



University of Huddersfield Repository

Lane, Mark

Using the AC Drive Motor as a Transducer for Detecting Electrical and Electromechanical Faults

Original Citation

Lane, Mark (2011) Using the AC Drive Motor as a Transducer for Detecting Electrical and Electromechanical Faults. Masters thesis, University of Huddersfield.

This version is available at <http://eprints.hud.ac.uk/id/eprint/10167/>

The University Repository is a digital collection of the research output of the University, available on Open Access. Copyright and Moral Rights for the items on this site are retained by the individual author and/or other copyright owners. Users may access full items free of charge; copies of full text items generally can be reproduced, displayed or performed and given to third parties in any format or medium for personal research or study, educational or not-for-profit purposes without prior permission or charge, provided:

- The authors, title and full bibliographic details is credited in any copy;
- A hyperlink and/or URL is included for the original metadata page; and
- The content is not changed in any way.

For more information, including our policy and submission procedure, please contact the Repository Team at: E.mailbox@hud.ac.uk.

<http://eprints.hud.ac.uk/>

MSc By Research

University of Huddersfield
School of Computing and Engineering

Using the AC Drive Motor as a Transducer for Detecting Electrical and Electromechanical Faults

Master of Science by Research

Student: Mark Lane
Supervisors: Dr Crinela Pislaru
 Professor Andrew Ball
 Dr Fengshou Gu

January 2011

Contents

	Page	
Abstract	iv	
Acknowledgements	v	
List of symbols	vi	
List of figures	viii	
List of tables	xi	
List of tables	xi	
Nomenclature	xii	
Chapter 1	Introduction	1-13
1.1	Research aims.....	1-2
1.2	Research objectives	1-2
1.3	Overview of thesis	1-3
Chapter 2	Literature review	2-4
2.1	Fault detection methods on motors using motor current signature analysis (MCSA)	2-4
2.2	Fault Detection using motor Instantaneous Angular Speed analysis (IAS)	2-6
2.3	Fault detection methods on inverter systems	2-6
2.4	Model-based condition monitoring.....	2-8
2.5	Fault detection using vibration analysis and advanced networks	2-9
Chapter 3	Theoretical aspects related to inverter-driven motor systems	3-11
3.1	Inverter Systems.....	3-11
3.1.1	Electric drive block diagram	3-12
3.1.2	Six-step VSI Inverter.....	3-13
3.1.3	PWM inverter.....	3-16
3.1.4	Sensorless Vector Drive Technology	3-17
3.1.5	Sensorless Flux-vector drive technology.....	3-18
3.1.6	Closed-loop flux-vector drive with field-orientated control.....	3-19
3.2	AC Motors (actuators).....	3-20
3.2.1	AC motor equivalent circuit and equations	3-27
3.2.2	AC motor mathematical model.....	3-29
Chapter 4	Design and practical implementation of the experimental test rig	4-31
4.1	Mechanical Test Rig Design.....	4-31

4.2	Test rig specification	4-33
4.3	Electrical Drive Specification	4-34
4.4	Test Rig Panel Equipment.....	4-36
4.5	Test Rig Panel	4-44
4.6	External Test Rig Equipment.....	4-46
Chapter 5	Improvement of experimental test rig performance by changing its configuration	5-53
5.1	Test Rig Modifications – Automation	5-53
5.1.1	Equipment used to automate the test rig - PLC	5-55
5.1.2	Example PLC Program operation.....	5-57
5.1.3	Test Rig PLC and operator screen.....	5-58
5.1.4	Test rig PLC control strategy.....	5-60
5.2	Test Rig Modifications – Closed-loop operation	5-61
5.3	Commissioning the test rig	5-62
5.4	Performance improvements	5-63
Chapter 6	Monitoring procedures for inverter-driven motor systems	6-64
6.1	Introduction to monitoring procedures	6-64
6.2	Motor fault detection	6-65
6.2.1	Motor supply	6-67
6.2.2	Motor speed.....	6-73
6.2.3	Motor vibration.....	6-74
6.2.4	Motor acoustic emissions	6-75
6.3	Inverter Fault Detection	6-75
6.3.1	Incipient Fault Diagnosis in Electrical Drives by Tuned Neural Networks	6-77
6.3.2	Fault Diagnostics in an Inverter Feeding an Induction Motor	6-80
6.3.3	Fault Detection of 3-Phase VSI using Wavelet-Fuzzy Algorithm	6-83
Chapter 7	Fault diagnosis of experimental inverter-driven motor system	7-85
7.1	Introduction	7-85
7.2	Data Acquisition System.....	7-85
7.3	Measurement of experimental data for healthy and faulty gearbox.....	7-89
Chapter 8	Conclusions and further work	8-102
8.1	Review of Objectives	8-102
8.2	Conclusions	8-104
8.3	Contributions to Knowledge and Understanding	8-106
8.4	Future work	8-106
8.4.1	Compatibility of existing condition monitoring methods with inverter-driven systems.....	8-107
8.4.2	Use of adaptive algorithms to signal motor faults.....	8-108

8.4.3	Improvement of measured inverter signals	8-108
8.4.4	Combining inverter and motor condition monitoring.....	8-109
8.4.5	Incorporating fault detection algorithms into existing automation/drive equipment 8-109	
8.4.6	Validating the fault detection algorithms.....	8-110
References		8-111
Appendix A	Gearbox Test Rig Modifications	8-2
A.1	Test rig modifications – mechanical and electrical works.....	8-2
A.2	Data acquisition system – modifications.....	8-5
Appendix B	PLC Program detail and Memory allocation	9-6
B.1	PLC Program design	9-6
B.1.1	PLC Program Structure	9-7
B.1.2	Operator screens.....	9-15
Appendix C	Commissioning tests	10-2
C.1	Test and calibration	10-2
C.2	PLC program verification	10-5
C.3	Tests to verify the automated test rig results.....	10-5
C.4	Actual Test Rig Operation Screenshots	10-23
Appendix D	Test rig schematics	10-1

Abstract

Condition monitoring of AC motors is a subject area that has received extensive research. Whether this monitoring is carried out on a scheduled basis by engineer intervention, or continuously using an on-line unit, the results of this testing enable preventative maintenance work to be carried out earlier, before any major failure occurs. Monitoring using vibration analysis is the most common and depending on the plant, can be done once or twice a year. This is usually limited to the condition of motor bearings and is not commonly used to detect failures in the motor electromagnetic systems. Monitoring units that use motor current measurements are also available, but these are less widely-used and usually on major plant motors (>250kW for example) that have a large capital outlay to replace.

The industry drivers – as always – are maximum plant and machinery uptime, with the minimal amount of scheduled maintenance. If maintenance is carried out too regularly, costs rise significantly not only due to the maintenance activity itself, but disruption to production schedules. Maintenance schedules that are too infrequent can result in an unacceptable rise in total failures of plant that are unexpected and may cause a significant amount of production disruption and downtime, especially if this occurs during out-of-hours working time.

However, industry now faces another big challenge and one that has had a good share of exposure over the last few years. It is of course, the drive to reduce carbon emissions and with it the amount of energy that a plant itself consumes. What has brought this more to the fore recently is the significant rise in energy costs. Whilst product margins have to remain the same, many companies energy costs have seen a two to three-fold increase in energy budgets in the last few years alone. For industry processes that have a significant amount of fan and pump applications, the manufacturers of low-cost AC inverters have saturated the lower-performance market of inverter drives such that any drive can control these type of fan and pump applications, where accurate speed control is not a major driver.

Unfortunately, this can be a step backwards for end-users of plant that use equipment to monitor motor condition via motor current signals. Additionally, vibration analysis that relies upon ‘base-lining’ motor data when the AC motor is running at base speed may not give accurate readings when the motor is under inverter control and running at a different speed.

For manufacturers of AC inverter drives in this low-end market, it can be difficult to sell a product from one manufacturer over another without the unit having a “USP”, or Unique Selling Proposition. Most decisions taken on inverter equipment purchase at this level are usually in favour of the equipment that costs the least to purchase. Credibility of manufacturers based on product history and perceived reliability cuts little ground with an ever cost-conscious industry.

This is where the research into diagnosis of faults on inverter driven motor systems can provide just this USP for manufacturers. If the incorporation of on-line diagnosis for simple inverter applications can be brought to a typical inverter unit at a reasonable cost, the manufacturer who can offer this gains a unique foothold in the marketplace – a drive that can monitor and signal that the motor it is driving is showing signs of early failure.

It will be sensible to limit this research to simple inverter applications as high-end inverter drives that operate equipment such as high-speed printing presses, rotary shears will be more difficult to model and simulate than a fan or pump application.

It is hoped that a typical inverter drive can relay enough detailed information about the load which it is driving to allow this to be used for abnormal motor load conditions as this will provide a platform on which to extend the research beyond this MSc and into the realms of incorporating such technology into a drive manufacturers

equipment. If this can be done without major modification to an inverter, then it may be easier to implement in equipment offered by different manufacturers.

It is quite possible that this technology could be licensed under a name that guarantees the performance of the condition monitoring algorithms and reliability from one drive manufacturer to another.

Acknowledgements

I would sincerely like to thank Professor Andrew Ball for his assistance in starting this research project as well as for his guidance along the way. I would also like to thank Dr. Fengshou Gu and my Director of Studies Dr. Crinela Pislaru who's assistance was invaluable in progressing the research.

An additional thanks to my Father, John Lane for his help in modifying the rig on-site and my mother for her motivation. This research is dedicated to my dear, late partner Lynn who was my guiding light all of the way.

List of symbols

AC	Alternating Current
AFD	Adjustable Frequency Drive
ANN	Artificial Neural Network
ASL	Above Sea Level
BNC	Bayonet Neill-Concelma (Type of connector, commonly used in Radio Frequency applications)
BP	BackPropagation
CMMS	Computerized Maintenance Management System
CSI	Current Source Inverter
CT	Current Transformer
DAQ	Data Acquisition System
DC	Direct Current
DOL	Direct On – Line
DSP	Digital Signal Processor
DWT	Discrete Wavelet Transform
EA	Evolutionary Algorithms
EEPROM	Electrically Erasable Programmable Read Only Memory
EPRI	Electrical Power Research Institute
FFT	Fast Fourier Transform
FL	Fuzzy Logic
FLC	Full Load Current
FLT	Full Load Torque
GA	Genetic Algorithm
GMM	Gaussian Mixture Model
GTO	Gate Turn-off Thyristor
HMI	Human machine interface (operator screen for control/visualisation of a control system)
HVAC	Heating, Ventilation And Control (for building management)
IAS	Instantaneous Angular Speed
IEEE	Institute of Electrical and Electronics Engineers
IGBT	Insulated Gate Bipolar Transistor
IP	Insulation Protection; Commonly referred to as 'IP Ratings'. Used to define the level of protection than an enclosure offers against contact with electrical parts and its resistance to dust or moisture.
IR	IR Losses. Usually referred to in context of : 'DC motor IR losses' where I = DC motor Armature Current; R = DC motor Armature Resistance.
LAD	LADder (PLC programming language format)
LDA	Linear Discriminant Analysis (credited to Fisher)
LRT	Locked Rotor Torque

MCSA	Motor Current Signature Analysis
MOSFET	Metal Oxide Semiconductor Field Effect Transistor
MRAS	Model Reference Adaptive System
NFMCSA	Notch Filtered Motor Current Analysis
PC	Personal Computer
PCI	Peripheral Card Interface
PI	Proportional Integral (used to define the terms used within a control loop. Example: 'PI controller')
PID	Proportional Integral Derivative (used to define the terms used within a control loop. Example: 'PID controller')
PII	Process Image Inputs (used in a PLC)
PIO	Process Image Outputs (used in a PLC)
PLC	Programmable Logic Controller
PPF	Pole Pass Frequency
PPI	Point-to Point Interface © Siemens AG
PPR	Pulses Per Revolution (for measuring encoder resolution)
PPU	Power Processing Unit
PWM	Pulse Width Modulation
RAM	Random Access Memory
RLS	Recursive Least Square
RMS	Root-Mean Squared
SCR	Semiconductor /Silicon Controlled Rectifier
STL	Structured Text Language (PLC programming language format)
VFD	Variable Frequency Drive
VSD	Variable Speed Drive
VVI	Variable Voltage Inverter

List of figures

Figure 3-1 - Block diagram of an electric drive [29]	3-13
Figure 3-2 - Variable Voltage Inverter (VVI) Basic Circuit Diagram [29].....	3-14
Figure 3-3 - Six-step VSI Block Diagram [29].....	3-14
Figure 3-4 - DC bus PI regulator diagram [30].....	3-15
Figure 3-5 - Six-step generator diagram [30].....	3-15
Figure 3-6 - Six-step firing pulses and motor current generated [29]	3-16
Figure 3-7 - PWM Inverter output switching waveform [31].....	3-16
Figure 3-8 - PWM inverter drive output [31].....	3-17
Figure 3-9 - Sensorless Vector Block Diagram [31]	3-18
Figure 3-10 - Sensorless Flux Vector Block Diagram [31].....	3-19
Figure 3-11 - Field Oriented Control Block Diagram.....	3-19
Figure 3-12 - Stator core detailing winding ‘slots’ [22]	3-20
Figure 3-13 - Phase pole winding details [22].....	3-20
Figure 3-14 - Rotor construction (a) – with laminations; (b) – laminations removed [22]	3-21
Figure 3-15 - AC Squirrel-cage motor exploded view [23].....	3-22
Figure 3-16 - AC Motor Torque Curve ; Redrawn from original diagram [24].....	3-24
Figure 3-17 - AC Motor torque/speed curve; Redrawn from original diagram [24].....	3-25
Figure 3-18 - Motor efficiency vs. loading curve; Redrawn from original diagram [24].....	3-26
Figure 3-19 - AC Equivalent Exact Circuit (one phase); Redrawn from original [25].....	3-27
Figure 3-20 - 3-phase supply waveform [27]	3-29
Figure 3-21 - Magnetic Linkages and voltages; Redrawn [28]	3-30
Figure 4-1 - Block diagram of test rig design.....	4-31
Figure 4-2 - Actual Gearbox Test Rig	4-32
Figure 4-3 - Block diagram of the experimental test rig.....	4-35
Figure 4-4 - Functional Block Diagram – 690+ Inverter, Frame C [32].....	4-38
Figure 4-5 - DC load motor diagram on the test rig	4-40
Figure 4-6 - Resistor bank view [34]	4-41
Figure 4-7 - Resistor bank internal wiring schematic [34].....	4-42
Figure 4-8 - Test rig control panel front	4-45
Figure 4-9 - Test rig control panel interior.....	4-46
Figure 4-10 - View of Helical Geared motor [35]	4-47
Figure 4-11 - Service factor table from David Brown Catalogue (page 65) [36]	4-47
Figure 4-12 - Cut-away view showing DC motor field/armature circuit; Re-drawn by ML [24].....	4-49
Figure 4-13 - Shunt-type DC motor as used on test rig	4-49
Figure 4-14 - DC Shunt motor speed, torque, voltage relationships.....	4-50
Figure 4-15 - Shunt wound machine circuit	4-50
Figure 4-16 - Power flow for Motor / Generator [25]	4-51
Figure 5-1 - Speed and load step operation	5-54
Figure 5-2 - Simple hard-wired control circuit using two switches	5-55
Figure 5-3 - Hard-wired control circuit shown in PLC software.....	5-55

Figure 5-4 - Simple PLC block diagram.....	5-56
Figure 5-5 - PLC Hardware rack block diagram	5-57
Figure 5-6 - PLC Program operation	5-58
Figure 5-7 - S7-222 PLC [37].....	5-59
Figure 5-8 - TP177 Micro Touch-screen [38].....	5-59
Figure 5-9 - Typical PPI network [37].....	5-59
Figure 5-10 - Step 7 MicroWIN programming software.....	5-60
Figure 5-11 - Test Rig PLC design philosophy	5-61
Figure 5-12 - Installing the HTTL Speed Feedback Technology Box Option [51]	5-62
Figure 5-13 - Single-ended encoder wiring [51].....	5-62
Figure 6-1 - Spectra of vibration and current signatures (0 -100 Hz) at 5.625 KW with no defects [3]	6-72
Figure 6-2 - Original and Notch-filtered current signals – healthy motor [4]	6-73
Figure 6-3 - Siemens Masterdrives Inverter Unit [47]	6-76
Figure 6-4 - Classification of common fault types [10].....	6-78
Figure 6-5 - Block diagram of an AC drive with highlight on the measurement location and processing flow [10].....	6-79
Figure 6-6 - Comparison between expected validation outputs and predicted [10].....	6-80
Figure 6-7 - Fuzzy logic fault diagnostics system [10]	6-81
Figure 6-8 - A voltage-fed PWM inverter system indicating the possible failure modes [14].....	6-82
Figure 6-9 - Inverter voltage spectra: (a) healthy case (b) one switch open (c) one switch short [14]	6-83
Figure 6-10 - A PWM voltage-fed inverter of induction motor (a) and after fault occurrence (b) [14]	6-84
Figure 7-1 - Setup for experimental gearbox test rig	7-86
Figure 7-2 - Mounting of motor encoder	7-86
Figure 7-3 - Three-phase current measuring unit.....	7-87
Figure 7-4 - Diagram of three phase measurement unit.....	7-88
Figure 7-5 - Diagram of measured signals	7-88
Figure 7-6 - Screenshot of measured signals.....	7-89
Figure 7-7 - Screenshot of operating status through 'dashboard'	7-89
Figure 7-8 - Simulation plots colour key	7-90
Figure 7-9 - Measured data for healthy gearbox – Test number 1	7-91
Figure 7-10 - Comparing motor torque (a) vs. armature current (b)	7-92
Figure 7-11 - Measured data for healthy gearbox – Test number 2	7-92
Figure 7-12 - Measured data for faulty gearbox – Test number 3	7-93
Figure 7-13 - Measured data for faulty gearbox – Test number 4	7-94
Figure 7-14 – Comparison of experimental data for Test number 1 and Test number 3	7-95
Figure 7-15 - Comparison between the actual AC motor phase currents	7-96
Figure 7-16 - Measured current signals for healthy and faulty gear set	7-97
Figure 7-17 - Experimental Test Rig System.....	7-97
Figure 7-18 - Model reference system used for data analysis.....	7-97
Figure 7-19 - Comparison of torque feedback values from drive measured between a healthy and faulty gear set	7-98
Figure 7-20 - Comparison between actual motor current signals for healthy and faulty gears.....	7-100
Figure 7-21 - Measured phase current waveform	7-101
Figure B-1 - Test Rig PLC Hardware components	8-2

Figure B-2 - Test rig panel exterior before and after modification	8-3
Figure B-3 - Test rig panel interior before and after modification	8-4
Figure B-4 - Diagram showing additional test rig signals.....	8-5
Figure B-5 - D-Type connector wiring for Data Acq. system (Optima Drawings)	8-5
Figure B-1 - PLC Program structure	9-8
Figure B-2 - Main Sequence (SBR0)	9-9
Figure B-3 - Subroutine SBR0 LAD network and symbols used	9-10
Figure B-4 - SBR2 Speed Sequence Diagram; State 2.....	9-11
Figure B-5 - Speed (SBR2) and Load (SBR4) state diagrams	9-12
Figure B-6 - Ramp function block	9-13
Figure B-7 - Ramp change calculation block.....	9-13
Figure B-8 - PLC Program Symbol Table for Test Rig Program (screenshot from S7-MicroWIN software).....	9-14
Figure B-9 - Main Operator Screen	9-15
Figure B-10 - 'Set-up' Screen	9-16
Figure B-11 - 'Recipe Screen 1'.....	9-17
Figure B-12 - Trending Display Screen.....	9-17
Figure C-1 - Field controller (maximum current potentiometer arrowed)	10-3
Figure C-2 - Analogue output scaling blocks [50]	10-6
Figure C-3 - 690+ Analogue output scaling function [50].....	10-6
Figure C-4 - 690+ Drive 'Feedbacks' Block [50]	10-6
Figure C-5 - 'Wiring' of inverter Feedbacks block to physical analogue outputs	10-7
Figure C-6 - Rig test 1a; 100% speed, varying load	10-9
Figure C-7 - Rig Test 1b; 100% speed, varying load.....	10-10
Figure C-8 - Rig Test 1c; 100% speed, varying load	10-11
Figure C-9 - Comparing AC inverter current feedback to actual measured instrument values	10-12
Figure C-10 - Commissioning Test 2; 30% load; Speed incremental steps	10-13
Figure C-11 - Commissioning Test 3; 60% load; Speed incremental steps	10-14
Figure C-12 - Commissioning Test 2; 30% load; Speed incremental steps	10-15
Figure C-13 - Commissioning Test 5a; 100% Load, Speed ramped 0 -100%	10-16
Figure C-14 - Commissioning Test 5a; 100% Load, Speed ramped 0 - 100%	10-17
Figure C-15 - Commissioning Test 5a; 100% Load, Speed ramped 0 - 100%	10-17
Figure C-16 - Repeat of Commissioning Test 5a; 100% Load, Speed ramped 0 - 100%.....	10-18
Figure C-17 - Test run 5c; Autotune performed.....	10-19
Figure C-18 - AC Motor no-load motor torque/speed plot	10-20
Figure C-19 - Test 7; verification of DC motor loading	10-21
Figure C-20 - Commissioning Test 8.....	10-22
Figure C-21 - Test 8 speed response comparison of	10-22
Figure C-22 - Current and torque response comparisons of.....	10-23
Figure C-23 - Operator Screen; Test Rig running in Auto	10-24
Figure C-24 - Trending Screen	10-24

List of tables

Table 4-1 - Gearbox Specification	4-33
Table 4-2 - Control transformer sizing	4-43
Table 4-3 - Control panel functions.....	4-45
Table 6-1 - Examples of motor failures arising from external system faults [40].....	6-66
Table 6-2 - Component failures in motors > 50hp and <=200 hp.....	6-66
Table 6-3 - Selected inverter fault codes [47].....	6-76
Table 6-4 - Selected inverter alarm codes [47].....	6-77
Table 6-5 - Experimental setup settings [10].....	6-79
Table 7-1 - Simulation data set for all healthy and faulty gear sets	7-90
Table 7-2 - Data plot signals and scaling factors.....	7-90
Table B-1 - PLC External Inputs	9-6
Table B-2 - PLC External Outputs	9-7
Table B-3 - Ramp function block inputs and outputs.....	9-13
Table B-4 - Operator Screen to PLC Data.....	9-18
Table B-5 - PLC to Operator Screen Data.....	9-19
Table C-1 - Main calibration parameters	10-2
Table C-2 - Calibration results table 1	10-2
Table C-3 - Calibration results table 2	10-3
Table C-4 - Calibration results table 3	10-4
Table C-5 - Operator screen value scaling.....	10-4
Table C-6 - 'Feedbacks' block observation data.....	10-7
Table C-7 - Scaling of drive output data	10-7
Table C-8 - Data logging channels - Commissioning tests.....	10-8
Table C-9 - Commissioning Test 1a Data	10-8
Table C-10 - Table of load readings; Test 1a	10-9
Table C-11 - Commissioning Test 2 Data	10-12
Table C-12 - Table of load readings; Test 2	10-13
Table C-13 - Table of load readings; Test 3	10-14
Table C-14 - Commissioning Test 4 Data	10-15
Table C-15 - Commissioning Test 5a Data	10-15
Table C-16 - 690+ Drive Autotune Parameters	10-20
Table C-17 - Commissioning Test 6 Data	10-20
Table C-18 - Commissioning Test 7 Data	10-21
Table C-19 - Graph points vs. load settings	10-22

Nomenclature

E_a	Voltage generated by rotation of armature in the field
f	Frequency (Hz)
h_g	Gearbox per unit efficiency
I_a	Armature current
I_m	Reactive or magnetising component of I_o
I_o	Current in magnetising branch of motor
I_p	Power component of I_o
J	Moment of inertia of the rotating components of the drive (kg.m^2)
J_l	Load inertia
J_{lr}	Load inertia referred to motor
n	Rev/sec
n_s	Rev/sec synchronous
N_l	Load Speed Rev/min
N_m	Motor Speed Rev/min
N_r	Rotor speed Rev/min
N_s	Synchronous speed Rev/min
p	Number of pole pairs
P_g	Air gap power per phase
P_m	Mechanical power output
R_a	Armature resistance
R_m	Magnetising resistance, representing iron losses
s	Slip
s	Fractional Slip (AC equivalent circuit)
T_f	Frictional torque loss
T_l	Load torque
T_l	Applied load
T_m	Motor torque / Mechanical torque (Newtons)
V_a	Applied armature voltage
ω_m	Mechanical angular rotation velocity ($2\pi n$ radians/s)
X_m	Magnetising resistance

Chapter 1 Introduction

AC motors are responsible for approximately 70% of all electricity consumed on the grid network and are used in 90% of all industrial motor applications for manufacturing processes of various forms. Depending on the size of these units, from 1 kilowatt to megawatts they can be costly items to replace. Even on smaller motors, lost production resulting from motor failure often costs manufacturing more in downtime than the actual motor is worth.

Demand for monitoring the condition of AC motors is now high as the pressure on processes is to perform with less and less profit margin and with vastly reduced down-time available on plant equipment. This places a heavy emphasis on the components used to perform day after day, with the minimum of maintenance input and the maximum amount of up-time.

There are many methods that can be used to monitor the condition of a motor and those such as vibration analysis rely on a person to manually perform the measurement task. Often, this is not possible due to the hazardous or inaccessible location of these motors, particularly when processes are running. It would be of great benefit to industry if the monitoring of motor condition could be done actively, be non-intrusive and run on a continuous basis using an unmodified, standard motor. Ideally, this form of monitoring would require no input from maintenance personnel and would signal potential failure conditions as and when they arise – not months later when manual checks are performed.

This approach tends towards requiring the motor to operate as a ‘transducer’ (since no other equipment will be fitted to the motor for diagnostic purposes), effectively using only the equipment fitted as standard to a typical motor in order to ‘feed-back’ information to a higher-level diagnostics system for the purposes of fault detection.

Condition-based monitoring of fixed-speed AC motor applications using the motor as a transducer is not a new research area. There are systems available on the market that can be wired non-intrusively into an existing AC motor application to monitor the motor behaviour and alarm when abnormal conditions exist. However, these systems rely on the motor operating at a continuous fixed-speed and coupled directly to the 3-phase supply. This is known industry-wide as Direct On-Line – DOL operation. Systems that rely on the motor operating in a DOL mode cannot be utilised on inverter-driven motor systems because the voltage, frequency and phase angles of motor current will vary as the motor speed is changed. As the use of inverter technology in industry becomes more widespread, the opportunity to perform diagnosis using these systems is no longer possible and manual measurement is required once again.

It follows that any new method developed to use the motor as transducer for the purposes of monitoring both the condition of the motor and the mechanical load that it drives must be compatible with AC inverter-driven motor systems.

1.1 Research aims

The aim of this research is to advance motor condition monitoring methods into the field of inverter-driven motor systems, rather than the fixed-speed non-inverter driven systems that have been the focus of much research up to now.

It is important to determine at the outset, whether any existing research has been undertaken into the specific area of using the AC motor as a transducer for detecting electrical and electromechanical faults on an inverter-driven motor system. This will ensure that the research is not duplicating any existing work and makes a valuable contribution to research in this field.

A study of all elements of inverter-driven motor systems will be required, from AC motor technology used through to the inverter-drive systems available on the automation market. This will include details of how modern flux-vector closed-loop and open-loop inverter systems operate, because any system that relies on the inverter to provide fault diagnosis will have to be compatible with the latest control methods available.

In order to test and simulate fault conditions, it will be important to have a test rig that contains all of the equipment required to perform these tests satisfactorily. Therefore, the design of a test rig, together with subsequent test and validation is incorporated into this research as a key contribution.

A series of tests run on healthy and faulty mechanical equipment will then be carried out. The most appropriate condition monitoring method will be used for the fault diagnosis of the test rig based on the differences between data sets for healthy and faulty gearbox.

1.2 Research objectives

The main objective of this project is to investigate the operation of an inverter-driven motor system with a view to determining whether the existing output signals on a typical AC inverter drive contain sufficient information so as to allow this to be used for purposes of condition monitoring and fault diagnosis on the driven motor system. The AC inverter must be from a latest-generation of drive and must not be modified from its original factory-delivered state. This will ensure that all results from the research are relevant to and useable with the current generation of modern inverter drives without requiring any modification.

The project objectives can be divided up into several parts and these are given below:

- Investigate actual motor condition monitoring techniques with a view to determine whether any existing research has been undertaken into the specific area of using the AC motor as a transducer together with the AC inverter signals for detecting electrical and electromechanical faults on an inverter-driven motor system.
- Research the latest state-of-the-art control strategies implemented in modern electrical drives.
- Design a practical test rig which will enable to measure relevant experimental data.
- Test and commission the operation of the rig to ensure design criteria are satisfied.

-
- Change the open-loop configuration of the test rig into the closed-loop configuration in order to increase the system performance and the accuracy of the test results.
 - Investigate the signals received from the inverter drive to ascertain their usefulness in detecting fault/non-fault conditions on the faulty equipment

1.3 Overview of thesis

An overview of the thesis is presented as follows.

Chapter 2 - contains a critical appraisal of the literature review about operation of the various existing fault diagnostic methods used on AC motor driven systems, AC Inverter drives and AC Inverter-driven motor systems is presented.

Chapter 3 - the theoretical aspects relating to inverter-driven motor systems are described. A study of all elements of these systems will be undertaken from the AC motor used through to the inverter-drive systems available on the automation market. This will include details of how modern flux-vector open-loop and closed-loop inverter systems operate.

Chapter 4 - the design of the test rig will be covered in detail. The operating specification that was created will be discussed, along with the equipment subsequently specified in order to control the test rig to an acceptable standard.

Chapter 5- the improvement of the experimental test rig performance by changing its configuration will be described, together with the equipment and design methods used.

Chapter 6 - the monitoring systems that have been developed and researched for use on AC motors and inverter systems are investigated and detailed.

Chapter 7 – the tests carried out on the actual test rig using healthy and faulty gear sets will be presented and the experimental data will be analysed.

Chapter 8 – contains the conclusions from the research performed and suggestions for future work.

The next chapter presents a critical appraisal of the exiting publications related to electrical drives and related condition monitoring methods.

Chapter 2

Literature review

This chapter describes a critical appraisal of the literature review about the operation of the various existing methods used for diagnosis on:

- AC motor systems
- AC Inverter drives
- AC Inverter-driven motor systems

Firstly, research on condition monitoring methods on motors involving measurements taken from motor speeds, vibration or current signals are detailed. Following on from this, investigation into the methods used for fault detection on the inverter drives is undertaken. This leads onto research work including model-based condition monitoring and those involving artificial neural networks.

2.1 Fault detection methods on motors using motor current signature analysis (MCSA)

Bo Liang's [1] research involved the condition monitoring and fault diagnosis of three-phase induction motors. Firstly, modelling of the three phase motor under different conditions and performing digital simulations of healthy and faulty inverter motor operation was carried out. This led to the second part of the research which was to evaluate the performance of range of fault detection and diagnostic techniques not limited to phase current analysis. The other techniques developed were vibration and transient speed variations. Finally, the research would lead to the development of fault detection and diagnostics for faults in three-phase induction motors based on novel signal processing techniques such as higher order spectral analysis and neural networks.

From the research, it was found that vibration analysis and per-phase current analysis are the most sensitive techniques for fault detection of induction motors. The success of neural networks developed for the same purposes of per-phase current fault detection were found to be dependent on the input variables used by the model. The fault detection models were developed to detect stator and rotor symmetries.

Jugrapong Treetrong [2] researched the use of parameter identification methods for the condition monitoring of electric motor drives. This would use MCSA as a basis for the research, but the efficiencies of these systems would be improved by the use of parameter identification techniques. A key element of the research would be that the system performing the parameter identification would have to work from available data (such as stator voltages, currents and the rotor speed) collected easily from the motor's power supply. The technique would not rely on any other intrusive equipment or sensors to help capture this data. To this end, a new technique of parameter estimation using the GA

(Genetic Algorithm) method would be used. This would use the MCSA signals without requiring any previous knowledge of the parameters to be estimated and without any other instruments.

Induction motor parameter estimation using the GA technique minimised the difference between the measured and predicted state variables for the motor. The results from testing concluded that the new scheme can estimate the parameters and predict motor condition with sufficient accuracy for motor fault diagnosis. It was found that the method can not only detect the faults, but can also quantify how many faults are happening in the induction motor.

Chinmaya Kar et al. [3] progressed MCSA research into motor gearbox loads, where load fluctuations on the gearbox and gear defects are two major sources of vibration. Fast Fourier Transforms, along with further processing using Discrete Wavelet Transform (DWT) to study the transients in MCSA. The drivers of this research were not due to the complexity involved in detecting faults from the analysed signals, but in actually needing the vibration measuring instruments. If these could be dispensed with and the same faults detected through MCSA, then this would be an important step in advancing MCSA further.

It was shown during the research that the use of Continuous Wavelet Transform (CWT) was unable to detect defects or load fluctuations. However, results did conclude that MCSA along with DWT can be a genuine replacement for conventional vibration monitoring.

Serkan Günal et al [4], researched a method whereby the main motor fundamental frequency of 50Hz (Europe) would be notch-filtered out before being fed into the fault detection process. This was known as the Notch-Filtered Motor Current Analysis (NFMCSA) method. The reasoning behind this method was that the spectral components of motor current (other than the fundamental component) carry required information for fault detection and it is easier to interpret this data once the fundamental component had been removed. The experimental verification of the proposed features and classifiers revealed that NFMCSA approach is a promising analysis especially considering the fact that high classification accuracy can be achieved even in case of structurally different machines with numerous different faults under varying motor load conditions.

Research undertaken by F. Gu et al [5], involved the use of induction motor current feedback signals to identify and quantify common faults within a two-stage reciprocating compressor based on bispectrum analysis. This theoretical basis is developed to understand the non-linear characteristics of current signals when the motor is driving a varying load under different faulty conditions. This work provides a novel approach to the analysis of stator current for the diagnosis of motor drive faults from downstream driving equipment and it was proved that the bispectrum feature gives rise to reliable fault classification results using non-intrusive methods.

Mohamed El Hachemi Benbouzid et al [6], realised that intensive research had been focused on MCSA methods and proposed to use advanced signal processing techniques on the stator motor current signals instead. In their investigations, the frequency signature of some asymmetrical motor faults were identified using advanced signal processing techniques such as high-resolution spectral analysis. Initial

experimental results clearly illustrated that stator current high-resolution spectral analysis is very sensitive to induction motor faults that modify the main spectral components, such as voltage unbalance and single-phasing effects. Experimental results demonstrated that the stator current high-resolution spectral analysis – proposed as a medium for induction motors faults detection – has definite advantages over the traditionally used FFT spectral analysis. Generally, this technique will be useful in detecting other fault conditions that modify the main spectral component signals.

2.2 Fault Detection using motor Instantaneous Angular Speed analysis (IAS)

Filippetti, F et al [7], researched using Artificial Intelligence techniques in induction machines diagnosis that including the ‘speed ripple’ effect. Torque ripples that occur due to the broken rotor bars in an AC induction machine manifest themselves as large speed fluctuations when using the high-resolution measuring device.

Rotor electrical faults of AC induction machines were used as the basis for this research together with a new, simple procedure based on a model which includes the speed ripple effect. Their research led to a new diagnostic index being developed, that was independent of the machine operating condition and inertia value, thus allowing the implementation of the diagnostic system to be achieved with a minimum of configuration intelligence.

This research validated the use of AI techniques because the improvements that they introduce in the diagnostic process and proved that in order to obtain an indication on the fault extent, faulty machine models are still essential.

Ahmed Yousef et al [8], researched the technique of instantaneous angular speed (IAS) condition monitoring applied to reciprocating and rotating machinery. This technique was used to detect broken rotor bars in such systems. Results from a broken rotor bar fault show that the power spectrum of the IAS signals could be used for the diagnosis of this failure mode.

The key features in this case are the use of the pole pass speed sidebands around the rotor speed components for the purposes of fault detection. These sidebands could be visible at high loads as in vibration and current signature monitoring.

2.3 Fault detection methods on inverter systems

B. Biswas *et al.* [9] researched current harmonics analysis of an inverter-fed induction motor drive system under fault conditions. They presented harmonic analysis of motor current signatures under different fault conditions of medium and high power Variable Frequency Drive (VFD) systems. The medium to high power ranges can be a significant capital investment, making early diagnosis of faults in this arena even more paramount. Computer simulation of a variable speed inverter-fed induction motor based on constant voltage/frequency (V/f) operation is implemented using Powersim (PSIM) simulation software. Frequency response characteristics of motor currents are compared to analyze fault conditions in the motor drive system.

The method used was to analyse each of the frequency responses for different fault conditions in the inverter and compare these to establish the utility of FFT algorithm to identify the nature of the fault. These faults were a fault at one of the six IGBT gate terminals, complete failure of one IGBT in the inverter module, and a line to ground fault at one of the motor phase terminals. It was found that the

frequency responses under three different fault conditions were distinctly different and the research was able to discriminate each of the different fault states.

A. Azzini *et al.* [10] researched the use of tuned neural networks to diagnose incipient fault diagnosis in electrical drives. In order to identify any decrease in efficiency and any loss in industrial application a suitable monitoring system for processes is often required. With their proposed approach, useful diagnostic indications can be obtained by a low-cost extension of the monitoring activity. In this way, the reliability of the obtained indications can be significantly increased considering the combination of advanced time-frequency transform, or time-scale, such as wavelets, and a new evolutionary optimisation approach based on Artificial Neural Networks (ANN's).

Their research had been successfully applied to a real-world electric machine fault diagnosis problem. The experiments showed that the algorithm is quite robust with regard to the setting of the parameters – it does not require so much fine-tuning of the parameters. Their adopted methodologies were able to give good results for fault / non-fault identification in electrical drives. This was especially advantageous as it was found that due to the use of both wavelet processing of the acquired current and EA evolution of the ANN is a very simple and easy to implement system for diagnostic purposes.

Khater, Faeka *et al.* [11] presented a fault diagnostics system for a three-phase voltage source inverter using rule-based fuzzy logic system. The system was developed as a rule-based fuzzy logic system for faults occurring on the inverter power semiconductor switches (IGBT's). Based on a time domain simulation model, the inverter different fault conditions are simulated with the resulting voltage spectrum providing the database for the fuzzy logic system. The developed fault diagnostics system is capable of identifying the type and location of the inverter fault.

The proposed fault diagnostics system resulted in a matrix that provides the fault condition according to the data base status

Rozailan Mamat *et al.* [12] considered the fault detection of 3-Phase VSI using Wavelet-Fuzzy Algorithm. A real-time condition monitoring algorithm for a 3-phase PWM inverter drive using fuzzy-logic was developed. It is designed to detect and identify the transistor open-circuit fault and an intermittent misfiring fault, which commonly occurs in the inverter drive system. The condition monitoring mechanism is based on discrete wavelet transform (DWT) and fuzzy logic (FL). With this method, stator currents are used as an input to the system – no direct access to the induction motor is required.

Rigorous testing – both theoretically and practically – of the system proved that it is robust and reliable. The features are directly extracted from the wavelet transform of the stator currents. The results clearly show that wavelet analysis together fuzzy logic, offers a great potential for monitoring and diagnosis of power electronic drives.

M. Abul Masrur *et al.* [13] researched intelligent Diagnosis of Open and Short Circuit Faults in Electric Drive Inverters For Real-Time Applications. A normal model and an extensive range of faulted models for the inverter-motor combination were developed and implemented using a generic commercial

simulation tool to generate voltages and current signals at a broad range of operating points selected by a machine learning algorithm. Extensive simulation experiments were conducted to test the system with added noise, and the results show that the structured neural network system which was trained by using the proposed machine learning approach gives high accuracy in detecting whether a faulty condition has occurred, thus isolating and pin-pointing to the type of faulty conditions occurring in power electronics inverter based electrical drives.

Three important sets of signals, namely the torque, and voltages and currents in different phases were used for the fault diagnostics. These signals were segmented simultaneously and diagnostic features were extracted from signal segments. The accuracy of the diagnostic results has reached more than 99% in average and furthermore, the authors presented a structured neural network system that is trained to detect and isolate any of the 15 faults in a three-phase induction motor in real-time. System performance is evaluated on the basis of time elapsed to detect a fault after it occurs and simulation results show that the proposed system takes less than 20 ms on an average to successfully detect and isolate a fault.

Debaprasad Kastha *et al.* [14] investigated Fault Modes of Voltage-Fed Inverter System for Induction Motor Drive. They recognised that knowledge about the fault mode behaviour of an converter system is extremely important from the standpoint of improved system design, protection and fault-tolerant control. They have undertaken a systematic investigation into the various fault modes of a voltage-fed PWM inverter system for induction motor drives and then developed a preliminary mathematical analysis for the key fault types. Such faults covered include input supply line faults to inverter drive transistor open and short-circuit faults. The predicted fault performances were then substantiated by simulation study. The study has been used to provide fault-tolerant control by determining the stresses in power components to allow operation to continue, post-fault by using steady-state operating regions. The research applied to inverters operating in the volts/hertz mode and the extensive simulation study was able to define the zone of operation where the drive can continue to operate safely in a degraded mode. In high-reliability process control environments, this is extremely important.

2.4 Model-based condition monitoring

Filippetti, F *et al* [15], presented the improvement of induction machine rotor fault diagnosis based on a neural network approach. By training the neural network using data sampled through experimental tests on healthy machines and through simulation in case of faulted machines, the diagnostic system can discern between “healthy” and “faulty” machines.

This was found to be a more robust method for on-line identification of induction machine rotor bar failures. The input and the output patterns to train the neural network were obtained using both experimental data related to healthy machines and computed data obtained from a faulted machine model as a simulator. In addition to this, the network was able to be introduced to manufacturing dissymmetry – inevitable in equipment – rather than by setting a fixed trigger threshold for distinguishing between healthy and faulty machines.

Filippetti, F et al [16], then further researched the application of expert systems, artificial neural networks (ANNs), and fuzzy logic systems that can be integrated into each other and used with more traditional techniques for fault diagnosis of electrical machines and drives. This research brings together the diagnosis of the induction machine itself and the AC converter drive including both open and closed-loop variants for detecting failed machine rotor bars.

Whilst the techniques covered are limited to only a number of practical implementations, it is believed that these techniques will have a significant role in electrical drive diagnostic systems. In particular, fuzzy-neural diagnostic systems will become extensively used for machine condition monitoring, potentially in self-repairing electrical drives.

Loránd Szabó et al [17], researched an Improved Condition Monitoring System for Induction Machines Using a Model-Based Fault Detection Approach. The monitoring system was based on improving the accuracy of fault detection by the combined application of two monitoring methods. A fault signal will only be generated when both methods indicate its presence in the electrical machine. The two fault detection methods used are MSCA (motor current signature analysis) and IAS (Instantaneous Angular Speed).

It was found that using two different monitoring methods at the same time improves the accuracy of the entire monitoring system following the correct operation of a vector controlled AC squirrel cage induction machine. However, with this paper, no actual simulated tests of motor faults was performed and the accuracy of the proposed system was not verified.

2.5 Fault detection using vibration analysis and advanced networks

Electric motor vibration creates additional power consumption and degrades the performance of the motor. To avoid unexpected equipment failures and obtain higher accuracy in diagnostic for the predictive maintenance of induction motors, on-line health monitoring systems play an important role to improve system reliability and availability. The recent developments in MEMS technology shows an increasing trend to integrate vibration analysis for fault diagnostic purposes. Vibration-based detection using an accelerometer is gaining popularity due to higher reliability of the devices, low power consumption and low cost.

To this end, Wei-Jen et al [18], presented a paper on a wireless health monitoring system for vibration analysis of induction motors. This paper presents the study of vibration due to the rotor imbalance. The technique of vibration detection and observation of vibration signal in the 3-phase induction machine is studied in this paper. A novel health monitoring system of the electric machine based on a wireless sensor network (ZigBee™/IEEE802.15.4 Standard) is also proposed and developed in this paper. Experimental results of the proposed severity detection technique of rotor vibration under different levels of imbalance conditions are investigated and discussed.

Research on the actual signal processing techniques required was studied and some of the more recent examples are cited.

Piotr Czech et al [19], presented research on classification of tooth gear wheel faults of a gearbox by multilayer perceptron (MLP) and continuous wavelet transform (CWT) simulated on a test rig stand. The outline of the research was to build classifiers of the local teeth damages in gear wheels, based on artificial neural networks (ANN's). The gear damage was in the form of a crack in the tooth base and the crumbling of a tooth tip.

As a result of the conducted research it was possible to build a correctly working classifier of both the type and advancement of the gear damage. However, it was found that the achieved classification error relies extensively on how the damaged model is prepared and the teaching method of the ANN in order to obtain accurate results.

Salem Al-Arbi et al [20], presented Early Diagnosis of Gear Transmission Failure based on Advanced Intelligence Analysis on vibration signals measured remotely. The research was concerned with investigating more reliable and effective approaches to the detection and diagnosis of different gear faults based on enabling techniques such as Time Synchronous Averaging (TSA), Spectrum analysis, Cepstrum analysis, Time-frequency analysis and Wavelet transforms. The sensors were mounted at two different locations, one on the gearbox and the other at the motor end.

It was found that spectral analysis based on TSA signals is a more appropriate solution to the remote fault diagnosis problem and the analysis results illustrate that spectral analysis based on TSA signals can achieve the same results at a remote position as when the sensor is mounted as close to the gear as possible.

Wavelet transforms were found to be the most effective due to factors such as allowing decomposition of signals at different scales, therefore allowing different gearbox transmission stages to be analysed, but further research work is required to confirm the operation of this in a real industrial environment.

The next chapter presents the theoretical aspects related to the operation of electrical drives including inverter-driven systems.

Chapter 3

Theoretical aspects related to inverter-driven motor systems

This chapter will describe the operation and theoretical aspects of inverter-driven motor systems on which this research is based. Study of the AC motor and inverter in detail is important, as the two effectively become one system for this research.

In the first instance, operation and theoretical equations of the AC asynchronous induction motor will be described. Following this, operation of modern inverter control systems will be detailed. From basic six-step inverters through to pulse-width-modulated sensorless vector units and then to devices operating in closed loop mode using motor encoder feedback. Closed-loop drive performance is discussed and comparisons made with other inverter operating modes.

3.1 Inverter Systems

An inverter-driven motor system controls the rotational speed of an alternating current (AC) electric motor by controlling the frequency and voltage of the electrical power supplied to the motor. This system is also called variable frequency drive (VFD), adjustable-frequency drive (AFD), and variable-speed drive (VSD). Variable-frequency drives are widely used in ventilation systems, pumps, elevators, conveyors, machine tools, etc. There are four basic design types of VFDs that are described briefly below:

a) Pulse Width Modulation (PWM) – this controller is extremely popular because it is affordable, highly reliable and reflects the least amount of harmonics back into its power source. The AC line supply voltage is the input signal for the converter (with diodes and large DC capacitors) which creates and maintains a stable DC bus voltage. The DC voltage feeds the inverter (now commonly with insulated gate bipolar transistors (IGBTs)) which regulate both voltage and frequency to the motor to produce a near sine wave like output.

PWM means that each transition of the alternating voltage output is actually a series of short pulses of varying widths. By varying the width of the pulses in each half cycle, the average power produced has a sine-like output. The number of transitions from positive to negative per second determines the actual frequency to the motor. The main advantages of PWM are: excellent input power factor; no motor cogging; high efficiency 92 - 96%; lower initial cost. However there are also several disadvantages: motor heating and insulation breakdown in some applications; non-regenerative operation; line-side power harmonics.

b) Current Source Inverter (CSI) - is the dual of a six-step voltage source inverter where the DC power supply is configured as a current source rather than a voltage source. The inverter SCRs

(Silicon Controlled Rectifiers) are switched in a six-step sequence to direct the current to a three-phase AC load as a stepped current waveform. CSI inverter could have load commutation and parallel capacitor commutation which are assisted by the input current regulation so it requires a large internal inductor to operate. The main advantages of CSIs are: reliability due to inherent current limiting operation; regenerative power capability; simple circuits. The main shortcomings are: large power harmonic generation back into power source; cogging below 6 Hz due to square wave output; poor input power factor due to SCR converter section.

c) Voltage Source Inverter (VSI) - uses an SCR converter section to regulate DC bus voltage. The inverter output is six-step output, the drive is a voltage regulator and uses transistors, SCRs or Gate Turn-Off thyristors (GTO's) to generate an adjustable frequency output to the motor. VSI's have the following advantages: simple design; applicable to multi-motor operations; operation is independent of load. The main disadvantages are: large power harmonic generation back into the power source; poor input power factor; cogging below 6 Hz due to square wave output; non-regenerative operation.

d) Flux Vector PWM drive – contains new power switching devices and smart 32-bit microprocessors to drive high torque, low RPM applications. The power section is the same as for all PWM drives and the motor's rotor position and speed are monitored in real time via a resolver or digital encoder for a full closed-loop system. In a sensorless vector control system, the motor speed is calculated from the voltage and current signals measured from the motor. From this information, the drive microprocessor determines and controls the motor actual speed, torque, and power produced. The vector control algorithms can be programmed into the motor or learned by the drive. These drives have the following advantages: excellent control of motor speed, torque, and power; quick response to changes in load, speed, and torque commands; ability to provide 100% rated torque at 0 speed; lower maintenance cost as compared to DC motors and drives.

The shortcomings of these drives are: higher initial cost in comparison to standard PWM drives; require special inverter-rated motors; and some drive manufacturer setup parameters are complex (although this is improving).

3.1.1 Electric drive block diagram

Figure 3-1 presents the components of an electric drive. The user introduces the input command (speed and /or position) into the controller which is sent to the Power Processing Unit (PPU). The electrical motor receives the electrical energy from the electric source and the command signal from the PPU. The electrical motor transforms the electrical power into mechanical energy which activates the mechanical load. The sensors are used to monitor the actual operating state of the drive and to feed back to the input of the controller an analogue or digital signal representing the output state. The actual and reference states are continually compared and if the actual state is different from the reference state an error signal is generated which the controller uses to force a change in the controllable parameters to eliminate the error by driving the system back towards the desired operating point. So the electrical drive is a feedback control system allowing the user to set a desired operating

state as a reference and the control system will automatically move the system to the desired operating point and maintain it at that point thereafter.

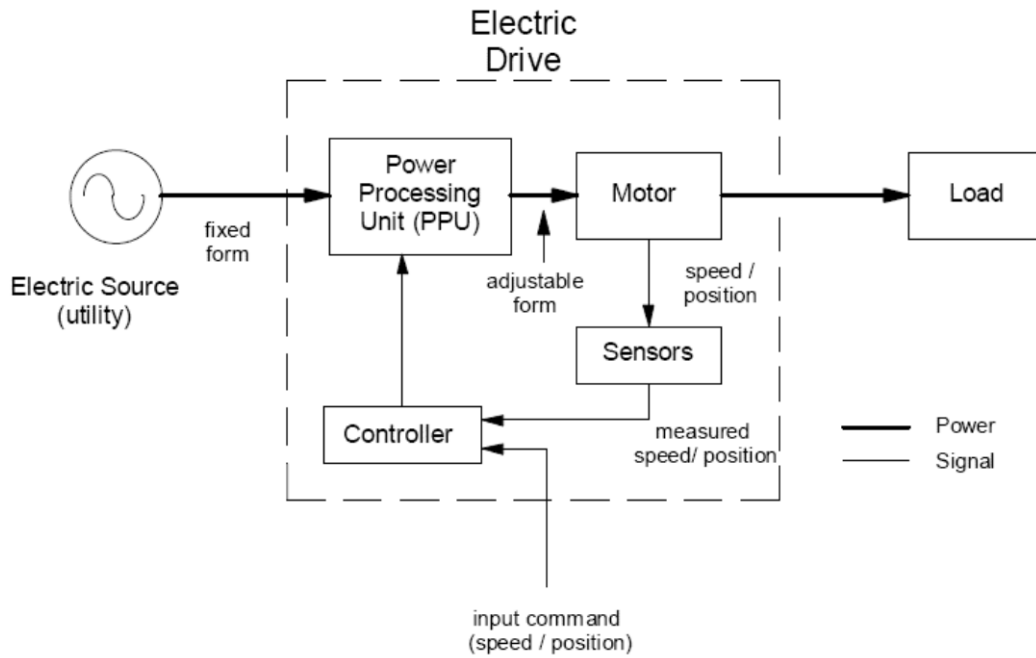


Figure 3-1 - Block diagram of an electric drive [29]

3.1.2 Six-step VSI Inverter

The most basic form of a six-step AC inverter is the Variable Voltage Inverter (VVI). The term 'six-step' comes from the fact that it takes six 60° switching steps to complete one full 360° cycle.

The VVI consists of an SCR (Semiconductor/Silicon Controlled Rectifier) circuit to convert the incoming AC voltage into DC. An SCR as opposed to just simply a bridge-rectifier arrangement is employed because the DC voltage needs to be controlled and regulated – this completes the 'Converter' section. A choke and capacitor make up the DC link section, helping to keep the converted DC voltage smooth and reduce ripple.

Finally, the output (Inverter) circuit consisting in modern drives of an IGBT (Insulated Gate Bipolar Transistor) circuit is used to convert the DC bus voltage into an 3-phase AC waveform. Older drives employed Thyristors, Bipolar Transistors or MOSFETS, but these are rarely used now. A diagram of this basic VVI is shown in Figure 3-2:

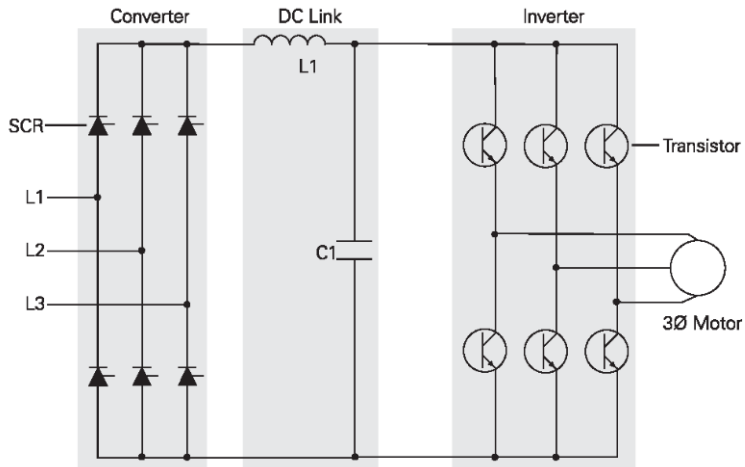


Figure 3-2 - Variable Voltage Inverter (VVI) Basic Circuit Diagram [29]

The circuit components of the six-step VSI are now described in more detail and Figure 3-3 below illustrates how all of the individual components function as part of a VSD controller and the control loops used.

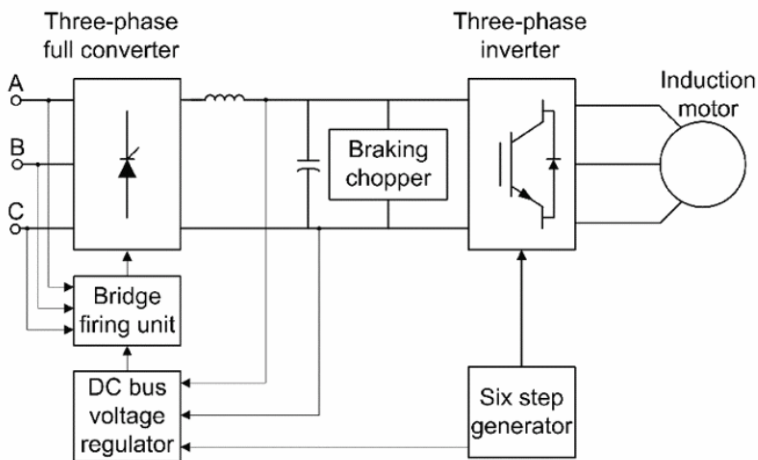


Figure 3-3 - Six-step VSI Block Diagram [29]

Bridge Firing Unit

The bridge firing unit is used to convert the firing angle, provided by the DC bus voltage regulator, into pulses applied to the thyristor gates. The bridge firing unit block contains notch filters applied to the voltage measurement to remove harmonics. The discrete synchronized six-pulse generator block is used to generate the pulses.

DC Bus Voltage Regulator and Braking Chopper

The DC bus voltage regulator is based on a PI controller and a hysteresis chopper logic. When the bus voltage decreases, the PI controller reduces the firing angle. When the bus voltage increases, the PI controller increases the firing angle. The chopper logic is based on hysteresis control. If the voltage reaches the upper hysteresis limit, the DC voltage controller toggles to braking mode and the chopper is activated, whereas the thyristor bridge is shut off. In chopper mode, the proportional action remains active but the integral gain is set to zero because the chopper dynamics are very high and the integral gain is useless. When the bus voltage reaches the hysteresis lower limit, the braking chopper is shut down and the thyristor bridge is reactivated. Figure 3-4 illustrates the DC bus PI regulator.

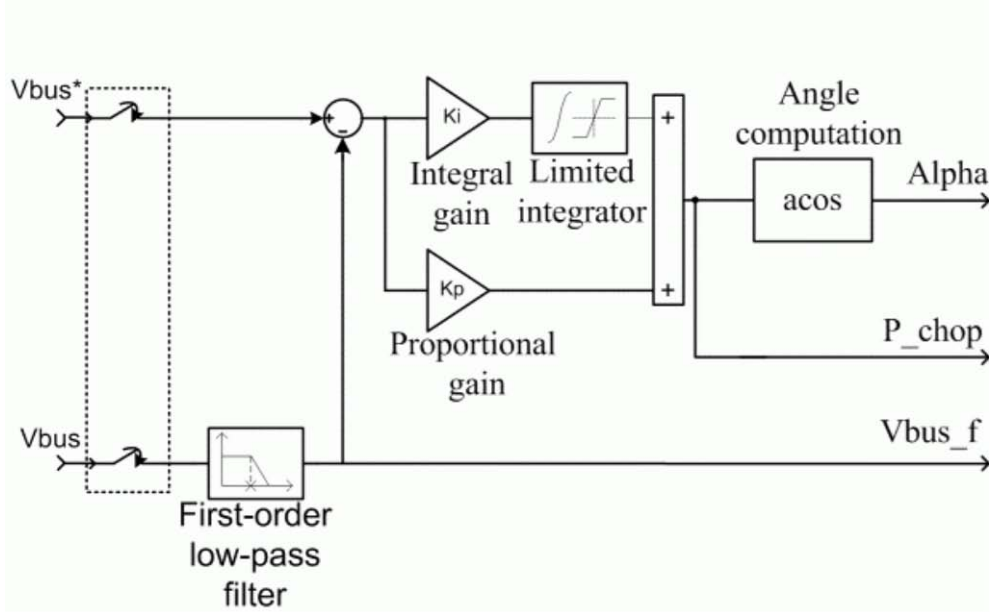


Figure 3-4 - DC bus PI regulator diagram [30]

Six-Step Generator

The six-step generator illustrated in Figure 3-5 contains six comparators to produce the six-step switching waveforms. Some supplementary logic enables a speed reversal by inverting two phases.

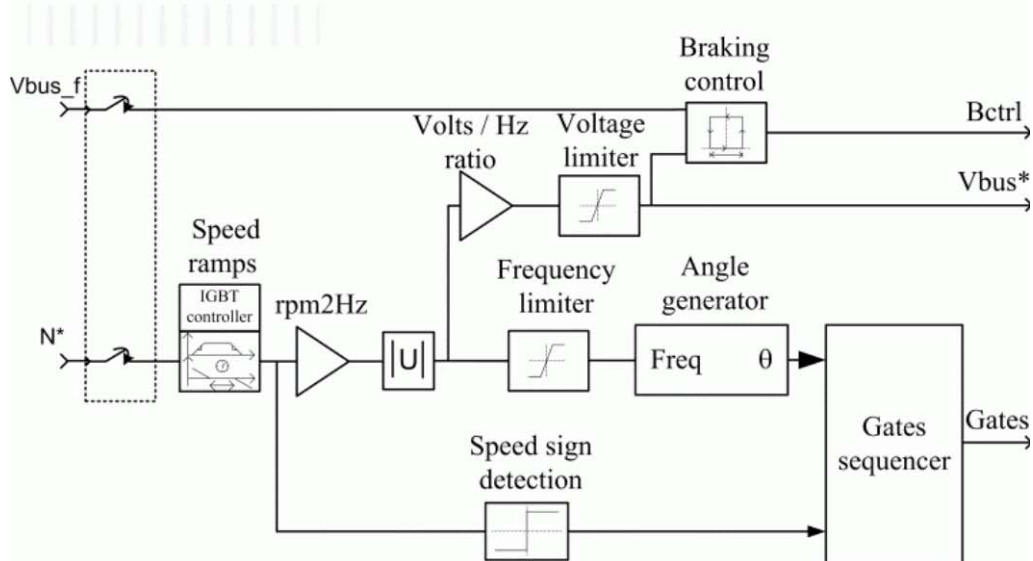


Figure 3-5 - Six-step generator diagram [30]

In the AC1 motor drive, the motor speed is not regulated in closed loop. Instead, the speed set point is used only to determine the motor voltage and frequency applied by the six-step inverter in order to maintain the (V/F) ratio (or the motor flux) constant from 0 to the nominal speed. Above nominal speed, the motor operates in the flux weakening mode; that is, the voltage is maintained constant at its nominal value while the frequency is increased proportionally to the speed set point.

When reversing speed, a short delay is required at the zero speed crossing so that air gap flux decays to zero.

The six-step pulses of the inverter circuit of the VVI are illustrated in Figure 3-6 below:

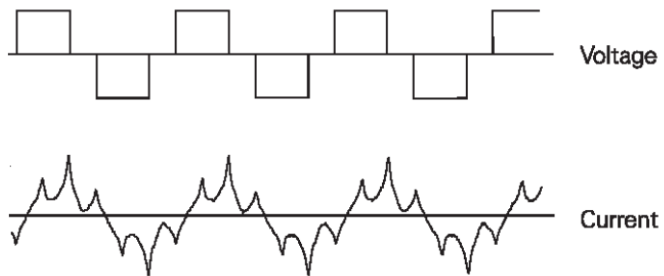


Figure 3-6 - Six-step firing pulses and motor current generated [29]

This method of switching is no longer used in AC inverters, due to the torque pulsations that occur in the AC motor each time one of the devices is switched. These torque pulsations manifest as 'cogging' in the motor and as the motor current is no longer sinusoidal, harmonic currents produced in the motor create additional heating, requiring de-rating of the motor.

However, because there is no high frequency carrier, a 6-Step type of inverter produces no audible noise in the AC motor.

3.1.3 PWM inverter

The block diagram of a PWM inverter is the same as for the six-step inverter. The major difference with a PWM inverter, however is how the 3-phase output to the motor is generated.

All modern VSI's now use PWM (Pulse Width Modulation), as this provides a more sinusoidal current output to control frequency and voltage supplied to the AC motor. Thus, they are more efficient and can provide a higher level of performance than the VVI or six-step units with no motor de-rating required.

The advent of PWM inverters brought with it the need to have a device capable of switching at a high-frequency and this is what an IGBT is designed to do. Typically, an IGBT can turn on in less than 400 nanoseconds and off in approximately 500 nanoseconds.

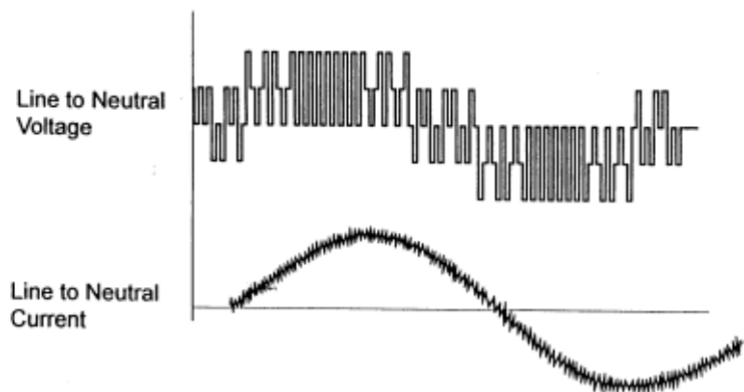


Figure 3-7 - PWM Inverter output switching waveform [31]

Observing Figure 3-7, it can be seen that the output of the PWM drive doesn't provide an exact replica of the AC input sine waveform. Instead, it provides voltage pulses that are at a constant amplitude.

The drive's control board signals the power device's control circuits to turn ON the waveform *positive half* or *negative half* of the power device. This alternating of positive and negative switching recreates

the 3-phase output. The longer the power device remains on, the higher the output voltage. The less time the power device is on, the lower the output voltage. Conversely, the longer the power device is off, the lower the output frequency with Figure 3-8 illustrating this.

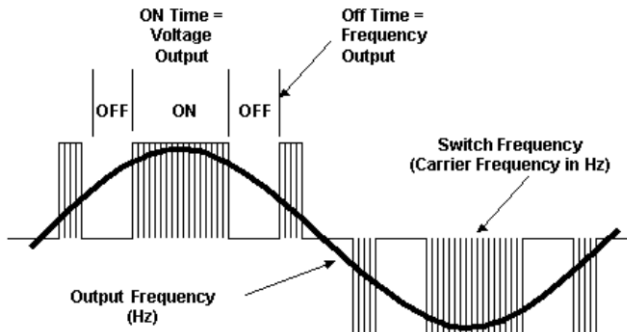


Figure 3-8 - PWM inverter drive output [31]

The speed at which power devices switch on and off is determined by the carrier frequency, also known as the switching frequency. The higher the switching frequency, the more resolution each PWM pulse contains. Typical switching frequencies are between 3KHz to 4Khz. The higher the switching frequency, the smoother the output waveform and therefore a higher resolution is obtained. However, higher switching frequencies decrease the efficiency of the drive because of increased heat in the power devices so a trade-off is made between resolution and efficiency.

High-performance drives have now taken PWM a step further and employ new technologies such as Sensorless Vector control to further improve motor performance. These are now described in more detail, with the Closed-loop flux-vector drive that uses encoder feedback being detailed last as this is the highest-performance drive offering.

3.1.4 Sensorless Vector Drive Technology

Sensorless Vector Control, like a V/Hz drive, continues to operate as a frequency control drive, with slip compensation keeping actual motor speed close to the desired speed. The Torque Current Estimator block determines the percent of current that is in phase with the voltage, providing an approximate torque current. This is used to estimate the amount of slip, providing better speed control under load. Figure 3-9 shows a typical Sensorless Vector drive block diagram.

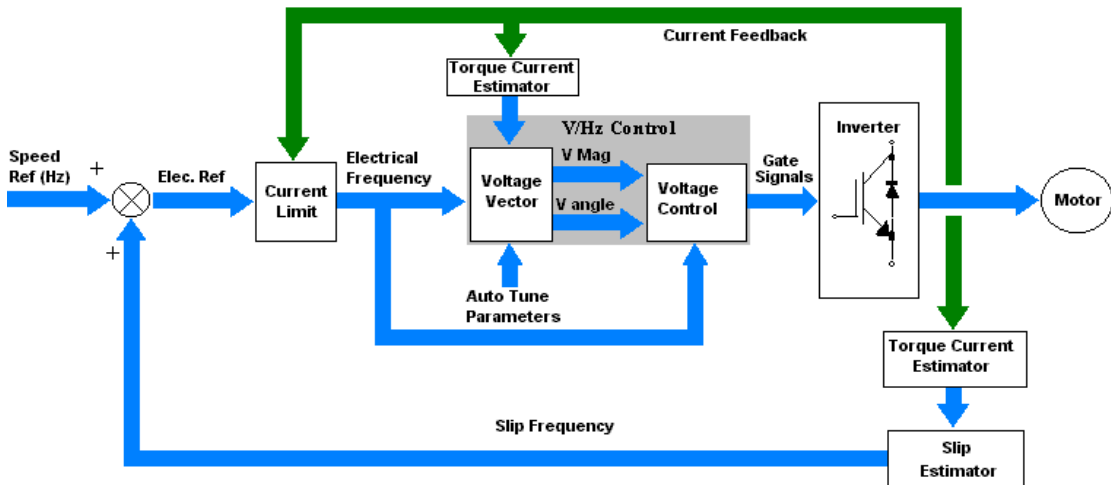


Figure 3-9 - Sensorless Vector Block Diagram [31]

The control improves upon the basic V/Hz control technique by providing both a magnitude and angle between the voltage and current. V/Hz drives only control the magnitude. Volts-angle (V angle in the figure) controls the amount of total motor current that goes into motor flux enabled by the Torque Current Estimator. By controlling this angle, low speed operation and torque control is improved over the standard V/Hz drive.

3.1.5 Sensorless Flux-vector drive technology

Sensorless flux vector control retains the basic core Volts/Hertz control philosophy and adds additional blocks around this core to improve the performance of the drive. A “current resolver” attempts to identify the flux and torque producing currents in the motor and makes these values available to other blocks in the drive. A current regulator that more accurately controls the motor replaces the current limit block. Notice that the output of the current regulator is still a frequency reference.

Early versions of Flux-vector drives required a speed feedback signal (typically an encoder) and also detailed information about the motor in order to properly identify the flux and torque currents. This led to the requirement for “matched motor/drive” combinations and many of the Siemens “Masterdrives” units had every motor type stored in the drive memory for such control. While there was nothing inherently wrong with this approach, it does limit the choice of motor to the end user and at the time, did not offer independent control of motor flux and torque. Figure 3-10 shows the additional components added to the sensorless vector drive.

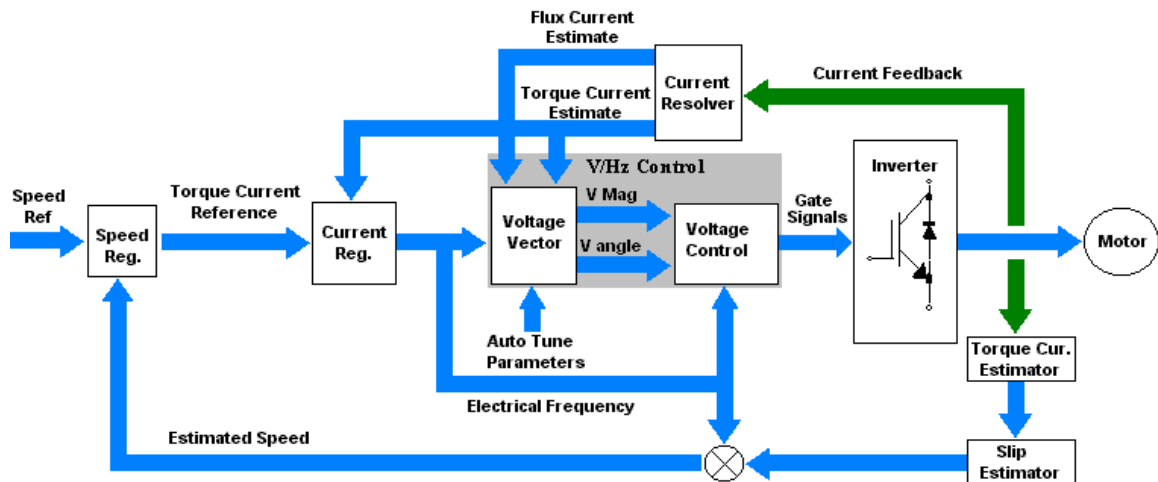


Figure 3-10 - Sensorless Flux Vector Block Diagram [31]

3.1.6 Closed-loop flux-vector drive with field-oriented control

The true closed-loop flux vector drive offers improved performance over the sensorless vector drive and modern units can now fully autotune to match completely the motor that they are controlling. These drives now employ field-oriented control that takes motor control a step further. What distinguishes a product using Field Oriented Control from a traditional vector product is its ability to *separate and independently* control (or regulate) the motor flux and torque. A block diagram of such a drive is given in Figure 3-11.

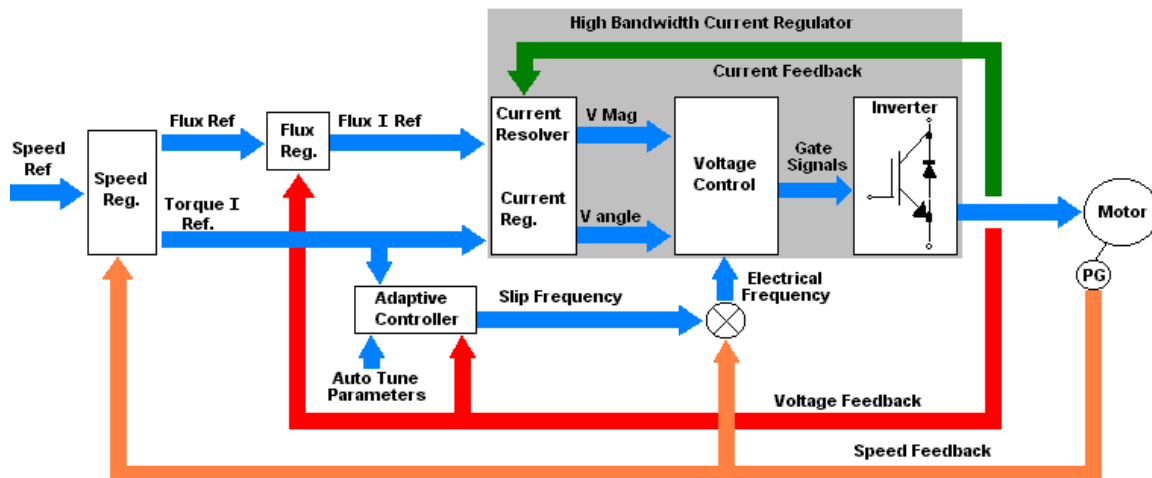


Figure 3-11 - Field Oriented Control Block Diagram

A high bandwidth current regulator that separates and controls the components of stator current replaces the Volts/Hertz core. The high bandwidth characteristics of this control eliminate nuisance trips due to shock loads and continuously adapt to changes in the motor and load characteristics. A separate adaptive controller uses information gained during auto tuning, actual reference information, and motor feedback information to give independent torque and flux control. This allows continuous regulation of the motor speed and torque. This is the type of controller that will be specified for the test rig.

3.2 AC Motors (actuators)

The type of AC motor used in this test rig for research purposes is an asynchronous squirrel-cage AC polyphase induction motor. The construction and principles behind the operation of this motor are detailed under this section sub-headings.

Construction - Stator

The asynchronous AC induction motor construction consists of a stator and rotor part. Unlike a DC machine, there is no electrical link between the stator and rotor through a commutator. The stator part consists of a defined number of pole windings that matches up to the number of pole windings in the rotor. These windings are embedded in slots that are cut into the laminated sections of the stator material (see Figure 3-12 below).

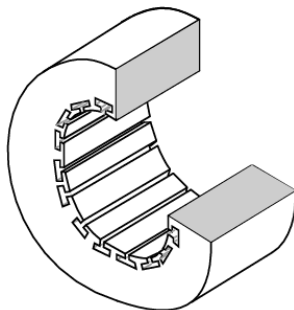


Figure 3-12 - Stator core detailing winding 'slots' [22]

The stator is made up of laminations made from thin insulated rings with slots punched from sheets of electrical grade steel. A stack of these is secured by end screws, which may also hold the end housings.

The pole windings are shown in Figure 3-13 below. Each phase of the supply is wound in opposing slots. Phase 1 is shown in green, 2 in red and 3 in blue.

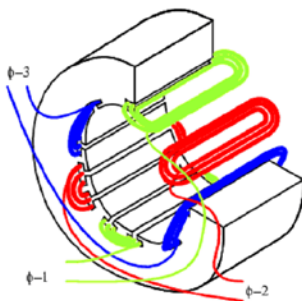


Figure 3-13 - Phase pole winding details [22]

Construction - rotor

The rotor consists of a shaft, a steel laminated rotor, and an embedded copper or aluminium squirrel cage. The illustration in Figure 3-14 (b) below shows the squirrel cage with the laminations removed.

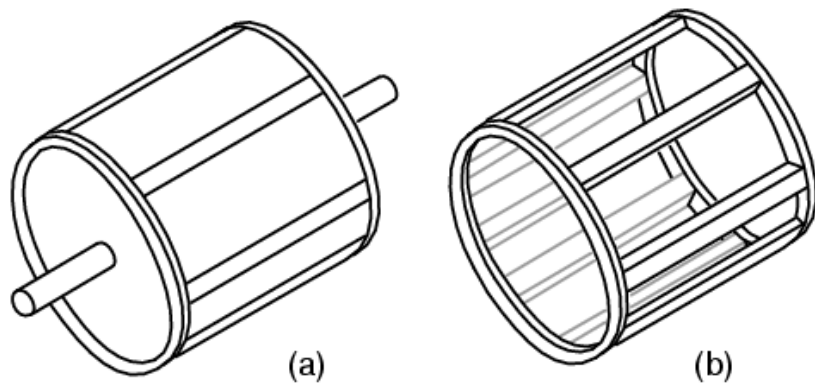


Figure 3-14 - Rotor construction (a) – with laminations; (b) – laminations removed [22]

There is a minimal air gap between the rotor and stator parts to allow the magnetic flux field to flow from stator to rotor, complete the magnetic circuit and provide electromotive force to the rotor.

The squirrel cage conductors may be skewed, twisted, with respect to the shaft. The misalignment with the stator slots reduces torque pulsations for smoother motor running.

Both rotor and stator cores are composed of a stack of insulated laminations. The laminations are coated with insulating oxide or varnish to minimize eddy current losses. The alloy used in the laminations is selected for low hysteresis losses.

Construction – bearings

An exploded view of a typical AC squirrel-cage motor is shown in Figure 3-15.

Each part is covered in detail under the diagram, but the general construction is as follows:

Parts IMB5 or IMB3 on the diagram below are the two possible motor front-end shields houses the motor bearing. Part IMB5 is a flange-style end housing that is usually used for mating directly to gearbox faces or into machinery housings. In this case, the motor may not be fitted with feet and is a flange-mounted motor. Part IMB3 is used where the motor is to be mounted on its feet – in this case a foot-mounted motor

The rear end shield, part 6.2 is common to either foot or flange mounted motor

Front and rear end-shield bearings, parts 1.60 and 6.10 hold the rotor shaft in place. The tolerance of these bearings is very tight as some rotors have as little as 0.1mm air gap between the rotor and stator.

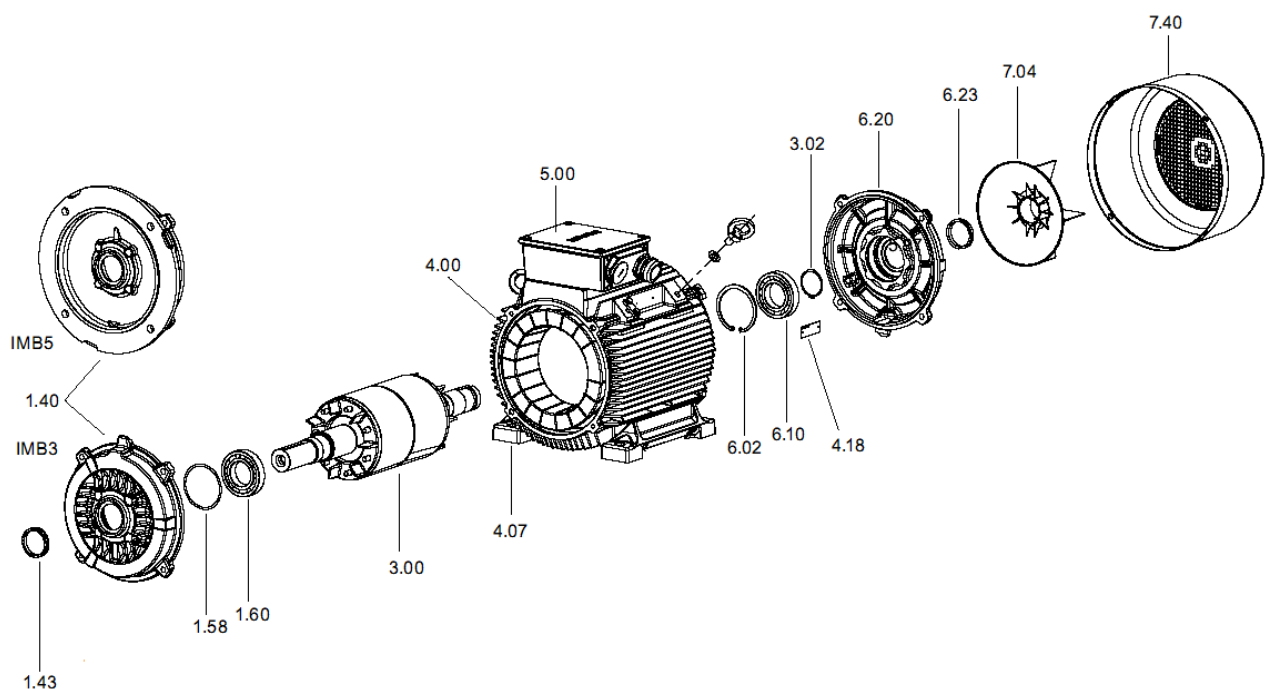


Figure 3-15 - AC Squirrel-cage motor exploded view [23]

Item	Description	Item	Description
1.40	End shield	4.07	Housing foot
1.43, 6.23	Shaft sealing ring	4.18	Rating plate
1.58	Spring washer	5.00	Terminal box, complete
1.60	Rolling-contact bearing	6.10	Rolling-contact bearing
3.00	Rotor, complete	6.20	End shield
3.02, 6.02	End bearing Circlip	7.04	Cooling fan
4.00	Stator, complete	7.40	Cooling fan cover

Direct on-line operation

AC asynchronous motors operate on the principle that the stator winding induces voltage and current into the rotor part so that there is a tangential force acting on the rotor due to the magnetic field and the motor rotor begins to turn if this force is sufficient to overcome the mechanical losses in the motor.

Motor Speed

With one pole pair isolated in a motor, the rotor rotates at a specific speed and this is defined as the base speed. The number of poles and the frequency applied determine this speed. A formula below allows the calculation of motor base speed based on the frequency, number of pole pairs of the motor and the fractional slip.

$$\frac{120 \cdot f}{p} \cdot \left(1 - \left(\left(n_s - n\right) / n_s\right)\right) \quad (3-1)$$

Where: f = Frequency; p = Number of pole pairs; n_s = rev/sec. synchronous; n = rev/sec.

There is one other factor that the equation above takes into account and that is motor slip. In an asynchronous machine, the rotor speed always lags behind the rotating magnetic field and the amount

by which the rotor lags behind the magnetic field is the amount of slip. A typical AC motor will exhibit between 3% and 5% slip.

Slip is required in order to generate motor torque. It is the action of the magnetic flux cutting the rotor conductors as it slips which develops torque. A loaded motor will slip in proportion to the mechanical load. If the rotor were to run at synchronous speed, there would be no stator flux cutting the rotor, no current induced in the rotor = no torque.

With one pole pair, and a supply frequency of 50Hz, a synchronous motor with no slip will rotate at 3000RPM. If the number of pole pairs is doubled, the synchronous speed is cut in half because the magnetic field rotates 180° in space for 360° of the electrical sine wave.

For example, the speed of a four pole motor (two pole pairs) with 2% slip connected to a 50Hz supply frequency will be:

$$\frac{120 \bullet 50}{2} \bullet \left(\frac{100 - 2}{100} \right) = 2940 \text{ RPM} \quad (3-2)$$

Motor Torque

When power is first applied to the motor, the rotor is at rest, while the stator magnetic field rotates at the synchronous speed N_s . The stator field is cutting the rotor at the synchronous speed N_s . The current induced in the rotor shorted turns is maximum, as is the frequency of the current and the frequency of this is equal to the line frequency. As the rotor speeds up, the rate at which stator flux cuts the rotor is the difference between synchronous speed N_s and actual rotor speed N_r or $(N_s - N_r)$. The ratio of actual flux cutting the rotor to synchronous speed is defined as slip:

$$s = \frac{N_s - N_r}{N_s} \quad (3-3)$$

Where: N_s = Synchronous speed; N_r = Rotor speed

The frequency of the current induced into the rotor conductors can only be as high as the line frequency at motor start. This then decreases as the rotor approaches synchronous speed. As already detailed under the previous section, at full motor loading (100% torque), slip will be a maximum of 5%. If the slip value is 2% at 50Hz, then the rotating stator magnetic field will be cutting the rotor at 1Hz. This 1Hz value is the difference between the synchronous speed and the actual rotor speed.

Motor torque curves

A typical motor torque curve for an asynchronous AC motor is shown in Figure 3-16:

Full load torque (FLT) is the safe, continuous torque rating of the motor

Full load current (FLC) is the safe, continuous motor current rating

Locked rotor torque (LRT) is around 50% higher than the FLT value and the Locked rotor current (LRC) is 500% of the FLC.

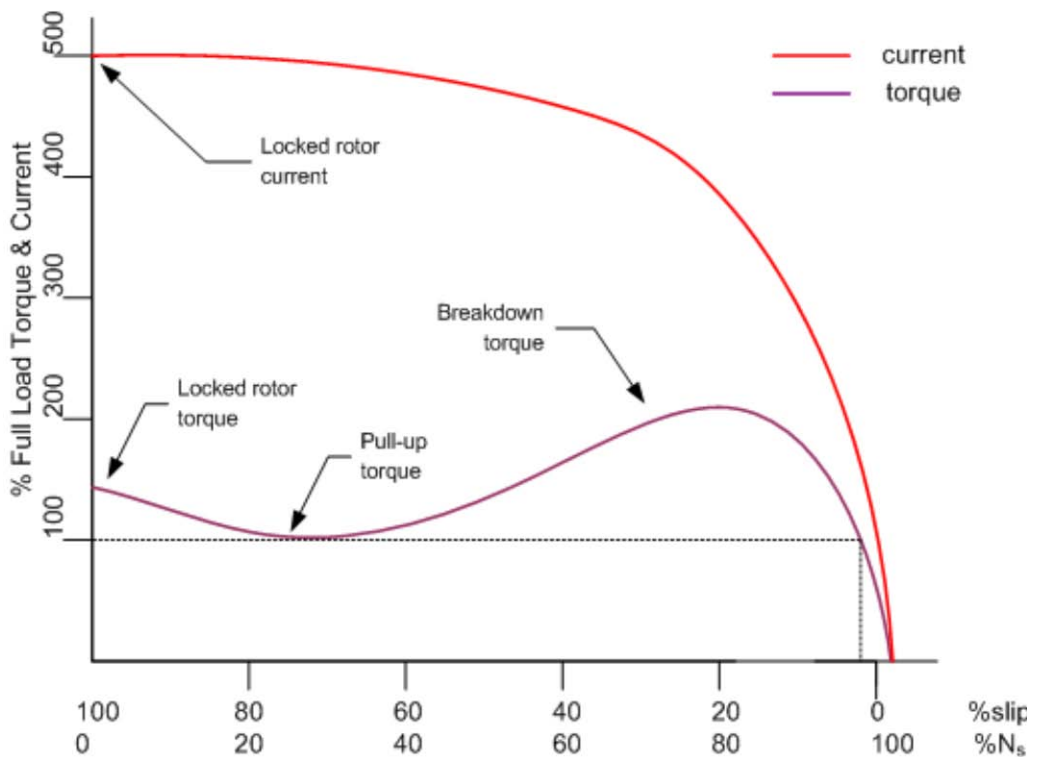


Figure 3-16 - AC Motor Torque Curve ; Redrawn from original diagram [24]

The motor current is high at start-up because the stationary rotor at start up behaves in a similar manner as if the secondary circuit were shorted-out on a transformer, resulting in the primary winding taking a high current.

As the rotor accelerates to within a few percent of synchronous speed, both torque and current will decrease substantially. Slip will be only a few percent during normal operation.

To the far right-hand side of the above figure, it can be seen that the torque, slip, and current will approach zero for a “no mechanical torque” load condition – at which point, the motor would reach synchronous speed.. This condition is likened to an open secondary transformer, where the primary only dissipates energy through eddy-current losses and circuit resistance as little resistance is reflected from the secondary (rotor) to the primary (stator). This would never happen under normal operating conditions.

Non-linear behaviour

An AC motor is inherently non-linear, especially when compared to a DC motor. This is because an AC motor relies on a single supply to provide both the magnetising field for the rotor and then to provide power enough to drive the rotor and generate torque.

The torque/speed curve given below shows this non-linear behaviour both in electromagnetic and mechanical torque terms as Figure 3-17 illustrates.

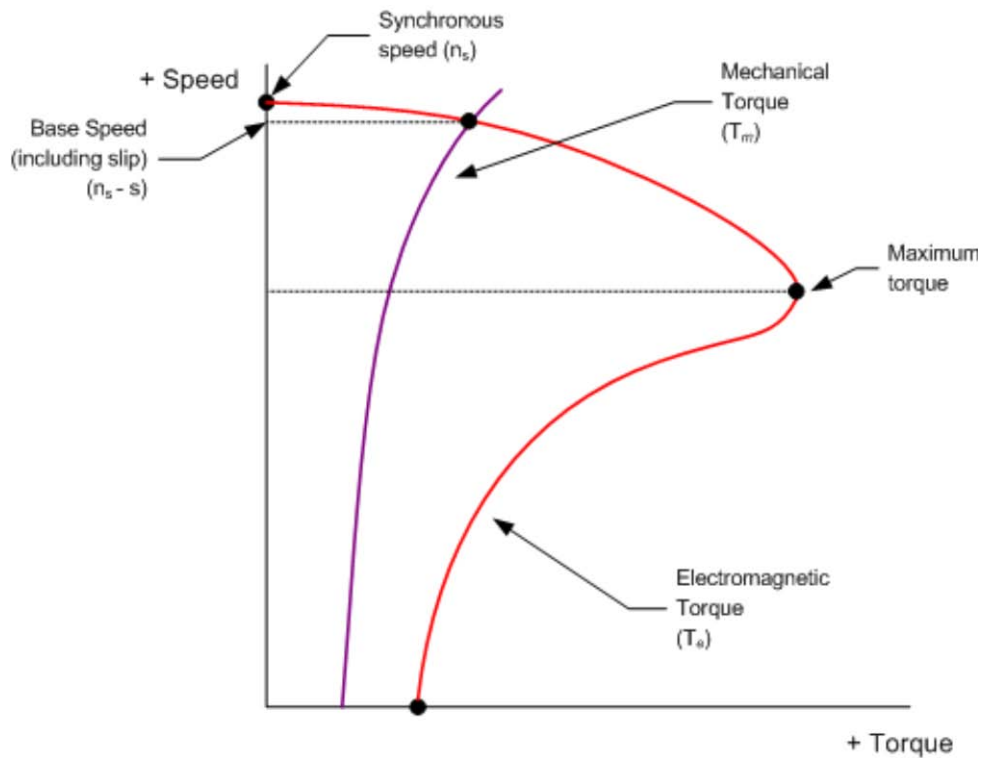


Figure 3-17 - AC Motor torque/speed curve; Redrawn from original diagram [24]

From zero speed ($n=0$) up to synchronous speed, the torque does not increase in a straight line, but does rise sharply as the motor base speed is reached. At this point, maximum motor torque is available for driving the load.

Motor efficiencies

Large three phase motors are more efficient than smaller 3-phase motors. This is due in part to the higher magnetising current ratio to torque-producing current ratio that smaller motors have.

Large induction motor efficiency can be as high as 95% at full load, though 90% is more common. Efficiency for a lightly loaded or no-loaded induction motor is poor because most of the current is involved with maintaining magnetizing flux. As the torque load is increased, more current is consumed in generating torque, while current associated with magnetizing remains fixed. Efficiency at 75% FLT can be slightly higher than that at 100% FLT and efficiency only really becomes poor below 25% FLT. The variation of efficiency with loading is shown in Figure 3-18 below:

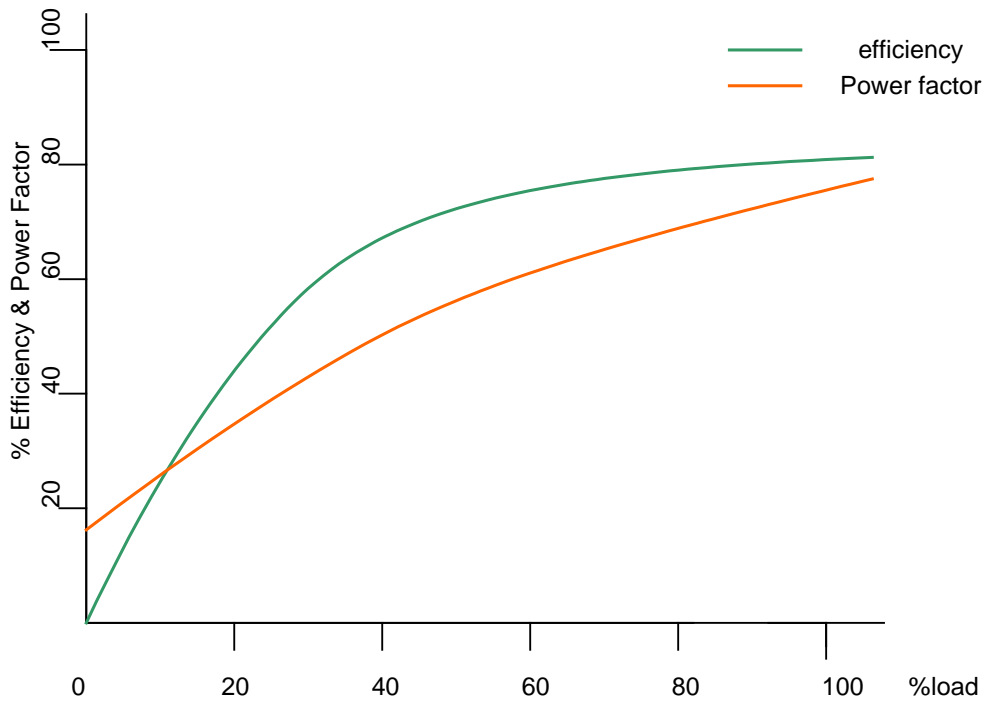


Figure 3-18 - Motor efficiency vs. loading curve; Redrawn from original diagram [24]

Just as important as the efficiency of the motor is the motor power factor. As the motor gets closer to its rated load, the power factor gets closer to unity (100% or 1.0). An inductive load will never achieve true unity power factor, but a good AC motor will get close to $0.86\cos\theta$ and this means that more of the power is going into actual work (torque produced) rather than being lost as heat.

Motor power and torque

Motor power is given by torque multiplied by speed of rotation:

$$P = T\omega \quad (3-4)$$

Where: P = Power (W)

T = Torque (Nm)

ω = Speed (rad/s)

Translating the above equation to take in the usual measurement of speed (RPM – revolutions per minute) the equation becomes that shown below:

$$P = \left(\frac{2\pi}{60} \right) \cdot T \cdot N \quad (3-5)$$

Where: N = Number of revolutions. Rev/min.

3.2.1 AC motor equivalent circuit and equations

The equivalent circuit for one phase of an AC machine is shown in Figure 3-19 below, and from this a formula is given that allows the torque output of an AC machine to be calculated using the equivalent circuit parameters:

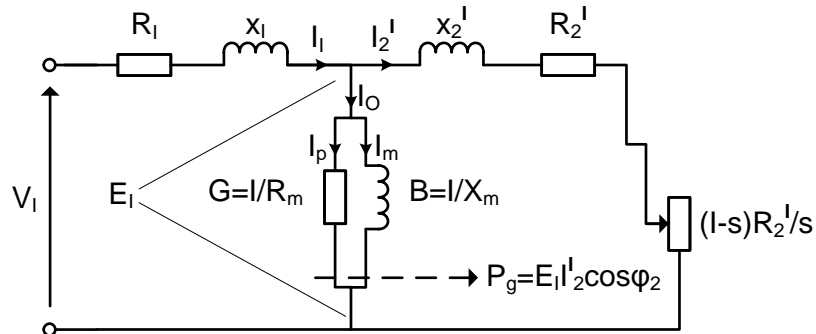


Figure 3-19 - AC Equivalent Exact Circuit (one phase); Redrawn from original [25]

I_o = Current in magnetising branch

I_p = Power component of I_o

I_m = Reactive or magnetising component of I_o

P_g = Air gap power per phase

R_m = Magnetising resistance, representing iron losses

s = Fractional slip = $(n_s - n) / n_s$

X_m = Magnetising resistance

The air gap power per phase $P_g = E_1 I'_2 \cos \varphi_2$ transferred magnetically from stator to rotor has two parts:

1. $I'_2 R'_2$ is converted into electrical power and associated with a voltage sE_1 . It is dissipated as heat loss
2. $(1-s)I'^2 R'_2 / s$ is converted to mechanical power and is associated with a voltage $(1-s)E_1$

For Figure 3-19 a power balance equation can be written. Rotor input/phase $E_1 I'_2 \cos \varphi_2 = P_g = I'^2 R'_2 / s$

or:

$$\begin{aligned}
 E_1 I'_2 \cos \varphi_2 &= E_1 I'_2 \frac{R'_2 / s}{Z'_2} &= I'^2 R'_2 &+ (1-s)I'^2 R'_2 / s \\
 &= I'^2 R'_2 / s &= \text{rotor Cu loss} &+ \text{mechanical output } P_m \\
 &= P_g &= sP_g &+ (1-s)P_g
 \end{aligned} \tag{3-6} [25]$$

For a motor, P_m will be taken as positive. It includes the torque loss which is virtually due to friction and windage only, since the rotor iron loss is negligible at normal slip frequency. At large values of motor slip, the effect of rotor iron loss must be allowed for in practise. For a generating machine, P_m would be

negative. The previous equation represents only one third of the total motor power, since it is expressed in phase values

Motor torque

The total torque developed electromechanically can be obtained from the previous equation and is given by:

$$T_e = 3 \frac{P_m}{\omega_m} = \frac{3P_g(1-s)}{2\pi n_s(1-s)} = \frac{3P_g}{2\pi n_s} \text{ Nm} \quad (3-7)$$

where:

P_m = Mechanical power output

P_g = Air gap power per phase

ω_m = Mechanical angular rotational velocity = $2\pi n$ radians/sec.

For any particular frequency and synchronous speed, the torque is directly proportional to the rotor input $3P_g$ since both P_m and ω_m vary as $(1-s)$. P_g itself is a function of speed. The torque can sometimes be expressed as $3P_g$ synchronous watts and from equation (3-7) this is equal to the torque in Newton-metres multiplied by the synchronous speed $\omega_s = 2\pi n_s$. A torque of one synchronous watt would develop one watt of power if acting at synchronous speed.

Writing equation (3-7) for the equivalent circuit shown in Figure 3-19, power P_g being calculated from $I_2'^2 R_2' / s$ the equation then becomes:

$$T_e = 3 \frac{P_m}{2\pi n_s} \times \frac{V_1^2}{(R_1 + R_2' / s)^2 + (x_1 + x_2')^2} \times \frac{R_2'}{s} \text{ Nm} \quad (3-8)$$

From this, a mathematical model of a mechanical mass drive system can be given by the equation:

$$J \frac{d\omega_r}{dt} = T_e - T_l - T_f \quad (3-9) [26]$$

J = Moment of inertia of the rotating components of the drive (kg.m^2)

T_l = Applied load

T_f = Frictional torque loss

The assumption made for deriving the above equation is that the output torque of a machine is predominately produced by the development of magnetic forces acting in a tangential direction on the magnetic material.

3.2.2 AC motor mathematical model

In order to understand the methods of monitoring procedures for inverter-driven motor systems, it is important to have knowledge of how the motor rotating field is generated and how the phase currents in the stator may be affected by adverse load conditions. Some motor condition monitoring systems using motor current signature analysis (MCSA) methods are based on the principle that all of the phase current signals are balanced under normal operating conditions.

In any three-phase motor system, the stator currents can be represented as $i_{S1}(t), i_{S2}(t), i_{S3}(t)$. The stator windings are positioned $\frac{2\pi}{3}$ radians or 120° apart and because each of the 3-phase supply currents is similarly displaced in time as given graphically in Figure 3-20:

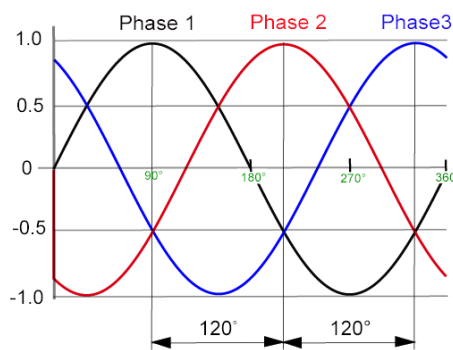


Figure 3-20 - 3-phase supply waveform [27]

then:

$$i_{S1}(t) + i_{S2}(t) + i_{S3}(t) = 0 \quad (3-10) [28]$$

is valid at any instance (the currents are balanced). Equations for the line-to-neutral voltages of the stator circuit are:

$$\begin{aligned} R_S i_{S1} + \frac{d\psi_{S1}}{dt} &= u_{S1}(t) \\ R_S i_{S2} + \frac{d\psi_{S2}}{dt} &= u_{S2}(t) \\ R_S i_{S3} + \frac{d\psi_{S3}}{dt} &= u_{S3}(t) \end{aligned} \quad (3-11)$$

And this is illustrated in Figure 3-21 below that details the magnetic linkages and voltages of the stator and rotor circuits:

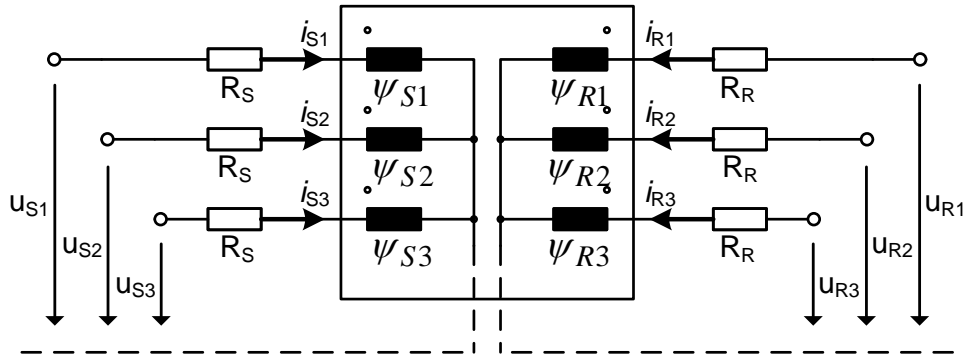


Figure 3-21 - Magnetic Linkages and voltages; Redrawn [28]

From this circuit, it is also found that the line-neutral stator voltages of the symmetrical AC machine are also balanced:

$$u_{S1}(t) + u_{S2}(t) + u_{S3}(t) \equiv 0 \quad (3-12)$$

The same can be said of the rotor winding, where the currents are also balanced, due to the assumed fictitious neutral point:

$$i_{R1}(t) + i_{R2}(t) + i_{R3}(t) \equiv 0 \quad (3-13)$$

The voltage equations for the rotor circuit are:

$$\begin{aligned} R_R i_{R1} + \frac{d\psi_{R1}}{dt} &= u_{R1}(t) \\ R_R i_{R2} + \frac{d\psi_{R2}}{dt} &= u_{R2}(t) \\ R_R i_{R3} + \frac{d\psi_{R3}}{dt} &= u_{R3}(t) \end{aligned} \quad (3-14)$$

From the above equations, it was proven that for a symmetrical three-phase winding fed by a set of symmetrical three-phase currents, the electrical machine components are balanced. Therefore, faults in the electrical circuit of the AC motor that distort the symmetry of the stator or rotor windings will cause disturbances in the motor operation and the analysis of such disturbances forms part of the condition monitoring of electrical machines.

The next chapter will cover the design and implementation of the experimental test rig in open loop configuration.

Chapter 4

Design and practical implementation of the experimental test rig

One of the key research contributions was to produce a test rig that can be used for simulating load conditions on an AC motor for the purposes of advancing research into motor diagnostics using the motor as a transducer. The test rig may also be used for other motor measurement tasks in the future. An important part of the test rig control system was to provide a reliable, easy-to-use rig that utilised the very latest in automation equipment available in the marketplace.

All aspects of the design, specification and operation of the gearbox test rig at the University of Huddersfield are covered. The mechanical control elements of the test rig will be considered first, followed by how the test rig is to operate. This will then lead onto how the design of the electrical control system was implemented to fulfil the operation and design criteria of the test rig according to the users requirements. DC motor principles for the type of motor used on this test rig will be covered at the end of this section.

4.1 Mechanical Test Rig Design

The mechanical design of the test rig had been undertaken by the University of Huddersfield engineering department and was fully completed prior to Optima Control Solutions involvement. At this stage, there was no electrical control system present to operate the rig.

The mechanical layout of the test rig is shown in Figure 4-1:

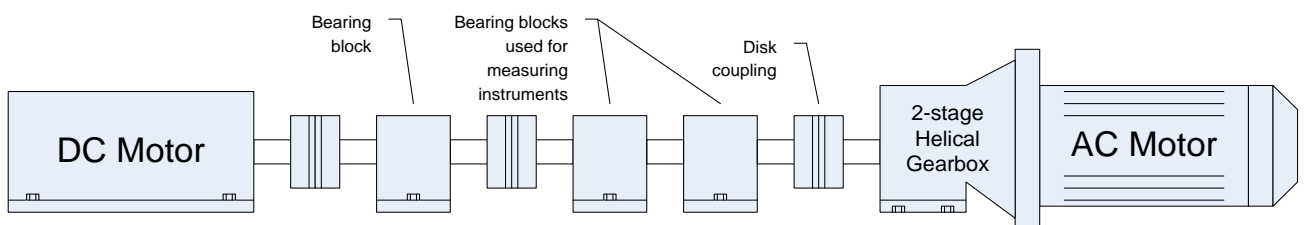


Figure 4-1 - Block diagram of test rig design

The AC motor will apply electromotive force to the test rig and be driven from an AC inverter. Directly coupled to the AC motor will be the two-stage gearbox that will have faults created in it for the purposes of detecting them via the AC motor current signals. Bearing stages in the middle of this test rig provide support for the line shaft from the coupling after the gearbox to the final coupling at the DC motor end. A DC motor will be used to vary the load on the AC Motor/Gearbox combination allowing varying loads to be applied on a faulty gear set for simulation of different load conditions.

The actual test rig is detailed in Figure 4-2:

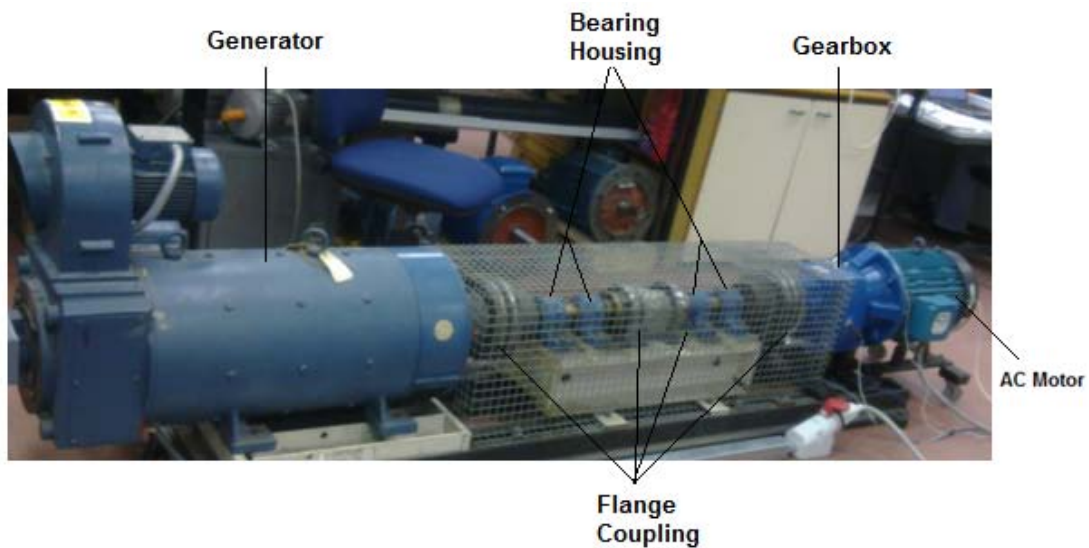


Figure 4-2 - Actual Gearbox Test Rig

Details of the test rig components are given thus:

AC Motor

Manufacturer: Invensys, Brook Crompton

Motor model: DA160MJ G 298659

Full load torque: 71.5 Nm Rotor inertia (J): 0.068 kgm 2

Rating plate data:

Power = 11 kW Voltage = 380 – 415 V Speed = 1470 rpm (for Y connection)

Power = 12.7 kW Voltage = 440 – 480 V Speed = 1760 rpm (for Δ connection)

Cos Θ = 0.88 Phase: 3 T.Rise: 80 Class: F IP: 55 IC 411 YR 02

The supply voltage at the University of Huddersfield is 415VAC 3-phase measured line-to-line. Reading from the motor nameplate data, the motor power will be 11kW with a no-load motor base speed of 1470RPM.

Motor Gearbox

Radicon IT TYPE: M07223.6BMCELA11.A ORDER No. 1008043

INPUT KW: 11KW DB OIL GRADE: 6E ASSEMBLY POSITION: 1A

The gearbox is of a planetary type, consisting of two gear sets (or stages). The first – or primary – set has two gears and the final set consists of two gears as well. The specification of the two sets is shown in the Table 4-1.

DC Motor (Generator)

The information from the DC motor rating plate is given below:

Size: SD 200XLC	No: G63801N	Power: 85 kW	Speed: 1750 rpm
-----------------	-------------	--------------	-----------------

Duty type: S1	Ins Class: F	Armature V: 460, A: 200	Enclosure: IP22
---------------	--------------	-------------------------	-----------------

Excitation V: 360V, I: 4.7A	Brgs DE. 6314 N.D.E.6309	Mass: 48.2Kg
-----------------------------	--------------------------	--------------

The unit is a shunt-wound DC motor, having a field supply that is completely separate from the armature circuit. There is no tachogenerator fitted to this motor. At the rear of the motor is a forced-ventilation cooling fan with a 415VAC supply rating of 4.2A.

Table 4-1 - Gearbox Specification

		Primary set PG0740.8/M07E	Final set M07-24.5B-C
Reduction ratio		0.810344828	4.538461538
No. of teeth		58/47	13/59
Contact ratio		1.45	1.469
Overlap ratio		2.89	1.289
Helix angle		27	13
Circular pitch at reference diameter	Normal	3.927	6.283
	Transverse	4.407	6.448
Circular pitch at running diameter	Normal	3.942	6.292
	Transverse	4.428	6.485
Circular pitch at base circle diameter	Normal	3.69	5.904
	Transverse	4.08	6.041

4.2 Test rig specification

In order that the test rig will meet the operational requirements of the user, it is important at the outset to agree how the unit is to operate, and with what equipment. This is best achieved by creating a project specification document that can be reviewed by both end user and designer, where any changes to the design can be made before the design process begins.

This section of the chapter will detail this initial specification and design process, with the next section covering the actual design itself in detail. The following control system elements were within the scope of the test rig design:

- Generate a project specification, review and discuss, sign-off
- Design the electrical control system
- Produce electrical circuit diagrams
- Configure and calibrate the AC drive system
- Build the enclosure
- Provide electrical installation of the enclosure to site equipment
- Perform a full functional test of both hardware and software elements on-site

An outline of the major sections within the project specification document are given here under separate headings:

General operation requirements

The key operational elements required of the test rig are:

- Test rig must operate off a standard 3-phase 415VAC supply; 32A rated

-
- Must be able to drive a 4-pole asynchronous AC motor, of rating 415VAC at 11kW continuously
 - Must be capable of dissipating the power generated by the test rig DC motor under full-load conditions
 - AC motor speed to be fully adjustable from 0Hz to 50Hz
 - DC motor load fully adjustable from 0% to 100%
 - Display of DC motor Field and Armature current must be provided
 - Display of AC motor speed must be provided
 - All operator controls to be conveniently mounted on the front of the enclosure

Control equipment

Requirements for the control equipment to be used in the test rig control system are:

- Must use the latest industry-standard equipment
- Equipment used must be readily available (no custom-designed equipment)
- All equipment must meet the latest CE and Low-voltage directives
- The unit must conform to relevant EMC requirements for use in the desired operating environment

The preference of equipment manufacturers to be installed in the University (whether fitted to this test rig or not) is:

Variable speed drive equipment:	Eurotherm/Parker SSD Drives
PLC:	Siemens
General control equipment:	Allen-Bradley
Circuit breakers / Protection:	Allen-Bradley

Safety circuit

For any installation that is controlling industrial equipment, the relevant standards for safety-related parts of the control system must be adhered to. For this control system, the safety standard is EN954-1. Because the test rig is completely guarded and there is no risk of operator injury during operation (no access to moving parts) a simple category 0 stop system will be employed. This is a coast-to-stop system and will be provided by the panel isolator that will completely remove all power from the equipment when switched off.

4.3 Electrical Drive Specification

The design of the electrical control system was contracted-out to Optima Control Solutions Limited after consultation with the relevant parties at the University.

In order that the control system design meets the customers requirements, it is important to manage the project correctly, whilst ensuring that all operating criteria are met. Thus, the project specification provides the template for the control system design. If any changes are made to the design as the project progresses, then the specification document will be modified for approval by the end user.

When designing any control system, the following factors must be taken into account when specifying the equipment to use:

- Suitability for task (power requirements, functionality, compatibility with other equipment)
- Cost versus performance balance (do not over-specify equipment)
- Manufacturer approved by end user
- Meets all requirements of EMC, and low-voltage directives and CE marked if appropriate
- Meets the project budget requirements

In order to specify the equipment correctly, a more detailed analysis of the operation required of the test rig is necessary.

The experimental test rig is to be an open loop system, utilising Start / Stop pushbuttons to control the inverter operation, with the system finding its own equilibrium state (see Figure 4-3). For the AC motor, the desired operating equilibrium may be the motor speed or angular position. When the mechanical load or supply voltage / frequency are changed, then the motor will find a new equilibrium state with different speed. The actual equilibrium state can be changed by forcing a change in the parameters over which the operator has control. The major elements of this system are given in the figure below:

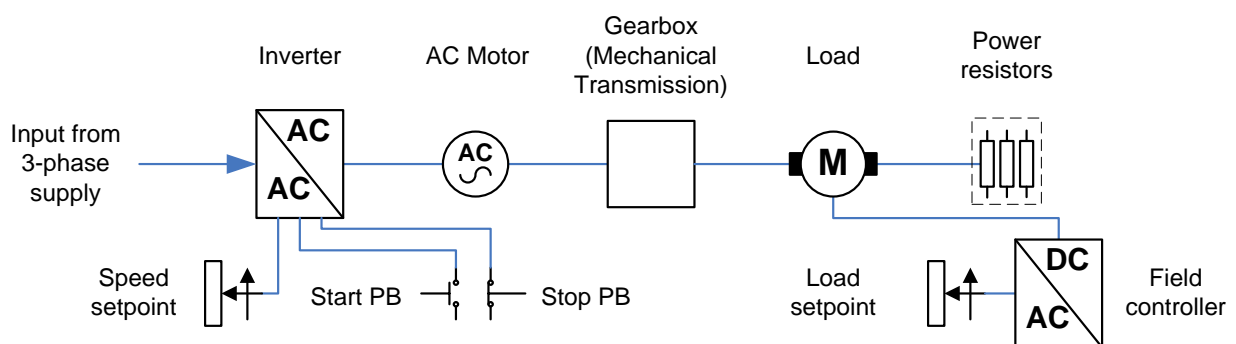


Figure 4-3 - Block diagram of the experimental test rig

The input signal from three-phase 415 VAC supply is sent to the inverter with a speed set point. This commands the AC squirrel-cage motor connected to the mechanical load (DC motor) through a gearbox (mechanical transmission). The DC motor is controlled by a DC drive connected to the field supply terminals and the energy generated from the DC motor is dumped to a resistor bank and dissipated as heat. A load setpoint will be fed into the DC drive for full adjustment of the mechanical load.

Inverter

As the equipment to be used must be to the current industry standard, an AC drive controller that utilises flux-vector PWM (Pulse Width Modulated) control will be specified. This then makes the test rig shown in Figure 4-3 a closed loop system, where the feedback loop comes from within the flux vector PWM drive itself (instead of an external encoder). For this reason there is a trend to refer to this as "Sensorless Vector" drive which operates as follows:

- A mathematical "model" of the motor operating parameters is created and stored by the drive microprocessor
- The microprocessor monitors the output current as the motor operates
- Actual motor current is compared to the model and the microprocessor determines from experience what the different current effects mean in terms of the motor performance

-
- Microprocessor executes the necessary error corrections (like the closed loop vector drive)

The only drawback is that the ability of the microprocessor to detect the subtle changes in electromagnetic field becomes more difficult as the motor gets slower. So the open loop vector drive is not reliable enough to use on cranes and hoists at zero speed, but can be used on the likes of this test rig where high performance at low speeds is not required. In any case, the motor to be used is not a force-ventilated type so cannot be run for long periods of time at low speeds otherwise the motor will overheat.

The drive must accept the following inputs:

- Speed setpoint
- Start signal
- Stop signal

The drive must have the following outputs:

- Scaled motor speed
- Scaled motor torque
- Scaled motor current

DC controller

The field controller (actually a DC Drive) will be responsible for maintaining a set field current to the DC motor from two phases of the incoming 3-phase supply. It must be capable of providing the required maximum motor field current continuously and must regulate the current accurately, to ensure a stable load setpoint on the test rig.

The controller must accept the following inputs:

- Load setpoint

The controller must have the following outputs:

- Scaled current output

Power Resistors

The power resistors must be capable of dissipating the energy output by the test rig on a continuous basis without overheating or degrading. Whilst it was more desirable to have the DC motor energy being regenerated to the mains supply, cost restrictions meant that the resistor bank was the only realistic option.

4.4 Test Rig Panel Equipment

Now the test rig basic design has been finalised, each of the major test rig control elements specified for this test rig will now be detailed, along with a description of their equipment operation. The theoretical aspects of AC inverter-driven motor systems has been covered in detail under section 3.

Inverter - Parker 690+ AC

The model of inverter chosen was a Parker 690+ AC Vector Drive. A 11kW drive was chosen for this application, as the test rig will not be operated with a motor greater than this rating in future. This model of drive was chosen due to the future performance upgrades that it offers and the ease to which these can be added-on at a later date. Also, the drive is fitted as standard with a host of programmable control blocks that can be used to perform a variety of tasks that may be useful in future test rig operations. Some of these blocks include:

-
- Two independent PID blocks
 - S-Ramp generator
 - Speed preset blocks
 - Logic blocks including AND, OR, NOT and timer functions

The 690+ series is a single range of AC drives designed to meet the needs of all variable speed applications from simple single motor speed control through to the most complicated integrated multi drive systems. At the heart of the 690+ is a highly advanced, 32-bit microprocessor-based motor control algorithm, to which can be added a host of control options that allow the drive to be tailored to meet exacting application requirements. These include options such as:

- Closed-loop encoder feedback
- Phase-lock control
- Industrial Fieldbus networks
- HVAC (Heating, Ventilation And Control for building management) systems

Three phase (380-500V) ratings are available from 0.37 to 355kW and single phase ratings (220-240V) from 0.37 to 2.2kW.

The drive will be programmed to provide the following control functions that will be operated on a keypad fitted to the front of the control panel door:

- Drive start
- Drive stop
- Speed setpoint adjustment from 0% to 100% speed (0 to 50Hz).

Once installed, the inverter will be tuned to match the AC motor it is driving and performance optimised for the test rig.

FULL TECHNICAL SPECIFICATION:

Power Supply – 220-240VAC ($\pm 10\%$) single or three phase; 380- 460VAC ($\pm 10\%$) three phase; (500V option available); Ambient – Constant torque ratings – 0-45°C (40°C with IP40 cover); Quadratic torque ratings – 0-40°C (35°C with IP40 cover) Derate from above temperatures to 50°C. Max Altitude up to 1000m ASL, derate 1% per 100m above 1000m; Overload – Constant torque ratings – 150% for 60 seconds, 180% for 1 second; Quadratic torque ratings – 115% for 10 seconds; Output Frequency – 0-480Hz Switching Frequency – Frame B 3,6 or 9kHz; Frame C, D, E and F 3 or 6kHz (all with audibly silent switching pattern) Dynamic Braking – Frame B and C standard; Frame D,E and F optional

The function diagram for the 690+ AC Vector drive as used in this test rig is given in Figure 4-4:

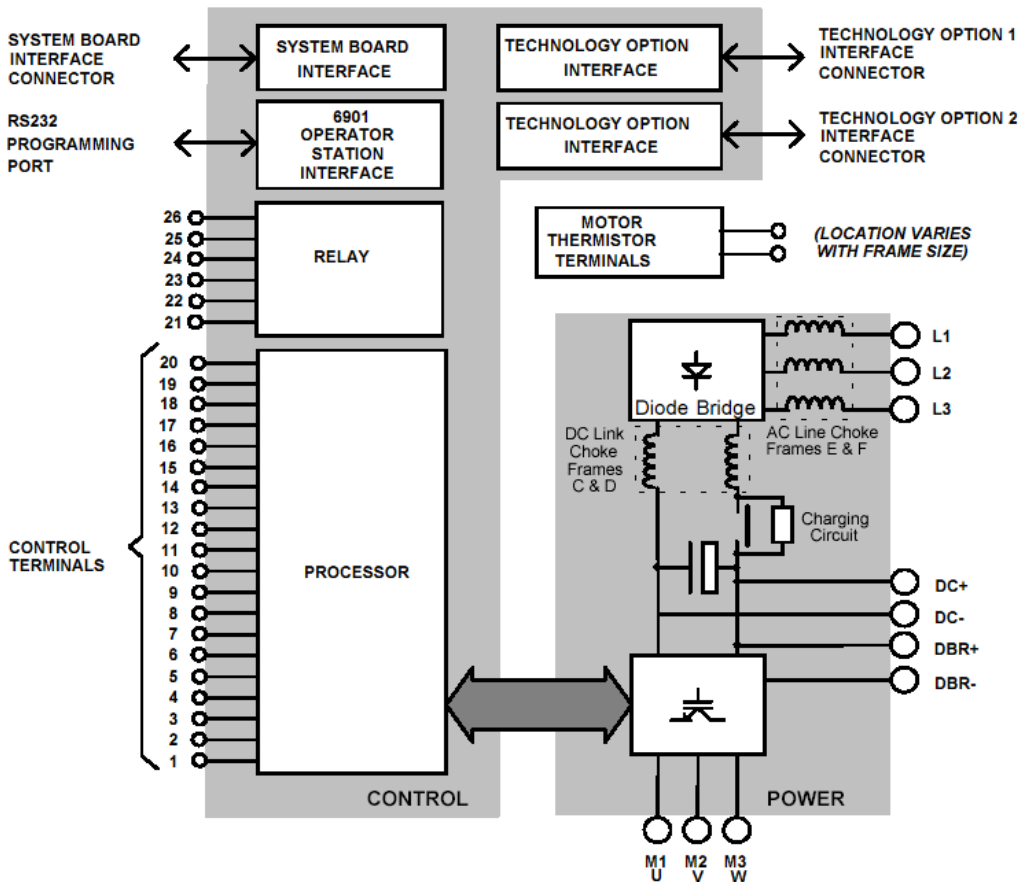


Figure 4-4 - Functional Block Diagram – 690+ Inverter, Frame C [32]

The drive processor uses an advanced 32-bit microprocessor-based motor control model and the operates as a 6-pulse PWM unit with a 3kHz switching frequency as standard. The features to be used on this test rig are briefly summarised below:

Control Terminals

These are used for supplying both analogue and digital signals to the processor. Digital signals will be used to indicate the status of the DC motor cooling fan and stop the AC drive should this develop a fault.

Relay Terminals

Three volt-free relay contacts are available to control auxiliary systems (2A maximum current rating). One output will be used to control the DC motor cooling fan whilst the AC drive is operating.

6901 Operator Station Interface

This facilitates connection of an external alpha-numeric display to the drive for operator control, engineer configuration and diagnostics.

Technology option

The technology option can be used to fit an optional motor encoder feedback module to the drive in order to facilitate operation in closed-loop vector mode. This may be required, in order to improve the performance of the test rig.

Operating modes of the inverter are as follows:

Open-loop (volts/frequency) control

The simple volts/frequency control mode of the 690+ drive takes the form of a speed reference command from an external source and varies both voltage and frequency applied to the motor. Additionally, the 690+ drive has a “slip compensation” block which helps to improve the speed control under varying load conditions by altering the frequency reference when the load changes to keep the actual motor speed close to the desired speed.

To summarise, this mode is ideal for basic motor speed control, or multiple motors driven in parallel.

Sensorless flux-vector control

High starting torque and tight speed regulation is provided by a sophisticated MRAS (Model Reference Adaptive System) motor control strategy. MRAS provides accurate speed simulation (without the need for any speed measuring transducer) by continually modelling the motor. There exist a number of different model reference adaptive control techniques such as parallel model, series model, direct model and indirect model.

To summarise, this mode provides for better speed regulation than Volts/frequency but without the additional expense of a motor feedback device.

Closed-loop vector control

Full closed-loop flux vector performance can be achieved with the 690+ drive by simply adding an encoder feedback ‘technology box’. This mode provides 100% continuous full load standstill torque plus a highly dynamic speed loop (up to 45 Hz bandwidth) that is more than sufficient for the most demanding of applications.

Inverter drive filter

For EMC (Electro-Magnetic Compatibility) purposes under EU regulation EN 61800-3, a filter is required for the inverter drive. Under EMC regulations, there are two emissions classes for electrical equipment, depending on the environment they are operating in. The environment for this equipment is non-residential so is class B (class A is residential).

The purpose of the filter is to protect other equipment operating in the same environment against potentially harmful conducted and radiated emissions. When fitted with this filter, the Inverter drive frame C (11kW) complies with:

- Conducted emissions for all environments (domestic and industrial)
- Radiated emissions for the “First Environment Restricted Distribution”

From the regulations, “First Environment Restricted Distribution” defines a mode of sales distribution in which the manufacturer (Parker SSD in this case) restricts the supply of equipment to suppliers, customers or users who separately or jointly have technical competence in the EMC requirements of the application of drives. This ensures that the equipment is put into service by competent personnel or companies and incorporated into the operating environment correctly. The “First Environment” is a location that can include domestic premises. It also includes establishments directly connected without intermediate transformer to a low-voltage power supply network which supplies buildings used for domestic purposes. The test lab at the University of Huddersfield shares its supply transformer with other rooms within the Technology campus and is therefore a “First Environment” location. The

majority of these rooms contain sensitive computing and instrumentation equipment so the emissions regulations are extremely important in ensuring that operation of the test rig does not unduly affect other users of equipment within the facility.

Compliance with EMC is not just about choosing the correct equipment – good design practise is essential. For example, in the design of the test rig, it will be stipulated that the AC motor must be wired in screened cable, be terminated using the correct EMC glands at the motor and the cable screen run uninterrupted back to the inverter. This essentially provides a “Faraday Cage” where the motor case, cable shield and drive cabinet all protect against harmful radiated emissions from the AC inverter drive.

Inside the control cabinet, low-voltage signal cables will be routed away from high-energy voltage cables and sensitive components separated from those that provide a source of radiated emissions.

DC Drive – Sprint 3200i DC 2Q

On the test rig used for measurements, the DC motor that provides the load to the AC motor will not be controlled from a DC drive. Instead, the motor will convert the energy generated by the loading to heat in a resistor bank. The field current of the DC motor will be controlled by a simple DC drive connected to two supply phases and configured to supply a current that will be pre-set by a potentiometer. This will allow the test rig to provide from 0 to 100% load on the AC motor. The circuit will be as shown in Figure 4-5:

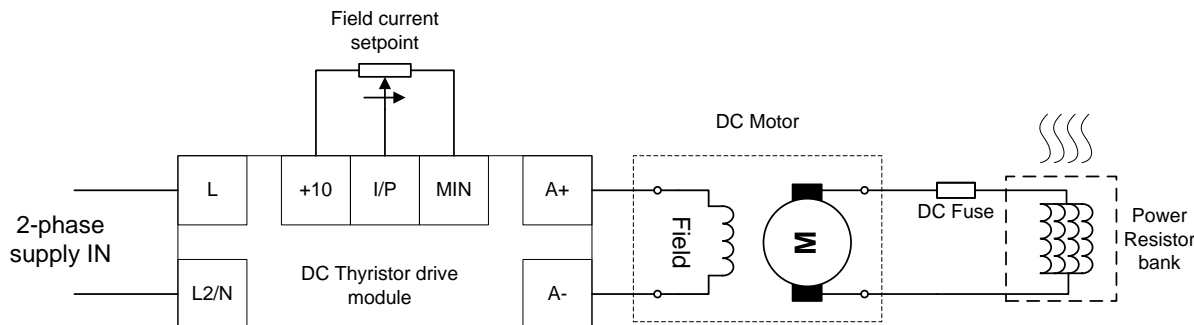


Figure 4-5 - DC load motor diagram on the test rig

The DC motor field controller is a DC thyristor drive that uses closed-loop control of the output current and feedback voltage to give precise control of the motor field. The drive is operated in a current-controller mode (conventionally if the drive was controlling a DC motor armature, it would be in speed control mode) with the demand signal being supplied from a potentiometer that will be mounted on the control panel front.

Because a DC motor exhibits a near-linear relationship between field current and armature current when used in this manner, if the motor field current is varied, then the motor load onto the AC motor will vary in proportion to this. The principles of the DC shunt machine will be covered in more detail later in this section.

This controller was chosen because it provides the closest field current match at 8A (the test rig motor requires 4.7A) so is cost-effective in terms of the “amperes rating : pounds cost” ratio. It is also a proven-unit and commonly used on low-cost DC drive systems in industry.

The controller also has an analogue output that can be used to indicate how much current the unit is outputting to the DC motor field. This is a buffered signal so is safe to connect to an external meter. In this case, a 0-10VDC meter will be scaled to read from 0 to 5A on the test rig panel to indicate to the operator how much field current they have chosen.

Once installed, the unit will be calibrated to match the field current required.

DC Motor Power Resistors

The size of the DC motor resistor bank was matched to that of the DC motor, should this motor/resistor bank combination be used on a test rig of a higher power rating.

The current rating of the resistor bank is 200A at 250VDC. This voltage rating is adequate for this test rig, as the AC motor is running at 1750RPM and the gearbox ratio is 3.675:1 approx., giving a final drive maximum speed of: 476RPM. As the DC motor output voltage is proportional to speed, at

maximum field voltage, the output voltage at 476RPM will be: $\left(\frac{476}{1750} \times 470\right) = 127 \text{ V.}$

A diagram courtesy of Electrohm Limited showing a view of the resistor bank with covers removed is shown in Figure 4-6:

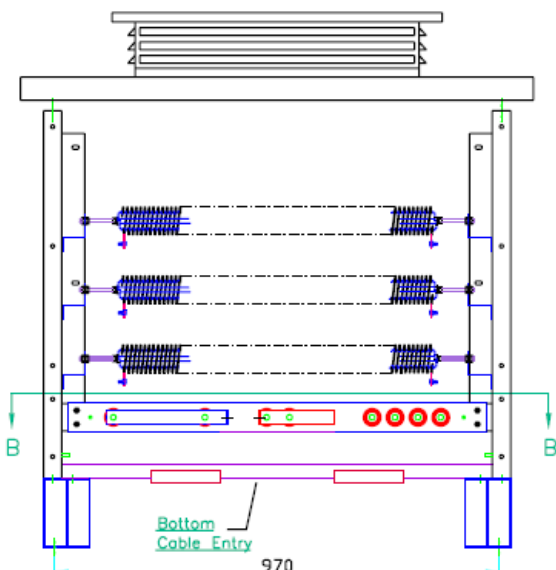
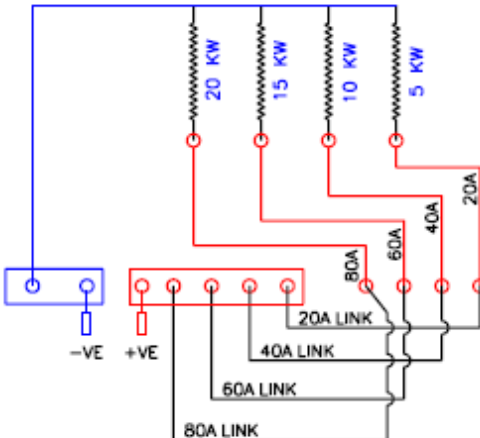


Figure 4-6 - Resistor bank view [34]

The schematic circuit given in Figure 4-7, courtesy of Electrohm Limited shows the connections made to each resistor section. For this application, all resistor sections will be left in-circuit.



Circuit Diagram

250 VDC

200 Amps

Figure 4-7 - Resistor bank internal wiring schematic [34]

Miniature circuit breaker – Inverter protection

It is important to protect the input stage of the drive against faults or surges in the power supply lines. This can be done by the use of fuses, or more commonly now in the form of 3-pole circuit breakers due to their low cost and ease of resetting. The unit chosen for this was an Allen-Bradley 3-pole 32A D-type, model 1492-SP. In case of short circuit or thermal overload, these devices are designed to protect equipment, systems and cables by quick disconnection. The Allen-Bradley units allow 10 to 20 times less let-through energy than conventional circuit breakers, resulting in less wire heating and minimizing damage to downstream components.

Other features of the 1492 range are:

- True IP2X finger safe design
- A positively trip-free mechanism (breaker operation cannot be defeated by holding the handle in the ON position)
- Time delay (D characteristic) for high inrush currents during inductive start-ups such as transformers and power supplies

Power Supplies: Switched Mode

Manufacturer: Allen-Bradley

The 1606-XLP Compact Power Supply was chosen due to its compact size as panel space is at a premium in the test rig enclosure. These devices are equipped with many of the same features and certifications as the XL devices, and support low-power applications. This power supply provides a cost-effective way to save space while delivering safe and reliable power.

- Rated outputs between 15...100 W (0.6...4.2 A at 24V DC)
- Multiple output voltages available
- Multiple single and three-phase inputs available for global applications
- Smaller, cost-effective solution for low power applications

Allen Bradley 140M-C2E-B63 Starter Motor Protector:

This is a 3-pole, 575 Volt Max. Motor Protector with an adjustable current range of 4-6.3A. It is used to protect the DC motor cooling fan motor against stalling and overcurrent conditions. There is an auxiliary contact fitted to this device that will stop the test rig from operating should the cooling fan trip. This will protect against damage to the DC motor caused by thermal effects. The specification of this device is detailed below:

- Isolator Module for Motor Protection Circuit Breakers
- Isolates the load for highest safety of equipment and staff
- Prevents unauthorized reconnection of power
- Padlock capability
- Ideal for preventive maintenance / plant shut downs
- Permits testing of circuit breakers and auxiliaries while disconnected

Motor Starter, Allen Bradley 100-C09*10:

This is the motor starter (referred to also as a contactor) used to operate the DC motor 3-phase cooling fan. Features of this unit are:

- AC and DC coil control
- Common accessories with other 100-C contactors
- IP2X finger protection
- Provisions for adding two conductors per terminal
- Meets IEC, CE, UL, and CSA standard requirements

Routeco Transformer

The transformer rating is calculated according to the load requirements of the equipment contained in the control panel. A transformer is required to bring the line-to-line voltage of 415VAC down to 110VAC for use by components such as the 24VDC power supply and DC motor cooling fan contactor. Total rating of the AC components was calculated as shown in Table 4-2:

Table 4-2 - Control transformer sizing

	Qty	Unit current (A)	Total (A)
Motor contactor	1	0.0636	0.0636
Power Supply	1	0.609	0.609
Cubicle Cooling Fans	2	0.32	0.64
Control relay	1	0.0909	0.0909
		Total current	1.4035 A
TX output voltage	110		154.385 VA

A 200VA transformer unit was chosen for this application.

DC Motor armature current transformer

In order to give indication to the operator of the rig how much armature current the DC motor is dissipating into the resistor bank, a current transformer will be fitted into one leg of the DC motor armature connections. This will convert the 0 – 200A current into a 0-10VDC signal that can be fed into an indicator on the panel. The specification of the current transformer was chosen so that the range

can be changed by altering jumpers on the unit to give more resolution if the full range of measured current is not used.

TECHNICAL SPECIFICATION:

Manufacturer:	LEM	Type:	DC Current transformer
Part #:	DK200-B10		
Power supply:	24VDC	Output signal:	0 – 10VDC
Jumper range:	Normal -	100A	
	Mid -	150A	
	High -	200A	

The setting was left on HIGH, to utilise the full range of the current transformer and to match the panel meter scaling that will indicate 200A with a 10V supply input . If better resolution is required at a later date, then a new panel meter with a lower scaling will need to be ordered instead.

DC Motor protection

Because the DC motor is acting as a generator, circuit protection in the armature circuit must be provided. This is to protect against severe damage both to the DC motor and potentially personnel working close by should the resistor bank short-circuit or develop a fault.

The type of fuse chosen for this purpose is a high-speed semiconductor fuse that has a fast-acting rupture time. These are commonly used in DC drive applications to protect the semiconductor devices in the drive, but their use here will ensure a fast disconnection of fault current with a potential clearing current of 22kA at 700V (the clearing current will be much higher for our lower-voltage motor) so we can be sure of safe and reliable fault disconnection.

Type: FWP-200A Description: Fuse link DC 200A

Manufacturer: Cooper Bussmann

Fuse carrier: BH1133

4.5 Test Rig Panel

The finished test rig panel is detailed in this section, along with a full description of the controls and photographs of the finished rig. The schematic diagrams are to be found under Appendix D.

The front of the test rig panel is shown in Figure 4-8, with the control elements indicated:

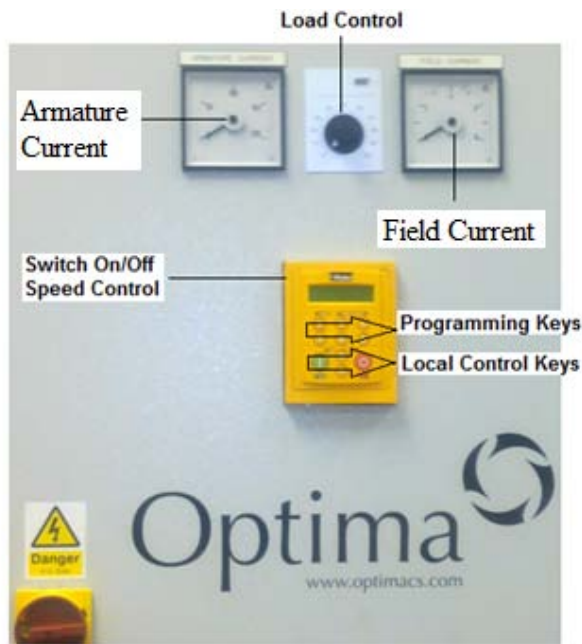


Figure 4-8 - Test rig control panel front

A brief description of the control panel functions is given in Table 4-3 below:

Table 4-3 - Control panel functions

Armature current	Indicates DC motor armature Amperes; Range: 0 to 200A max. This indication is taken from the DC motor current transformer output.
Load control	Used to control DC motor field current from 0% to 100%. This potentiometer is fed directly into the DC Field Controller
Field Current	Indicates DC motor field current; Range: 0 to 5.0A max. This output is fed from the buffered output of the DC field controller
Switch On/Off Speed Control (Local Control Keys)	Pushbuttons control AC Drive Start/Stop Red (Stop); Green (Start) This keypad is connected to the inverter drive by the use of a serial communications lead. The keypad normally resides on the drive front, but an optional remote panel-mount kit was chosen to mount the keypad on the test rig panel front.
Programming keys	These are Used to access AC inverter drive parameters; Under normal operating conditions, the keypad is used to increase or decrease the motor set speed. If desired, an engineer mode can be selected to modify parameters such as speed loop tuning, ramp times, etc.

The internal design of the test rig control cabinet is shown in the Figure 4-9.

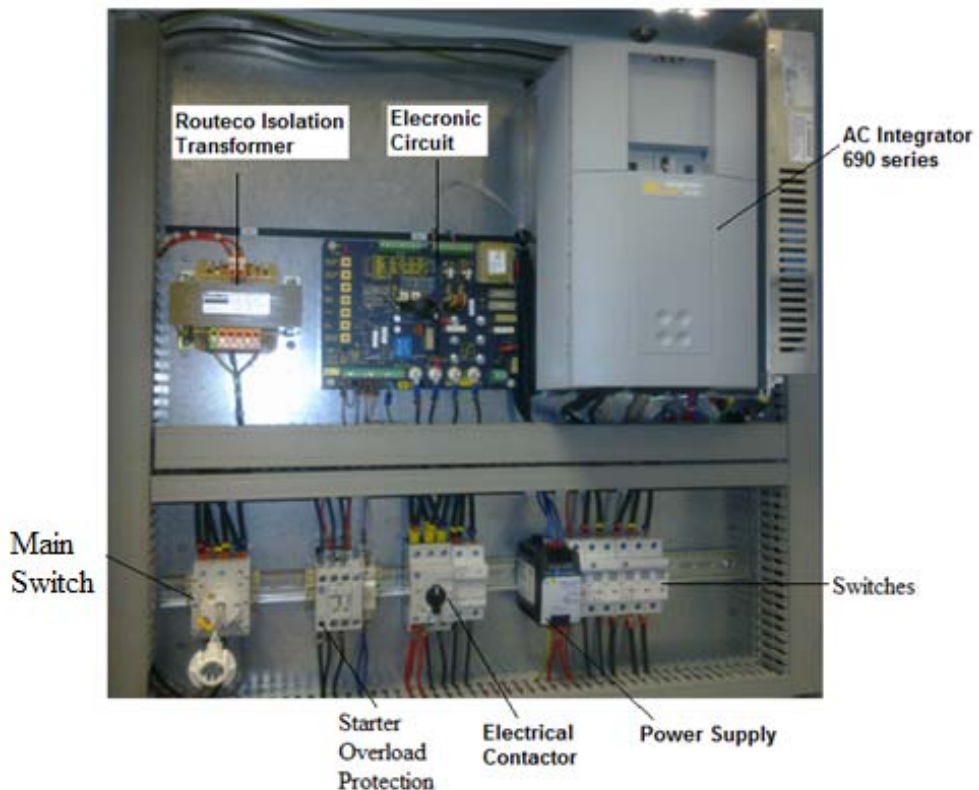


Figure 4-9 - Test rig control panel interior

All of the elements described previously are shown above. Room has been deliberately left to allow for other components to be installed in future. This is standard practise when building control system panels and typically, 20% free space should be left in any control panel for future use.

4.6 External Test Rig Equipment

This section describes in greater detail, any existing equipment that is outside of the scope of the test rig design (excluding the AC motor that was detailed in Chapter 3).

Mechanical Transmission – Gearbox Set

The need for combined motor gearboxes on an AC machines has been driven by machinery designers and end users who require a convenient, compact design that comes as a complete package without the need for additional mechanical components between motor and gearbox. The requirement to drive low-speed loads that require a high-torque has also been a factor, because at any given power, torque in an AC motor is inversely proportional to speed. High-torque, low-speed motors exist, but these are usually confined to DC machines as their AC equivalents run at a much lower power factor and generate much more heat than the high-speed motors. It is now considered more efficient to use step-down gearboxes for driving lower-speed loads at higher torque values.

Most motors now come with a motor-gearbox combination as an option that saves having to couple the motor up to a gearbox supplied separately. The motor is usually flange-mounted and mates directly to the gearbox front flange plate. One of the industry leaders in motor-gearbox combinations is SEW Eurodrive.

A cut-away view of a helical motor gearbox combination – similar to the type used on the test rig – is shown in Figure 4-10:



Figure 4-10 - View of Helical Geared motor [35]

Gearbox efficiencies

Most motor gearboxes can achieve up to 98% efficiency, with this increasing as the rated power output of the unit increases. Because of this, the motor gearbox can usually be kept at the desired operating temperature by natural convection cooling.

If we wished to size a motor up to drive a gearbox load, then account of service factors and gearbox efficiency should be included. The service factor for the gearbox used on the test rig is 1.18 according to the David Brown catalogue (see page extract below):

N2 R/MIN	i	M2 Nm	Fm	N	Unit Designation		Kg	
Output Speed	Ratio	Output Torque	Service Factor	Overhung Load	Column Entry 1 Through 20 Spaces to be filled when entering order		Weight	Motor Size
392	3.68	258	1.18	7040	M 0 7 2 2 3 . 6 _ M _ _ _ _ 1 1 . A _ _		128	160M

Figure 4-11 - Service factor table from David Brown Catalogue (page 65) [36]

If we wished to size a motor up for driving a load rated at 1000W using a helical in-line gearbox, we assume 98% efficiency for the gearbox as manufacturers rarely state their gearbox efficiencies (the Siemens web-site does not declare any motor gearbox efficiencies for it's equipment). P_m = Motor power required; P_l = Load power required;

$$P_m = P_l \cdot \text{eff} = 1000 \cdot \left(\frac{1}{0.98} \right) = 1020\text{W} \quad (4-1)$$

As a rule-of-thumb, motors should be rated at 10% over the input power of the gearbox to allow for factors such as site conditions and mechanical wear. Therefore, 1020W motor power then becomes: 1122W.

We can now calculate the total power required to drive the load by multiplying this figure by the service factor provided by the gearbox manufacturer, giving:

$$P_m = 1122 \cdot 1.4 = 1570\text{W} \quad (4-2)$$

By taking into account all of the above factors, the designer can be assured that any expected transient loads to the gearbox are allowed for and that the motor will adequately drive the load for the duration of the gearbox's intended service life. Other service factors can apply for different load types and these are readily available.

Motor output torque and inertia

As torque is inversely proportional to speed, the torque requirement of the motor reflected back through the gearbox is determined by the gearbox ratio. The following equation shows this:

$$T_m = T_I \left(\frac{N_I}{N_m} \right) \quad (4-3)$$

Where: T_m = Motor torque arising mechanically (Nm); T_I = Load torque; N_I = Load Speed; N_m = Motor Speed.

For example, if a load required 563Nm of torque and the input to output speed ratio was 1456:182RPM (assume that the driving motor is a 415VAC 4-pole motor with base speed of 1456RPM driving the load through an 8:1 ratio gearbox), the required motor torque would be:

$$T_m = 563 \left(\frac{182}{1456} \right) = 70.37 \text{Nm} \quad (4-4)$$

Because the speed ratio is fixed, any losses due to friction or otherwise will result in a loss of final output torque at the gearbox shaft. If the gearbox efficiency is taken into account, then equation 4-3 becomes:

$$T_m = \left(\frac{T_I}{\eta_g} \right) \bullet \left(\frac{N_I}{N_m} \right) \quad (4-5)$$

Where: η_g = gearbox per unit efficiency

For acceleration and deceleration, the inertia of the system needs to be considered. The inertia of the load is reflected back to the motor and determined by the gearbox input and output speeds: J_{lr} = Load inertia referred to motor; J_l = Load inertia;

$$J_{lr} = J_l \left(\frac{N_I}{N_m} \right)^2 \quad (4-6)$$

DC Shunt Motor

The DC shunt motor will be acting as a generator in this application. To understand how the motor is to operate in this test rig, it is important to have a knowledge of how the machine operates and what the expected behaviour of the DC motor is likely to be.

DC motors are amongst the earliest of motor types. Their main advantage is to be able to be battery-powered and run at a variable speed easily by simply varying the DC supply voltage to the motor armature. The main disadvantage with DC machines is the need to have a commutator in order to generate current within the rotor windings. The main period of DC use was when supplies were predominantly DC, but since then their use has become the first choice in railway traction applications, on-board ships and for battery-powered vehicles.

As with an AC motor, the DC motor comprises stator and rotor parts. Unlike an AC motor, however the DC shunt-type motor is made up of two distinctly separate electrical circuits. The stator windings (referred to as the Field) provide the magnetising current for the motor. These field windings generate lines of magnetic flux that flow around the blue shaded area of Figure 4-12 – the stator. Where there is a small air gap between the armature and stator, the magnetic field remains as strong as it is through the field core and the lines of magnetic flux cut through the armature windings. The field circuit is low-

current with many coil turns generating the magnetic field and the field current only increases slightly with a large increases in DC motor power.

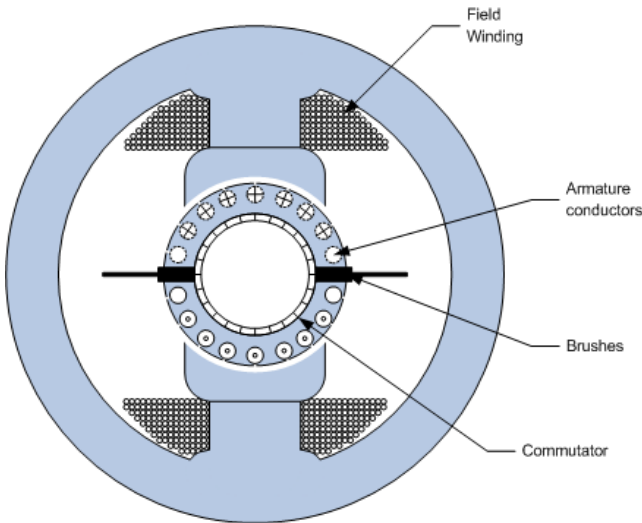


Figure 4-12 - Cut-away view showing DC motor field/armature circuit; Re-drawn by ML [24]

The rotor windings (referred to as the Armature) provide the motoring power of the DC machine and is a high-current circuit. In order to transfer voltage to the rotor, the DC machine relies on slip rings and brushes. The rotor circuit current increases proportionally with motor power – these two parameters being directly related. A circuit diagram for the DC shunt machine is given in Figure 4-13:

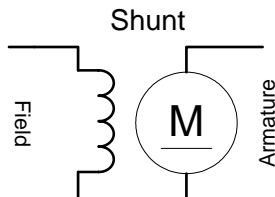


Figure 4-13 - Shunt-type DC motor as used on test rig

In a shunt motor, the field coils are connected in parallel with the armature coil. Compared to other types of DC motor, shunt-wound motors generate the least torque for a given current, but their advantage is that the speed varies very little with load. They will not run away under no-load conditions, but may if the field windings fail. Their use is found in constant-speed applications with varying load, such as:

- Extruders
- Machine line-shafts
- Constant-torque applications where good speed regulation is required

In a control system where the armature voltage is varied to control speed, the speed is almost directly proportional to the voltage applied. A shunt motor also has the advantage of a near-linear torque-to-current curve up to the motor's base speed. Figure 4-14 on the next page illustrates this.

As can be seen from Figure 4-14, motor speed is proportional to armature voltage up until the motor base speed (the speed available at maximum armature voltage). If the motor speed is desired to be increased above base speed then the field must be weakened. This can be done by reducing the field current, whereupon the motor speed will increase linearly (speed is approximately inversely

proportional to field current). Above the base speed point, the armature current and voltage remain at the maximum values. In addition, once above base speed, the torque available from the armature drops off linearly with the increase in speed.

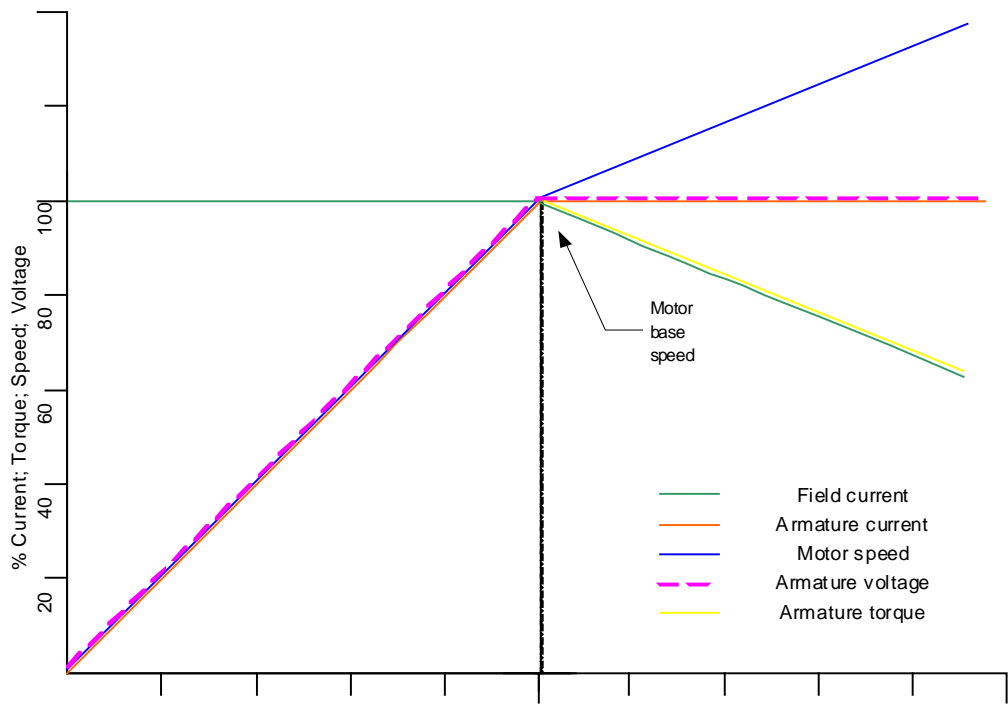


Figure 4-14 - DC Shunt motor speed, torque, voltage relationships

Shunt machine equations:

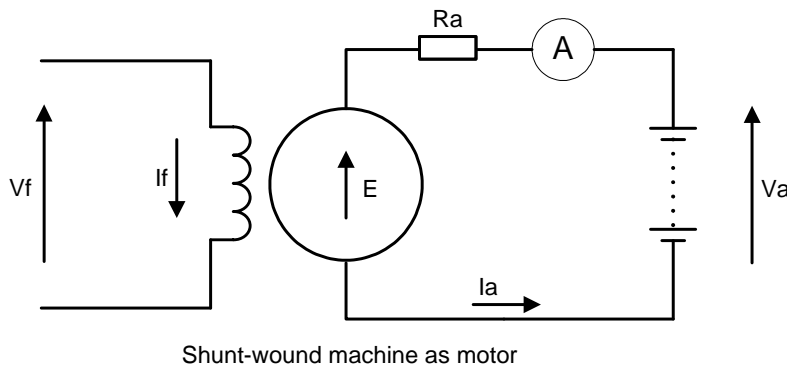


Figure 4-15 - Shunt wound machine circuit

For the shunt machine shown in Figure 4-5, the relationship between armature voltage and current is given by the equation below:

$$V_a = E_a + I_a R_a \quad (4-7)$$

Where: V_a = Applied voltage; E_a = voltage generated by rotation of armature in the field; I_a = armature current; R_a = armature resistance.

The IR part of the equation takes into account the losses in the armature circuit caused by resistance of coils and brush-gear, although this is usually small, so E_a is approximately equal to V_a .

If Equation 4-7 is multiplied by armature current, then a power balance equation for a DC machine is formed:

$$V_a I_a = EI_a + I_a^2 R_a \quad (4-8)$$

Then, the mechanical power $E \bullet I_a$ can be equated to torque times speed product:

$$T_e \bullet \omega_m \text{ gives: } T_e = \left(\frac{E}{\omega_m} \right) \bullet I_a = k_\phi \bullet I_a \quad (4-9)$$

Where: k_ϕ = Flux factor; generated volts per radian/sec. or torque per ampere

Any losses caused by resistance in the armature circuit become more apparent. DC motor I^2R losses can often be significant in larger DC machines and these usually have to be taken into account when calibrating a DC motor drive.

Electromechanical relationship

The armature current which will be drawn from the supply to drive a particular mechanical load, with V and R known can be calculated using the following equation. The smaller value that results from this equation is the one required.

$$I_a = \frac{|V \pm \sqrt{(V^2 - 4 \bullet R \bullet \omega_m \bullet T_m)}|}{2R} \quad (4-10)$$

Where: ω_m = Mechanical angular rotation velocity ($2\pi n$ rad/s); T_m = mechanical torque (Newtons)

When re-arranged, this equation will be useful in translating motor armature current into effective motor torque produced.

A steady-state diagram for a DC machine when operating either as a motor or generator is given in Figure 4-16 below:

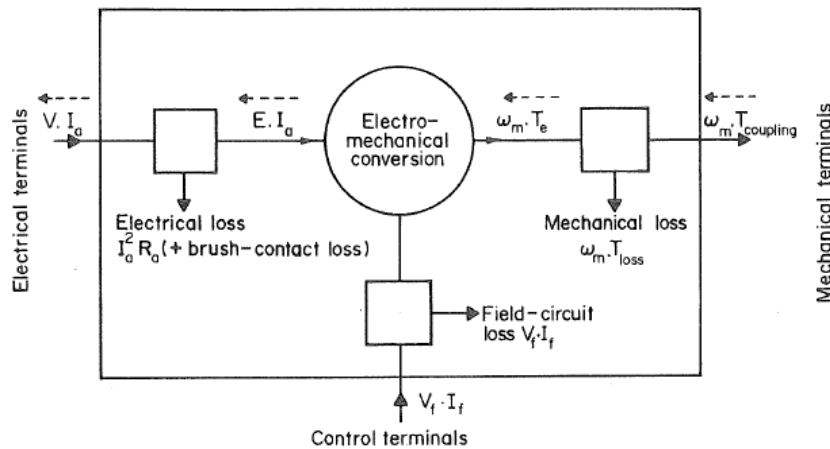


Figure 4-16 - Power flow for Motor / Generator [25]

The equation for a mechanical source $T_e = T_m = T_{coupling} + T_{loss}$, analogous to $E = V + RI$ if the DC machine was motoring. Mechanical losses are replaced by IR losses in the armature circuit if the machine was motoring.

$$\text{Magnetisation characteristic: } k_\phi = f(I_f, I_a) = \left(\frac{Pz_s}{\pi} \right) \bullet \phi_m \approx f(I_f) \quad (4-11)$$

Electromechanical relationship:

$$T_e = k_V \phi \bullet I_a \quad (4-12)$$

So, the torque value, T_e is proportional to the armature current and is linear. If the torque/speed curve of the motor is available, given the known speed ω_m then the corresponding value of T_m can be read off the curve.

The implications of the DC motor behaviour when applied to operation in the test rig must be fully understood. From Figure 4-14, it can be stated that motor armature current is directly proportional to field current and behaves in a near-linear manner up to the field-weakening range. As we will not run into this ‘field-weakened’ range with the test rig in its current configuration (the maximum speed of 1750RPM on the DC motor rating plate will not be exceeded), if the motor field current is varied, then the motor load onto the AC motor will vary in proportion to this.

This test rig DC motor controller will keep the DC motor field in current control, so the voltage will be regulated in order to achieve the required field current. This is a field control method commonly used in high-performance DC drives, because in practise it achieves a constant field flux strength regardless of motor temperature and the resultant change in field resistance. If the field were purely in voltage control mode, then there would be higher flux generated at lower motor temperatures and lower flux at higher temperatures.

Wiring diagrams for the rig are given under Appendix D and commissioning tests used to verify the correct functioning of the test rig to specification are contained in Appendix C for those interested in how the operation of the rig was validated.

The next chapter describes how the open-loop configuration for the test rig is changed to a closed-loop configuration in order to improve the performance of the practical test rig.

Chapter 5

Improvement of experimental test rig performance by changing its configuration

Because test results obtained with the original test rig design did not provide the consistency and repeatability of test criteria required, the test rig was to become fully automated and programmable to satisfy the strict test conditions required. This chapter firstly describes the design modifications and equipment required in order to fully automate the test rig. The equipment used is conveyed next, followed by the commissioning and test of the automation system.

As applications for AC drives have advanced, it is necessary to provide test equipment that is capable of emulating the high-performance end of AC vector drives. Upgrading of the AC inverter drive from Sensorless Vector to full Closed-Loop vector control by the addition of an incremental motor encoder gives the performance upgrade required. The details of this upgrade are described herein.

5.1 Test Rig Modifications – Automation

It is necessary to clearly define what the requirements of the new test rig automation system will be so that there is a good understanding of what system will be installed in the test rig panel. This will allow individuals from various backgrounds (mechanical or electrical) to make useful and informed comments or alterations to the specification.

The modifications required to the test rig are necessary in order to allow a repeatable, deterministic series of tests to be undertaken in order to keep the motor speed and load profile identical through each test run. Each test run will allow faults to be introduced into the mechanical or electrical system whilst keeping the test condition parameters exactly the same from one test run to another.

At present, the test rig relies on a manual speed setpoint and load setting. This cannot be repeated accurately enough from run to run, so automation of the fundamental test rig control signals is required. These signals are:

- AC motor speed setting
- DC motor load setting

For each of the signals above, a step sequence will be generated that can be set to run for any amount of time, with any value for speed or load to be set. The following parameters can be entered for each step:

- Step sequence start value (Speed or load setting; 0% to 100%)
- Step sequence end value (Speed or load setting; 0% to 100%)
- Step ramp time (In seconds – defines the time taken to reach the next speed or load setpoint)
- Step sequence holding time (In seconds – This is the amount of time each sequence step will be held before the next step is run)

For setting-up the test rig and programming the step sequence values, an operator screen will be provided. This will replace the existing start/stop pushbuttons on the drive operating keypad and the load setting potentiometer. However, these will be physically retained on the control panel as the drive keypad in particular allows detailed AC drive diagnostic data to be displayed.

These modifications will allow tests to be run without the continuous supervision by an operator. Figure 5-1 details how the sequence might run in an easy-to-interpret manner.

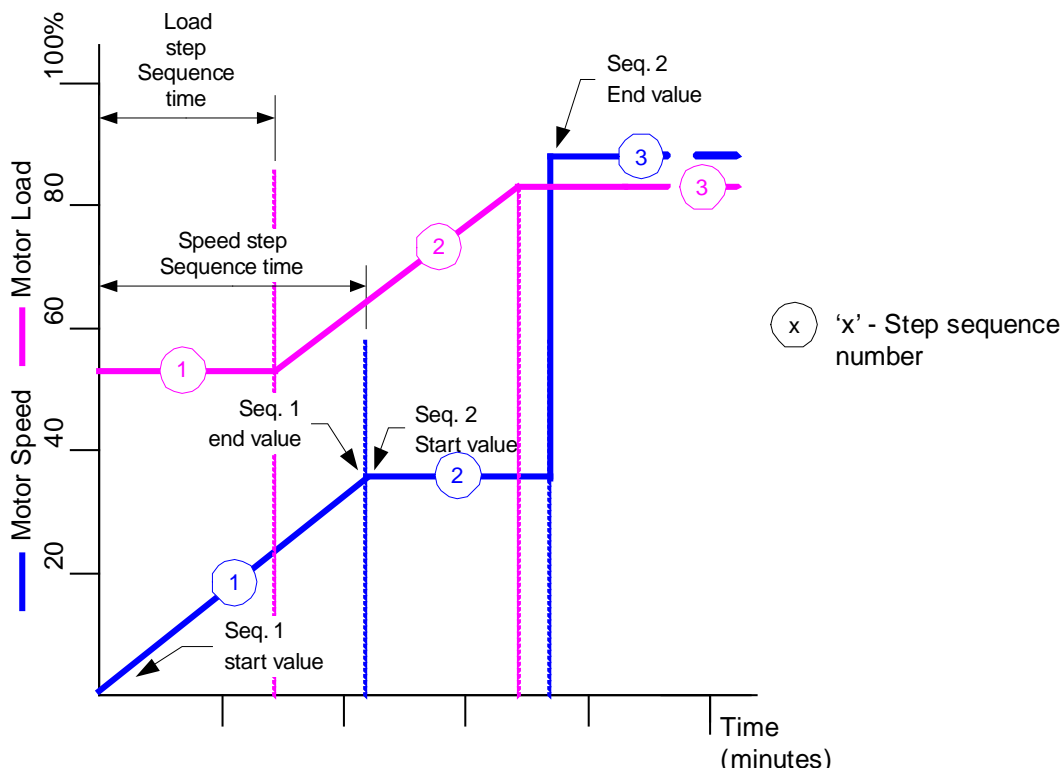


Figure 5-1 - Speed and load step operation

The step sequences for speed and load will be separated. This will allow for independent variation of load or speed. The sequences will initially be developed to either provide 'step' or ramped' changes in load or speed. To demonstrate the operation, some of the conditions in Figure 5-1 are described:

- a) Seq. 1 start value to Seq. 1 end value (in blue) is a ramped speed setpoint change from 0% at the start of **Step 1** of the sequence to just over 30% at the end of the sequence, the duration of the sequence being determined by the 'Speed step Sequence Time' value. Step 2 then takes over and runs at this speed until **Step 3**, whereupon the setpoint is given a step change up to just over 80% speed.
- b) Seq. 1 start value for the load is over 50%, which is maintained for the duration of 'Load Step Sequence Time'. At Step 2, the load setting is ramped to just over 80% setpoint and then at Step 3, this value is maintained.

Possible future developments of the test rig software could include:

- Additional algorithms written to perform curved load or speed demands rather than the straight line ramps shown in the diagram. These can be developed at a later date once the initial test measurements have been started.
- An external input could be used to modulate the load demand on the test rig. This could be a 0-10VDC signal provided by a signal generator to simulate a cyclic load, such as that from a compressor.

5.1.1 Equipment used to automate the test rig - PLC

A PLC was chosen as the most appropriate method of automating the test rig. The PLC operation is described under this section, with a view to proving why this was the most appropriate choice.

A PLC (Programmable Logic Controller) is a device that was originally developed to replace traditional hard-wired relay logic for machine control. As machines became more complex, the task of controlling these through relay logic started to become onerous and when faults occurred, they were very difficult to trace. In addition, modifying the control operation slightly could require many days work of re-wiring and testing again.

Now, instead of physically wiring relay contacts together to relay coil, all of the “wiring” is now done internally in software. The relay coil in this case is now an output from the PLC.

Figure 5-2below shows how “Key 1” and “Key 2” would be wired in an electrical circuit and Figure 5-3 shows how this circuit would look in a real PLC program. As can be seen, there is not much difference and basic machine functions are relatively easy to program in a PLC.

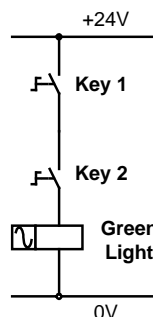


Figure 5-2 - Simple hard-wired control circuit using two switches

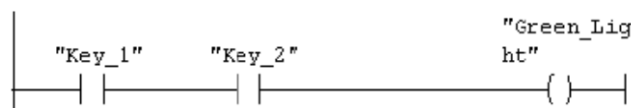


Figure 5-3 - Hard-wired control circuit shown in PLC software

Figure 5-4 illustrates the basic building blocks of a PLC in block-diagram form. The elements of this are described on the following page:

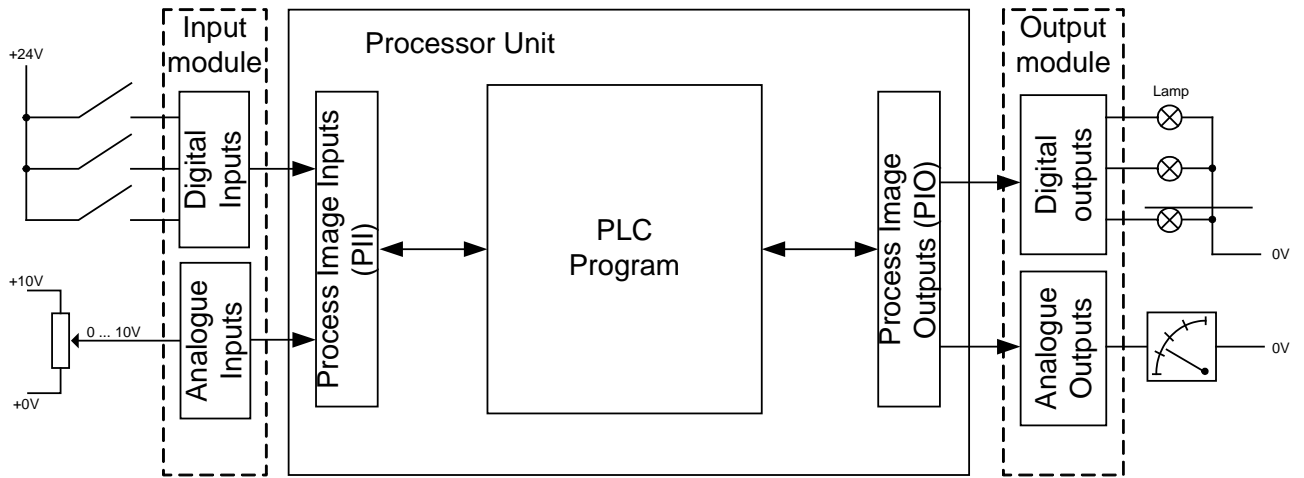


Figure 5-4 - Simple PLC block diagram

Processor unit - The processor unit houses the main PLC processor, memory expansion card slots (if available), back-up memory (battery or flash EEPROM). The processor has a high-speed communication bus system that is used to talk to the various expansion modules. Some of the possible expansion modules are detailed below.

Input modules - Input modules can take various types of inputs, ranging from digital (24VDC, 110/240VAC), to analogue (0-10VDC, 4-20 mA). As the input signals are high-voltage, the modules protect the processor by isolating the high-voltage input signals from the low-voltage ones used by the processor. Damaging an input module with over-voltage will not damage the processor.

The function of these modules is to convert and process the input signals so that the processor can read and interpret the values so they can be used by the program.

Output modules - Output modules are designed to allow the signals from the PLC program to be output in a form that can be used to control equipment or signal to users what is happening within the PLC program. Without output modules, a PLC would simply be a processor of information with no means of outputting this to the real-world. Output signals can be in the form of digital (24VDC, 110/240VAC), or analogue voltage/current (0-10VDC, 4-20 mA).

Figure 5-5 is included to show how the units shown in Figure 5-4 are represented in physical hardware and descriptions of each element follow.

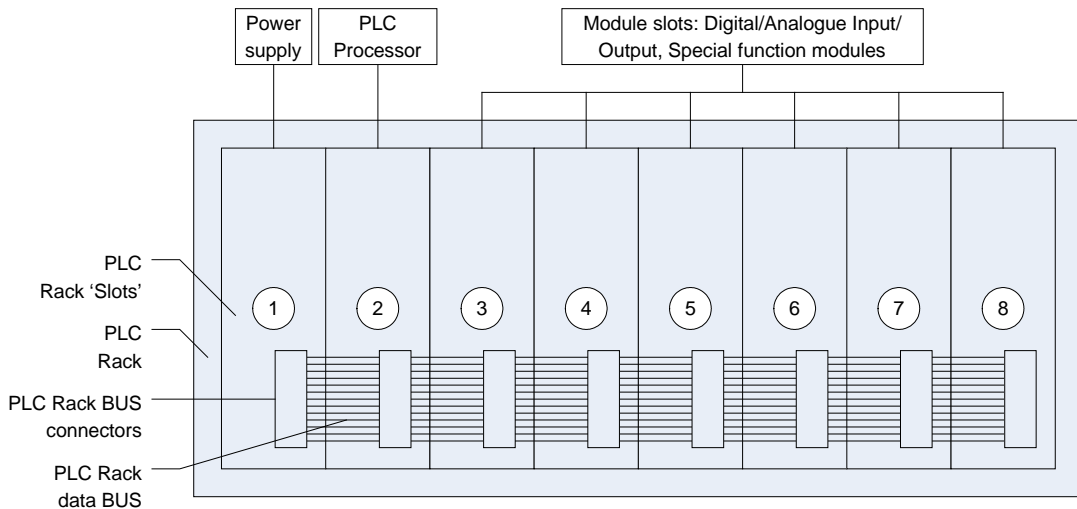


Figure 5-5 - PLC Hardware rack block diagram

PLC Rack - A PLC rack can vary in design from one manufacturer to another but always follows the same basic design principles. A rack can be ordered with a number of free 'slots' according to how many add-on PLC modules are required. The larger an application (and therefore PLC program) then the more 'slots' can be specified. A maximum number is usually 17 but additional racks can be added to a PLC application if all of the slots become used up. The number of additional racks can be anything up to an additional 9 for a Siemens PLC system. The rack shown in Figure 5-5 has a total of 8 slots.

PLC Rack Slots - With the exception of slots 1 and 2, any module type can be plugged into any slot of the rack. Slot 1 is always reserved for the PLC power supply, slot 2 is reserved for the PLC processor.

PLC Rack BUS connections - Each rack slot provides a BUS connection to the rack chassis backplane that each module plugs into. Alternatively, a ribbon cable may be used to connect modules together that provides the same function as the rack BUS.

PLC Rack data BUS - The data BUS is a parallel communications network that allows the PLC to communicate with the modules connected into the rack for the purposes of retrieving input data from input modules or outputting data to output modules.

PLC Slot designations - Any PLC slot from 3 upwards can be used to house any module type (input, output, analogue or digital) except for slots 1 and 2 which have their own dedicated function.

Slot 1: The power supply is always located in slot 1 of the rack. The power supply takes an industrial-standard control voltage of either 110VAC or 24VDC and converts this to the voltages required by the PLC and all of the expansion modules. Typically 1.2V, 3.3V,+5V and 24V power supply lines are supplied to the rack BUS for an Allen-Bradley PLC system, other manufacturers can differ.

Slot 2: The PLC Processor occupies slot 2 and controls the data bus. In addition to reading inputs and writing outputs to modules, the PLC is also responsible for retrieving diagnostic data from faulty modules and signalling this to the main PLC program.

5.1.2 Example PLC Program operation

Figure 5-6 shows a typical PLC program operation:

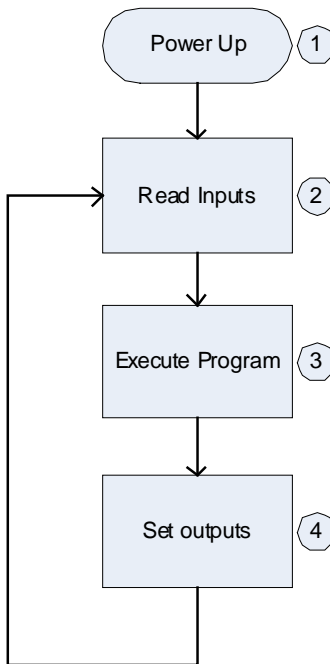


Figure 5-6 - PLC Program operation

Inputs are read into the PII ‘process image input’ table so that during the PLC process scan, each input remains constant for the entire scan even if it does actually change state whilst the program is being executed. This allows for consistent and predictable program behaviour.

Modern PLC’s have come much further than just replacing relay logic. They are now as fast as many home computers in performing mathematical calculations for operations such as PID control loops and other custom-written mathematical control functions.

The additional features of modern PLC’s does not detract from their main function – that of machine control with regular, synchronised process functions. Unlike a PC that ‘multi-tasks’ and processes commands asynchronously and with no guarantee of execution time, a PLC is designed to allow functions to be processed at a set frequency.

5.1.3 Test Rig PLC and operator screen

The test rig PLC chosen was a Siemens S7-222 PLC, order code 6ES7212-1AB23-0XB0 and is shown in Figure 5-7. The reason for this choice was:

- Cost effective, but powerful with up to 4kbytes of programming memory
- 8 Digital Inputs, 6 Digital Outputs included as standard
- Expandable with up to 3 additional modules for analogue/digital inputs/outputs
- Communicates to Siemens Touch-screen via PPI network
- PLC has already been used by University of Huddersfield previously and programming software exists for this

The PLC would be expanded with the following additional cards in order to provide the analogue control signals required to drive the test rig:

- 4-way analogue input module
- 2-way analogue output module



Figure 5-7 - S7-222 PLC [37]

Operator touch-screen

Siemens manufacture a touch-screen that is designed to communicate with the S7-200 PLC over the PPI network. The screen is programmed using Siemens WinCC Flexible Micro 2008 software. This software allows the user to freely program a number of operator screens that can contain input/output values, pushbuttons, text lists, graphics, trending displays. All of the values used by the screen are programmed and referenced to the internal variables in the PLC. Communication to the PLC is established by setting the correct communication protocol, baud rates and individual addresses for each device.

The model of the touch-screen is TP177 Micro and this is shown in Figure 5-8:



Figure 5-8 - TP177 Micro Touch-screen [38]

PLC communication to / from screen

The network that the S7-200 PLC communicates to the touch screen is a PPI (a Siemens term). PPI is a master-slave protocol: the master devices send requests to the slave devices, and the slave devices respond. A typical PPI network is illustrated in Figure 5-9:

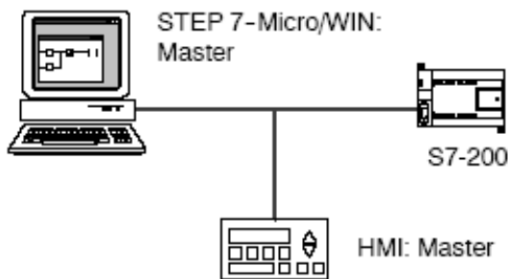


Figure 5-9 - Typical PPI network [37]

The HMI (Touch-screen) operates as master on the test rig PPI network – it gives the read/write instructions to the PLC. When the Laptop is connected to the network, it is also a master, but the network supports multiple masters and communication is shared between the two devices (Laptop and HMI). In this configuration, all devices are given a unique network address (the maximum number of devices on the network is 32).

PLC Programming software

Siemens Step 7 MicroWIN 32 is used to create the PLC program used by the test rig and an overview of the software is given in Figure 5-10 below:

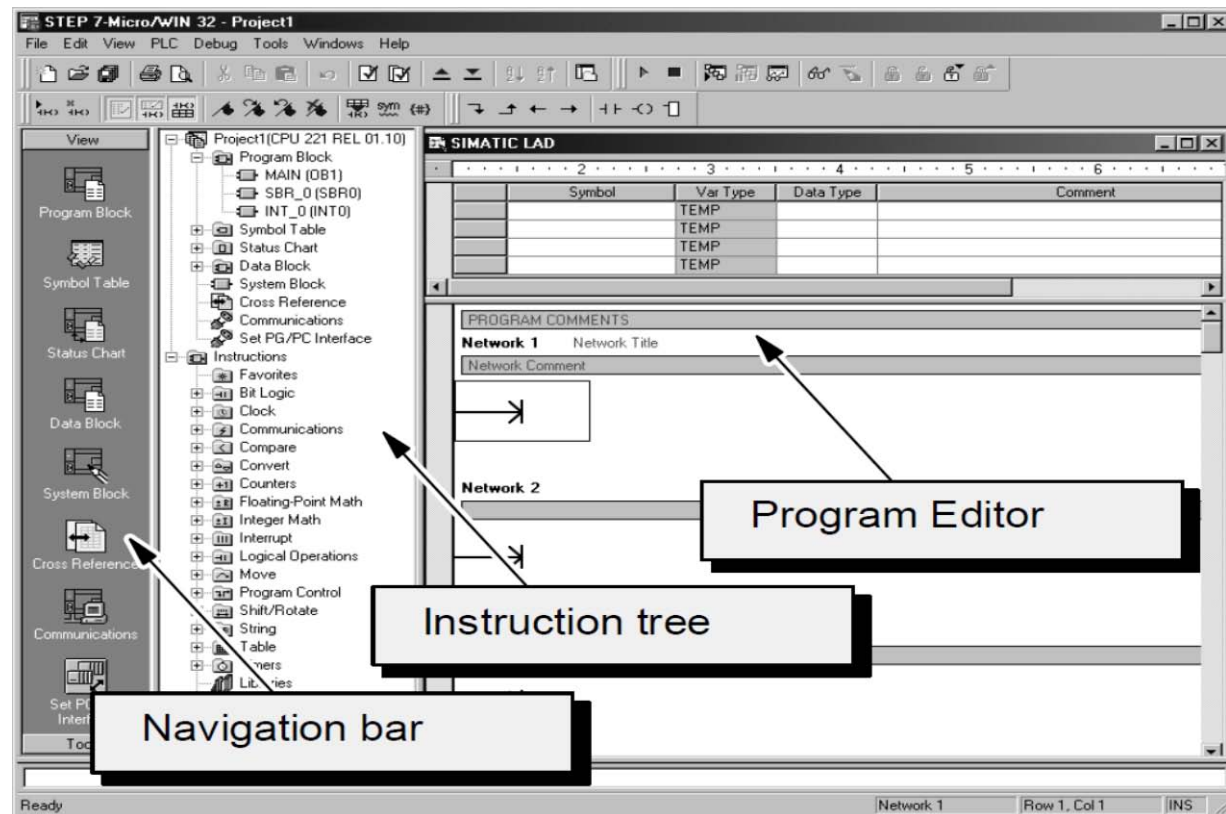


Figure 5-10 - Step 7 MicroWIN programming software

Programming can be done in:

- STL (Structured Text Language). This text-based concept is very similar to assembly language programming
- LAD (LADder diagram format). This displays the program as a graphical representation similar to electrical wiring diagrams

5.1.4 Test rig PLC control strategy

This section will detail how the PLC will be incorporated into the existing test rig and how the program will operate in a block-diagram format. This is given in Figure 5-11.

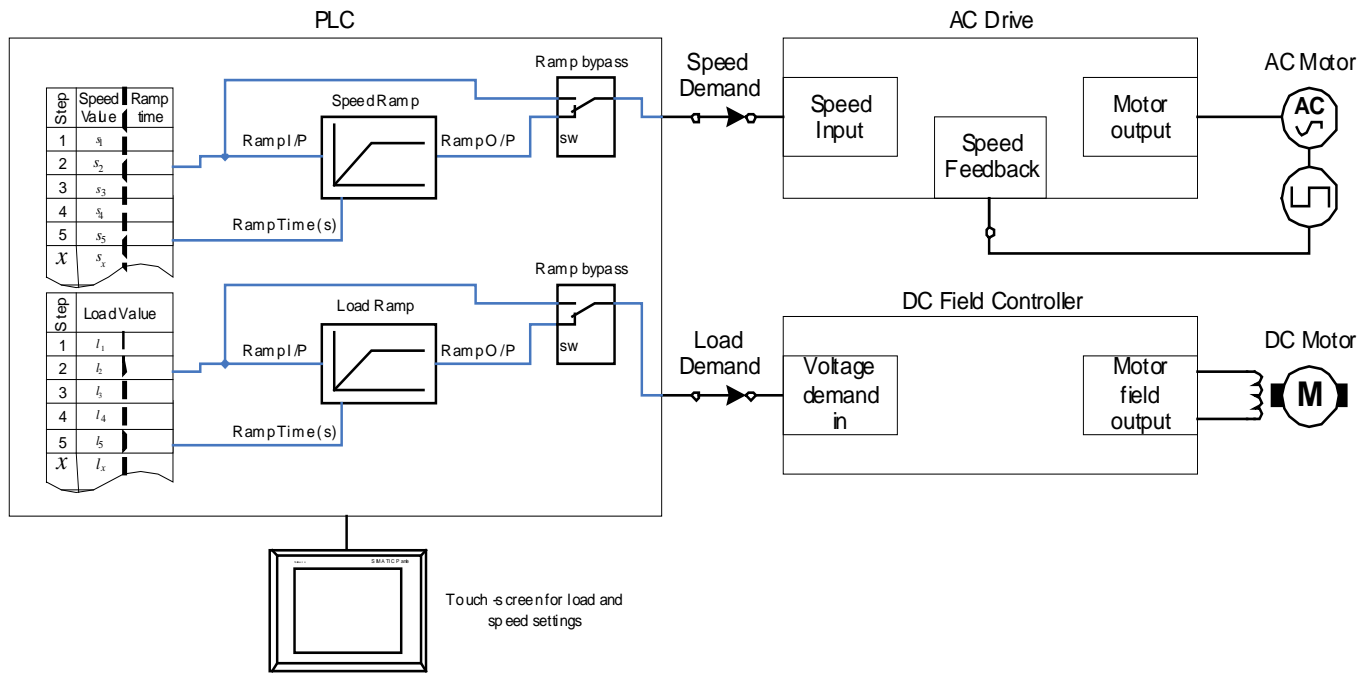


Figure 5-11 - Test Rig PLC design philosophy

From studying the diagram, the PLC block contains on the left-hand side, the program sequence steps (the first 1 – 5 are shown) with two outputs being fed to a ramp generator. Each step sequence has a time delay associated with it. When the time delay has expired, the PLC program will move onto the next step. A step-change of input will be fed into the ramp generator and this will provide an output that changes at a rate determined by the ramp time from the old value to the new step-change value.

A touch-screen will be provided to enter test rig operating data, rather than entering it step-by-step using the PLC programming tools and this will be situated on the control panel door. The screen allows the test rig to be operated by non PLC-literate engineers.

Further information on how the PLC program is structured and software state diagrams to describe how each sequence operates is given under Appendix B.

The test rig modifications for the PLC are detailed in Appendix A.

5.2 Test Rig Modifications – Closed-loop operation

To upgrade the 690+ Vector drive to full closed-loop operation, an encoder ‘Technology Box’ as termed by Parker SSD Drives would be fitted to the existing inverter. As part of this upgrade, an encoder would be fitted to the motor for speed feedback purposes and connected into the inverter drive. Closed-loop encoder control allows the motor torque and speed to be more finely controlled with speed holding of typically $\pm 0.1\%$. Fitting of the encoder signal box is straightforward, is simply plugs into the front of the drive, see Figure 5-12.

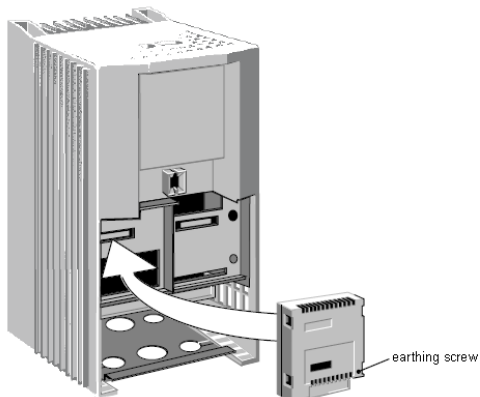


Figure 5-12 - Installing the HTL Speed Feedback Technology Box Option [51]

The encoder used on the motor provided pulse outputs of A, B and a once-per-revolution marker pulse. The connection diagram given in Figure 5-13 was followed and all of the unused pulse connection inputs were grounded to terminal 11 on the encoder board.

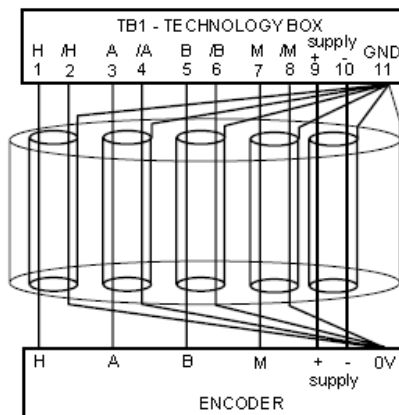


Figure 5-13 - Single-ended encoder wiring [51]

Once wired correctly, the drive was configured to the correct number of encoder pulses, in this case 1000. The mode of operation was set to quadrature, that gives direction and speed from the two pulses.

5.3 Commissioning the test rig

After installation of the new control equipment, it was necessary to fully test the operation of the new PLC program to ensure that the operation met the original design specification.

The equipment required to commission the test rig was

- Laptop, complete with:
 - PLC programming software (Siemens 'Step 7 MicroWIN Version 4.0')
 - Touch-screen programming software (Siemens 'WinCC Flexible Micro 2008 version')
 - Drive programming software (Parker SSD 'DSE Lite')
- Laptop programming leads:
 - Siemens CP5512 PCMCIA communication adaptor (PLC Programming and on-line diagnostics)

-
- Siemens Serial to PPI converter (programming touch-screen)
 - Parker SSD serial communication lead (Drive programming and on-line monitoring)
 - Fluke DM85 Multimeter complete with fused test leads
 - Hand-held current-clamp meter 0-200A range, AC/DC voltage
 - Hand-held digital tachometer

Full details of the commissioning tests performed and the results obtained are given in Appendix C.

After the commissioning tests had been carried out, an assessment was made as to the improvement of the test rig performance both from the PLC automation aspect and for the drive performance improvements by changing into closed-loop mode. These improvements are detailed in the next section.

5.4 Performance improvements

PLC Automation

The accuracy of test results obtained by using the PLC to automate the test rig was confirmed by thorough commissioning tests. Figure C-8 on page 10-11 in Appendix B compares two results from separate test runs to compare the consistency of the test runs. It was shown that the test conditions did not vary from one run to the next, so automation of the test rig has seen a major advance in performance of the rig in this aspect.

Motor performance

Improved motor performance by converting the test rig AC drive into true closed-loop mode is shown in Figure C-21 and Figure C-22 on page 10-22 under Appendix B. The speed holding of the test rig motor is significantly improved and allows the test rig to simulate operation of high-performance closed-loop vector drives for the purposes of fault detection.

The next chapter will detail the monitoring systems that have been developed and researched for use on AC motors and inverter systems.

Chapter 6

Monitoring procedures for inverter-driven motor systems

Key trends for condition monitoring are summarised along with some of the more common motor failures experienced by industry. Research methods used to detect some of these motor faults are then described. Attention is then drawn to inverter faults and current techniques used to detect these. Fuzzy logic and neural network systems for learning and adapting fault detection algorithms complete the chapter.

6.1 Introduction to monitoring procedures

There are many methods in use that provide condition monitoring for induction motor-driven systems. The popularity of the induction motor has seen it being used for a wide-range of industrial applications and a considerable amount of data has been obtained as to how the motor fails and the common causes of failure.

This initial research leads others to develop systems that can detect the causes of failure at an early enough stage so as to allow corrective action to be taken on the equipment. It is highly desirable in industry to have the maximum amount of up-time available on equipment with the minimal amount of intervention and preventative maintenance. Indeed, there are mathematical maintenance models that are used to try and ascertain the most efficient frequency of maintenance. These are based on Stochastic modelling but this topic is outside the scope of research. Nevertheless, it gives an insight into the drivers in industry that are being used to bring the level of maintenance intervention down.

As stated previously, because the induction motor is so popular in industry then any system that can actively monitor the motor and give reliable indication of the inception of faults will help prevent downtime by indicating that preventative maintenance is required before the motor fails catastrophically. Quite often, types of mechanical faults such as cracked or broken rotor bars/end-ring, minor bearing damage, and misalignments which do not completely block (stall) the rotor, may cause noise and excessive currents and heat during the steady-state operation of the motor that remains undetected by the user.

Conventional motor overload units usually guard against frequent starting and blocked rotor but may not trip under the conditions mentioned previously. Of course, Such protection is only activated in response to a fault which has already happened, whereas condition monitoring aims to identify the cause and give the operator time to respond before the trip occurs.

There are both invasive and non-invasive methods are used to measure motor vibration, temperature, speed and torque variations for detection of motor abnormalities. The most advanced of all of these methods, however is based upon using motor current signature analysis (MCSA), since it has been found that the motor current signals contain the required information that can be used for fault detection without requiring additional hardware to be fitted to the motor.

Seven Key Trends for condition monitoring in 21st century

Sandy Dunn [39] identified seven key trends for condition monitoring:

- The development of smart sensors, and other low-cost on-line monitoring systems that will permit the cost-effective continuous monitoring of key equipment items
- The increasing provision of built-in vibration sensors as standard features in large motors, pumps, turbines and other large equipment items
- Increasingly sophisticated condition monitoring software, with rapidly developing "expert" diagnosis capabilities
- The acceptance of Condition Monitoring within the "mainstream" of Operations and Maintenance, with Production operators increasingly utilising Condition Monitoring technologies as part of their day-to-day duties
- Increasing integration, and acceptance of common standards for interfacing Condition Monitoring software with CMMS and Process Control software
- An increasing focus on the business implications and applications of Condition Monitoring technologies, leading to the utilisation of Condition Monitoring technologies to improve equipment reliability and performance, rather than to merely predict component failure.
- A reduction in the cost-per-point of applying Condition Monitoring technologies - possibly leading to more widespread use of these technologies

These trends identified by Sandy Dunn are written from a maintenance perspective and are aimed at improving the way that industry monitors and plans plant maintenance on equipment. Now that users of such equipment are accepting that active or at the least regular manual condition monitoring is a key part of their day-to-day running of the plant, then any such system that can integrate easily into existing plant equipment will find favour in the marketplace.

6.2 Motor fault detection

Methods of fault detection that were researched were found to each measure different core motor data sources:

- Motor supply
- Motor speed
- Vibration
- Acoustics

There are a number of methods used for each of the core motor data sources in order to detect motor faults and each of these has been studied in detail. Methods for detecting motor faults are detailed in the following chapters following the headings given in the list above, but first the categorisation of motor faults will be examined.

Motor faults

Motor faults can be categorised into the following electrical, thermal or mechanical faults and these are given in Table 6-1:

Table 6-1 - Examples of motor failures arising from external system faults [40]

Mechanical	Shock loads Bearing failure Misalignment Mechanical unbalance Loss of lubricant
Thermal	Overload Stall Single phasing Loss of coolant/inadequate cooling Harmonic heating
Electrical	Insulation breakdown due to: <ul style="list-style-type: none">– Contamination– Vibration/mechanical damage– Thermal cycling– Overvoltage Broken rotor bars/rotor windings due to: <ul style="list-style-type: none">– Overspeed– Frequent starts– Harmonic heating– Lamination damage
Commutator, slip rings and brushgear (DC motors)	Overheating Contamination Excessive sparking

Further to this table of possible failures, two comprehensive studies have been carried out into the most common induction motor fault occurrences in industry. The first of these, in 1986 was undertaken by the Electrical Power Research Institute (EPRI) [41], [42] and in 1987, the IEEE (Institute of Electrical and Electronics Engineers) published the results of their survey [43], [44], [45]. The results of these studies are shown in Table 6-2:

Table 6-2 - Component failures in motors > 50hp and <=200 hp

Rank	Failed Component	Percent of total
1	Insulation > Ground	17.9
2	Sleeve bearing	11.4
3	Ball bearing	5.5
4	Oil Leakage	4.8
5	Thrust bearing	3.9
6	Insulation-Turn	3.5
7	Squirrel-cage winding	3.5

8	Bearing Seal	2.2
9	Roller bearing	2.0
10	Shaft	1.8
11	Loose blocking	1.6
12	Oil system	1.1
13	Stator slot wedges	1.1
14	Accessories	1.1
15	Frame	0.9
16	Loose rotor iron	0.8
17	Line cable	0.8
18	Coil connections	0.7
19	Balance weights	0.6
20	Other unspecified	34.8

From the total list of 19 specified faults, there are a total of 5 directly attributable to the electrical wiring or winding part of the motor. The remaining faults are all mechanical and some of these are not related to the drive-train part of the motor.

Each of the fault detection methods will now be covered under each of the four core motor data sources outlined previously.

6.2.1 Motor supply

Each method researched in this section involves the measurement of signals from the motor supply terminals. This could be resistance, inductance, current, or voltage signals being supplied to the motor. In effect, these measurement methods require no other measuring instrument to be connected to the motor and the motor remains unmodified from its original form supplied by the manufacturer.

Some of the methods studied involve the detection of asymmetrical conditions in the motor – this is covered in principle under heading “3.2.2 -AC motor mathematical model” and helps the understanding of how these are to be applied.

Other methods involve the modelling of healthy motor parameters and then comparing these with the normal running data returned from the motor to detect differences between data sets.

Stator Phase Currents

Bo Liang [1] researched using stator phase current analysis to detect asymmetrical faults in the motor caused by either broken rotor bars, stator winding faults, or asymmetrical phase supply voltages.

A broken rotor bar in an induction motor was known to cause asymmetry, resulting in modulation of the air gap flux as the rotor turns. This will in turn be reflected in the stator winding currents so that the main supply frequency component ω_1 will be observed with a series of $(1 \pm 2ns)\omega_1, n = 1, 2, \dots$ sideband components.

When asymmetrical conditions are existing in the motor, sidebands appear around the pole pair related supply frequency. It was noted that at greater motor load and therefore increased motor slip, these sidebands were more pronounced. The sidebands were more apparent from phase current analysis

than in the vibration analysis Bo Liang undertook (see section). However, with the motor under no load, broken rotor bars were not detectable because the low currents flowing in the rotor give rise to very little asymmetries.

Phase current analysis is advantageous as the motor supply cables can be accessed anywhere from the switch room to the motor and the data acquisition can be non-invasive as current measurement is via hall-effect devices – there is no direct wiring-in to the motor circuit.

Parameter Identification/Estimation Methods

Juggrapong Treetrong, [2] researched Recursive Least Square (RLS) and Genetic Algorithm (GA) methods.

RLS (Recursive Least Square) method

RLS had been used in this research to estimate parameters for the motor stator. For RLS to function, data on the motor characteristics has to be obtained ‘off-line’. This requires de-coupling of the motor from any load and performing a series of tests on the motor to provide ‘base-line’ data. These tests are given below:

DC Test

A DC test is used to determine stator resistance. This is how a modern inverter drive will also perform the measurement – the inverter fitted to the test rig will have this feature built-in. As there is no induced voltage to the rotor and no rotor current, we have a true measurement of the stator resistance. Stator resistance is calculated as:

$$R_S = \frac{v_{DC}}{2i_1} \quad (6-1)$$

Where: v_{DC} = Test DC voltage applied; i_1 = Stator current flow

for a star-connected AC motor as there will be two stator windings in series at the motor terminals used for the test.

No-load test

The no-load test is used to measure rotational losses from the induction motor and find information from its magnetisation currents – the losses in this case being only windage and frictional losses. The test results give:

- Input power
- Currents from each of the three phases
- Supply frequency
- Line voltage

Locked-rotor test

For this test, the rotor must be locked in position mechanically so it can not rotate. A low voltage (90 volts) of normal frequency is applied to the motor stator windings.

The following motor parameters are calculated:

- Power factor
- Total motor circuit impedance, made up of

- Stator resistance
- Rotor resistance
- Stator leakage reactance
- Rotor leakage reactance

Genetic Algorithm (GA) method

This method is useful to estimate the values of rotor and stator parameters using the motor nameplate data without the intrusive tests that the RLS method requires.

The flux linkage model and torque model of an induction motor is adapted to the estimation. The scheme is developed to obtain all the motor parameters: stator and rotor resistance, stator and rotor leaking reactance and magnetizing reactance to provide good 'base-line' motor parameters so that estimated vs. actual motor parameters can be compared to help diagnose faults more effectively.

The GA scheme was evaluated with different motor sizes and different load levels using simulation tests and then by the experimental data of the induction motors under normal operating conditions at different load levels and then under fault conditions at differing loads. The results from both tests show that the new scheme can estimate the parameters and predict the motor condition with sufficient accuracy for motor fault diagnosis.

Motor current signature analysis (MCSA)

MCSA is based on the principle that the motor current signal provides the necessary data content required for fault detection. The signal processing tools of Fourier, Wavelet, and Hilbert–Huang transformations are applied to the acquired motor current data to extract the detail necessary for motor fault detection.

Each of the motor phase supplies contain current components that are a direct by-product of unique rotating flux components caused by faults such as broken rotor bars, air gap eccentricity, and shorted turns 'T' in low voltage stator windings and others. MCSA can detect these problems at an early stage and thus avoid secondary damage and complete failure of the motor.

MCSA is a system used for analyzing or trending dynamic, Energized systems. Proper analysis of MCSA results will assist the technician in identifying:

- Incoming winding health
- Stator winding health
- Rotor Health
- Air gap static and dynamic eccentricity
- Coupling health, including direct, belted and
- Geared systems
- Load issues
- System load and efficiency
- Bearing health

Basic steps for analysis

There are a number of simple steps that can be used for analysis using MCSA. These are as follows:

-
1. Map out an overview of the system being analyzed.
 2. Determine the complaints related to the system in question. For instance, is the reason for further investigation due to the equipment being operated improperly, rather than known regular machine faults, and is there other data that can be used for analysis.
 3. Take data.
 4. Review data and analyze:
 - a. Review the 10 second snapshot of current to view the operation over that time period
 - b. Review low frequency demodulated current to view the condition of the rotor and identify any load-related issues.
 - c. Review high frequency demodulated current and voltage in order to determine other faults including electrical and mechanical health.

Most faults can be determined at a glance, with many rules being similar for both MCSA and vibration analysis. In addition, there are several rules that should be considered:

- Pole Pass Frequency (PPF) sidebands around the line frequency indicate rotor bar faults. The higher the peaks, the greater the faults.
- Harmonic Pole Pass Frequencies often relate to casting voids or loose rotor bars.
- Non-PPF sidebands that cause a ‘raised noise floor’ around the line frequency peak normally relate to driven load looseness or other driven problems.
- ‘Raised noise floor’ signatures relate to such things as looseness or cavitations.
- Peaks that show in current and voltage relate to electrical issues, such as incoming power disturbances, loose wiring connections.
- Peaks that show in current only relate to winding and mechanical faults.
- Peak pairs that do not relate to running speed or line frequency are most often bearing related problems.

MCSA using a modified bispectrum for fault diagnosis of downstream mechanical equipment

Research undertaken by F. Gu [5] et al, involved the use of induction motor current feedback signals to identify and quantify common faults within a two-stage reciprocating compressor based on bispectrum analysis. This theoretical basis is developed to understand the non-linear characteristics of current signals when the motor is driving a varying load under different faulty conditions. Although conventional bispectrum representation of current signal allows the inclusion of phase information and the elimination of Gaussian noise, it produces unstable results due to random phase variation of the sideband components in the current signal. A modified bispectrum based on the amplitude modulation feature of the current signal is then adopted to combine both lower sidebands and higher sidebands simultaneously and hence characterise the current signal more accurately. Based on the new bispectrum analysis, a more effective diagnostic feature is developed – named Normalised Bispectral Peak – for fault classification. In association with the Kurtosis value of the raw current signal, the bispectrum feature gives rise to reliable fault classification results. In particular, the low feature values can differentiate such faults as belt looseness from other fault cases. Even different degrees of

discharge valve leakage and inter-cooler leakage can be separated easily using two linear classifiers. This work provides a novel approach to the analysis of stator current for the diagnosis of motor drive faults from downstream driving equipment.

Monitoring gear vibrations through MCSA and wavelet transforms

Chinmaya Kar et al [3], progressed MCSA research into motor gearbox loads, where load fluctuations on the gearbox and gear defects are two major sources of vibration. Using MCSA may be favourable as conventional measurement of vibration in the gearbox is not easy because of difficulties in mounting the vibration transducers in certain environments due to gearbox inaccessibility. In this paper, a multi-stage transmission gearbox (one with and one without defects) has been studied with a view to replacing conventional vibration monitoring by using MCSA.

It has been observed through Fast Fourier Transform (FFT) analysis that low frequencies of the vibration signatures have sidebands across the line frequency of the motor current whereas high frequencies of vibration signatures are difficult to detect. To this end, Discrete Wavelet Transform (DWT) is suggested to decompose the current signal, and FFT analysis is carried out with the decomposed current signal to trace the sidebands of the high frequencies of vibration. The advantage of DWT technique to study the transients in MCSA has also been cited. The inability of Continuous Wavelet Transform (CWT) in detecting either defects or load fluctuation has been shown. The results indicate that MCSA along with DWT can be a genuine replacement for conventional vibration monitoring.

FFT analysis of current and vibration signals

Figure 6-1 shows the spectra of the steady vibration signatures and current signatures of the gearbox. With no defect, one defect in the 2nd gear (defect-1) and two defects in the 2nd gear (defect-2) at 5.625kW load condition, within the frequency range 0–100 Hz. The following observations were made:

1. The rotating shaft frequencies such as input shaft frequency (f_1), lay shaft frequency (f_2) and output shaft frequency (f_3) are of the order of 49, 30 and 20 Hz respectively and hence lie within 0–100 Hz range. In all the vibration spectra, prominent frequencies such as f_1 , f_2 , f_3 are observed. In some cases, harmonics of f_1 and f_3 are also detected. The corresponding Sidebands of the rotating frequencies across the line frequency (f_e) are observed in the current Spectra.
2. Rotor eccentricity in the induction motor ... is also traced by examining the Remaining sidebands of the line frequency in the current signatures. These are shown by a line Drawn in the spectra. Since the amount of load affects the rotor speed, the slip factor also Changes in each case. The amplitudes of the sidebands due to rotor eccentricity are very large after the load removal than those before the load removal. It is due to the fact that the load acts as a damping factor for vibrations due to the rotor eccentricity.
3. In an induction motor, the speed is normally inversely proportional to the load applied. However, it was noted that when coupled to a gearbox, a large fluctuation of speed in the order of 0.5 Hz (30 RPM) is observed. It has been observed that a defect-free gear running at 3.75kW load has input shaft speed of 49.7 rpm whereas at 1.875 kW, it is 49.4 rpm – one would expect a higher load to reduce the motor speed, not increase it. The reason is that the gearbox casing vibration is retransmitted back to the gearbox drivetrain through the flexible rolling element bearing, and as a result, a very large excitation of the gearbox takes place due to various time-varying parameters like tooth mesh stiffness, frictional

forces and torques and bearing forces. This causes the large speed fluctuations observed. It was concluded that tracking of the rotating speed is not effective in monitoring of the gearbox condition.

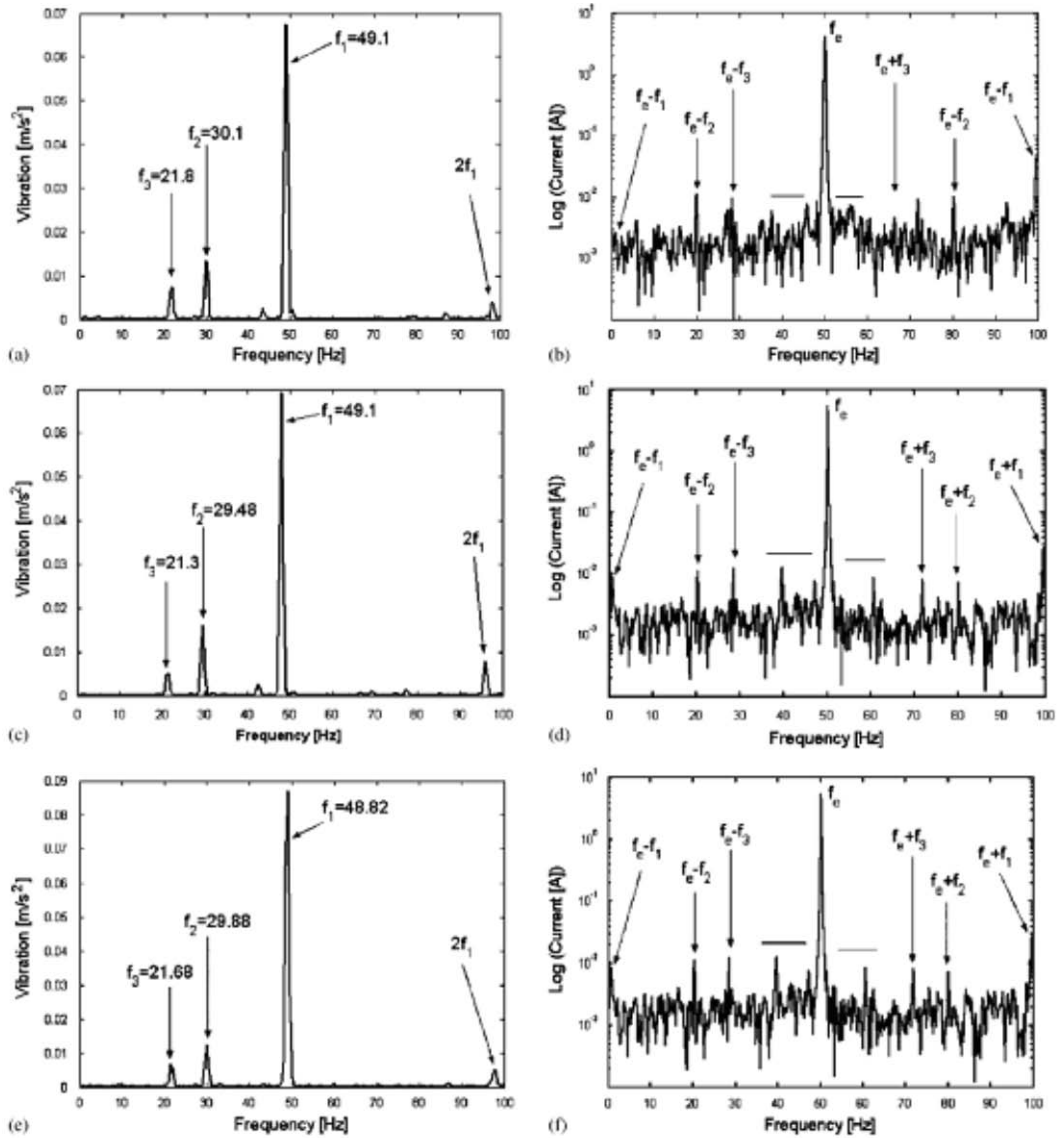


Figure 6-1 - Spectra of vibration and current signatures (0 -100 Hz) at 5.625 KW with no defects [3]

Induction machine condition monitoring using Notch-Filtered Motor Current Analysis (NFMCSA)

Serkan Günal et al [4], researched a method whereby the main motor fundamental frequency of 50Hz (Europe) would be notch-filtered out before being fed into the fault detection process. The reasoning behind this being that the spectral components of motor current other than the fundamental component carry required information for fault detection. The distinguishing approach in this research was to utilize only localized time-domain information instead of employment of spectral information (such as Fourier or wavelet domain) which are commonly used in most of the previous works.

What sets this research apart from other methods is that existing methods considered faults of either broken rotor bars or defected bearings with the developed fault classification and detection methods being tested with identical motors (same manufacturer) and one of these would always be the healthy

reference. This research added a second (and completely different) healthy motor to the test. When the classification algorithm was performed with two healthy motors and five faulty ones, the healthy motors were successfully classified from faulty motors in spite of the clear differences between the two healthy motors.

Motor current waveform data is acquired from both healthy and faulty motors at a sampling rate of 20 kHz with 16 bit vertical resolution. Real-time notch-filtering was performed with a DSP based programmable filter. Careful inspection of the current waveform reveals that the waveform consists of a fundamental harmonic which constitutes the largest factor of the signal, and a noise-like additive waveform which is relatively subtle and therefore occluded by the fundamental. By eliminating the fundamental harmonic, the subtle details which actually carry the necessary information are emphasized. This can be seen in Figure 6-2 below:

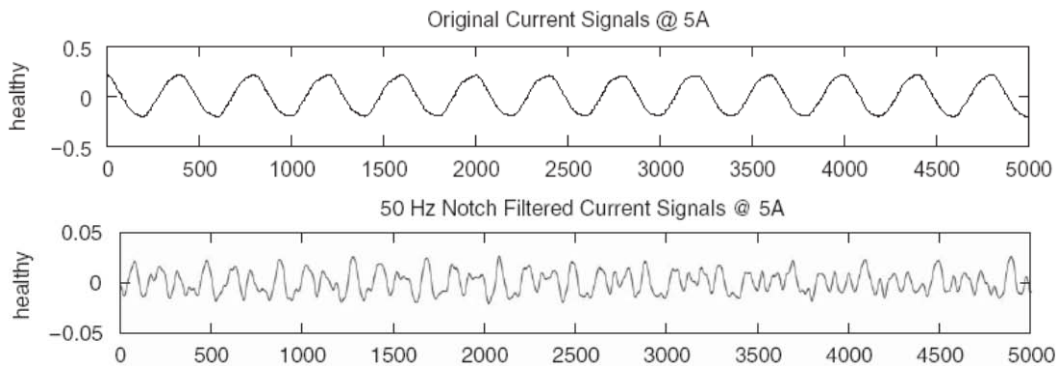


Figure 6-2 - Original and Notch-filtered current signals – healthy motor [4]

The classification of faulty motors with the proposed parameters was performed using three classifiers:

- Bayesian
- Gaussian mixture model (GMM)
- Fisher's linear discriminant analysis (LDA)

to verify the effectiveness and the success of the proposed feature set. Experimental verification of the proposed features and classifiers revealed that NFMCSA approach is a promising analysis especially considering the fact that high classification accuracy can be achieved even in case of structurally different machines with numerous different faults under varying motor load conditions.

6.2.2 Motor speed

The motor speed – when measured with sufficient accuracy – can also be used to diagnose valuable information about how the motor is performing. If the speed resolution is high enough, then rapid changes in speed measured over one motor revolution can be further processed to study the relevance of these speed changes in relation to motor condition.

Transient Speed Analysis to detect rotor or stator asymmetrical faults

Filippetti, F et al [7], researched using Artificial Intelligence techniques in induction machines diagnosis including the speed ripple effect. transient speed analysis methods for detecting motor stator or rotor asymmetrical faults using a high resolution encoder and performing additional speed monitoring. Torque ripples that occur due to the broken rotor bars manifest as large speed fluctuations when using the high-resolution measuring device.

The speed ripples are at the same frequency as those that occur when measuring the stator currents, so the same principles of detection would apply.

However, the conclusions found that motor inertia and load could absorb the speed ripples, especially with only one broken rotor bar. The sensitivity of this detection method was therefore dependant upon the load type but the speed spectrum detection method "provided valuable information in identifying frequency components $2s\omega_1$ and $2\omega_1$ caused by pulsating torque.".

Instantaneous angular speed monitoring of electric motors

Ahmed Yousef et al [8], researched the lesser-known technique of instantaneous angular speed (IAS) condition monitoring applied to reciprocating and rotating machinery.

In practice, many mechanical systems in engineering applications rotate with a varying speed, despite the assumption they rotate at a constant speed. This sub-revolution varying speed data contains significant information about reciprocating and rotating machinery parts. In diesel engines, for example, angular speed variations can reflect the characteristics of gas pressure in cylinders, which can be used to diagnose engine combustion related faults and efficiency.

The principle of IAS extraction

Many techniques can be used to extract IAS from an incremental rotary encoder signal. Sweeney and Randall (1996) overviewed these techniques including carrier tracking, pulse timing, frequency domain block-shift transforms, frequency domain zoom demodulation and Hilbert transforms.

The Accuracy of the first two techniques: (carrier tracking and pulse timing) is determined by the Hardware resources available. This limits the wide application due to the cost of the required hardware and the non-generic nature of these techniques. The last three techniques use essentially the same principles to obtain the IAS signals. These methods are developed based on fast Fourier transform (FFT) and rely largely on digital signal processing. In addition, the raw data can be collected using a low cost general-purpose ADC device (data accuracy can be as low as eight bits). As rapid advances have been made in computational capability, FFT-based techniques have great potential as generic approaches for use in a wide range of applications.

The residual IAS signal extraction can be summarised in four steps:

1. Band-pass filtering.
2. Analytic representation (Hilbert transform).
3. Carrier frequency removal (frequency shifting).
4. Angle calculation and differentiation.

These IAS features were utilised to predict the operating condition of an electric motor. Results from a broken rotor bar fault show that the power spectrum of the IAS signals could be used for the diagnosis of this failure mode. The key features in this case are the pole pass speed sidebands around the rotor speed components. These sidebands could be visible at high loads as in vibration and current signature monitoring.

6.2.3 Motor vibration

Of all the motor condition monitoring methods, vibration analysis is one of the most widely used in industry and therefore most developed. As imminent failure of a motor can be directly related to the

level and frequency of motor vibration detected, this method provides a reliable indicator of motor condition.

For each type of mechanical failure of a motor (given under on page) the analysis of the data will be examined with a different set of reference parameters, since each mechanical component will have differing frequency characteristics. Some common detection methods using vibration analysis are given below.

Detecting Rotor or Stator Asymmetrical Faults

Bo Liang [1] researched using vibration analysis to detect asymmetrical faults in the motor caused by either broken rotor bars, stator winding faults, or asymmetrical phase supply voltages.

By spectrally analysing the motor phase currents using FFT's (Fast-Fourier-Transforms) the predominant characteristic frequency $2\omega_l$ for stator asymmetry and $-2s\omega_l$ for rotor symmetry that exist below the rotor frequency ω_r , can be seen when such asymmetrical faults are present.

Comparisons can be made between sets of data from a healthy motor and those from a motor with broken rotor bars.

The conclusions from these results were that stator and rotor faults could be clearly detected by vibration spectrum analysis. The characteristic asymmetric stator fault symptom of a sideband at two times the supply frequency on the spectral display is substantially increased when stator asymmetry exists.

Some disadvantages with this method were that in order to accurately detect faults present in the motor, knowledge of the motor structure is required due to the differing frequency responses of different motors.

6.2.4 Motor acoustic emissions

The techniques that can be used to interpret and analyse data from the above sources are:

- Stator Phase Current Analysis
- Application of Higher Order Spectrum Analysis to Induction Motor Fault Diagnosis
- Application of Neural Networks to Induction Motor Fault Diagnosis

Not all the data analysis methods given apply to all data sources but each data source description will be followed by the analytical methods for each.

6.3 Inverter Fault Detection

With the development of power electronics, microprocessors and digital signal processors (DSP's), induction motors are predominantly fed from pulse width modulation (PWM) inverters for variable-speed operation. This section will detail the existing methods used for fault detection and/or prediction of faults on inverter-driven motor systems. Whilst monitoring of motor current signals is important, there are failures that can occur in PWM inverter drives that often the drive cannot detect.

Whilst incipient motor faults can lead to premature motor failure, the same can be said of inverter drive faults. If left undetected, certain inverter faults can lead to eventual failure of the motor [46]. For example, the intermittent failure of a switching device in one of the phases can cause imbalances in rotor phase currents and heat up the motor.

Some of the methods researched can detect and identify the transistor open-circuit fault and an intermittent misfiring fault, which commonly occurs in the inverter drive system.

In order to maintain a high-uptime of equipment, advance warning and a controlled shutdown are desirable in order to keep the plant running effectively. If advance warning is made available soon enough, standby equipment can be arranged, or in some instances a 'hot-swap' may take place with one inverter being 'switched-out' of circuit whilst the other then regains control of the process.

If motor faults can also be diagnosed using signals supplied from the inverter to the motor, then this is a further advance that will have considerable potential in industry.

Faults detected by the Siemens PWM inverter

Some of the faults that can be detected by a Siemens Masterdrives AC PWM inverter shown in Figure 6-3 are listed in Table 6-3



Figure 6-3 - Siemens Masterdrives Inverter Unit [47]

Faults will cause the drive to immediately shut-down in order to protect itself, or the motor it is driving.

Table 6-3 - Selected inverter fault codes [47]

Fault code	Description
F011 - Over-current	Over-current shutdown has occurred. The shutdown threshold has been exceeded. Check the converter output for short-circuit or earth fault
F020 - Excess temperature of Motor	The motor temperature limit value has been exceeded. Check: Motor (load, ventilation etc.); Sensor for cable break, short-circuit
F023 - Excess temperature of Inverter	The limit value of the inverter temperature has been undershot or exceeded. Check: That minimum and maximum ambient temperature from 0°C to 45°C
F025, 26, 27 - UCE upper switch/UCE Phase L1, L2, L3	The current limit of the inverter output switch for phase 1 has exceeded its limit

Whilst the fault cause is of interest to the user, the process that the motor is controlling is now stopped and no advance warning of the fault has been given. This is not desirable for continuous process industries (extrusion, for example where plants run 24-7 and shutting-down a machine takes 2-3 days to restart).

On the other hand, drive alarm codes give more imminent warning of failure, so these signals may give indication of possible future failures. Table 6-4 gives some of these alarms from the same drives manual that a system could use to warn the user that there is a potential problem arising.

Table 6-4 - Selected inverter alarm codes [47]

Alarm code	Description
A023 Motor temperature	Check: the motor (load, ventilation, etc.). Read off the current temperature in r009 Motor Temperature
A025 I2t converter	If the current load state is maintained, a thermal overload of the converter occurs. The converter will lower the max. current limit
A034 Setpoint/actual value Deviation	The difference between frequency setpoint/actual value is greater than the parameterized value and the control monitoring time has elapsed.
A042 Motor stall/block	Motor is stalled or blocked.

As can be seen from the above table, the list of potential alarms that the drive can indicate before an actual trip occurs are limited.

The alarm is generally triggered from basic information such as the motor temperature (from a simple pt100 temperature sensor) or total failure of part of the IGBT (I2t) converter using the drive's in-built current transformers. However, with the IGBT's, no indication is given as to whether each gate of the firing circuit is operating as it should – a fault is only generated if the device overloads. There is no alarm indication for open-circuit and the motor may commutate (albeit with poor response and control) with a failing firing circuit, especially if the fault is intermittent.

Faults not detected by inverter drives – future work

AC inverter drives cannot detect subtle faults on individual elements of the PWM circuit or motor faults such as those covered in chapter 4 (broken rotor bars, shorted stator windings) so other external monitoring systems would be required to improve the level of fault diagnosis that can be obtained.

This data could be transmitted from the drive, across a high-speed network (some AC drives now support Ethernet protocols) to allow further signal processing by a higher-level system. Once these systems have been proven, and as the data processing capabilities of AC vector drives become more powerful, this could be re-integrated into the drive control software.

Some of the methods used for inverter fault detection are given next.

6.3.1 Incipient Fault Diagnosis in Electrical Drives by Tuned Neural Networks

A. Azzini et-al [10], researched a diagnostic tool that can be added to an AC drive control system using non-invasive techniques (requiring no modification of the AC inverter) or dedicated sensors. Their research was based on using the AC inverter input terminals as the only accessible point on the system.

With the proposed approach, useful diagnostic indications can be obtained by a low-cost extension of the monitoring activity. In this way, the reliability of the obtained indications can be significantly increased considering the combination of advanced time frequency transform, or time - scale, such as wavelets, and a new evolutionary optimisation approach based on Artificial Neural Networks (ANNs).

Due to the variety of different AC drive designs, a system that relied on accessing the internal control elements of an inverter would be difficult to implement in the real-world and most inverter units are

generally considered by their users to be a 'black box' where there is no modification work ever undertaken inside the unit. The concept of opening the unit up to access internal components and signals is not an approach that would be appropriate, since with new equipment, this would almost certainly invalidate the manufacturer's warranty.

A system of fault detection that is totally customised to the application, using dedicated sensors for the purpose is bound to achieve a level of diagnosis that is more reliable than a system that does not. Clearly, there is a trade-off to be made. The trade-off is that in many applications, it is more important to recognise a fault or no-fault condition in the unit without needing any further information (i.e. which particular component inside the inverter has failed). Further diagnosis can be done off-line once the unit has been replaced. Providing that an abnormal condition can be reliably detected in the beginning of the fault situation, then this will be of great importance to the user of the equipment. Some typical faults were identified, classified and studied in this research and Figure 6-4 details these:

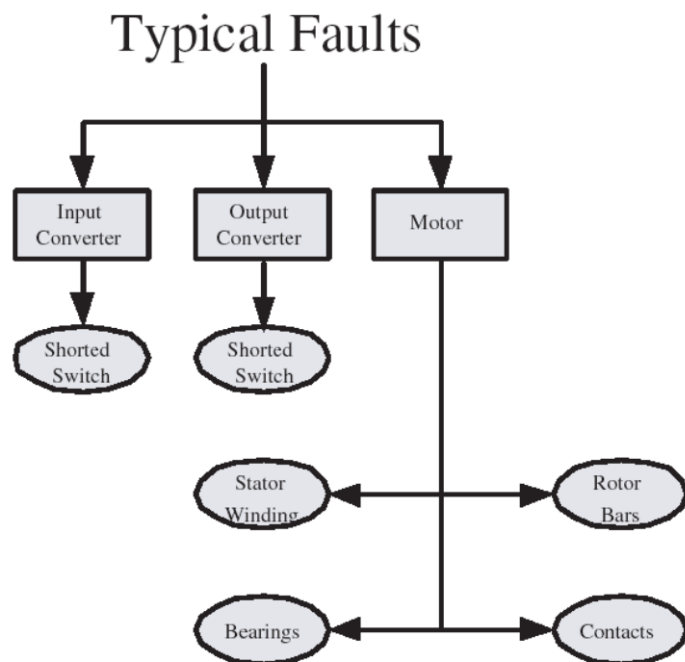


Figure 6-4 - Classification of common fault types [10]

The research involved the use of Artificial Neural Networks (ANN's) and in particular "biologically inspired computational models that use evolutionary algorithms (EAs) in conjunction with artificial neural networks (ANNs) to solve selected problems."

A block diagram of the actual inverter system investigated is shown in Figure 6-5 below:

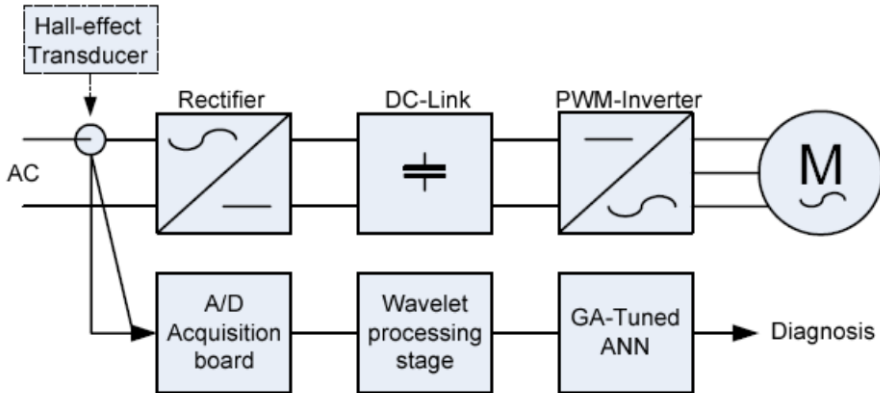


Figure 6-5 - Block diagram of an AC drive with highlight on the measurement location and processing flow [10]

The operation of the system in relation to measurement and processing of data is as follows:

- The current signals are acquired at the input terminal of a PWM inverter connected to a three-phase induction motor (230V, 50Hz).
- The numerical representation of the current signals are then elaborated by a Matlab function to perform wavelet processing [48], [49]:
 - o Perform the wavelet decomposition using the mother wavelet Daubechies 3;
 - o For each level of decomposition extract the coefficients with maximum value;
 - o Build a vector of selected coefficients and normalize the vector to infinity norm;
 - o Associate it to a fault index C equal to 1 (fault condition), or 0 (normal condition).

The tests were run on a motor with an inserted fault of high resistance in one of the rotor phases. The experimental settings are given in Table 6-5 below:

Table 6-5 - Experimental setup settings [10]

Motor			Inverter
Condition	Location	Fault Type	Frequency
Fault	Rotor	Additional 50 Ω on KL phase	10
Fault	Rotor	Additional 100 Ω on KL phase	25
Fault	Rotor	Additional 200 Ω on KL phase	30
Fault	Rotor	Additional 500 Ω on KL phase	45
Non Fault	No Location	No Fault	10
Non Fault	No Location	No Fault	25
Non Fault	No Location	No Fault	30
Fault	Rotor	Phase K open	10
Fault	Rotor	Phase L open	25
Fault	Rotor	Phase M open	30
...

Ten simulation runs were performed for each of the conditions above so the network could learn the condition effectively. Figure 6-6 illustrates the expected condition (No fault – 0; Fault – 1) along with what the ANN algorithm produced. The expected result is indicated by a solid marker and the ANN result by an asterisk:

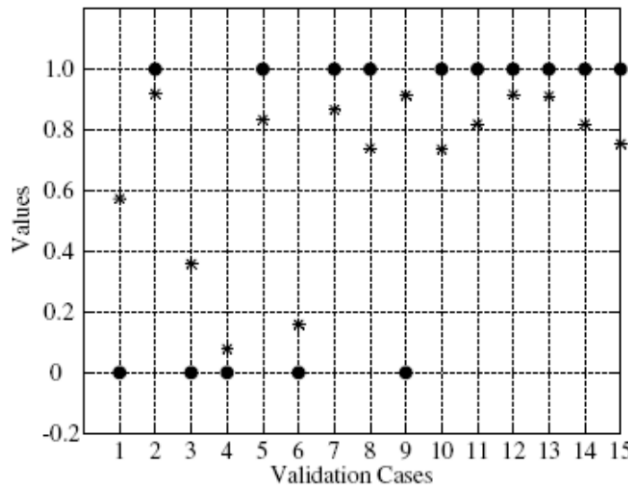


Figure 6-6 - Comparison between expected validation outputs and predicted [10]

The conclusions from these experiments showed that the ANN approach has been successfully applied to a real-world electric machine fault diagnosis problem. The methodologies were found by the researchers to give good results in fault and non-fault identification in electrical drive. Results obtained on the real-world problem compared well against alternative approaches based on the conventional training of a pre-defined neuro-fuzzy network with backpropagation (BP).

This research indicates that despite the Inverter being seen as a potential barrier to collecting useful information from the motor under fault conditions, if the correct data analysis is applied, good information on the motor condition can still be obtained from the supply signals. This research will be especially useful if the motor and inverter are combined into a single package (as some newer designs are) and the unit is in a remote location.

6.3.2 Fault Diagnostics in an Inverter Feeding an Induction Motor

Khater Faeka et-al [11], studied using fuzzy logic to diagnose faults on a three-phase voltage source inverter. The research was based on a time-domain model and different inverter faults were simulated with the resulting voltage spectrum being used to provide the database for the fuzzy logic system to work from.

In contrast to the previous research under heading 6.3.1, this concentrates on developing fault diagnosis for the Inverter itself. This was due to the fact that while several techniques have been developed for fault diagnostics and fault diagnostics model of an induction machine, there has been limited work carried out to investigate fault diagnostics in the inverter. The research was to propose an adequate method to determine fault types and their location in the inverter. Figure 6-7 illustrates the drive system with data monitoring and processing feeding the developed fault diagnostics (FD) system.

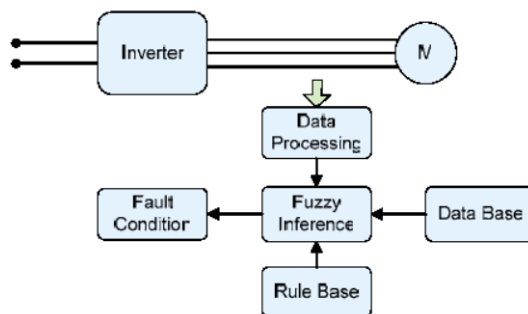


Figure 6-7 - Fuzzy logic fault diagnostics system [10]

Some techniques have previously been developed for detecting inverter faults and these are listed below:

- Open-switch FD in the voltage source inverter (VSI) feeding a synchronous machine drive system. The techniques utilize measurement of voltages at key points of the drive system and an analytical model
- Detection based on knowledge model using either current-vector trajectory or the instantaneous frequency to detect and identify the fault of an open transistor in the inverter.
- Knowledge-based expert system approach has been presented for fault diagnosis of a 3-phase inverter except the fly wheeling diodes – however limited to the most probable defect since the measurement information with Fourier analysis was not able to result explicit determination of the fault.

The fault modes of the VSI were investigated for the key fault types taken from the document published by Debapradad Kastha et-al [14]:

1. Input supply single line to ground fault (F1)
2. Rectifier diode short-circuit fault (F2)
3. Earth fault on dc bus (F3)
4. DC link capacitor short-circuit fault (F4)
5. Transistor base drive open fault (F5)
6. Transistor short-circuit fault (F6)
7. Line-to-line short circuit at machine terminal (F7)
8. Single line to ground fault at machine terminal (F8)

These are shown in Figure 6-8:

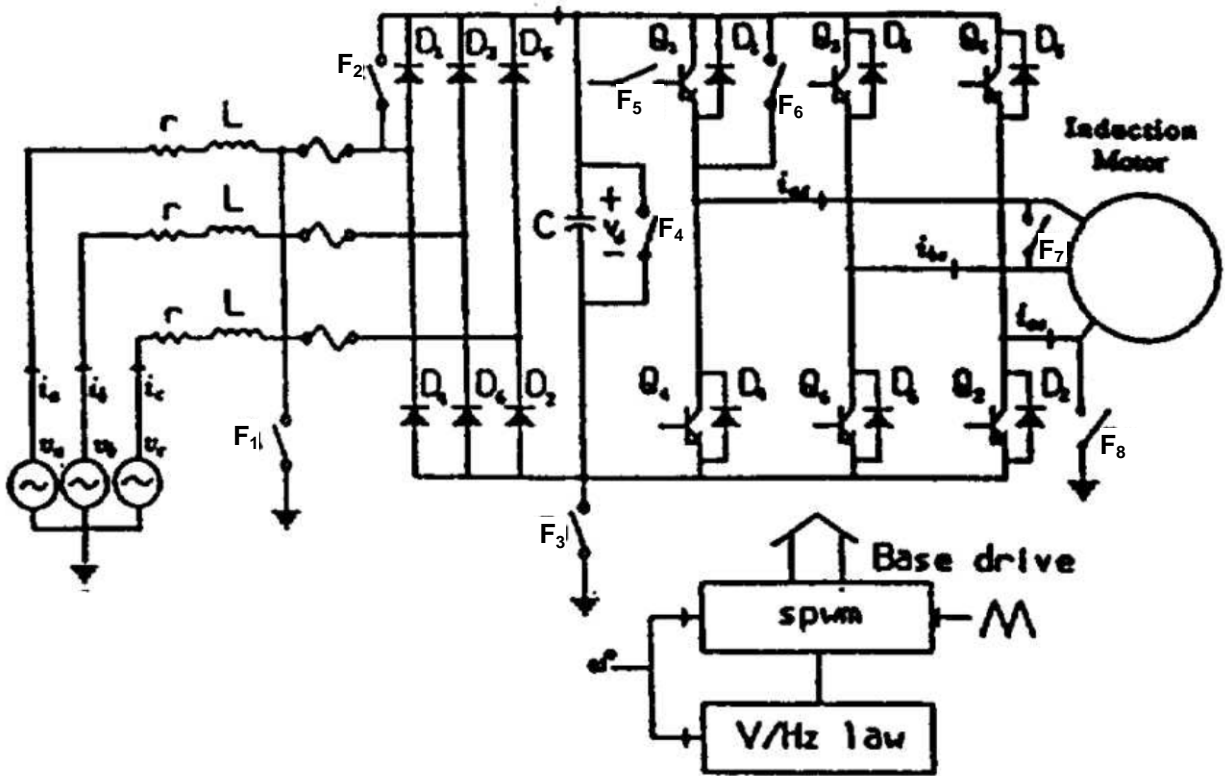


Figure 6-8 - A voltage-fed PWM inverter system indicating the possible failure modes [14]

This study concentrates on the IGBT circuit switches and rightly notes that "...short circuit faults at the inverter output occur as short circuit at the machine terminals and thus protection system activates the circuit breaker but often fails to define faults in the power semiconductor switches (IGBTs)." [54] As stated at the beginning of this chapter.

Faults that can occur in the drive IGBT circuits are:

1. Open circuit faults in :
 - a. One switch (upper or lower)
 - b. Two switches for different phases (same side of dc bus)
 - c. Two switches for different phases (different sides of dc bus)
2. Short circuit faults in :
 - a. One switch (upper or lower)
 - b. Two switches for different phases (same side of dc bus)

Simulation models were developed for healthy and differing fault conditions (open and short-circuit faults) to provide details on the waveform and the spectrum of voltage and current both before and after the fault occurrences. FFT's were used on the signals obtained and it was found that each fault condition had a distinct "salient waveform feature" that distinguished it from other faults.

This is indicated in the figure shown next (phases a, b, and c shown from top to bottom). The healthy inverter case indicates no even harmonic components and no dc components (Figure 6-9(a)) whereas (b) shows with one of the six switches open that even harmonic components appear in all phases in particular the second harmonic with the largest value occurs in phase A.

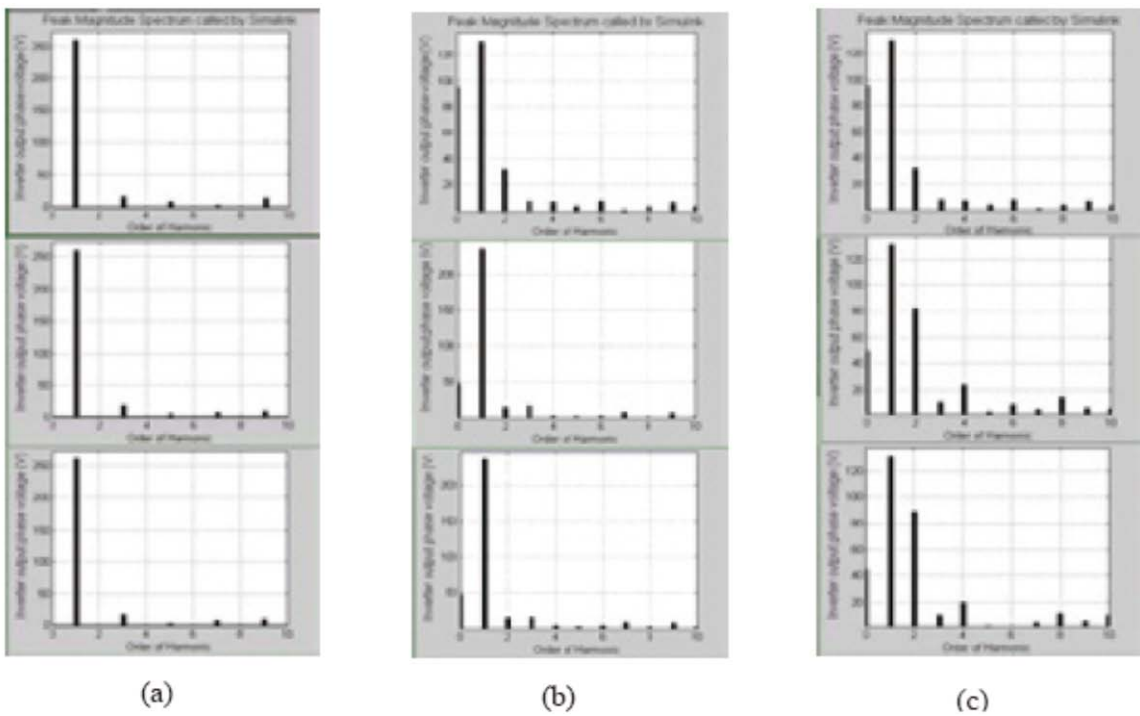


Figure 6-9 - Inverter voltage spectra: (a) healthy case (b) one switch open (c) one switch short [14]

6.3.3 Fault Detection of 3-Phase VSI using Wavelet-Fuzzy Algorithm

Research carried out by M.Rozailan Mamat et al [12], was designed to help detect firing faults in the IGBT circuit of the inverter drive. Results were promising - the developed system was rigorously assessed theoretically and experimentally, and it was shown that the system is robust and reliable. The system uses a real-time condition-monitoring algorithm for 3-phase pulse width modulation (PWM) inverter in fuzzy speed controlled induction machine.

They found that by analysing the supply variations to the motor after component failure and creating equivalent circuits for this, they could create algorithms for the faults that a higher system would use to provide the base-line for fault indication. One examination was of a MOSFET transistor failure (T1 in case of Figure 6-10)

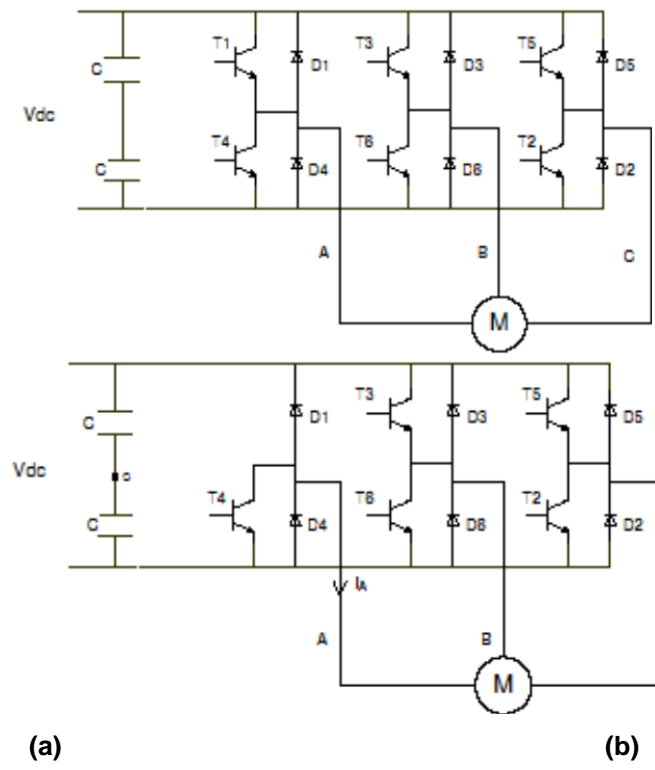


Figure 6-10 - A PWM voltage-fed inverter of induction motor (a) and after fault occurrence (b)

[14]

This chapter describes the methods used to perform testing on the experimental test rig. Following on from the successful commissioning and validation of the test rig equipment, it is now possible to proceed with testing and record accurate results.

Chapter 7

Fault diagnosis of experimental inverter-driven motor system

Particulars of the data acquisition equipment are firstly presented. Following on from this, the testing on healthy gearbox equipment is described. Testing then proceeds to the faulty gearbox equipment and at the end of all tests, results from the two tests are compared and analysed.

7.1 Introduction

A fault is implemented on the motor gearbox fitted to the test rig (see the technical details for healthy gearbox in Table 4-1) and the experimental data is compared between healthy and faulty gearbox. These tests take the form of a model-based approach, whereby a healthy system is first tested and used as a baseline for the results. Testing on faulty system is hoped to reveal differences in the model data compared to the actual faulty data.

The data collection equipment will be described, followed by the actual tests and results obtained. All commissioning tests have been performed prior to this run (see Appendix C) so the results can be relied upon to be accurate. Modifications made to the data acquisition system to collect additional information from the modified test rig are given in Appendix A.

7.2 Data Acquisition System

Data from the test rig will be fed to an external data monitoring system. Transducers, namely an accelerometer and angular speed encoder, have been fitted directly on the test rig. Each transducer produces a voltage output proportional to the amplitude of the measured parameter and each is connected to a data acquisition (DAQ) system by coaxial BNC cables to reduce signal noise.

The placement of transducers is presented in Figure 7-1

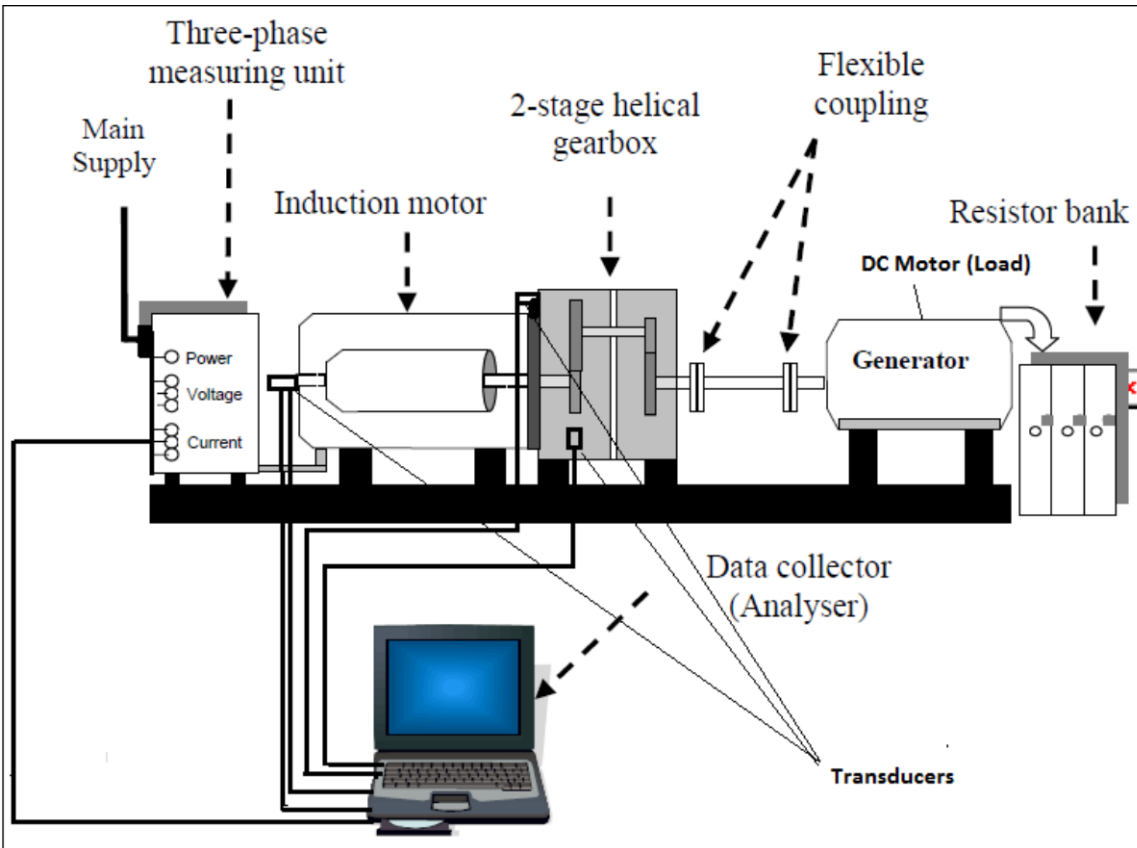


Figure 7-1 - Setup for experimental gearbox test rig

Accelerometers with frequency range 0-40 kHz, sensitivity 74mv/ms-2, and acceleration of up to 2000ms-2 are positioned directly at the side of the gearbox itself and at the top induction motor flange (near gearbox) to measure vibration levels. Each accelerometer is connected via a screw-threaded brass stud bonded to the casing with ceramic cement, which helps avoid over-heating.

Shaft Encoder - An incremental optical encoder (Manufacturer: Hengstler; Type: RS32-O/100ER) is used to measure Instantaneous Angular Speed (IAS). It is fitted to the end of induction motor shaft itself via a bracket mounted to the fan cowl (see Figure 7-2). The encoder is directly connected to the computer via the DAQ system. There will be 100 pulses per revolution of the motor.



Figure 7-2 - Mounting of motor encoder

Specification of the encoder is as follows;

Shaft diameter: 5 mm / 6 mm

Absolute maximum speed: max. 6,000 RPM

Vibration proof (IEC 68-2-6): 100 m/s² (10 ... 2,000 Hz)

Devices for Current and Electrical Power Measurement – A digital photo and diagram of the three-phase current measurement unit are presented in Figure 7-3 and Figure 7-4 respectively. The motor current and voltage in each phase are measured using a PCB-mounted hall-effect current transformer (CT). A measured value for the current in each line is fed into the DAQ unit, which converts this into a voltage measurement, provides appropriate filtering and anti-aliasing, and feeds the signals to the data collection channel of a data collector / analyser. Thus, this unit can be used to measure the instantaneous current in each of the three phases, the instantaneous voltage of each of the three phases and the instantaneous electrical power supplied by each of the three phases.

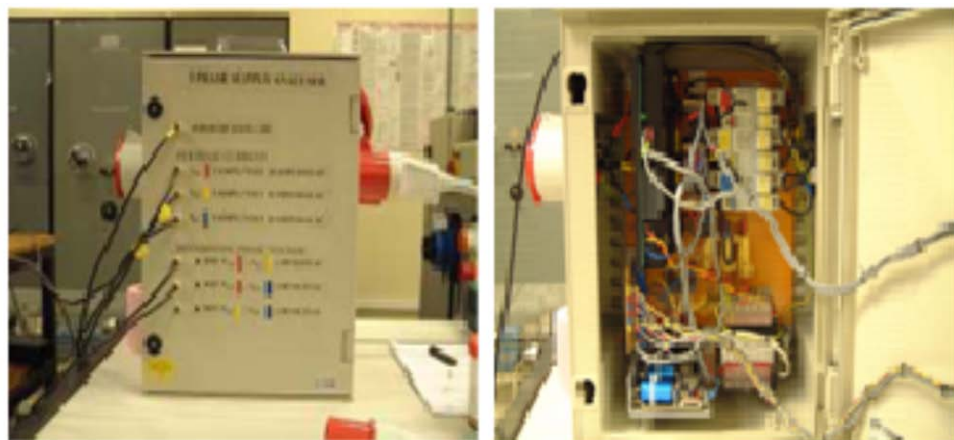


Figure 7-3 - Three-phase current measuring unit

In Figure 7-4;

VL_1L_2 , VL_2L_3 and VL_1L_3 are line to line voltages;

IL_1 , IL_2 and IL_3 are the three line currents.

- = Hall Effect Voltage Transducer
- = Hall Effect Current Transducer

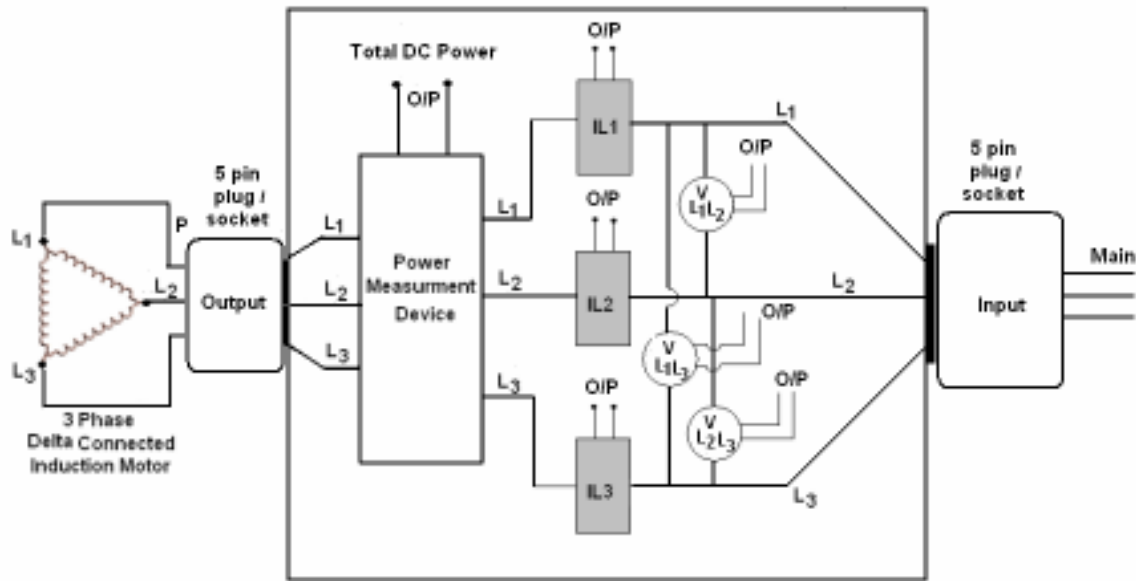


Figure 7-4 - Diagram of three phase measurement unit

Data acquisition process

The data acquisition system is configured to take a maximum of 15 channels, of which a total of 10 will actually be used for this condition monitoring application. A PC card is connected to a spare PCI (Peripheral Card Interface) slot in the computer. This configuration is shown in Figure 7-5 below:

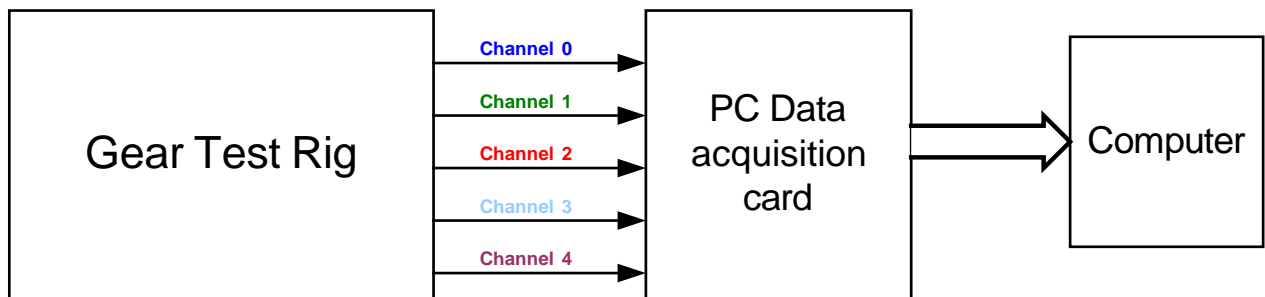


Figure 7-5 - Diagram of measured signals

Channel 0 – Blue: signal from shaft encoder (1 pulse / revolution) to determine average speed calculation

Channel 1 – Dark Green: Signal from shaft encoder (100 pulses / revolution) for Instantaneous Angular Speed

Channel 2 – Bright Red: Motor current

Channel 3 – Yellow: Vibration signal from gearbox

Channel 4 – Dark magenta - vibration signal from motor flange

These five signals are measured from the test rig and sent to the data acquisition system which is connected with a software package allowing the display of virtual instruments on the computer screen.

The data acquisition system display is shown in Figure 7-6:

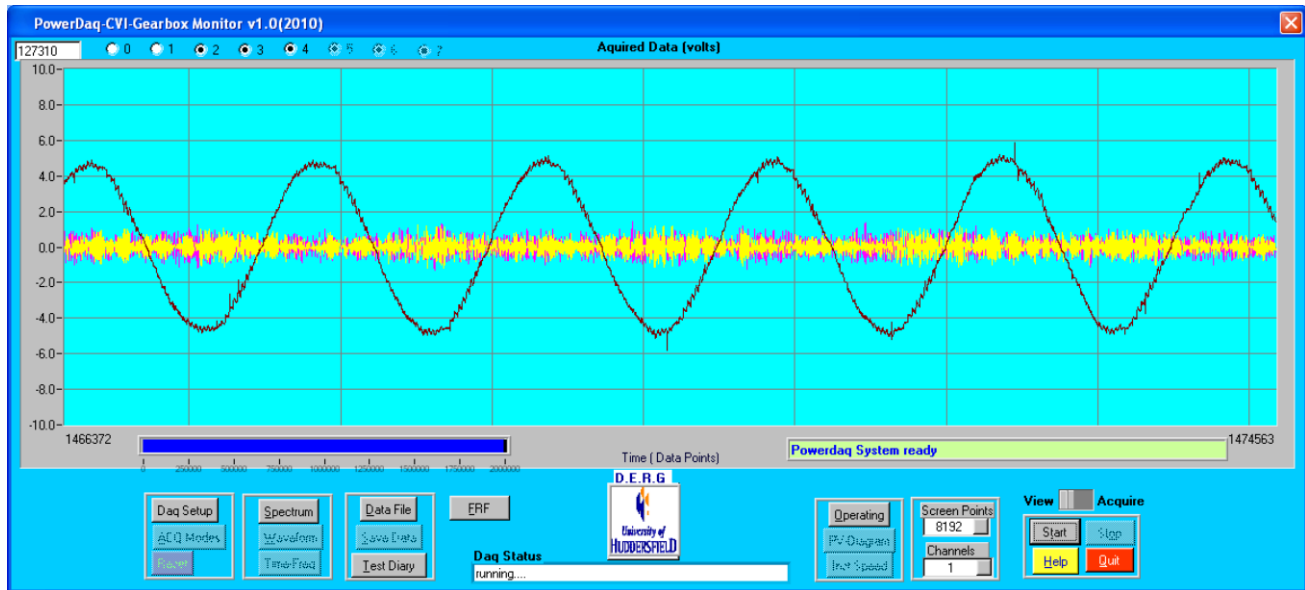


Figure 7-6 - Screenshot of measured signals

Also, the software allows the display of operating conditions through a real-time ‘dashboard’ in Figure 7-7:

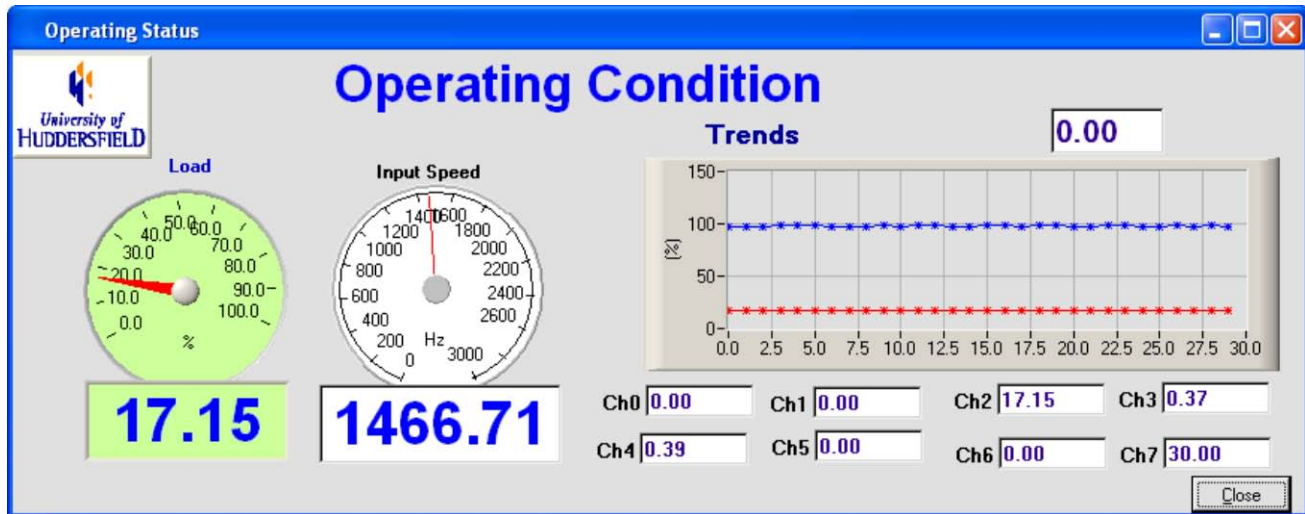


Figure 7-7 - Screenshot of operating status through 'dashboard'

7.3 Measurement of experimental data for healthy and faulty gearbox

Two sets of tests will be performed for the healthy gearbox and another two sets of tests will be done for faulty gearbox in order to check the repeatability and reliability of the measurement procedures. Figure 7-9 and Figure 7-11 contain the measured values for the healthy gearbox for the following variables: DC motor armature current; load set; AC motor speed feedback; AC motor torque feedback; AC motor current; AC motor speed demand. The same variables are measured after the fault (introducing a break in tooth number 47 from the gearbox primary drive set) was implemented in the gearbox and the results are shown in Figure 7-12 and Figure 7-13.

The commands included in the PLC program are set manually on the operator screen and their relevant details are shown in Table 7-1.

Table 7-1 - Simulation data set for all healthy and faulty gear sets

Step	Speed (%)	Load (%)	Time (s)
1	100	0	60
2	100	20	60
3	100	40	60
4	100	60	60
5	100	80	60
6	100	100	60

A key for each of the data plots in the graph is as follows together with a description and scaling factors:

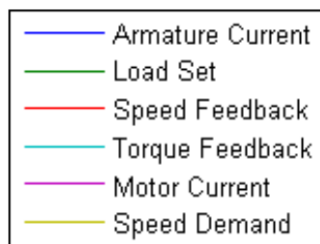


Figure 7-8 - Simulation plots colour key

Table 7-2 below gives more information on each of these signals collected:

Table 7-2 - Data plot signals and scaling factors

Value	Description	Scaling
Armature current	Measured current in DC motor armature from a C.T. mounted on the resistor bank	0 – 100% = 0 to 200A
Load set	Load set by the test rig PLC and output to the DC motor field controller	0 – 100% = 0 to 4.0A Field current
Speed feedback	AC motor speed feedback indicated by the AC inverter	0 – 100% = 0 to 1470 RPM
Torque feedback	AC motor torque feedback indicated by the AC inverter	0 – 100% = 0 to 71.5 Nm (Full-load-torque)
Motor current	AC motor torque feedback indicated by the AC inverter	0 – 100% = 0 to 20.9 A
Speed demand	Speed output from the test rig PLC to the AC Inverter	0 – 100% = 0 to 1470 RPM

Measured data for healthy gearbox (Test number 1)

Figure 7-9 shows the measured values for the healthy gearbox and the following aspects are worthy to be noted:

1. The load setpoint has been set to give an actual torque feedback of 20, 40, 60, 80%, rather than a load setpoint of 20, 40, 60 and 80%. This is due to the relationship between

- the DC motor load and the motor torque feedback not being entirely linear (i.e. a load setting of 20% will not yield a 20% torque feedback from the motor).
2. The DC motor armature current follows the increase in DC motor field current in the same proportion, as we would expect – the relationship between DC motor field current and armature current produced was proved to be linear during the commissioning tests.

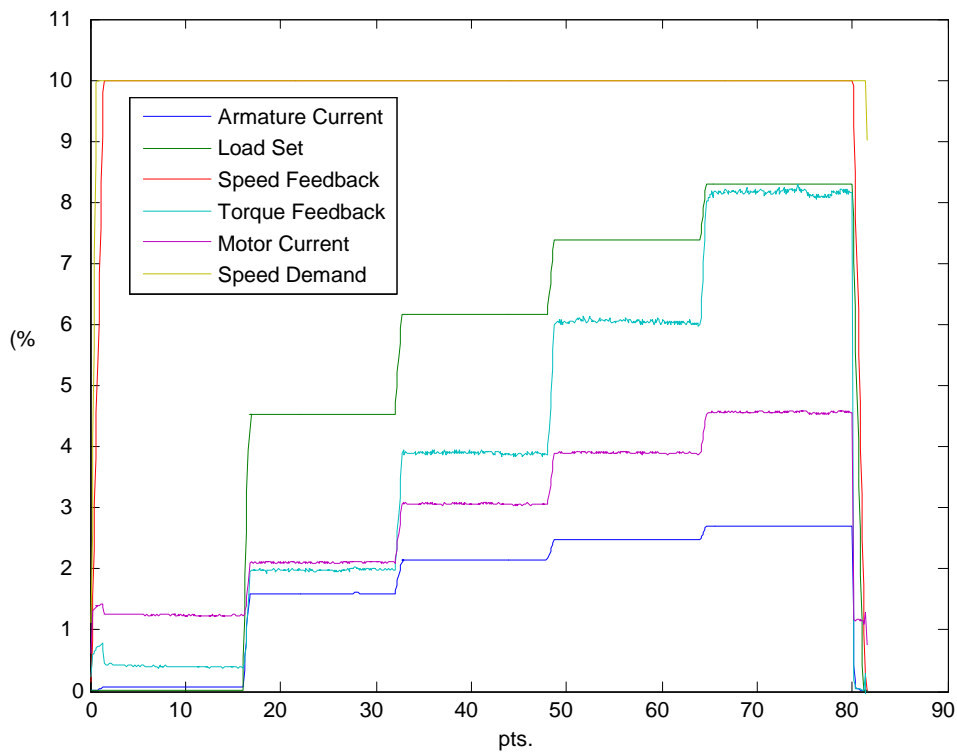


Figure 7-9 - Measured data for healthy gearbox – Test number 1

The healthy gearbox shows that a flat torque response exists at each of the load settings. At the 60% torque figure, motor torque is observed to fall away slightly before the next load increase is applied and at 80% torque, there is a dip in the torque feedback before the end of the test is complete.

Figure 7-10 shows that the lowest point on the graph for torque feedback can be observed at data point 762. By plotting the torque feedback and DC motor armature current, it can be seen that the two values follow the same pattern. Therefore, it could be said that the dip in motor torque was not gearbox-related, but due to a fall in armature current. This could be the field controller, but because no active measurement of field current is being taken, this is difficult to prove.

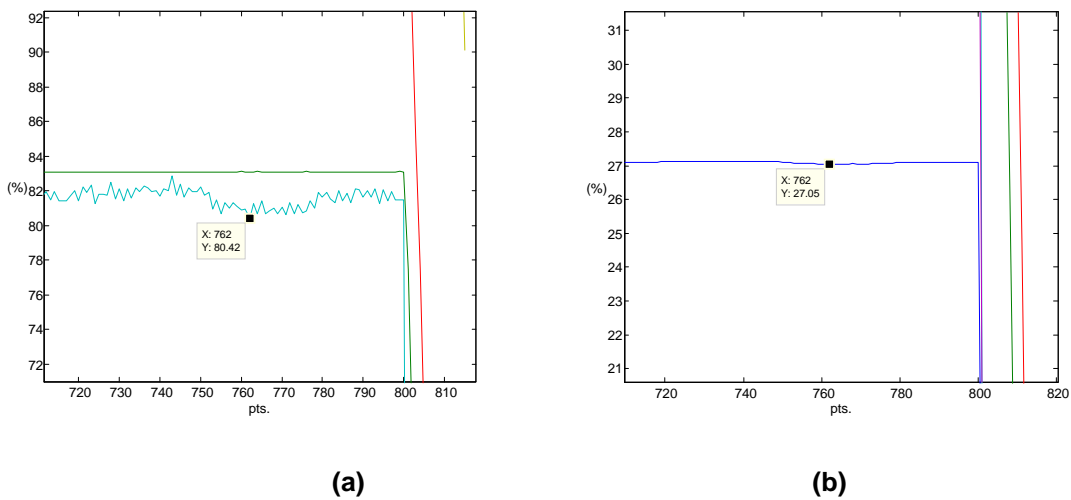


Figure 7-10 - Comparing motor torque (a) vs. armature current (b)

Measured data for healthy gearbox (Test number 2)

Test number 2 will follow exactly the same load test parameters and the measured data is presented in Figure 7-11.

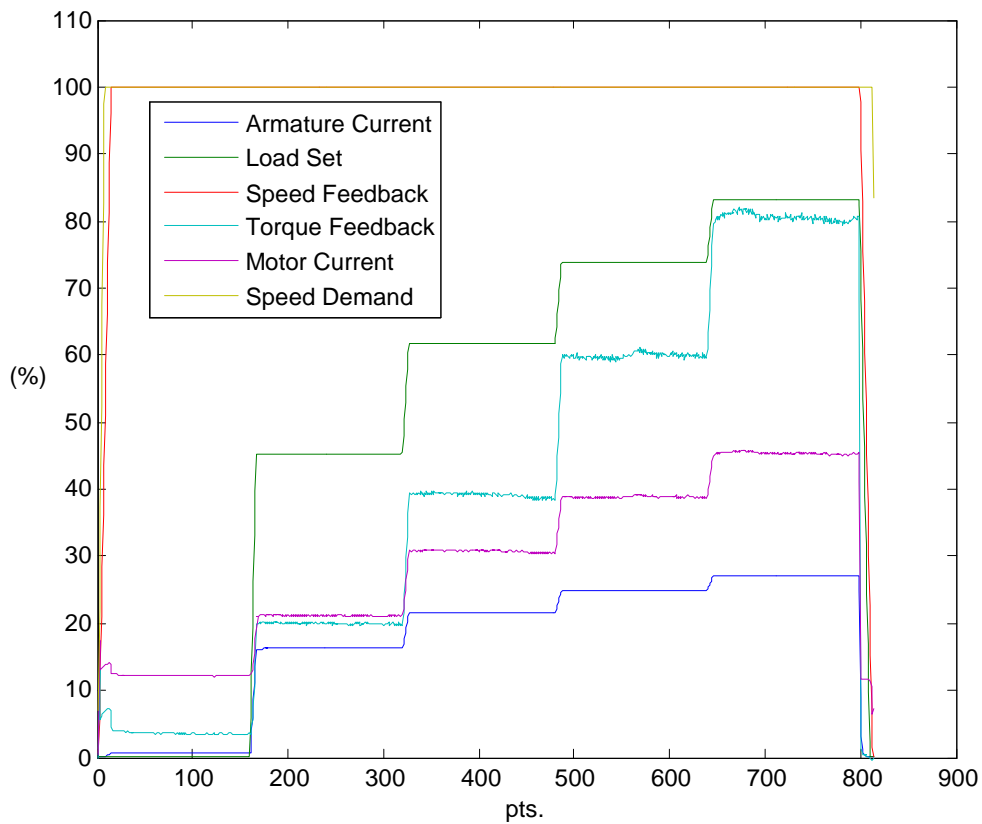


Figure 7-11 - Measured data for healthy gearbox – Test number 2

The motor torque readings at 60% and 80% show a greater disturbance in Figure 7-11 than Figure 7-9. Mid-way through the 60% torque feedback, the value sees a minimum of 59% and a maximum of 61%. The 80% value peaks at up to 82%, before falling back to 79%. Again, if this is compared to the DC

motor armature plot, it can be seen that this is repeated therefore it was concluded that the measurement procedures are reliable.

Measured data for faulty gearbox (Test number 3)

The same commands have been applied to the PLC and the following variables have been measured for the faulty gearbox: DC motor armature current; load set; AC motor speed feedback; AC motor torque feedback; AC motor current; AC motor speed demand. These variables are the inverter drive signals.

The experimental data for Test number 3 is shown in Figure 7-12:

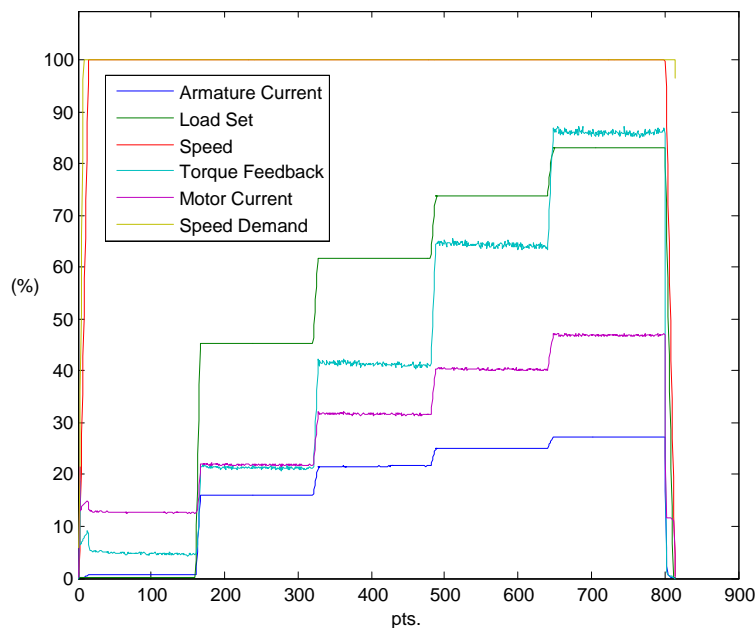


Figure 7-12 - Measured data for faulty gearbox – Test number 3

Measured data for faulty gearbox (Test number 4)

The second test is done for the faulty gearbox and the measured results are presented in Figure 7-13:

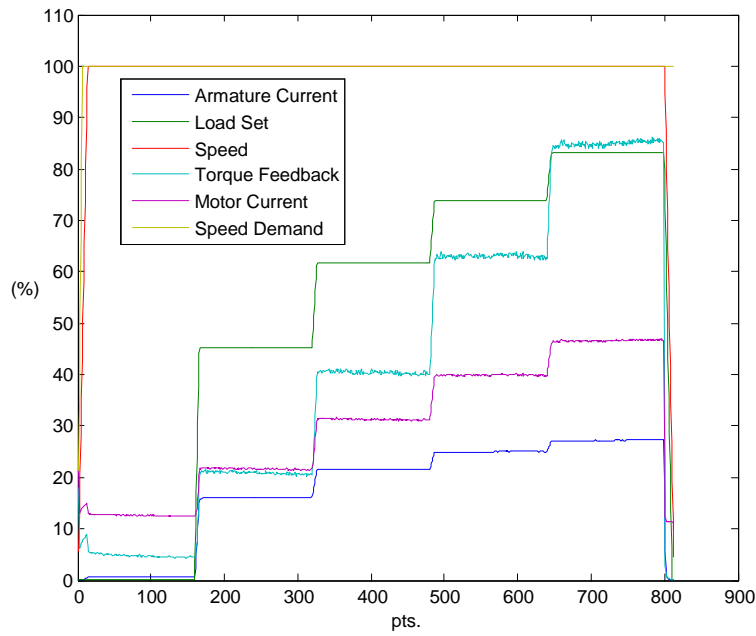


Figure 7-13 - Measured data for faulty gearbox – Test number 4

Once again the comparison of the experimental data for the faulty gearbox produced good results (there were no major differences between the measured values) so the conclusion was that the measurement procedures are reliable.

Comparison between measured data for Test number 1 and Test number 3

The experimental data measured by the inverter for healthy gearbox (solid line) is plotted on the same graph with the measured results for faulty gearbox (dotted line) and is shown in Figure 7-14

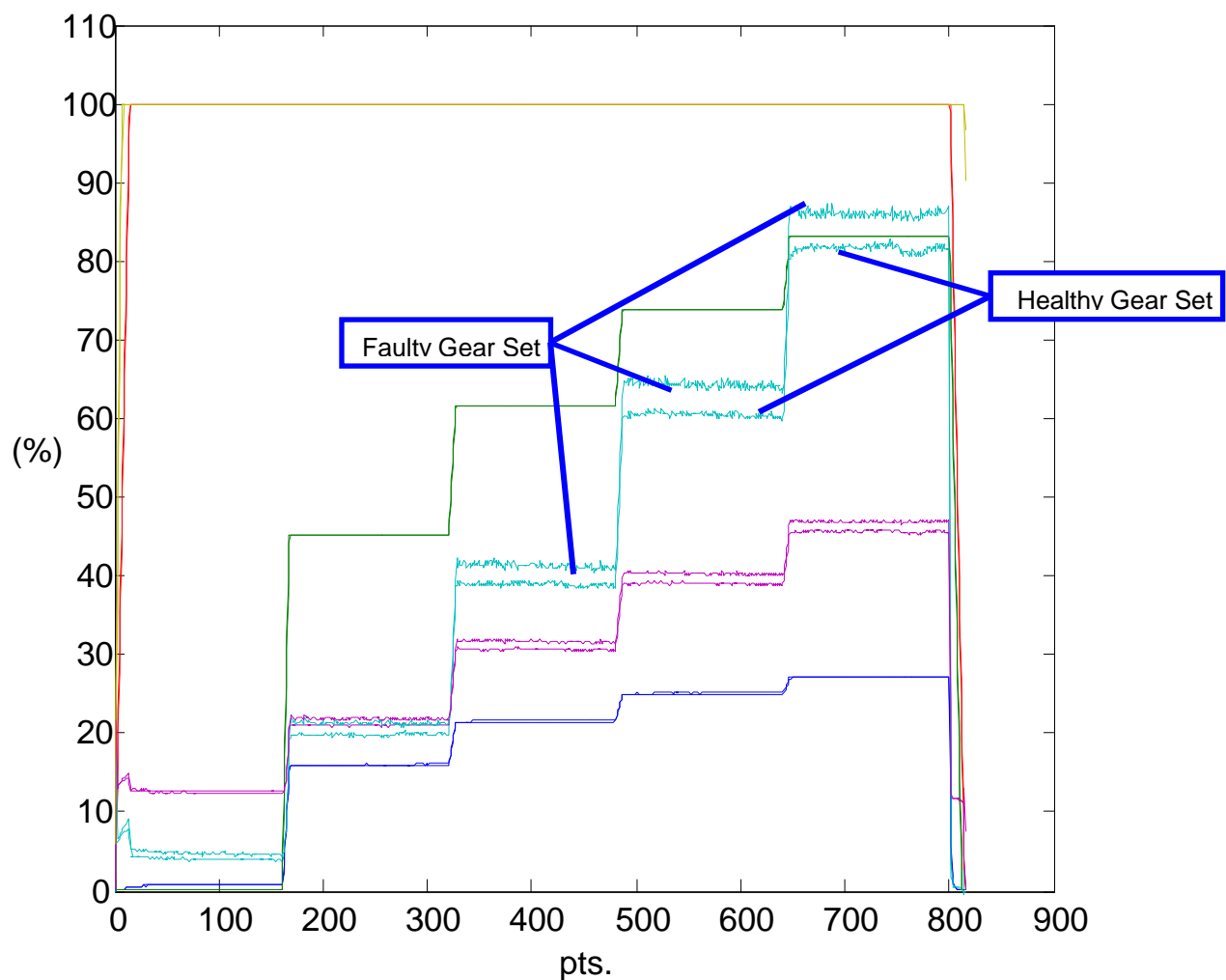


Figure 7-14 – Comparison of experimental data for Test number 1 and Test number 3

Healthy gear set: Solid line

Faulty gear set: Dotted line

From the two sets of results, it is immediately clear that the torque feedback from the drive with the faulty gear set is higher than that of the healthy set because it is necessary to produce more work to overcome this defect. In addition to this, the torque demand is higher once the load setpoint has changed, gradually dropping off as the test rig stabilises. The same can be said of the motor current value. The motor speed feedback remains constant throughout the range of loads applied.

Comparison between the actual AC motor phase currents for test number 1 and test number 3

Comparing actual motor currents (measured from a C.T. in one of the motor phases) between Test number 1 and test number 3, the effect of the faulty gear set on motor current can be seen to manifest itself in a different manner to that observed from experimental data measured by the inverter (see Figure 7-14) and it is presented in Figure 7-15.

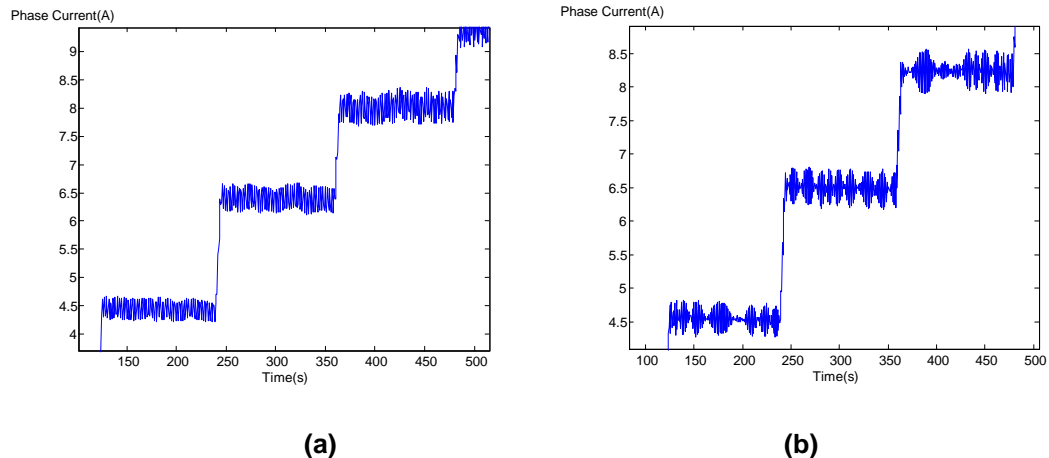


Figure 7-15 - Comparison between the actual AC motor phase currents
(a) healthy gearbox ; (b) faulty gearbox

Torque pulsations from Figure 7-15 (b) have a different pattern than those from Figure 7-15 (a) as expected. These pulses can last between 20 and 5 second periods and there are no such oscillations observed on the healthy gear set. One suggestion is that these pulses can occur on a system that is ‘under-damped’ in terms of gain values applied to the speed or current loop. As the faulty gear rotates, there is potential for greater backlash in the gearbox and this will reduce the damping effect of the load that the motor is driving, the result being an oscillation in the drive speed loop and therefore the current demand to the motor.

The sampling rate of the DAQ system limits the examination to a time-domain analysis – the rate is too low to allow FFT to be performed and a frequency analysis to be performed.

By comparing each of the healthy and faulty data gearbox sets on the same graph, the differences in the signals become easier to visualise. Figure 7-16 below gives the two actual measured current signals and it is obvious that the values for the motor actual current for a faulty gearbox become greater than the actual motor current when a healthy gearbox is installed in the electrical drive. This was expected because the torque feedback is increasing and the controller has to produce higher demand values in order to compensate for a faulty mechanical transmission. The inverter signals follow the same pattern therefore it is possible to use them instead of actual motor current for fault-detection purposes and more details about the usefulness of using these signals are presented in Chapter 8 (section 8.4).

The comparison between measured current signals for healthy and faulty gearbox is showing that the AC motor (actuator) can be used as a transducer for detecting electrical and electromechanical faults on an inverter-driven motor system. The next step was to analyse in more depth the differences between the two sets of measured data and the next paragraph is explaining this approach.

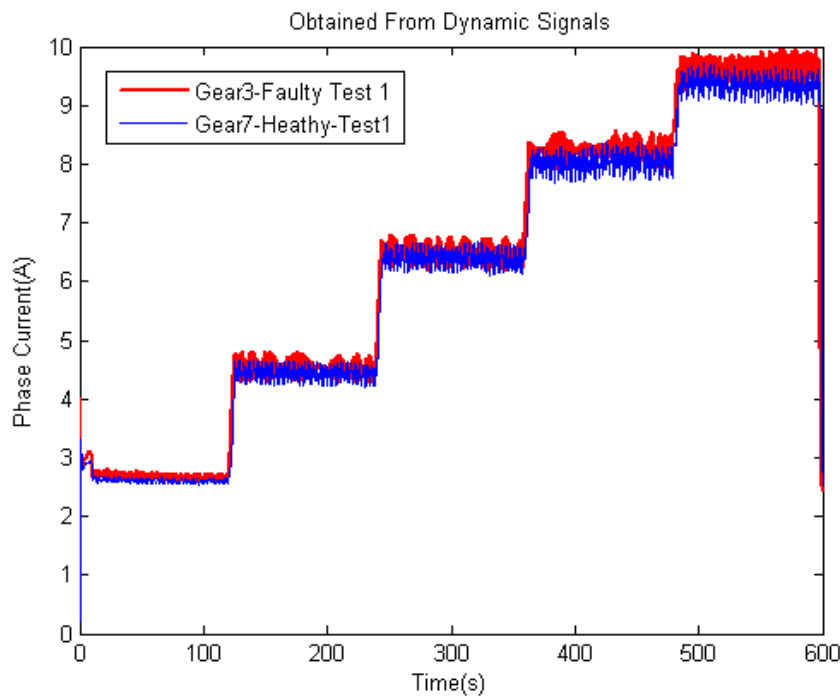


Figure 7-16 - Measured current signals for healthy and faulty gear set

Advanced data analysis for the differences between the measured inverter drive torque feedback for Test number 1 and Test number 3

Several Matlab programs implementing algorithms for advanced data analysis have been produced by the researchers from Diagnostic Engineering Research Centre within the University of Huddersfield. I would like to express my special thanks to Dr Fengshou Gu for giving me access to these programs and assisting me on using the programs to analyse the experimental data.

The data analysis is based on the system modelling method. The system on the experimental test rig is shown by Figure 7-17.

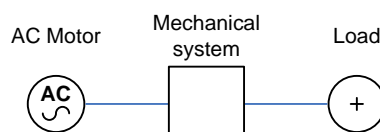


Figure 7-17 - Experimental Test Rig System

The healthy data set is then used as the 'System Model' reference for the model. When the test rig faulty data is obtained, this is given as the 'Actual System' in the model shown in Figure 7-18 :

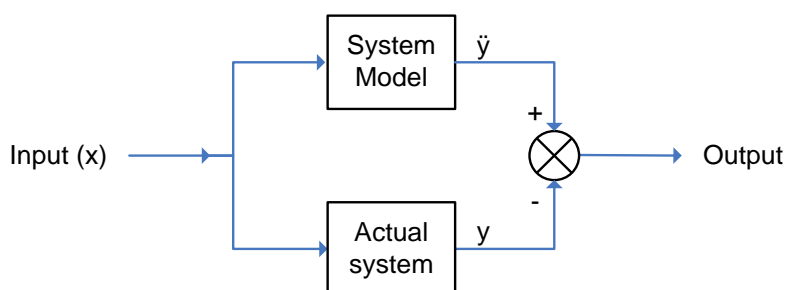


Figure 7-18 - Model reference system used for data analysis

If both sets of data were the same, the output from the model system ($y - \hat{y}$) would be zero. Any faults present in the actual system will bring the output from the system above zero.

Figure 7-19 shows the results for the comparison of measured torque feedback values between the healthy and faulty gear set. The following steps have been taken:

1. A simple subtraction of torque feedback is taken between the values from each set over time;
2. The root-mean-squared value of differences in the % torque feedback is calculated at each data points to measure the difference;
3. The difference is normalised by nominal current to remove the effect of load settings

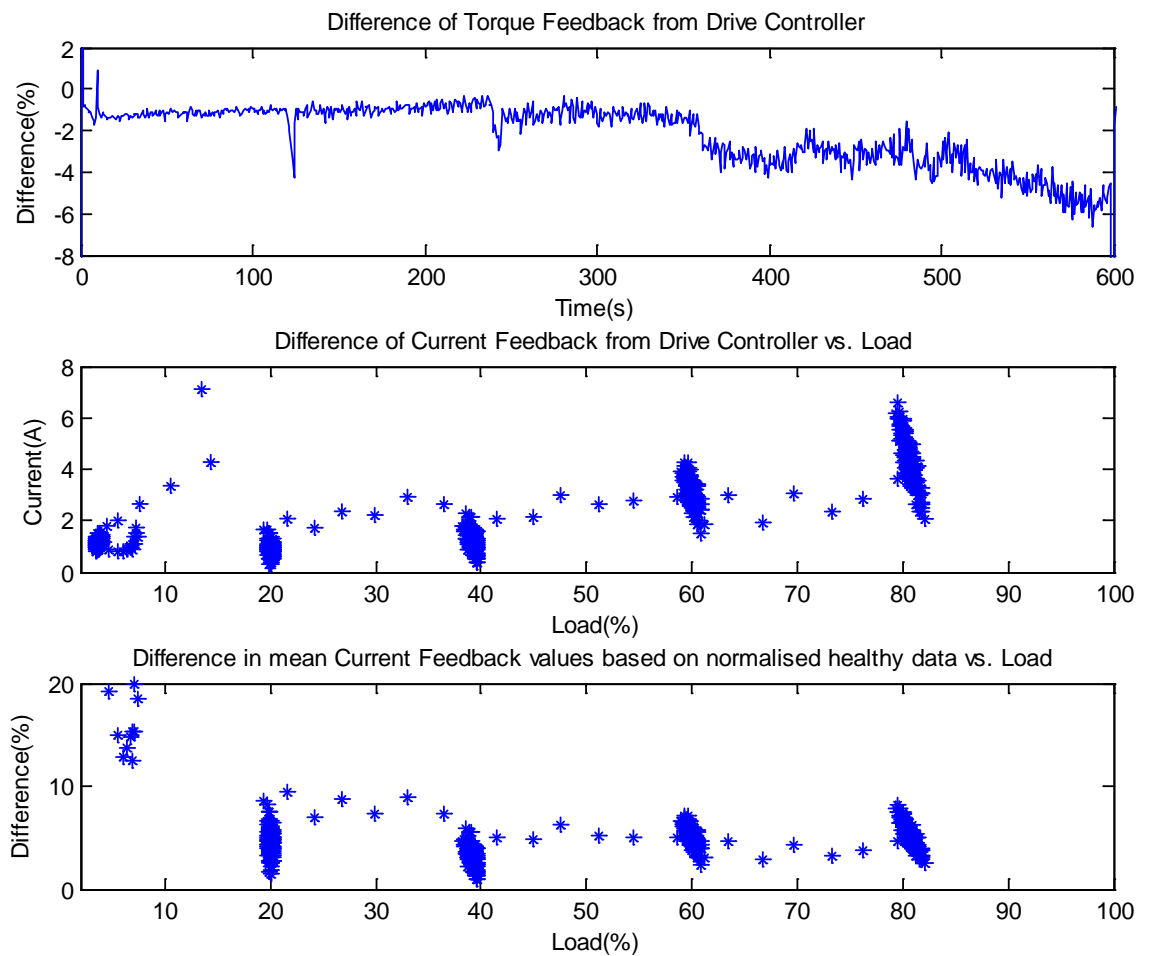


Figure 7-19 - Comparison of torque feedback values from drive measured between a healthy and faulty gear set

As shown in Figure 7-19, the normalised data set (bottom) shows that the error percentage stays the same at each load level, whilst the non-normalised data (middle) naturally gives a higher % difference at higher values of torque, as this is where the greatest difference in values occurs. RMS (Root-Mean-Squared) values are used for the non-normalised data because the peak deviation between the measured signals is so high. Both the middle and bottom data sets indicate the output from our model reference system shown in Figure 7-18.

For a monitoring system that is to trigger faults from a percentage value difference being greater than a set threshold, then the normalised data analysis method is preferred. There will be no requirement to modify the threshold value as the value of torque feedback increases because the data is normalised dynamically to the healthy data set.

If both data sets were from healthy gearboxes, we would expect the points at each load setting to be grouped closer together to form a circle pattern, rather than a line.

Advanced data analysis for the differences between the actual current feedback (measured by Current Transformer) Test number 1 and Test number 3

Figure 7-20 shows the results for the comparison of measured actual current feedback between the healthy and faulty gear set after following the three steps mentioned above.

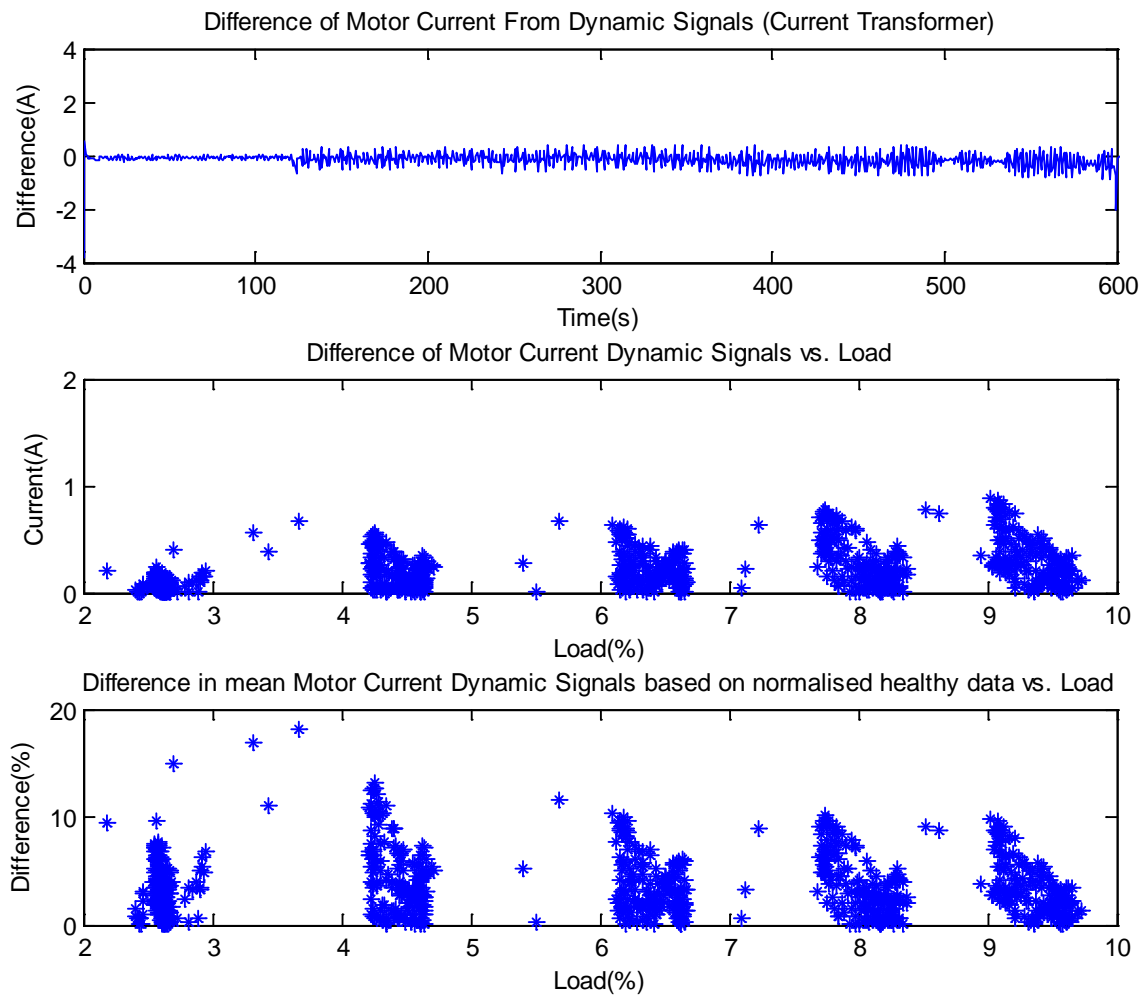


Figure 7-20 - Comparison between actual motor current signals for healthy and faulty gears

The grouping of this data is more spread-out at each load, but it must be considered that the actual current value is non-sinusoidal coming from the PWM drive and the X-axis data spread is due to the fluctuations in currents measured as the drive switches and these fluctuations are not 'in-phase' from one test run to the next. If we zoom into the phase current signal measured, the 'sawtooth' current signal obtained can clearly be seen

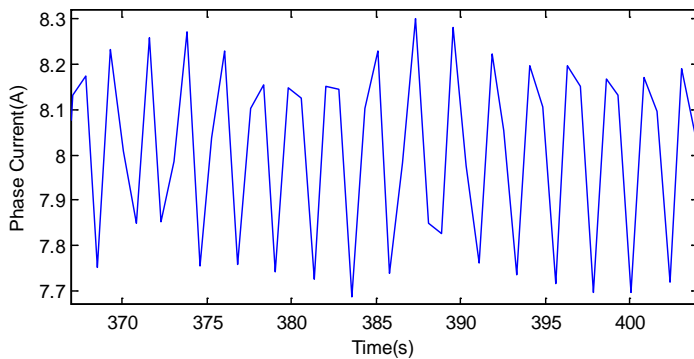


Figure 7-21 - Measured phase current waveform

If we try and subtract one current signal directly from the other, it becomes impossible to overlay the peaks of each signal exactly and that is where the wide data spread on the x-axis occurs.

However, by comparing the two results from Figure 7-19 and Figure 7-20 it can be seen that the drive torque output gives a sufficiently detailed signal to allow a comparison to be made between healthy and faulty gear sets from the torque signal obtained.

This is important, as it may be possible to perform additional data analysis on the signals output from a standard inverter drive. The 32-bit microprocessor that the inverter drive uses will rely on accurate current and voltage signals being measured by the drives own instruments. These signals may lose some resolution before being fed out to the drive analogue outputs but sufficient resolution may be retained.

After this initial research work was completed, the test rig has subsequently been used by the department to advance other methods of motor condition monitoring. These include vibration monitoring, instantaneous speed analysis and acoustic measurements. The rig will form a key part of allowing the department of diagnostic research to continue the advancement of motor condition monitoring.

The next chapter contains the conclusions of this research project and suggestions for further work.

Chapter 8

Conclusions and further work

This chapter will present a review of the project objectives and achievements. Following from these, conclusions obtained from the research work will be discussed. The key contributions are summarised separately. Finally, future work which is helpful in further development of the methods investigated in this thesis is discussed.

8.1 Review of Objectives

A review of the initial project objectives and achievements is given in this section.

Objective 1. Investigate actual motor condition monitoring techniques with a view to determining whether any existing research has been undertaken into the specific area of using the AC motor as a transducer together with the AC inverter signals for detecting electrical and electromechanical faults on an inverter-driven motor system.

Achievement 1. It was important to ensure that the research undertaken is not duplicating any existing works. From the literature review, it became clear that the area of using the inverter drive output signals to monitor and detect faults in the driven equipment is not one that has been studied in any detail. Therefore, the research work could continue in the knowledge that any results obtained would be a valuable research contribution in this field.

Objective 2. Research the operation of modern AC Flux-vector controllers with a view to using the latest inverter controller methods for these tests.

Achievement 2. The use of a Parker 690+ AC Vector Drive ensures that this test rig is using one of the most modern AC vector inverters on the market. Operation of the drive in true closed-loop mode with motor feedback encoder gives a high level of performance from a standard AC asynchronous motor. Results obtained from this rig can then be stated to be from with the most up-to-date drive technology and therefore the research is not restricted to use on old technology.

Objective 3. Design a test rig, using equipment that will meet the demands of the research work to be undertaken.

Achievement 3. The test rig design was successful as the most up-to-date drive equipment had been specified and incorporated into the rig, whilst keeping the project cost within the budget constraints. This equipment could also be upgraded in future if the test rig research demands changed.

Objective 4. Test and commission operation of the rig to ensure design criteria are satisfied. This will also involve running simulated test runs on the rig and analysing any results obtained.

Achievement 4. After designing and specifying the test rig from a clean sheet, the rig was then commissioned to ensure that the performance of the rig was up to the designed standard. However, after successful commissioning, initial research work was attempted on the test rig for an application

involving detecting motor gearbox faults. After running a series of tests, it was impossible to create identical test conditions for any test run. If any two sets of results could not be compared under like-for-like test conditions, then no further research could be carried out.

Objective 5. Design and implement improvements to the test rig if these improvements can be proven to return more accurate test results.

Achievement 5. A design to automate the test rig was developed to meet the conditions for repeatable tests. The incorporation of a PLC (Programmable Logic Controller), together with means of programming test conditions into the PLC, was shown to provide the test conditions required of the rig.

Objective 6. Perform simulated tests to prove that the test rig is providing accurate and repeatable test conditions

Achievement 6. From thorough testing, it was found that the test rig PLC modifications carried out as part of this research provided consistent control signals to operate the test rig and therefore maintained identical test runs. This was important as a research project commissioned by David Brown had to guarantee the same test conditions for each run to determine if there were different test results obtained from healthy and faulty gear sets. The modifications allowed this work to be carried out satisfactorily and results detailed in Chapter 7 provide conclusive proof of this.

Objective 7. Use the test rig to run a series of tests on healthy and faulty equipment.

Achievement 7. The PLC-automated test rig was eventually required to satisfy research demands on a key application involving motor gearboxes from a major manufacturer. This allowed both healthy and faulty gear sets to be exchanged in order to introduce the desired faults.

Objective 8. Investigate the signals received from the inverter drive to ascertain their usefulness in detecting fault/non-fault conditions on the faulty equipment

Achievement 8. Data was collected from the gearbox test rig and analysed using MATLAB. From a series of tests performed on the healthy and faulty gear sets, some clear differences in the signals received from the inverter were noted. This provided an important step forward in the research to show that there is good potential in using these signals to detect downstream mechanical faults. The detection method is novel as it uses the drive signals to monitor the load, rather than the motor currents.

8.2 Conclusions

Based upon these achievements, we can conclude that:

- The decision to design and build a test rig using the most up-to-date closed-loop drive technology provided an important starting point for this research. Closed-loop vector drive technology is unlikely to advance much further than it is at present, except by incorporating the technology into ever-smaller drive footprints, so any results obtained will remain valid for the foreseeable future. A modern closed-loop drive (such as the Parker 690+ unit) can provide the feedback signals required by an external data-logging system without any modification. Three analogue outputs were used in this case and this allowed the internal feedback signals of motor speed, current and torque to be ported out for measurement by external instrumentation with ease.
- The importance of selecting a mechanical fault that is typical of what will be encountered in industry is vital to ensure that the research will have value in industry. This came in the form of a true research project commissioned by David Brown to determine if gearbox faults could be detected by using the AC motor as transducer. Originally, this research was to be performed using a direct on-line (DOL) AC motor running at fixed-frequency but the principle of using the inverter drive signals to detect the fault was to be used instead. The gearbox chosen was a standard two-stage gearbox using two sets of helical gears. David Brown defined the faults to be simulated and provided actual faulty gear sets for this purpose. Having real-world faults present in the gearbox that were specified by the manufacturer provided ideal fault test conditions and paves the way for this research to be used on the many applications that use helical gearbox technology in industry.
- In an environment where tests are to be performed on a repeat basis, there must be a guarantee that one test is run in an identical manner to another. Test runs initially performed on the non-automated test rig highlighted clear flaws in the testing methods used. Test conditions were that the motor was to run at a fixed-speed, with an increasing load applied in steps. Upon analysis of the first few tests, it could be seen that there was not one single set of test run conditions that could be compared to another. Whether this was the load setting, or the time taken to run at each load not being the same, it was always the case that there were slight differences. Human beings are not robots and whilst every effort can be made to operate the test rig under the same conditions from one run to the next, in practise this will not happen – and didn't. It follows that without an absolute defined set of repeatable test conditions, it is impossible to compare any two sets of results and any research relying on these results would be invalid.
- The use of a PLC to automate the test rig provided a vital guarantee of consistent test conditions. When the results of two identical tests are analysed and compared against each other, an assurance can be given that any deviation from the expected conditions is as a result of factors external to the control system, rather than anomalies in the test procedure itself. In this research, automation allowed a reliable base line data source to be obtained from the series of load tests run

on the healthy motor gearbox unit. Knowing that the test conditions would be identical, load tests run on the known faulty motor gearbox set could be run and results of the two tests compared like-for-like.

- From the tests, it has been shown that for a particular mechanical fault introduced, the inverter drive signals have provided sufficient information to allow a difference between healthy and faulty gear sets to be observed. The data has been analysed and feedback provided to David Brown who are pleased with the results obtained.
- Although the data was captured and analysed using a low-sampling frequency (1 second interval), meaning that only a time-domain visualisation could be carried out, the difference between healthy and faulty gearbox data could still be clearly seen. Because of the low signal-processing overhead that this brings, application of these methods will become easier to incorporate in general automation equipment. Memory storage becomes less of an issue, as does the processing overhead on the hardware – it is not desirable for the monitoring software to take up the majority of processing time on equipment who's primary function is controlling the plant or equipment. The appeal of this method of fault diagnosis is therefore greatly enhanced for both automation equipment manufacturers and end-users.
- Monitoring methods such as MCSA rely on a high level of data storage and analysis, with a significant cost and performance implication on the equipment used to perform the analysis. As this used standard drive output signals, the cost and complexity to implement this method is significantly reduced over other methods. This should ensure that the technology is more readily embraced by industry than other methods.
- There is significant interest from industry in motor and mechanical sub-system condition monitoring – as shown in the work commissioned for David Brown. The customers of Optima Control Solutions Ltd. have regular vibration analysis checks carried out on key plant equipment. Often, this has shown to be valuable in detecting early failures. In July 2010, vibration analysis led to a new inverter motor being replaced only six months into service. The unit had failed due to an assembly issue in production (early end roller-bearing failure). Had this remained undetected for a year or so, the unit would have to be replaced at the end users cost. As it stood, the unit was replaced free of charge by the manufacturer, saving the user hundreds of pounds. Bringing the cost and availability of condition monitoring systems down is key to getting established in customer sites. If this is as simple as linking up to drives and monitoring the key output signals, then this method of detecting mechanical failure has a high commercial value.

8.3 Contributions to Knowledge and Understanding

Contribution I: The practical design and implementation of an experimental test rig for the particular purpose of detecting motor faults using the inverter signals was an essential part of the research programme. This made sure that the correct equipment was used and that the test rig would give the required level of performance. It also allowed the rig to be fully tested to the design criteria and in future the test rig can be calibrated on a yearly basis to ensure that it still conforms to the original design specification.

Contribution II: Improvement of the test rig performance by upgrading to closed-loop control was provided. As applications for AC drives have advanced, it is necessary to provide test equipment that is capable of emulating the high-performance end of AC vector drives. By adding additional optional equipment to the existing AC vector drive used in the test rig it is now possible to offer this operating mode for testing. At present, this form of AC asynchronous motor control is still the most advanced method on offer and is unlikely to be superseded in the near future.

Contribution III: Automation of the test rig by a using PLC (Programmable Logic Controller) to drive test rig operation. This implementation represents an important contribution to several research projects done by the researchers from the Diagnostic Engineering Research Centre within the University of Huddersfield. The use of a PLC to automate the test rig provided an important step to guaranteeing consistent test conditions. Thus, for this test rig guarantees can be made that one test condition is identical to another allowing verifiable results to be obtained.

Contribution IV: Detection of gearbox faults using the inverter drive signals. Because the area of MCSA has seen so much research undertaken, it is important to research other means of condition monitoring. The use of inverter-driven systems in modern industry is now so widespread and detection methods that are not compatible with such systems will have limited applications. This model-driven method of detecting faults using the inverter signals is a logical forward step to take and it is hoped that this particular area of research will now receive much more attention in the coming years. The research carried out in this thesis is an important step in driving this further.

8.4 Future work

The initial research work can be concluded as a success, but needs to be progressed further in order for this method to provide an automated non-intrusive monitoring technique that provides reliable fault indication in real-world inverter-driven systems. For example, this research has been performed using a fixed speed for all tests, which may not be applicable to some inverter-driven systems.

Progression of the research is important, as existing methods involving motor condition monitoring through vibration, speed, or current measurements are mostly limited to applications that run at a fixed speed and on non-inverter, DOL (Direct-On-Line) systems. If progression does not happen, then these condition-monitoring techniques will be left behind as more and more AC motor applications become inverter-driven as a result of energy saving measures required by industry.

8.4.1 Compatibility of existing condition monitoring methods with inverter-driven systems

Inverter-driven motor systems can present issues to existing research involving motor condition monitoring through vibration, speed, or current measurements. Further research is required in order to validate these existing motor condition monitoring methods with inverter technology. Existing methods are listed, along with the effects that an inverter drive may present to these methods:

Vibration, speed and current measurement

On current analysis methods, a varying speed may compromise fault diagnosis that relies on the presence of harmonic data shown as sidebands of the main 50Hz carrier frequency to detect fault conditions. These sidebands will experience frequency-shift and amplitude variation as the motor speed and frequency is varied.

Speed variation will also affect vibration and angular speed monitoring systems as the reference data point of speed may be constantly changing. For vibration analysis, this will mean that the frequency components measured will shift and unless the system monitoring these signals compensates, false triggering of faults may occur. As speed analysis relies on measuring subtle changes in rotor angular speed, this may be affected by inverter technology as at a motor speed of 1500RPM, an inverter with 3kHz switching frequency can affect the rotor speed up to two times in one revolution and more if the motor is running slower.

Motor Current Signature Analysis (MCSA) – phase current noise

Complications with diagnostics involving motor current signals stem from the fact that each phase output waveform from a modern PWM drive is not sinusoidal. Because of the manner in which a PWM drive operates, there is effectively a modulated carrier signal (the switching frequency of the drive) imposed over the main 50Hz frequency. Additionally, as the drive does not always switch on and off for one full carrier cycle – but parts of it – the motor phase signal is enriched with harmonic content. It follows that any system relying upon monitoring low-amplitude sideband frequencies around the main motor carrier to observe faults (NFMCSA – Notch-Filtered Motor Current Signature Analysis, for example) may find that these low-amplitude sideband frequencies are swamped by the many harmonics that a PWM drive produces. In a typical AC vector drive manual, there are no less than 50 harmonic currents listed [32] all with varying degrees of amplitude, decaying as the harmonic number increases.

Initial analysis of motor phase current data from the test rig was performed using a high sampling frequency, then processing the signals using FFT (Fast Fourier Transform) techniques to analyse the frequency content of the motor phase current signals. This revealed sideband frequencies that were numerous and not generally of fixed frequency. Whilst the main carrier signal could be clearly seen, the sideband content had more of a ‘white-noise’ appearance about it. NFMCSA methods would clearly struggle to pick out the required data in this ‘noisy’ environment.

Motor Current Signature Analysis (MCSA) – motor slip

However, this is not the only barrier to using MCSA. Phase current signature analysis as researched by Bo Liang [1] relied upon the fact that the sidebands appeared more prominently when the motor was at a higher load, with more slip occurring. Between 0 and 25% load, the sidebands were not visible, because of the small amount of slip that occurs. A closed-loop inverter drive compensates for

increased motor slip by increasing the supply frequency to maintain base speed. With limited slip at higher loads due to this slip compensation, there may be no motor sidebands and therefore no indication of the motor broken rotor bar faults being studied.

The phase current analysis method used by Bo Liang and others will require further testing on AC closed-loop systems to confirm if this still gives reliable fault indication. It may be possible to adapt some of these existing methods to use the inverter-generated signals for the purposes of fault detection.

All of the above issues strengthen the case for using the inverter drive output signals for condition monitoring on inverter-driven systems.

8.4.2 Use of adaptive algorithms to signal motor faults

Although the test results obtained from this research have not been incorporated into a system that can automatically signal faults after learning base-line data, this is an area that shows a lot of potential for further work. Some of this work could see the inverter drive signals being used with adaptive algorithm techniques to learn the motor operating conditions over a range of motor speeds. This would firstly be limited to machinery that has a constant, predictable operating mode such as fans or pumps. Systems that experience sudden changes in load, such as conveyors or lift/hoist systems may not be suitable. The algorithms would be tested on suitable industrial inverter-drive applications and their use then proven out in the field.

8.4.3 Improvement of measured inverter signals

At present, the resolution of the inverter signals is unknown and as the research progresses, it may be necessary to extract greater information from the drive signals. Closer co-operation with a drive manufacturer will be required to determine more information about the intended feedback signals being used. For example, the torque, speed and current signals are output from the drive via analogue signals at the moment. Information is not given in the drives manual as to the output resolution of these signals (12 bit plus sign, for example) or the sampling rate. It may be possible that higher resolution signals at a higher sampling rate can be retrieved over Fieldbus, for example, as the drive internal processor is 32-bit. One would expect the 32-bit processor to be working from measured signals to the same resolution. Without the introduced latency and potential for noise that analogue signals have, the Fieldbus data can be read directly into a data acquisition system for further processing.

This will be possible on the existing rig, and may be the next key step in this research. The Parker 690+ AC Vector drive has an Ethernet 'technology box' available. The manual for this does not state the data transfer rate available, or the bit resolution of parameters available from the drive, however this data should be obtainable from the UK manufacturer. Even closer co-operation with the drive manufacturer may lead to a special version of firmware being issued that allows 32-bit data to be passed across the Ethernet network if this is not currently available and improves the data analysis.

8.4.4 Combining inverter and motor condition monitoring

Condition monitoring of inverter drives for fault diagnosis is not a new research area. It has been considered that although electric motor problems can occur for a variety of reasons – ranging from design faults and poor manufacturing quality to incorrect design application, or harsh operating conditions on-site – what can also have an influence on the failure of motors, is the inverter itself. If the drive output circuit is intermittently failing, or the feedback device on closed-loop systems is providing incorrect speed data, the motor can be stressed with the harmonic content of currents due to ‘misfiring’ of the inverter output circuit or higher phase currents than are necessary to achieve a given speed. MCSA for motor failure and Wavelet-fuzzy algorithms for inverter failure are just two types of methods that can be applied to inverter-driven motor systems for early fault diagnosis.

It is therefore important to consider how condition monitoring for both motor and inverter could be applied as a whole to the inverter-motor system. An inverter that can signal potential failure of both itself and the motor it is driving will have a serious commercial interest for drives manufacturers, providing the end-user has confidence that the drive is not indicating potential failure too soon, necessitating a premature drive replacement. There is the potential for a perceived conflict-of-interest to occur and this may prove to be a barrier to such a system being wholeheartedly embraced by the end-users of inverter equipment.

8.4.5 Incorporating fault detection algorithms into existing automation/drive equipment

A useful step would be to incorporate the motor condition monitoring algorithms into industrial automation equipment. This could be in the drive itself, or a supervisory system that reads data from the drive over a proprietary network (Ethernet, for example). Such algorithms would need to function on systems that do not require a high signal processing rate, or large amounts of data storage overhead if they are to be incorporated into AC inverter drives or PLC (Programmable Logic Controller) systems.

If this could be incorporated into a drive, the technology could be licensed to drive manufacturers for use in their equipment. This would advance industrial AC motor condition monitoring into a readily available product and provide manufacturers with a unique selling proposition. As inverter drive technology stands, there is little to separate manufacturers in terms of performance or features. Most decisions taken with regard to which manufacturer is chosen for an application is down to price, perceived brand reliability, or simply personal preference. The first drive manufacturer to offer motor condition monitoring as an optional extra will certainly steal an advantage over competitors.

Alternatively, now that most drive manufacturers (Parker amongst them) provide Ethernet connectivity, it may be possible to transfer data out of the drive at a higher rate and process this data in an industrial PC located in the plant. The majority of modern factory automation systems have higher-level Fieldbus systems (namely Ethernet) to process data for operators and supervisors, so it should be possible to incorporate the algorithmic software into these systems and market this as a separate ‘bolt-on’ package.

8.4.6 Validating the fault detection algorithms

Final stages of the research would see the algorithms implemented on suitable industrial applications in industry. As many inverter systems are used on fans and pumps for energy saving, then these should be some of the first target systems. The load profile is not overtly affected by normal operating conditions and so can easily be base-lined. If faults can be detected – especially those that might impact on the energy savings offered by such systems – then this potentially a very large market area.

References

- [1] Bo Liang, "Condition monitoring and Fault Diagnosis of Three-Phase Induction Motors", Department of Mechanical Engineering, University of Manchester 2001
- [2] Jugrapong Treetrong, "The Use of Parameter Identification Methods for the Condition Monitoring of Electric Motor Drives", Faculty of Engineering and Physical Science", University of Manchester, 2009
- [3] Chinmaya Kar, A.R. Mohanty. (22 September 2004). Monitoring gear vibrations through motor current signature analysis and wavelet transform. Mechanical Engineering Department, Indian Institute of Technology, Kharagpur 721 302, India, Mechanical Systems and Signal Processing.
- [4] Serkan Günal, Doğan Gökhan Ece, Ömer Nezih Gerek, "Induction machine condition monitoring using notch-filtered motor current." Anadolu University, Department of Electric and Electronics Engineering, Eskisehir, Turkey.
- [5] F.Gu, Y.Shaob, N.Huc, A.Naid a, A.D.Ball a. (7 December 2009). Electrical motor current signal analysis using a modified bi spectrum for Fault diagnosis of downstream mechanical equipment. *Mechanical Systems and Signal Processing*. 2 (1), 1-5
- [6] M. E. H. Benbouzid¹, M. Vieira and C. Theys²; Induction Motors' Faults Detection and Localization Using Stator Current Advanced Signal Processing Techniques; University of Picardie "Jules Verne" 80000 Amiens, France¹; Laboratoire d'Informatique, Signaux et Systèmes, CNRS & University of Nice "Sophia Antipolis," 06041 Nice, France²
- [7] Filippetti, F., Franceschini, G. and Tassoni, C. "AI techniques in induction machines diagnosis including the speed ripple effect", IEEE Transactions on Industry Applications, Vol. 34, No.1, 1998.
- [8] Ahmed Yousef, Ben Sasi, Fengshou Gu, Bradley S. Payne and Andrew Ball. (Number 2 - 2004). "Instantaneous angular speed monitoring of electric motors". Quality in Maintenance Engineering. 10 (2), pp. 123-135.
- [9] B. Biswas, "Current Harmonics Analysis of Inverter-Fed Induction Motor Drive System under Fault Conditions ", Electrical Engineering Department of Haldia Institute of Technology, Haldia, West Bengal
- [10] A. Azzini, L. Cristaldi, M. Lazzaroni, A. Monti, F. Ponci, A.G.B. Tettamanzi; "Incipient Fault Diagnosis in Electrical Drives by Tuned Neural Networks"; 1Dipartimento di Tecnologie dell'Informazione, Universita degli Studi di Milano, via Bramante, 65 – 26013 Crema, Italy
- [11] Khater, Faeka and abu El-Sebah, "Fault Diagnostics in an Inverter Feeding an Induction Motor"; Mohamed Electronics Research Institute - Dokki, Cairo, Egypt; Osama, Mohamed High Institute of Engineering – Six October City, Egypt
- [12] Rozailan Mamat, M Rizon, M.S. Khanniche, "Fault Detection of 3-Phase VSI using Wavelet-Fuzzy Algorithm"; 1Terengganu Advanced Technical Institute, Terengganu, Malaysia.

-
- [13] M. Abul Masrur, Senior Member, IEEE, ZhiHang Chen, and Yi Lu Murphey, Senior Member, IEEE; "Intelligent Diagnosis of Open and Short Circuit Faults in Electric Drive Inverters For Real-Time Applications"; US Army RDECOM-TARDEC 6501 E 11 Mile Rd Warren, MI 48397-5000, USA Univ. of Michigan-Dearborn, Dearborn, MI 48128, USA
 - [14] Debaprasad Kastha, "Investigation of Fault Modes of Voltage-Fed Inverter System for Induction Motor Drive"; University of Tennessee, Knoxville
 - [15] Fiorenzo Filippetti¹, Giovanni Franceschini, Carla Tassoni²; "Neural Networks Aided On-Line Diagnostics of Induction Motor Rotor Faults"; Department of Electric Engineering, University of Bologna, 40136 Bologna, Italy¹; University of Parma, 43100 Parma, Italy²; 1995
 - [16] Fiorenzo Filippetti¹, Giovanni Franceschini, Carla Tassoni²; "Recent Developments of Induction Motor Drives Fault Diagnosis Using AI Techniques"; Department of Electric Engineering, University of Bologna, 40136 Bologna, Italy¹; University of Parma, 43100 Parma, Italy²
 - [17] Loránd SZABÓ¹, Károly Ágoston BIRÓ¹, Dénes FODOR², Ernő KOVÁCS³; "Improved Condition Monitoring System for Induction Machines Using a Model-Based Fault Detection Approach"; Department of Electrical Machines, Technical University of Cluj P.O. Box 358, RO-400750 Cluj, Romania¹; Department of Automation, Faculty of Information Technology, Pannon University Veszprém Egyetem u. 10, H-8200 Veszprém, Hungary²; Department of Electrical and Electronic Engineering, University of Miskolc H-3515 Miskolc-Egyetemváros, Hungary³.
 - [18] Korkua, Suratsavadee, Jain Himanshu, Lee Wei-Jen, Kwan Chiman; "Wireless health monitoring system for vibration detection of induction motors." Industrial and Commercial Power Systems Technical Conference (I&CPS); 9-13 May 2010
 - [19] Piotr Czech¹, Bogusław Łazarz², Henryk Madej³, Grzegorz Wojnar⁴; "Classification of tooth gear wheel faults of gearbox working in the circulating power test rig by multilayer perceptron and continuous wavelet transform"; ¹⁻⁴Faculty Of Transport, Silesian University Of Technology, Gliwice, Poland
 - [20] Salem Al-Arbi, Fengshou Gu, Luyang Guan, Andrew Ball, A. Naid; "Gearbox Fault Diagnosis based on Vibration Signals Measured Remotely"; School of Computing and Engineering, University of Huddersfield; 2009
 - [21] William T. Thomson*, Ronald J. Gilmore**, "Motor Current Signature Analysis To Detect Faults In Induction Motor Drives—Fundamentals, Data Interpretation, And Industrial Case Histories"; * - Director and Consultant EM Diagnostics Ltd, Alford, Aberdeenshire, Scotland; ** - Discipline Technical Authority (Electrical Engineering), AMEC Upstream Oil & Gas, Nigg, Aberdeen, Scotland
 - [22] Diagrams from: <http://electoprojects.com/motors/tesla-induction-motors-1.htm>; Last used: 29th November 2010;
 - [23] Diagram from: Siemens Operating Instructions 10/2008 English for IEC Low-voltage Motors; Siemens AG Industry Sector, Nürnberg Germany; © 10/2008

-
- [24] European Electric Motors; Written by Dr David G Searle; A Drives and Controls Publication, published on behalf of Eurotherm Drives Ltd. New Courtwick Way, Littlehampton, West Sussex, BN17 7PD; ISBN 0 907485 10 3
 - [25] Electrical Machines and their Applications 4th Edition; Author: John Hindmarsh 1985
 - [26] Novotny, D.W. "Vector control and Dynamic of AC Drives", Oxford University Press Inc., New York, 1996
 - [27] From: http://en.wikipedia.org/wiki/File:3_phase_AC_waveform.svg; Last used 29th November 2010; Source File:3-fas-spänningar.svg; "Author: J Messerly, modification of original svg by User: SiriusA". This figure illustrates one voltage cycle of a three-phase system, labelled 0 to 360° (2 π radians) along the time axis. The plotted line colours represent each phase component.
 - [28] Werner Leonhard, "Control of Electrical Drives", 2nd Completely Revised and Enlarged Edition, Technische Universität Braunschweig , 1997
 - [29] Siemens Industry USA; Basics of AC Drives; www.sea.siemens.com/step/pdfs/acd_2.pdf; Last Used: 29th November 2010
 - [30] Six-step Inverter Block Diagram; <http://www.mathworks.com/access/helpdesk/help/toolbox/phsmod/powersys/ref/sixstepvsiinductionmotordrive.html>; Last Used: 29th November 2010
 - [31] Control Technologies Manual PWM AC Drives Revision 1.0;
 - [32] 690+ Series AC Drive Frame B, C, D, E & F Installation Product Manual HA465492U004 Copyright Eurotherm Drives Limited 2009
 - [33] European Electric Motors; Written by Dr David G Searle; A Drives and Controls Publication, published on behalf of Eurotherm Drives Ltd. New Courtwick Way, Littlehampton, West Sussex, BN17 7PD; ISBN 0 907485 10 3
 - [34] Resistor Load Bank; 50kW, 250VDC; Drawing number: FE 081073 Issue B; Electrohm Limited Ohms House, Woodlands Business Park, Ystradgynlais, Swansea, SA9 1JW
 - [35] Helical geared motor view taken from: <http://www.radicon.com/geared-motor-series-m.php> Radicon Website (formerly David Brown)
 - [36] David Brown Radicon Series M Helical In Line Technical Catalogue Up to - 90kW / 110,000 Nm; Catalogue number: CM-1.02GBD1009
 - [37] Siemens S7-200 Programmable Controller System Manual; Edition 08/2005 A5E00307987—02 Copyright Siemens AG 2004 All rights reserved
 - [38] Images taken from: <http://www.automation.siemens.com/bilddb/index.aspx?lang=en> Siemens Automation and Drives Image Database Website Portal; Last used 03rd December 2010
 - [39] Sandy Dunn. (2009). Condition Monitoring in the 21st Century; <http://www.plant-maintenance.com/articles/ConMon21stCentury.shtml> (Accessed 28-11-2010)
 - [40] J Apsley , ERA Report 93-0776R, ERA Project 44-02-1819 Task F; December 1993; "Condition Monitoring Of Inverter Fed Motors"; ERA Technology Limited, Cleeve Road, Surrey, England.

-
- [41] Albrecht P.F. et al "Assessment of the reliability of motors in utility applications – Part 1", IEEE Transactions on Energy Conversion, Vol. EC-1, No.1, March 1986, pp. 39-46
 - [42] Albrecht P.F. et al "Assessment of the reliability of motors in utility applications – Part 2", IEEE Transactions on Energy Conversion, Vol. EC-2, No.3, September 1987, pp. 396-406
 - [43] O'Donnell, P. "Report of large motor reliability survey of industrial and commercial installations – Part 1", IEEE Transactions on Industry Applications Vol. 21, No.4, July 1985, pp.853-864
 - [44] O'Donnell, P. "Report of large motor reliability survey of industrial and commercial installations – Part 2", IEEE Transactions on Industry Applications Vol. 21, No.4, July 1985, pp.865-872
 - [45] O'Donnell, P. "Report of large motor reliability survey of industrial and commercial installations – Part 3", IEEE Transactions on Industry Applications Vol. 23, No.1, January 1987, pp.153-158
 - [46] Penman, J., M.N. Dey, A.J. Tait and W.E. Bryan, 1986. "Condition monitoring of electrical drives". IEE Proc. B Electrical Power Application, 133: pp. 142-148.
 - [47] Operating Instructions Siemens Simovert Masterdrives Frequency Converter (AC-AC)
© Siemens AG 2009
 - [48] I. Daubechies, "Ten Lectures on Wavelet," Society for Industrial and Applied Mathematics, Philadelphia, Pennsylvania, 1992
 - [49] S. Mallat, "A Wavelet Tour of Signal Processing," Academic Press, San Diego, CA, 1999
 - [50] 690+ Series AC Drive Frame B, C, D, E & F Software Product Manual HA465038U005
Copyright Eurotherm Drives Limited 2009
 - [51] Parker SSD Drives HTTL Speed Feedback Communications Option Technical Manual
for 690+ Frame C+ HA467152U001 Issue 7

Appendix A Gearbox Test Rig Modifications

A.1 Test rig modifications – mechanical and electrical works

The final stage of implementing the test rig modifications comes in the form of installing the actual equipment inside the existing test rig control panel. The existing control panel had sufficient space inside the panel and on the panel door to accommodate the additional equipment – the initial design philosophy of leaving the 20% free space had proved beneficial in this case.

Internal modifications

The PLC would be mounted in space available at the top left of the control panel backplate. A 24VDC power supply would be taken from the existing power supply unit inside the panel. It was calculated that there was enough capacity in this to feed both the PLC and touch-screen that were to be fitted. A DIN-rail to mount the PLC on would be installed and additional trunking to contain the cables would be fitted above the PLC to keep the installation neat and be in-keeping with the rest of the control panel work.

Wiring the PLC into the existing circuit required some modifications to the internal wiring, detailed on the electrical schematics that are included in Appendix D. The internal modifications required the following additions:

- 4 off Fused terminals were fitted to protect the PLC and the expansion modules against excessive fault over-currents that may damage the modules. 4x20mm glass fast-acting fuses of 1A rating were used.
- New terminal block sections installed for future expansion, wired to the spare inputs and outputs on the PLC

Wiring the PLC

The PLC wiring was completed before the equipment was installed in the test rig as this would save time during the installation. Approximately 2 metres of cable was left from each of the PLC terminals to free ends and all of the cables were marked-up with numbers. Two hours were spent making off the PLC cabling that included both ferrule termination and cable numbering to allow ease of identification.

A close-up image of the PLC detailing the modules used can be seen in Figure B-1:

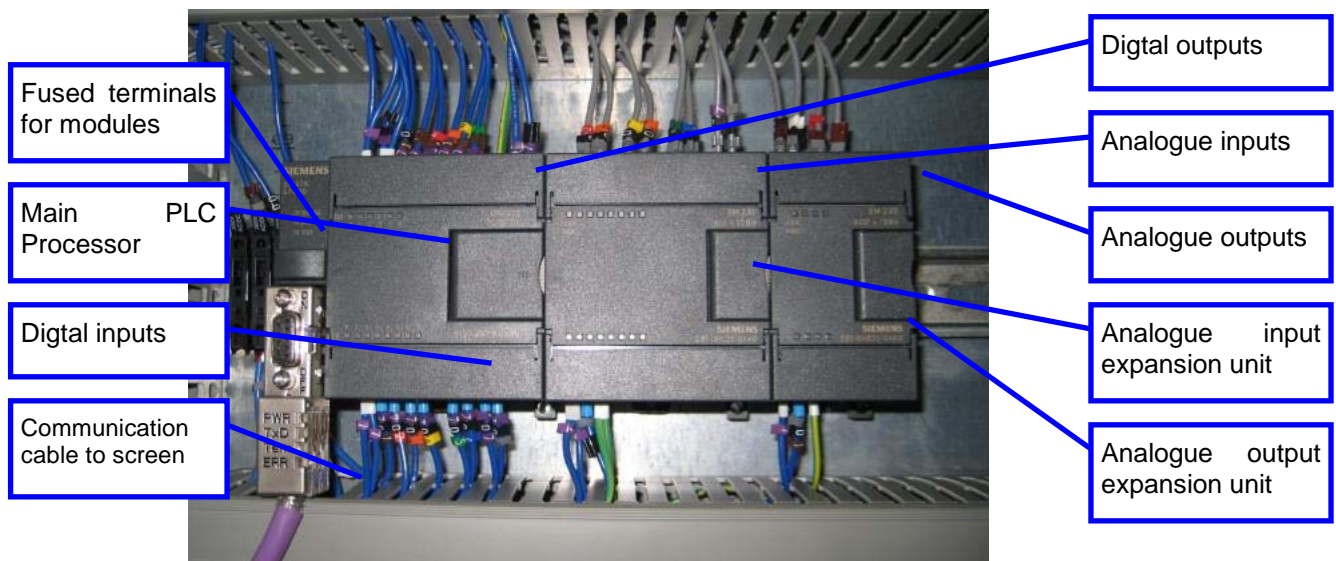


Figure B-1 - Test Rig PLC Hardware components

Spare terminals were left for future expansion of the test rig PLC to avoid the inconvenience of adding extra cabling in future. These are for digital inputs and outputs and may be used for external control/signalling to/from the test rig if required.

External

The now obsolete manual load potentiometer would be left on the front panel in case it may be required in future. The operating keypad for the drive would also be maintained as it is useful in providing diagnostic information on the status of the drive.

A new hole would be cut-out of the panel door to fit the new screen into. New power supply (24VDC) and a network cable (PPI interface to communicate from Screen to PLC) would be routed from the backplate to the panel door. Images of the test rig before (left) and after (right) the modification work was undertaken are shown in Figure B-2 and Figure B-3 below:



Figure B-2 - Test rig panel exterior before and after modification

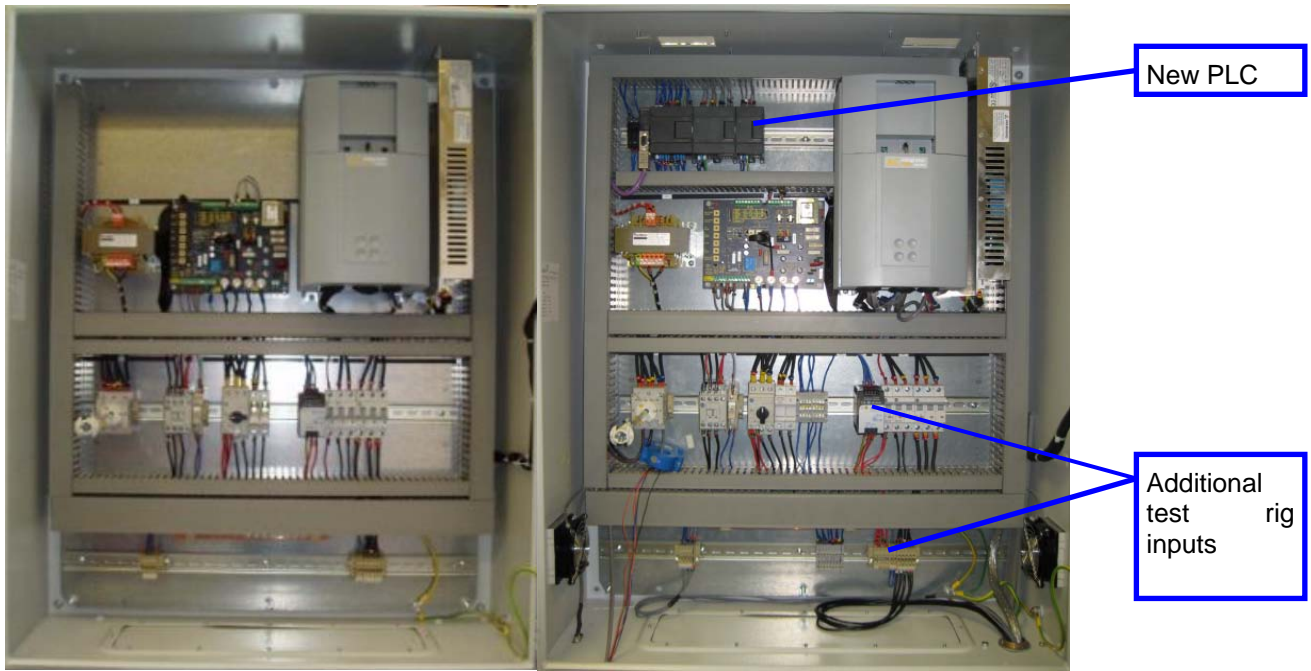


Figure B-3 - Test rig panel interior before and after modification

The modification work took approximately 8 hours to complete at the University and was done in an evening while the rig was not being used.

A.2 Data acquisition system – modifications

After the test rig modifications as detailed in Chapter 5 were completed, additional signals were added to those already present on the data acquisition system. These were necessary on two fronts:

- To verify that the automated signals were correct on each test run
- To determine if the feedback signals from the inverter drive could be used for fault diagnosis on this test rig.

The channel configuration was now as shown in Figure B-4:

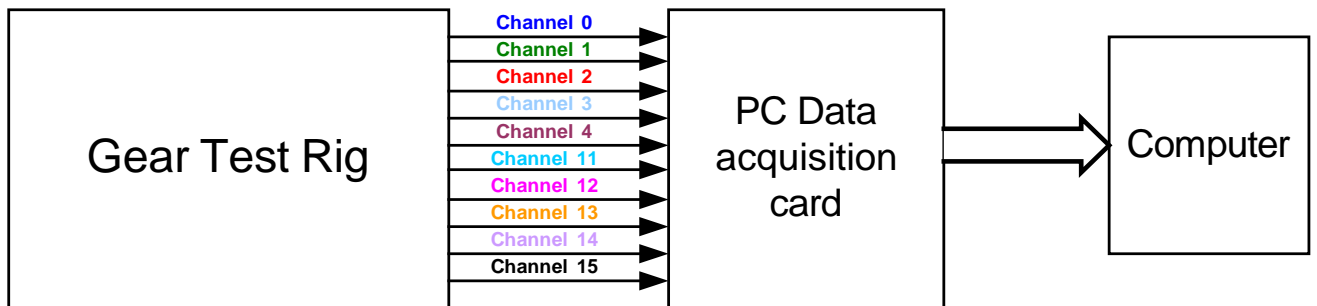


Figure B-4 - Diagram showing additional test rig signals

Channel 11 – Cyan:	DC Motor Armature current
Channel 12 – Magenta:	Automated load setting; PLC > Field controller
Channel 13 – Orange:	Inverter drive speed feedback
Channel 14 – Lavender:	Inverter drive motor current feedback
Channel 15 – Black:	Automated speed setting; PLC > Inverter drive

These were made available to the data acquisition system by the fitting of a 9-way D-type connector to the bottom of the test rig panel. This will be wired according to the diagram below:

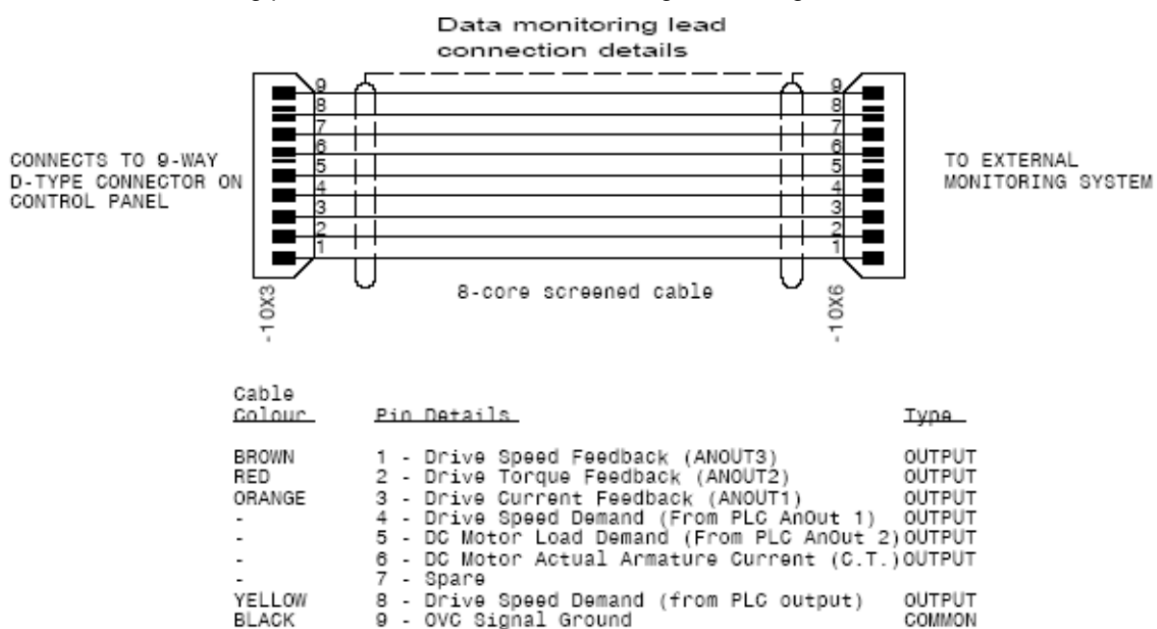


Figure B-5 - D-Type connector wiring for Data Acq. system (Optima Drawings)

Appendix B PLC Program detail and Memory allocation

This appendix provides additional data to accompany Chapter 5, for the test rig modifications concerning the operation of the PLC software and how this is structured.

B.1 PLC Program design

The PLC will have a data block assigned to store speed values and ramp times for each step. A similar data block will be used for the load values and ramp times. A “Data Block” is an assigned area of memory that contains contiguous values of data grouped together for ease of organisation and programming.

Each step sequence (maximum of 20 steps programmed) will output either a speed or load value to the ramp block and a ramp time for each sequence step. If the ramp time is zero, then the ramp output will be bypassed for that step using the ramp “switch” and the raw output will be fed directly to the AC inverter drive or DC field controller.

Consistency of tests

Because a PLC has predictable program cycle scan times, it can be relied upon to perform consistent tests from one test to the next using the same data. This is important, as inconsistent test cycles will produce inconclusive results.

PLC Inputs

The PLC inputs are defined as follows in Table B-1:

Table B-1 - PLC External Inputs

Type:	Description	Function / Scaling
Analogue	Speed feedback from AC inverter	0 – 10V = 0 to 100% calibrated speed
Analogue	DC Motor field controller feedback	0 – 10V = 0 to 4.7A Field current
Analogue	Current feedback from AC inverter	0 – 10V = 0 to 100% calibrated speed
Analogue	DC Motor armature current feedback from current transformer	0 – 10V = 0 to 207A (maximum armature current)
Digital	DC Field controller health	1 – Controller healthy
Digital	AC Inverter health	1 – Inverter healthy
Digital	AC Inverter at zero speed	1 – Motor at zero speed

PLC Outputs

The PLC outputs are defined as follows in Table B-2:

Table B-2 - PLC External Outputs

Type:	Description	Function / Scaling
Analogue	Speed setpoint to AC inverter	Control speed of AC motor according to the program demands 0 – 10V = 0 to 100% calibrated speed
Analogue	Load setpoint to DC field controller	Vary the AC motor load demand according to the program demands 0 – 10V = 0 to 100% calibrated load
Digital	AC drive start	0 – Stop AC Drive 1 – Start AC Drive

Operator Screen Data

The data that the operator enters into touch-screen to run the test rig needs to be stored in the PLC for use by the program.

PLC data is organised into the following groups:

- WORD/INT's for storing of speed or load setpoint values as integers. The format of WORD data in the PLC is MW(x) where 'x' is the unique address number.
- BOOLean (bit) data for operator pushbuttons. The format of BOOL data is Mx.x where 'x.x' is the unique address.

Some of the integer values are held in non-volatile RAM in the PLC so that when power is turned off to the test rig, the values are not lost. Each data value has a unique address and the operator screen can read or write values into these address areas. The tables are grouped into data that is either sent from the screen to the PLC (input values) or from the PLC to the screen (output values). Not all data values are shown below for every speed or load setting, but the main data types are given:

B.1.1 PLC Program Structure

The structure of the PLC program is shown below. The program is made up of MAIN routines (these are fixed in the PLC) and SBR routines (sub-routines that are written specifically for the application and can be called freely in the PLC program, sometimes more than once).

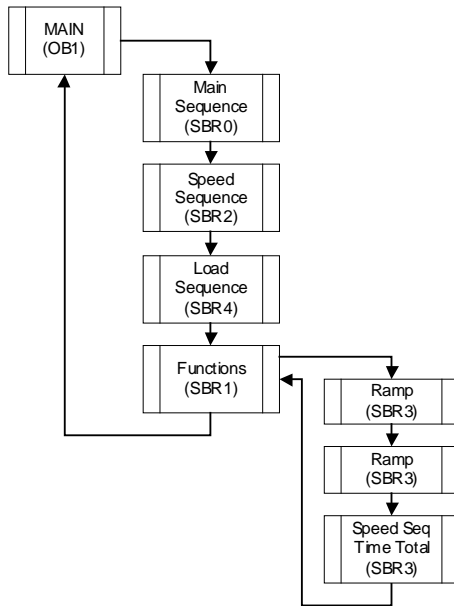


Figure B-1 - PLC Program structure

A description of each program function is given below:

MAIN (OB1)

This is the main routine that the PLC calls at every program scan. This program cannot be deleted and all of the functions required for the test rig to operate are contained in this routine. Any subroutines written are called from this 'Master' program as well.

Main Sequence (SBR0)

The Main Sequence provides the main control of the speed and load state sequences. This sequence ensures that the operator follows all of the correct set-up screens before operating the test rig.

A state diagram programming approach was used for the software design as it allows the operation of the test rig to be finalised before the software is written. It should be possible to define any control system operation by a definite number of operational steps. Once each step has been clearly defined, writing the software from this becomes far more straightforward and allows ease of fault finding because if the program is halted at a particular state, it can clearly be seen what operation is required to move the program on. Another advantage is that operation of the software can be viewed with ease by people with no programming knowledge or background.

In the main state diagram written for this test rig and shown in Figure B-2, the state operations are as follows:

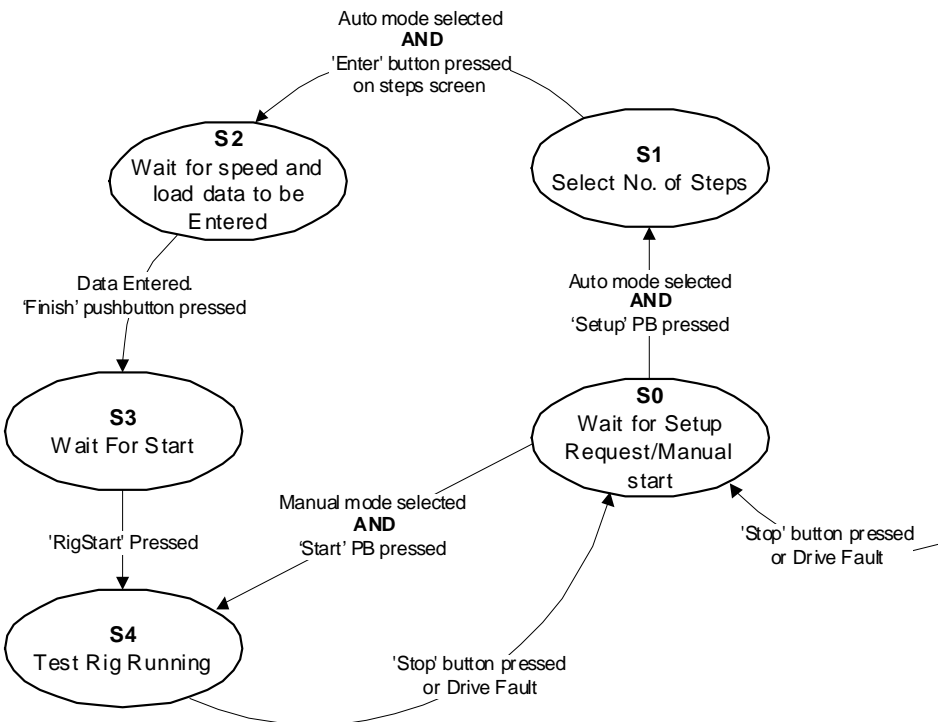


Figure B-2 - Main Sequence (SBR0)

S0 - The test rig is idle. The AC inverter and DC drive are de-energised.

Auto mode: To proceed from this state, the test rig operator must press the 'Set-up' pushbutton on the main operator screen. The program proceeds to state S1.

Manual mode: To proceed from this state, the test rig operator must press the 'Manual Start' pushbutton. The program proceeds to state S4.

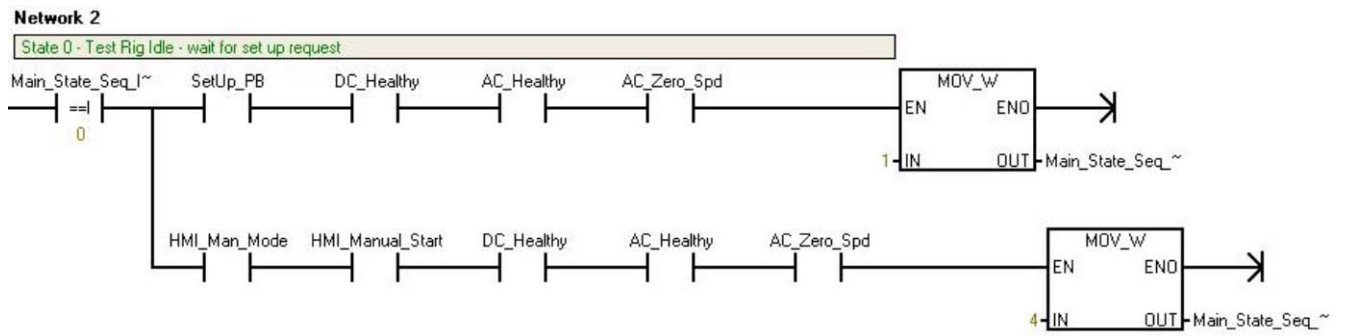
S1 - The test rig is idle. Once the number of speed and load sequence steps have been entered on-screen, the operator must press the 'Enter' pushbutton to confirm this. The program proceeds to state S2.

S2 - The test rig is idle. The operator will enter the required speed and load data on each screen (there are 4 screens with 5 speed and load data parameter sets on each – described later in this section, [Chapter: B.1.2 - Operator screens page 9-15]) then press the 'Finish' pushbutton. The program proceeds to state S3.

S3 - The test rig is idle. The operator will now be returned to the main operator screen, where the 'Auto Start' pushbutton will now be displayed. Until all of the above steps have been completed, the 'Auto Start' pushbutton will not be displayed. Once this button is pressed, the program proceeds to state S4.

S3 - The test rig is running. The AC inverter and DC field generator are enabled and the test rig will run all of the programmed speed and load sequence steps. The test rig can be stopped by pressing the 'Stop' pushbutton. The test rig will also stop if there is a fault on either the AC inverter, DC field generator, or the DC motor cooling fan.

Translation of the main sequence SBR0 design into the PLC's native programming language (LADder) logic can be seen in Figure B-3 below. The program is represented in the top half of the figure and the symbols used by the network are included below.



Symbol	Address	Comment
AC_Healthy	I0.1	
AC_Zero_Spd	I0.2	
DC_Healthy	I0.0	
HMI_Man_Mode	M0.7	HMI > PLC '1' - Select Manual Mode for operation (not sequence)
HMI_Manual_Start	M2.0	HMI > PLC 'Start' pushbutton in manual control area on Operator screen
Main_State_Seq_IN	VW0	
Main_State_Seq_OUT	VW2	
SetUp_PB	M0.1	HMI > PLC 'Setup' pushbutton on operator screen

Figure B-3 - Subroutine SBR0 LAD network and symbols used

As this is state **0** (zero) – initial program state – the equality statement “= =I” is used to only run the operations in this network if the value ‘Main_State_Seq_IN’ is equal to 0. There are two parallel routes that the program can take. The top route will advance the state sequence engine to stage **1** if all the conditions are met (or ‘True’). The symbols -| |- represent logic states, unless there is text inside the symbol (as is the case with the instruction at the top left). If all logic cases are TRUE (1), then the end statement of MOVE_W will move a value of ‘1’ into the variable ‘Main_State_Seq_OUT’. At the end of the subroutine, the integer ‘Main_State_Seq_OUT’ will be written to integer ‘Main_State_Seq_IN’. This is to ensure that when the state condition changes, a full PLC scan occurs of all other subroutines before the next state sequence is advanced. The bottom route will similarly allow an advance to state **4** if all of the conditions are met.

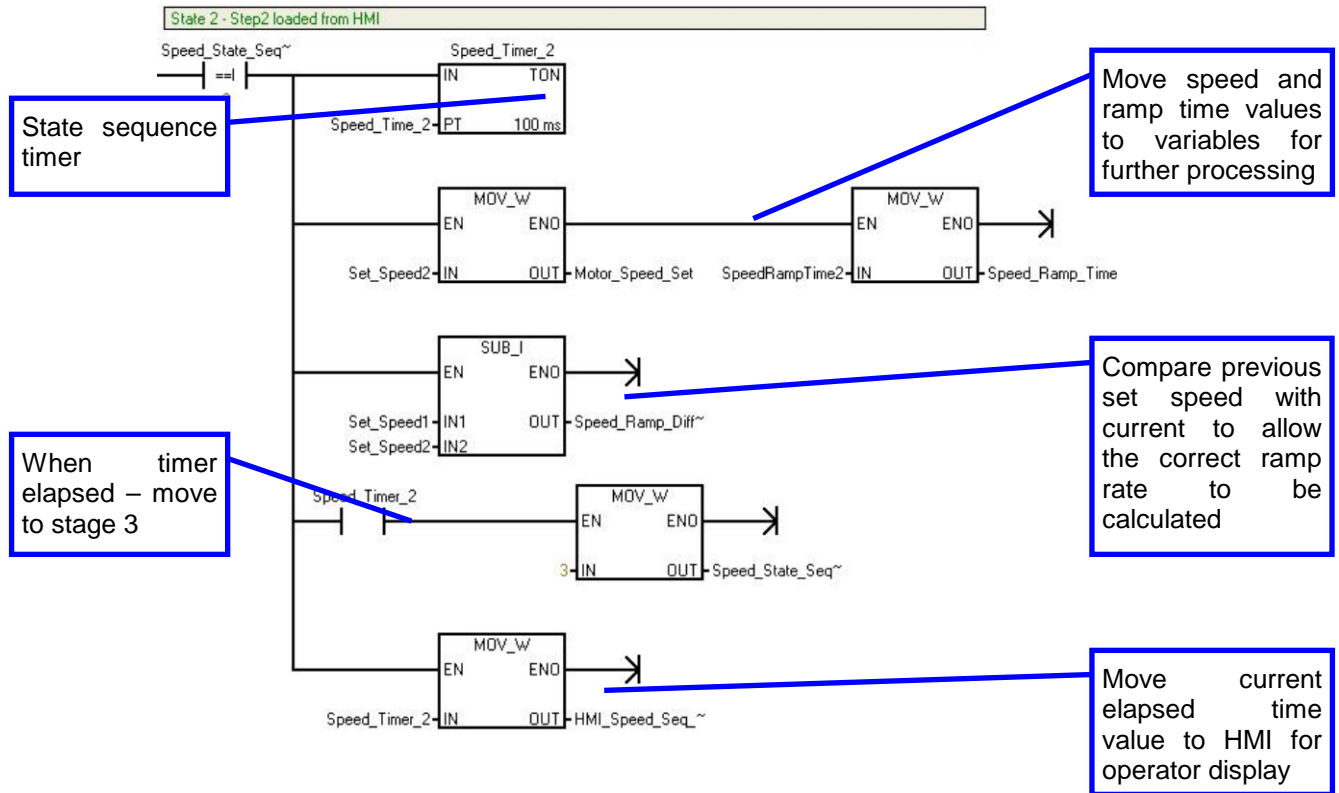
This corresponds to Figure B-2 on the previous page, where it can be seen that there are only two possible transitions from State 0 – the selection of Auto mode (State 1) or Manual (State 4). Auto mode is selected initially by pressing the ‘Set-up’ pushbutton on the screen – represented by symbol ‘M0.1 – SetUp_PB’ in the PLC program. Manual mode is enabled by selecting ‘Manual’ on the touch-screen – symbol ‘M0.7 – HMI_Man_Mode’. State programming allows the program operation to be easily modified in future and faults with operation to be quickly traced because if the program is stopped, the condition for transition to the next state can easily be identified.

Speed Sequence (SBR2)

The speed sequencer has been written to allow up to 20 different speeds to be run on the test rig, each with its own ramp time from one setpoint to the next and time to run each speed before the next step is run. This can be seen in (a).

On state **1**, the program writes the speed setpoint to be run <VW14 - Set_Speed1...> to the integer value <VW316 - Motor_Speed_Set>. The ramp time for state **1**, <VW16 - SpeedRampTime1> is written to the integer value <VW342 - Speed_Ramp_Time>. Both these integer values are fed into the RAMP function SBR3 to set the speed and ramp time in which to achieve it. State 2 operates in the

same manner, writing the speed and ramp time values for state **2** to the ramp block – this continues up until state 20 (the last state). The state sequence is timed by the ‘Speed_Timer_2’ value and when the TON (on-delay timer) has expired, the bit associated with it is set to state **1** and the sequence moves to the next state. State **2** is displayed in Figure B-4:



Symbol	Address	Comment
HMI_Speed_Seq_Time	Vw308	PLC > HMI Scaling: 10 = 1 second
Motor_Speed_Set	Vw316	PLC > HMI Motor Speed Setpoint
Set_Speed1	Vw14	HMI > PLC; Scaling: 0 to 100.00% on screen = 0 to 32,700 in PLC
Set_Speed2	Vw20	HMI > PLC
Speed_Ramp_Diff_INT	Vw340	Difference in speed value for ramp block sent from state sequence
Speed_Ramp_Time	Vw342	Speed ramp time send from state sequence to RFG
Speed_State_Seq_IN	Vw4	
Speed_State_Seq_OUT	Vw6	
Speed_Time_2	Vw18	HMI > PLC
Speed_Timer_2	T38	
SpeedRampTime2	Vw22	HMI > PLC Units: 10 = 1s

Figure B-4 - SBR2 Speed Sequence Diagram; State 2

Load Sequence (SBR4)

A separate load sequencer has been written to allow different load patterns to be programmed independently of the speed set-points. A maximum of 20 load steps can be programmed each with its own ramp time from one load setpoint to the next and time to run at each load before the next step is run.

The load and speed sequences are given in Figure B-5. Some multiple states (steps 3 through 19) are left out for clarity, but there are 20 running states each in total for the speed and load sequences, giving up to 40 different speed/load combinations. The structure of the stage sequencer for load settings is the same as the speed sequencer so program detail on this does not warrant inclusion.

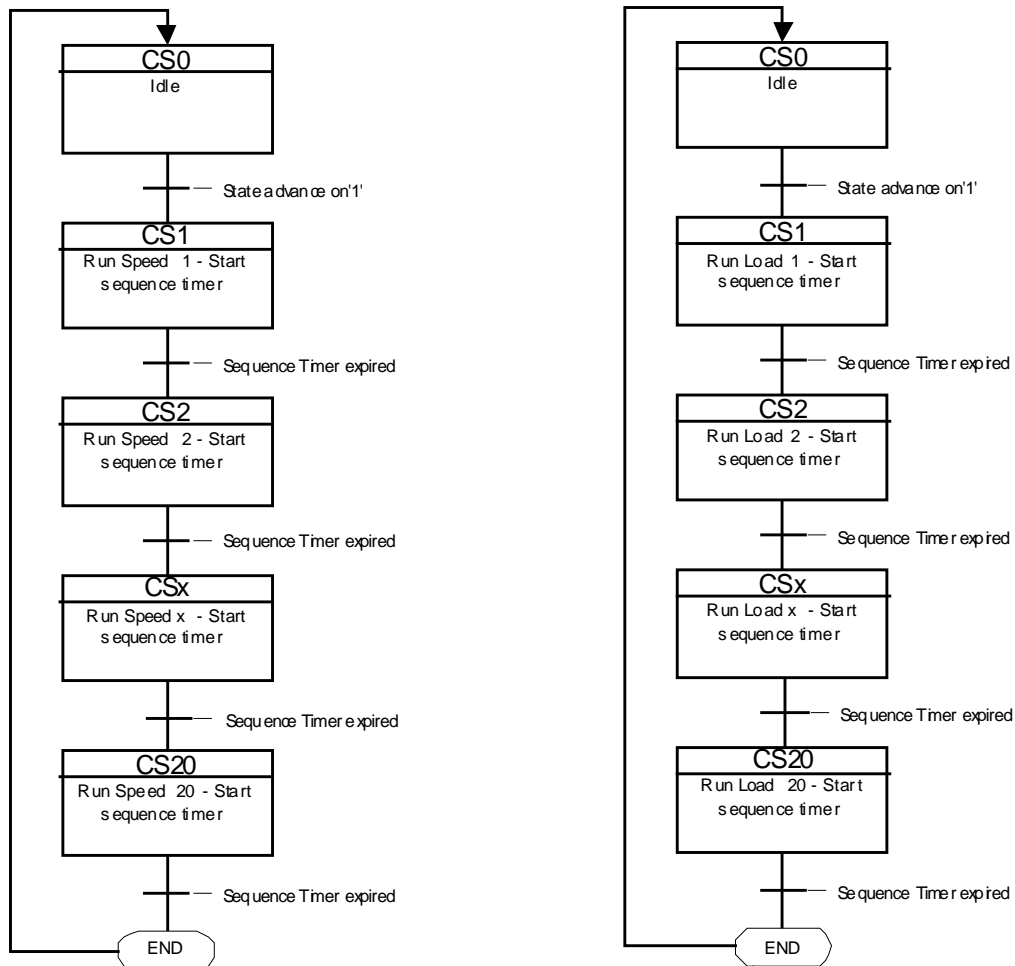


Figure B-5 - Speed (SBR2) and Load (SBR4) state diagrams

Functions (SBR1)

This subroutine performs the following tasks:

- Calculates and generates the ramped speed and load setpoints before outputting to the AC drive and DC field controllers respectively. The **Ramp function (SBR3)** is called to generate the ramped setpoints. The setpoint values are then scaled or offset to give the required output voltage.
- Scale and move PLC analogue inputs to internal PLC registers for outputting to the operator HMI
- Subroutine '**Speed Seq Time Total**' (**SBR5**) calculates the total speed and load sequence times so the operator can ensure they are equal and correct if necessary
- Operates the PLC digital outputs to control the AC drive and DC field controller

Ramp Function (SBR3)

The ramp function block is shown in Figure B-6. The RAMP function limits the rise and fall of the floating-point variable 'IN' and returns the calculated floating point value as variable 'OUT'.

The parameters input to the block are given in the table below. REAL data type is a floating-point variable. As the variables input from the operator screen are INTeger format, they must be converted

to floating-point values before being passed to this function. The RAMP function block has been written by Siemens for the S7-200 Processor.

Table B-3 - Ramp function block inputs and outputs

Symbol	Type	Description / Function / Scaling
IN	REAL	Input value for RAMP block
MAX_VARIATION	REAL	Maximum output variation; Units per second
OUT	REAL	Ramp output value

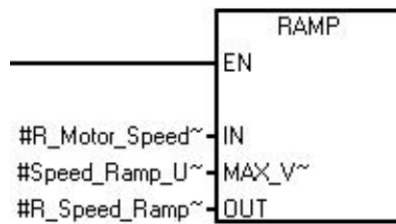


Figure B-6 - Ramp function block

Ramp times are usually defined for the maximum range of a value. For example, an AC inverter may have a ramp time set of 10 seconds. The drive will therefore take 10 seconds to ramp from zero speed to 100% speed. If the speed setpoint changed from 0% to 10%, the drive would take 1 second to ramp up to 10%. This is not what is required for our application. Instead, we require the ramp time to be effective for each speed change. In order to achieve this, we will calculate the maximum variation in units per second dynamically in the PLC program according to the current speed set and the next speed value to reach given in the following formula:

$$\left(\frac{(\text{New Speed Setpoint}) - (\text{Current Speed Setpoint})}{\text{Ramp Time (s)}} \right) \text{ABS} = \text{MAX_VARIATION} \quad (9-1)$$

ABS is a notional command that converts the result to always be a positive integer number. The MAX_VARIATION value is sent to the RAMP block. For example, we require a ramp time of 5 seconds from the current speed of 10% to 50%.

$$\text{Maximum variation units/second} = \left(\frac{50 - 10}{5} \right) \text{ABS} = 8.0 \quad (9-2)$$

The following function has been written to perform this calculation:

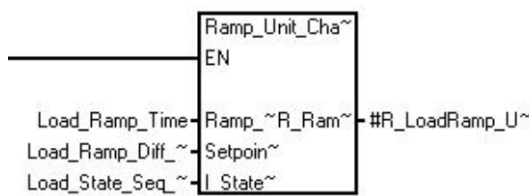


Figure B-7 - Ramp change calculation block

PLC variables

The symbol editor is used to declare all of the global program variables. These include the variables that are sent to and from the HMI). An extract from the actual program symbol table is shown below:

	Symbol	Address	Comment
1	Speed_to_Drive	AQW0	0 to 32000 = 0 to 10V
2	Load_to_Drive	AQW2	0 to 32000 = 0 to 10V
3	DC_Healthy	I0.0	'1' - DC Drive Healthy
4	AC_Healthy	I0.1	'1' - AC Drive Healthy
5	AC_Zero_Spd	I0.2	'1' - AC Drive at zero speed
6	SetUp_PB	M0.1	HMI > PLC 'Setup' pushbutton on operator screen
7	Steps_PB	M0.2	HMI > PLC 'Enter' pushbutton on Steps entry screen
8	Finish_PB	M0.3	HMI > PLC 'Enter' pushbutton on Speed & Load sequence set-up screen
9	RigStart_PB	M0.4	HMI > PLC 'Start' Pushbutton on Operator screen
10	RigStop_PB	M0.5	HMI > PLC 'Stop' Pushbutton on Operator screen
11	Allow_Start	M0.6	PLC > HMI Show Start PB on Operator Screen
12	HMI_Man_Mode	M0.7	HMI > PLC '1' - Select Manual Mode for operation (not sequence)
13	Rig_Running	M1.0	PLC > HMI '1' Test rig is running
14	Sequence_Times_Not_Eq	M1.3	PLC > HMI: Warning that speed and load sequence times are not equal
15	HMI_Manual_Start	M2.0	HMI > PLC 'Start' pushbutton in manual control area on Operator screen
16	HMI_Manual_Stop	M2.1	HMI > PLC 'Stop' pushbutton in manual control area on Operator screen
17	HMI_Repeat_Select	M2.2	HMI > PLC Select to repeat the speed sequence or not
18	Speed_Steps_HMI	Mw10	HMI > PLC Number of speed sequence steps required set on 'Steps entry' screen
19	Load_Steps_HMI	Mw12	HMI > PLC Number of load sequence steps required set on 'Steps entry' screen
20	Speed_To_Drive_INT	Mw14	PLC > Drive analogue output prior to scaling
21	Load_To_Drive_INT	Mw16	PLC > Drive analogue output prior to scaling

Figure B-8 - PLC Program Symbol Table for Test Rig Program (screenshot from S7-MicroWIN software)

B.1.2 Operator screens

The operator screens have been written on a Siemens TP177A unit that interfaces to the S7-200 PLC via a PPI connection (Point-to-Point Interface) that handles all of the data transfer between screen and PLC. The operation of the protocol is invisible to the programmer – the transfer of data values to and from the PLC is performed automatically and no communications routine is required.

The editing software used is Siemens WinCC Flexible Micro edition software. Each screen will be shown and the functions on the screen identified:

Main operator screen

This screen is the main screen used to operate the test rig once all of the parameters have been set-up. Auto or Manual running modes can be selected from this screen. **Automatic** mode runs the test rig according to data set up in the ‘Recipe Screens’. The speed and load setpoints are run from one value to another automatically and an option is provided to ‘Repeat’ the test rig operation continuously.

Manual mode allows a set speed and load to be run on the test rig for general operation.

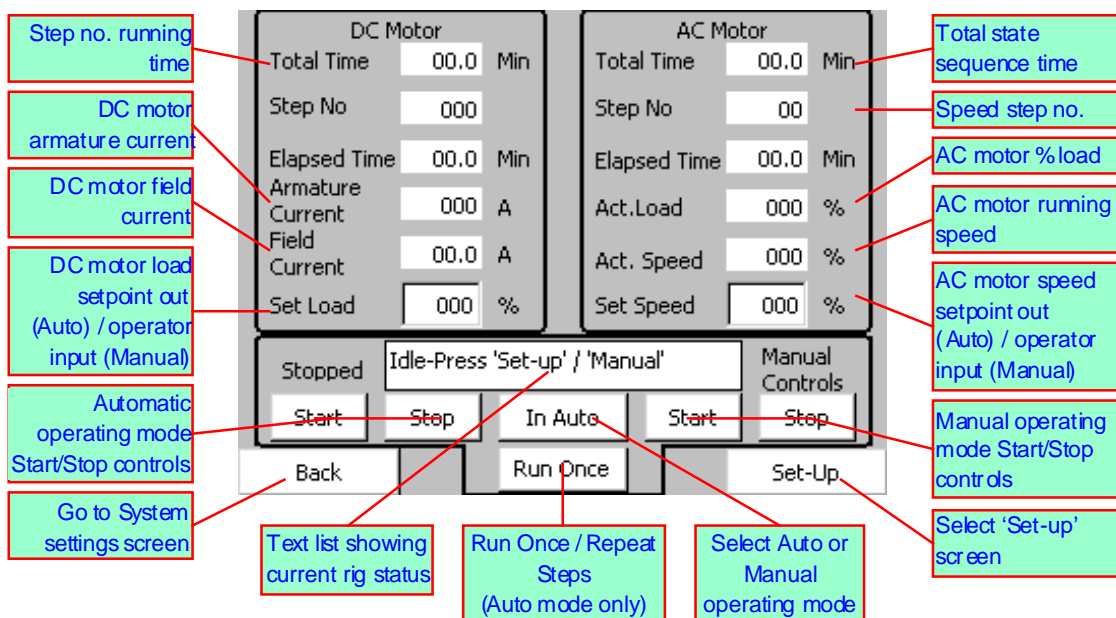


Figure B-9 - Main Operator Screen

This screen can be left at any time that the test rig is running without affecting operation.

All the DC motor status information is on the left of the screen. The load of the DC motor can be set here if the test rig is in manual mode, otherwise the load setting that is being sent to the DC motor from the auto sequence is shown. Other useful information is the total time that has been set for the load test to run and what step sequence is currently in operation.

The AC motor information is on the right of the screen. AC motor speed can be set here in manual mode and the actual motor speed and load percentage value can be viewed as well.

At the bottom middle of the screen is a text list showing the test rig status. If the test rig is not responding to user input, it is useful to check this to see which user step the test rig is waiting for if it cannot be operated for whatever reason.

Selecting Auto or Manual mode is performed by pressing the toggle button in the middle-bottom of the screen. By default, the test rig always starts-up in Automatic mode.

Automatic mode – Single Cycle:

'Start' and 'Stop' pushbuttons for this mode are at the bottom-left of the screen. The 'Start' pushbutton will only be shown once the number of steps required has been entered, all of the sequence step data has been filled in and the 'Finish' key pressed on this page. The test rig can be stopped at any time by pressing 'Stop'. The automatic mode can either operate as a single-step (runs through all steps and speeds then stops) or continuously where after the last step has finished, the test rig will start again from step 1 without stopping.

To switch modes, use the toggle button to select 'Run Once' or 'Repeat'.

Manual mode:

Manual mode operation keys are at the bottom-right of the screen. These are only shown if the test rig is in manual mode. 'Start' and 'Stop' buttons control the test rig.

The speed and load setpoint displays on the screen now change to input values so the operator can manually alter the values. A ramp time of 10 seconds is automatically applied to these setpoint values to protect the drive and load against sudden load or speed changes.

'Set-up' Screen

This screen lets the operator input the required number of speed values and load values to be run in sequence on the test rig. Once the number of steps has been entered, pressing the 'Enter' button will move to the 'Recipe' screens.

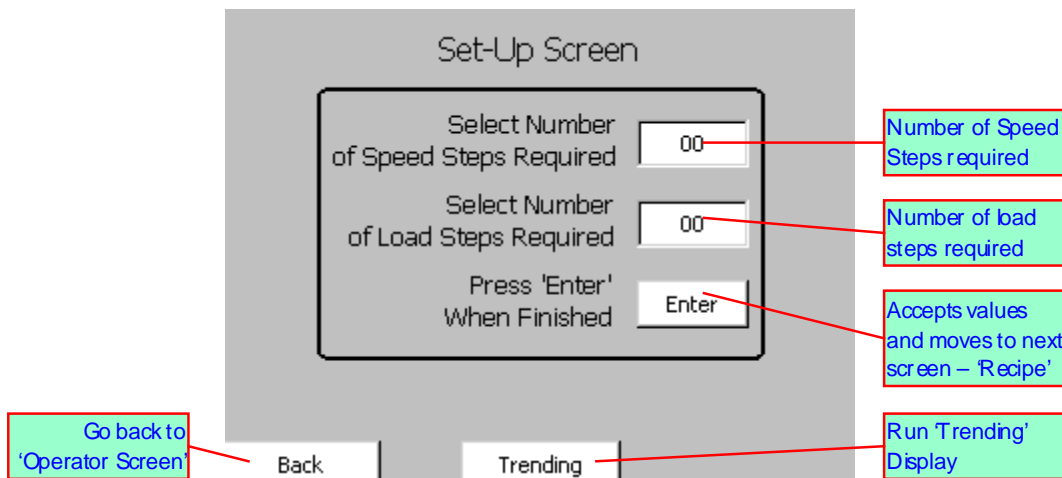


Figure B-10 - 'Set-up' Screen

To allow trending of values to assist with diagnostics, a trend screen is included on the display. Press the 'Trending' button to open the trend screen.

'Recipe' Screen

This screen is repeated 4 times for entry of up to 20 recipe steps for each of the load and speed sequences. Only the number of steps that were entered on the previous page will be shown, if the number of steps is lower than the step numbers shown on-screen, then blanks will be displayed on-screen. Once recipe entry is complete, pressing 'Finish' will return to the main Operator Screen.

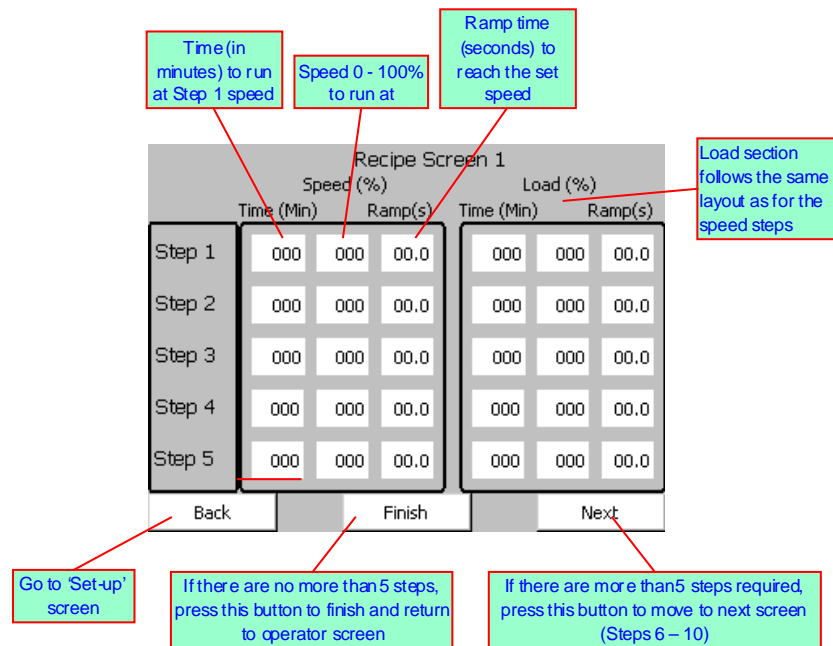


Figure B-11 - 'Recipe Screen 1'

Trend screen

The trend screen is configured to show the following values in a continuous display with an update rate of 1 second. The trend screen is shown below:

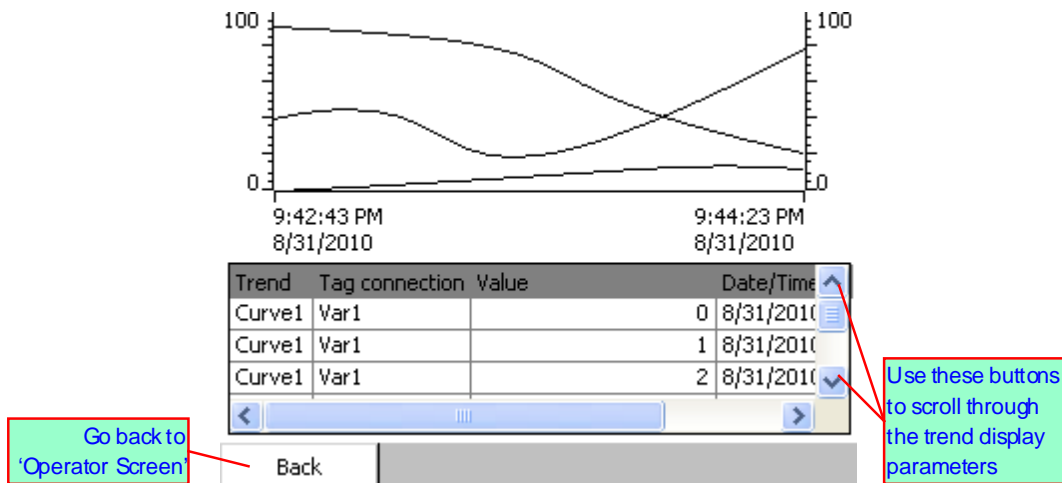


Figure B-12 - Trending Display Screen

This display is not intended to be used for accurate measurements, but as a general indication of test rig operation.

A list of inputs to and from the PLC to the operator display screen is given on the following pages. These inputs and outputs allow the operator to control the test rig and monitor its operation.

HMI > PLC (Inputs)

Table B-4 - Operator Screen to PLC Data

Address	Symbol	Description / Function / Scaling
M0.1	SetUp_PB	'Setup' pushbutton on operator screen
M0.2	Steps_PB	'Enter' pushbutton on Steps entry screen
M0.3	Finish_PB	'Enter' pushbutton on Speed & Load sequence set-up screen
M0.4	RigStart_PB	'Start' Pushbutton on Operator screen
M0.5	RigStop_PB	'Stop' Pushbutton on Operator screen
M0.7	HMI_Man_Mode	Select Manual Mode on Operator screen ('1' – Manual mode)
M2.0	HMI_Manual_Start	'Start' pushbutton in manual control area on Operator screen
M2.1	HMI_Manual_Stop	'Stop' pushbutton in manual control area on Operator screen
MW10 ^N	Speed_Steps_HMI	Number of speed sequence steps required set on 'Steps entry' screen; Value: 0 to 20
MW12 ^N	Load_Steps_HMI	Number of load sequence steps required set on 'Steps entry' screen; Value: 0 to 20
VW12...	Speed_Time_1	Recipe screen - Time to run at speed setting 1; Scaling: 0 to 50.0 minutes on screen = 0 to 30,000 in PLC
VW126*		
VW14...	Set_Speed1	Recipe screen - Speed to run at on step 1; Scaling: 0 to 100.00% on screen = 0 to 32,700 in PLC
VW128*		
VW16...	SpeedRampTime1	Recipe screen - Time to reach the speed setting; Scaling: 0 to 60.0 seconds on screen = 0 to 600 in PLC
VW130*		
VW150...	Load_Time_1	Recipe screen - Time to run at load setting 1; Scaling: 0 to 50.0 minutes on screen = 0 to 30,000 in PLC
VW264*		
VW152...	Load1	Recipe screen - Load to run at on step 1; Scaling: 0 to 100.00% on screen = 0 to 32,700 in PLC
VW266*		
VW154...	LoadRamp_1	Recipe screen – Time to reach the load setting; Scaling: 0 to 60.0 seconds on screen = 0 to 600 in PLC
VW268*		
VW270	HMI_Man_Speed	Operator screen – Manual speed setting; Scaling: 0 to 100% on screen = 0 to 32,700 in PLC
VW272	HMI_Man_Load	Operator screen – Manual load setting; Scaling: 0 to 100% on screen = 0 to 32,700 in PLC

^N - non-volatile memory area

* - total of 20 values, one for each step sequence (the next step addresses are offset by 6 – VW12, 18, 24 etc.)

PLC >HMI (Outputs)

Table B-5 - PLC to Operator Screen Data

Address	Symbol	Description / Function / Scaling
M0.6	Allow_Start	'1' - Show Start PB on Operator Screen
M1.0	Rig_Running	'1' - 'Test rig is running' status for screen
VW2	Main_State_Seq_OUT	Main state sequence number to indicate status of the test rig to operator and guide them as to the operation or next steps required. Values 0 to 4 are converted to a text list for display purposes with the following text displayed for each value: 0: "Idle – Press 'Set-up' or 'Manual' Pushbutton" 1: "Press 'Steps' Pushbutton" 2: "Press 'Finish' Pushbutton" 3: "Press 'Start' Pushbutton" 4: "Test Rig Running"
VW298	HMI_DC_Mot_Curr	DC Motor Armature Current Feedback; Scaling: 0 to 200A on screen = 0 to 32,700 in PLC
VW300	HMI_AC_Speed	AC motor actual speed; Scaling: 0 to 100% on screen = 0 to 32,700 in PLC
VW302	HMI_DC_Field_Current	DC Motor Field Current; Scaling: 0 – 4.7A on screen = 0 – 32700 in PLC
VW304	HMI_AC_Current	AC motor actual current; Scaling: 0 to 100% on screen = 0 to 32,700 in PLC
VW308	HMI_Speed_Seq_Time	Current elapsed time of the speed sequence step; Scaling: 0 to 50.0 minutes on screen = 0 to 30,000 in PLC
VW310	HMI_Load_Seq_Time	Current elapsed time of the load sequence step; Scaling: 0 to 50.0 minutes on screen = 0 to 30,000 in PLC
VW312	HMI_Speed_Step_No	Current step number of the speed sequence that is running; Value: 0 to 20
VW314	HMI_Load_Step_No	Current step number of the load sequence that is running; Value: 0 to 20
VW316	Motor_Speed_Set	Motor speed setpoint from the PLC to the AC drive; 0 to 100% on screen = 0 to 32,700 in PLC (0 to 10V at drive)
VW318	DC_Motor_Load_Set	Setpoint from the PLC to the DC motor field controller; 0 to 100% on screen = 0 to 32,700 in PLC (0 to 10V at controller)

Appendix C Commissioning tests

This appendix details the commissioning tests performed on the test rig and consists of four main sections.

C.1 The first test is for the initial calibration of all equipment used on the test rig, from the AC inverter to DC motor loading, after the PLC modification works were undertaken (first described in Chapter 5).

C.2 The second details the tests carried out to confirm the correct operation of the test rig automation PLC program.

C.3 The third section confirms the correct operation of the PLC program together with the calibrated test rig to ensure that the automation standard required of the test rig has been met and that consistent test result measurements can be carried out. Analysis of the modification works and the final results obtained are discussed in section C.3, page 10-5.

C.4 This gives actual pictures of the working operator screen taken during commissioning.

C.1 Test and calibration

In order to ensure the correct operation of the test rig, it is important to ensure that the rig is operating to specification. If the test rig is not calibrated correctly, then any results obtained from the rig will be invalid. The specification of the test rig is:

Maximum speed: 1750RPM

Maximum load (AC motor): 80% of motor F.L.C.

The following main parameters, given in Table C-1 can be adjusted to give the desired test rig operation:

Table C-1 - Main calibration parameters

Equipment	Parameter	Description / Function / Scaling
AC Drive	Maximum speed	Motor maximum speed RPM set to 1470RPM
	Motor Current	Motor maximum current (A) set to 20.7A
DC Field controller	Maximum current	Maximum DC motor field current adjustment potentiometer

The test rig has two modes of operation, Manual and Automatic. To test the rig calibration, the following test runs were carried out and the results noted. The values for these results were taken from the AC drive operating keypad on the front of the test rig:

Table C-2 - Calibration results table 1

Test conditions	Parameter	Value
100% speed	Motor speed	1470RPM
0% Load	Motor current A	≈3.6A (Motor F.L.C. 11.2A)
100% speed	Motor speed	1200 – 1400 RPM (oscillating)
100% Load	Motor current A	22 – 31A (oscillating)

The maximum load value of the AC motor was being exceeded and the drive was limiting the motor current after a period of time running at over 150% rated motor current. The drive manual states "Output Overload Motoring 150% for 60s, 180% for 0.5s short term rating" [60]. After 60 seconds of

running at 150% current, the drive will limit the motor output voltage to reduce the current. This limitation was occurring in an oscillating manner – the drive limiting maximum current down to approx 90% in order to protect itself and the motor, then restoring 150% current after a time, before limiting it again. If the test rig was to operate in this manner for a length of time, the motor could be damaged due to being thermally overload. This was the reason for limiting the maximum loading to 80% of motor FLC to protect against accidental against test-rig misuse.

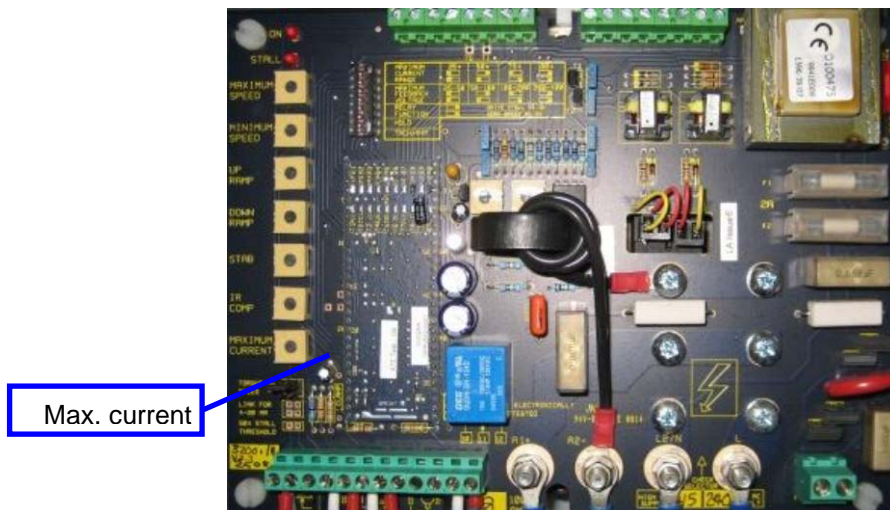


Figure C-1 - Field controller (maximum current potentiometer arrowed)

The current of the DC field was reduced by using the adjustment potentiometer on the field controller (see following diagram). After this adjustment, the test results were taken again.

Table C-3 - Calibration results table 2

Test conditions	Parameter	Value
100% speed	AC Motor speed	1470 RPM (steady) – confirmed by using hand-held tacho to verify RPM value
100% Load	AC Motor current A	18A (steady)
	DC Motor current A	40A (from current-clamp meter)

Calibration checks 1:	Expected Value	Actual value	Result
Maximum motor speed	1470RPM	1470RPM	PASS
AC motor loading	18A	18A	PASS

The current transformer used to measure the DC motor current was checked next. The specification for this units is:

DC Current range:	0 to 200A (DC Motor maximum current rating)
Supply voltage:	24VDC
Output voltage:	0 to 10VDC (0.5% accuracy)

For the test below, the following result was taken:

Table C-4 - Calibration results table 3

Test conditions	Parameter	Value
100% speed	DC Motor current A	27.8A (measured from current-clamp meter)
80% Load	Output from C.T.	1.3V

The current, I measured from the CT can be calculated as the a ratio of the maximum output voltage:

$$I = \frac{1.3}{10} \bullet 200 = 26A$$

This was deemed to be of sufficient accuracy as the CT is purely for indication, not actual measurement.

<u>Calibration checks 2:</u>	<u>Expected Value</u>	<u>Actual value</u>	<u>Result</u>
DC motor current transformer	27.8A	26A	PASS

Calibrating the operator screen

Now that it was confirmed the DC test rig was operating to specification, the operator screen of the PLC would need calibrating to indicate correct values for the test rig .

The scaling of operator screen values is as follows:

Table C-5 - Operator screen value scaling

Parameter	PLC Value	Screen Display Value
DC Armature current	0 to 32700	0 to 200A (scaling determined by maximum CT rating and max. DC motor current)
DC Field Current	0 to 32700	0 to 4.2A
AC Motor Actual Load	0 to 26160	0 to 100% (Note 100% load is indicated for actual 80% load: $32700 \times 0.8 = 26160$ maximum PLC value)
AC Motor Actual Speed	0 to 32700	0 to 100%

The PLC scales analogue inputs according to the following specification. Analogue output values are scaled in the same manner.

<u>PLC Integer value:</u>	<u>Input voltage:</u>
0 to 32,700	0 to 10VDC

It is common to scale the display to the maximum value possible from the input, although in reality this will never be realised. One example is the DC armature current. From commissioning tests performed, the maximum expected current is 40A and this equates as a voltage input to the PLC of 2VDC.

The only screen display that has been purposely configured to not be a true representation of an input is the AC motor load value. The test rig screen has been calibrated to indicate 100% load demand and feedback, with the drive at 80% load, so the rig motor cannot be overloaded.

C.2 PLC program verification

Once the test rig had been calibrated, the next series of tests would validate the correct operation of the program sequence.

For this, Siemens Step7 Microwin32 software was used and the programming Laptop connected to the PLC using the CP5512 interface adaptor. This allows the program to be monitored on-line and even program changes to be made whilst the test rig is running.

The design diagrams for the software were printed out and these were used to check the program operation against the original design.

Initial testing revealed problems with:

- Ramped setpoints from one step to the next not operating (setpoint changing immediately)
- Ramp times from step to step not equalling the values set on-screen
- Test rig not stopping correctly and failing to re-start

Another problem became evident as the program operation was improved during testing – the PLC ran out of memory. The PLC has a maximum of 4kbytes for program data and the automation program had exceeded 4.2kbytes. This required some subroutines to be re-written to use the program instructions more effectively (less operations). Eventually with much re-writing of program code, the size was reduced to 3.8kbytes. This allows for some program modifications to be made in future without reaching the PLC limit.

Eventually, the issues found were fixed over the next few weeks of test rig operation. A list of faults found by other users of the test rig was made and these were corrected at subsequent visits to the University.

C.3 Tests to verify the automated test rig results

Initial testing

There are various conditions under which the test rig can be operated. The speed and load can be set to any value, for any period of time but it is important to ensure that the rig can be trusted to perform concurrent tests in a repeatable and accurate manner. This will guarantee that test data obtained from the test rig can indeed be trusted to form an accurate base for analysing and comparing good vs. bad conditions on whatever the motor is controlling. If the speed or load conditions are not repeatable, then the test data is all but invalid.

The first series of tests will involve setting some speeds and loads for the test rig to operate under, then repeating these a number of times whilst recording sampled data from the rig and analysing this later on.

Signals required from the inverter

The type of inverter fitted to the Bearing Test Rig is a Parker SSD 690+ 11kW AC Vector Drive. This inverter comes as standard with three analogue outputs. These can be configured to output +/-10V, 5V or 4 – 20mA depending on the application requirements.

There are a total of three analogue outputs that are used for signal analysis.

Analogue output configuration

In each 690+ drive, there are ranges of freely configurable blocks provided as standard that the user can program for their application. The blocks that control the analogue outputs are shown in Figure C-2 below:

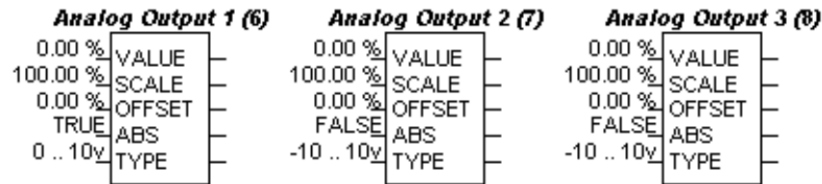


Figure C-2 - Analogue output scaling blocks [50]

The scaling, type and offset of each analogue output is programmable, with the source of the output being selected from the parameter 'VALUE' on the block. The internal structure of the block is shown in the Figure C-3 below:

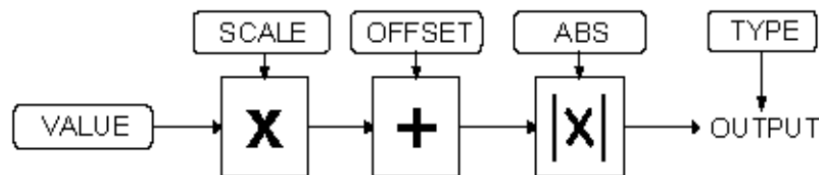


Figure C-3 - 690+ Analogue output scaling function [50]

Selection of signal for analysis

Upon investigation of the various feedback signals that the Parker 690+ drive provides, there are not many that could be useful for detailed signal analysis. For example, it is not possible to monitor the current of each phase separately (although the drive does this internally in order to monitor and control the motor) or the voltage of each individual phase.

There is, in fact only one 'Feedback' block that might provide some of the signals required for analysis and this is shown in below:

<i>Feedbacks</i>	
DC LINK VOLTS	0 V
TERMINAL VOLTS	0 V
SPEED FEEDBACK RPM	0.00 rpm
SPEED FEEDBACK REV/S	0.00 rev/s
SPEED FEEDBACK %	0.00 %
ENCODER FEEDBACK %	0.00 %
ENCODER COUNT	0
TORQUE FEEDBACK	0.00 %
FIELD FEEDBACK	0.00 %
MOTOR CURRENT %	0.00 %
MOTOR CURRENT	0.0 A
* 10.0 V	
* 2048	
* FALSE	
* QUADRATURE	
FALSE	
ENCODER SUPPLY	
ENCODER LINES	
ENCODER INVERT	
ENCODER MODE	
QUADRATIC TORQUE	

Figure C-4 - 690+ Drive 'Feedbacks' Block [50]

This feedback block allows some of the motor data to be observed and some of the more useful outputs are given in Table C-6:

Table C-6 - 'Feedbacks' block observation data

Parameter	Description
SPEED FEEDBACK RPM	In SENSORLESS VECTOR mode (no encoder feedback fitted to the test rig drive) the parameter shows the calculated mechanical speed of the motor in a percentage, scaled from 0 – 100% = 0 RPM > 'Maximum motor RPM' calibration value set in the drive
TORQUE FEEDBACK	Shows the estimated motor torque, as a percentage of rated motor torque
MOTOR CURRENT %	This diagnostic contains the level of rms line current being drawn from the Inverter and is seen as a % of the MOTOR CURRENT parameter setting in the MOTOR DATA function block.
MOTOR CURRENT	This diagnostic contains the level of rms line current being drawn from the Inverter.

From the table shown previously, the parameters TORQUE FEEDBACK and MOTOR CURRENT and SPEED FEEDBACK % will be linked to the test rig by a 9-way D-Type socket mounted to the test rig for this purpose.

The outputs were not scaled so the following output will be output from the drive for the signal conditions as follows:

Table C-7 - Scaling of drive output data

Parameter	Drive Value	Output value
TORQUE FEEDBACK %	0 to 100% Motor torque	0 to 10VDC
MOTOR CURRENT %	0 to 20.6A = (Includes magnetising current)	0 to 10VDC
SPEED FEEDBACK RPM	0 to 1470 RPM	0 to 10VDC

The actual configuration of drive analogue outputs is shown in Figure C-5 below:

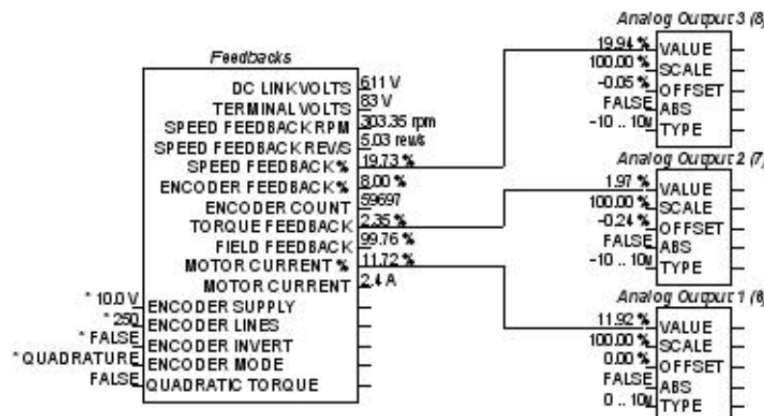


Figure C-5 - 'Wiring' of inverter Feedbacks block to physical analogue outputs

This figure is taken from a screenshot of the actual drive configuration program, 'DSELite' provided by Parker Hannifin SSD Drives for the purposes of programming their inverter drive equipment.

Trial simulation tests

The trial simulation tests are designed to ensure that the test rig is operating in a reliable and predictable manner over the range of operating conditions applied so that any future results obtained from the rig can be shown to be accurate. Tests will be performed with known good equipment to use as a base-line for all results. It may be found that the test rig is not operating satisfactorily under these trial tests, even though initial commissioning tests under 'C.1 - Test and calibration' may have found the operation to be as expected. The drive on this test rig will have to undergo a series of trial tests to prove its performance and although it is not always possible to recreate all the conditions under which an item of equipment will be operated, these tests will provide a useful starting point.

In addition to the main rig equipment (PLC and Drive), these tests would also confirm that the data logger was reading data correctly and that any scaling of values was accurate and representative of actual data. Verifiable data can only come from an accurate and quantified data source. If there were any errors at the data collection point, this will leave any results obtained open to question.

Test rig equipment notes

The Parker 690+ inverter was initially selected to run in 'Sensorless Vector Mode' for these tests. Test results will be analysed using a graph generated by a Matlab[®] routine from the test rig data. The data logging system records data from a maximum of 18 channels, but we are interested only in data from four channels recorded from the rig:

Table C-8 - Data logging channels - Commissioning tests

Channel	Description	Source
12	Speed feedback %	AC Inverter Analogue Output 1
13	Torque feedback %	AC Inverter Analogue Output 2
14	Motor current %	AC Inverter Analogue Output 3
15	Speed demand %	PLC Analogue Output 1

Commissioning Test # 1a

The speeds, load values and times that the rig is to run for are as below:

Table C-9 - Commissioning Test 1a Data

Step	Speed (%)	Load (%)	Time (s)
1	100	20	60
2	100	40	60
3	100	60	60
4	100	80	60
5	100	100	60

Total test running time: 5 minutes

The speed (%) is a percentage of the maximum calibrated motor speed for the test rig AC motor. The maximum speed of this is: RPM

The load (%) value is a percentage of the maximum field current of the DC machine. However, the DC field controller has been set to only allow a maximum of 80% load to be AC motor at full speed to avoid running the motor at 100% load for long periods of time and risk burning out the motor. So, when a load value is set, this will need scaling down by a factor of 0.8 to read the correct results on the graphs. Three tests will be run using the above settings and the data from the test rig recorded for each.

The output from this first run is given in Figure C-6:

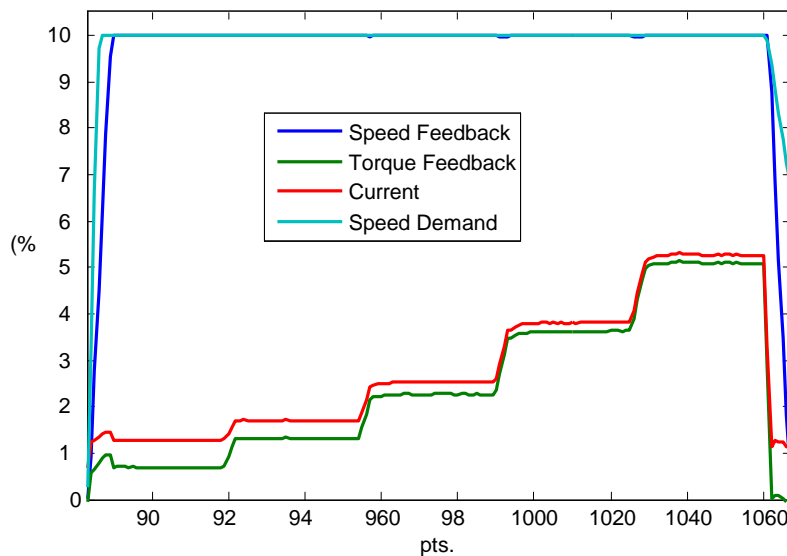


Figure C-6 - Rig test 1a; 100% speed, varying load

Although the load values are: 20, 40, 60, 80 and 100%, the motor actual torque does not reflect this. Part of this is due to the DC load 100% being calibrated for a maximum of 80% motor load. However, the values read back are lower than expected – we should be achieving 80% load at full AC motor speed. The table of results obtained from manual readings obtained with a manual voltmeter is given below (0 – 10 VDC voltage converted into percentages by multiplying by 10):

Table C-10 - Table of load readings; Test 1a

Step	Speed (%)	Actual Load (%)
1	20	6.92
2	40	13.17
3	60	22.68
4	80	36.21
5	100	50.94

The initial results also show that the DC motor cannot generate full load unless the AC motor is running at full speed. Power (if motoring), and load (generating) in this case depend on the: Power = Speed x Torque equation. A lower AC motor speed yields lower armature voltage on the DC machine, therefore lower torque and therefore reduced power. As the DC motor is feeding into a resistor bank (no

armature supply for generating an opposing force to the AC motor at lower speeds) there is no way around this.

The test will be run a further two times and the results from these compared to the first test run.

Commissioning Test # 1b

This test is the same as test #1a and the results will be compared on a graph by overlaying test 1b over test 1a and seeing if they are the same. The graphs are shown in Figure C-7:

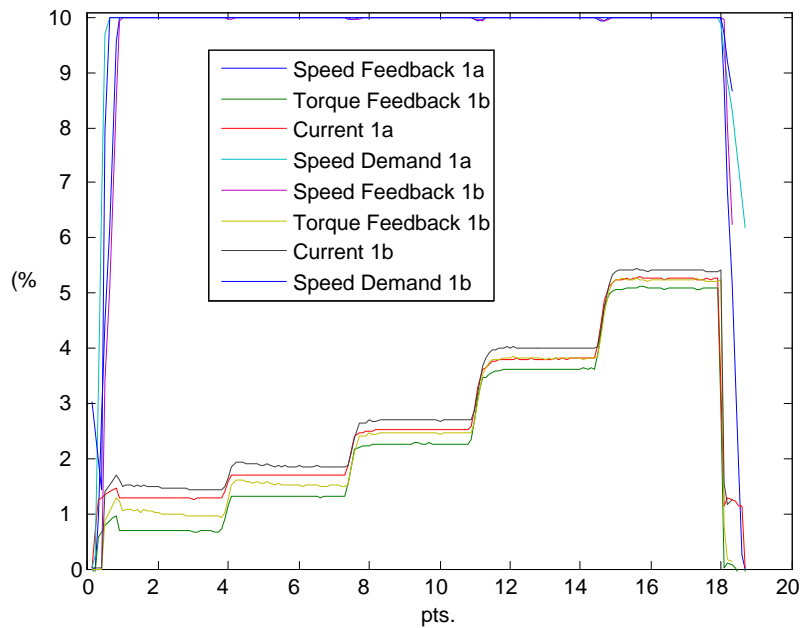


Figure C-7 - Rig Test 1b; 100% speed, varying load

The speed response is almost identical but the current feedback and torque feedbacks behave differently on each run. Run 1b feedbacks are slightly higher than run 1a. The test will be run again and the results from test 1b overlaid with test 1c:

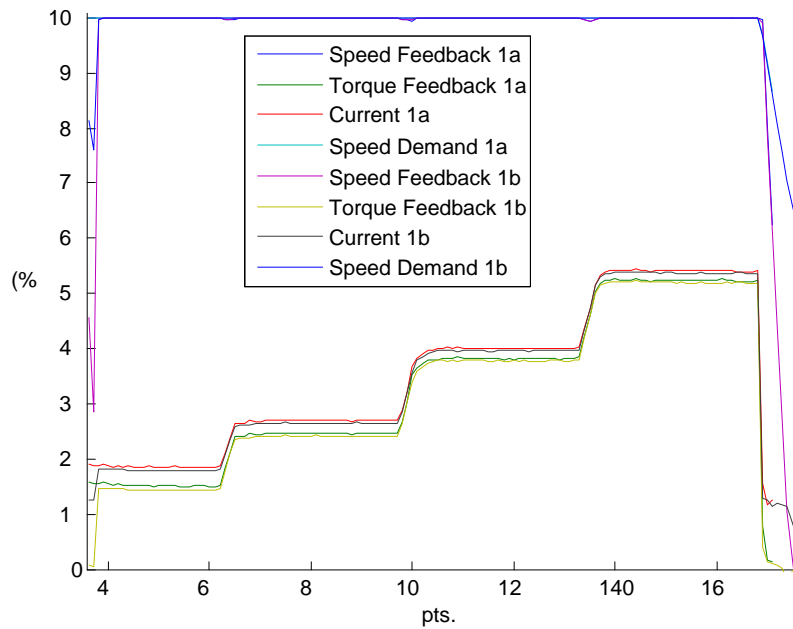


Figure C-8 - Rig Test 1c; 100% speed, varying load

The results from this run are almost identical. The important aspects to note from the results are:

- Rate of rise and timing of current steps is accurate and repeatable although current feedbacks may differ slightly
- The speed rate of change of demand and the speed feedback is repeatable

Figure C-8 confirms that the test rig PLC is providing consistent control signals to operate the test rig, even through the readings back from the test rig may not be the same from one run to the next.

The chart below shows the run from Test 1b comparing the motor current feedback from the inverter analogue output to that read by electronics monitoring the current in one of the motor phases to see if the signals are comparable.

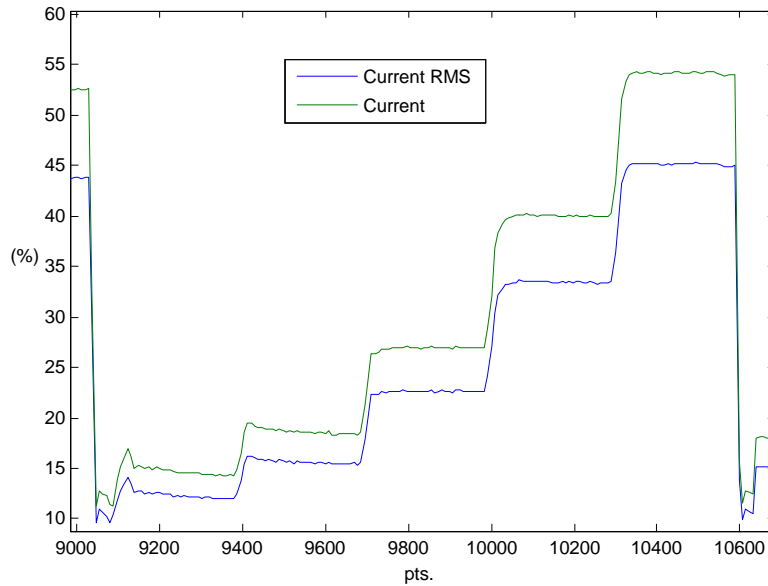


Figure C-9 - Comparing AC inverter current feedback to actual measured instrument values

The magnitude readings of the current feedbacks are not equal as there were some scaling issues during recording of data, but the intention is to show that the analogue output from the drive is representative of the actual motor current at the sampling rates we are running for these tests.

There appear to be some scaling issues with what the graph is showing and what the results were when viewed on the data logger dashboard. This dashboard runs on the PC used to gather data from the test rig. When the tests were run, the motor torque of approximately 80% at full speed that was read from the AC drive display matched that shown on the dashboard. The scaling factors will be investigated and these tests run again.

Commissioning Test #2

Test 2 will determine how a constant load setpoint on the DC motor (constant field current) affects the load that the AC motor sees when the speed is increased in steps. The test data is as given in Table C-11:

Table C-11 - Commissioning Test 2 Data

Step	Speed (%)	Load (%)	Time (s)
1	20	30	60
2	40	30	60
3	60	30	60
4	80	30	60
5	100	30	60

This test was run and the following Figure C-10 obtained

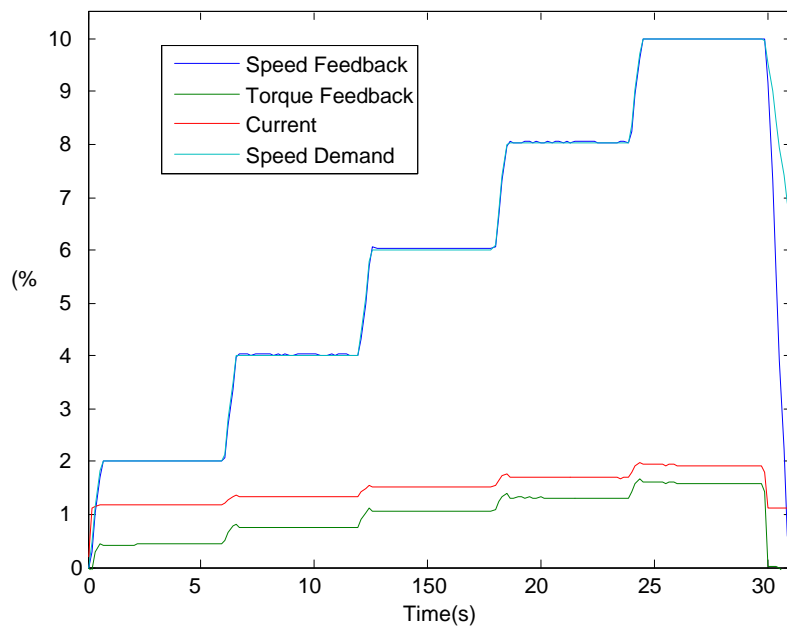


Figure C-10 - Commissioning Test 2; 30% load; Speed incremental steps

The motor torque feedback only reaches near the load setting when the motor is at full speed. The DC motor does not act as a constant load to the AC machine, although in real-world situations the motor load will rarely remain constant over a range of motor speeds.

The graph shows how the motor current is not a good indicator of true motor load, especially at lighter loads due to the magnetising current required that is present even before the motor begins to turn.

Helpfully, the drive also provides a motor torque output that offsets the magnetising current taken by the motor from the feedback readings to give a true indication of the motor load. As can be seen from the red and green graphs, the increase in motor torque for a given speed is more linear on the torque reading than for the current.

The above results also show that at 30% field current setting on the DC motor the maximum factored load on the AC motor should be: $30 \times 0.8 = 24\%$. The results are given in Table C-12.

Table C-12 - Table of load readings; Test 2

Step	Speed (%)	Actual Load (%) Motor torque	Step change
1	20	4.40	
2	40	7.51	3.11%
3	60	10.49	2.98%
4	80	13.17	2.68%
5	100	15.82	2.65%

The DC motor loading to the AC motor at full speed is far short of what we would expect, as the reading should be nearer 18%. This could be due to scaling issues as reported in test 1c, so this test will be run again as test 3.

Commissioning Test #3

Test 3 is similar to test 2, but with the DC motor load increased from 30% to 60%. This test was run and the following Figure C-11 obtained

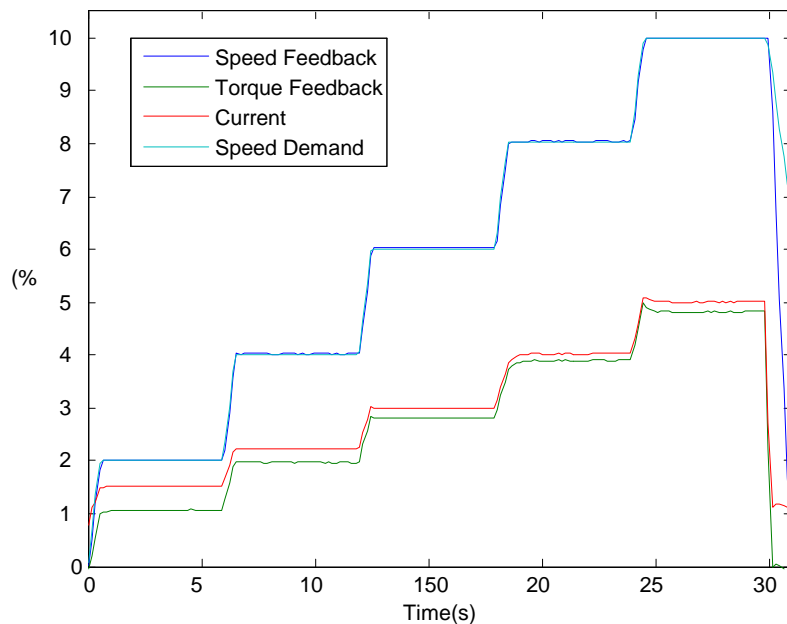


Figure C-11 - Commissioning Test 3; 60% load; Speed incremental steps

The results are given in Table C-13 below:

Table C-13 - Table of load readings; Test 3

Step	Speed (%)	Actual Load (%) Motor torque	Step change
1	20	10.72	
2	40	19.66	8.94%
3	60	28.13	8.47%
4	80	38.67	10.54%
5	100	48.15	9.48%

The actual maximum load value is now 48.15%, compared to the factored theoretical value of: $60\% \times 0.8 = 48$. This is the load value that we would expect from the AC motor and shows that the DC motor load to the AC motor may not be directly proportional to the field current supply. There must be some non-linearity in the DC motor speed/current relationship especially at lower field currents.

Commissioning Test #4

This test is run to see how the AC motor is loaded when the DC motor is set to give 100% load (factored to 80% actual) and the AC motor is ramped up linearly in speed. This will test how the DC motor actual load behaves under the full speed range of the AC motor.

Table C-14 gives the settings that were made on the test rig screen. With the AC motor initially at zero speed, with full field current on the DC motor this allows the field controller to stabilise.

Table C-14 - Commissioning Test 4 Data

Step	Speed (%)	Load (%)	Ramp time	Time (s)
1	0	100		60
2	100	100	60	60
3	0	100		60

Figure C-12 shows the initial run:

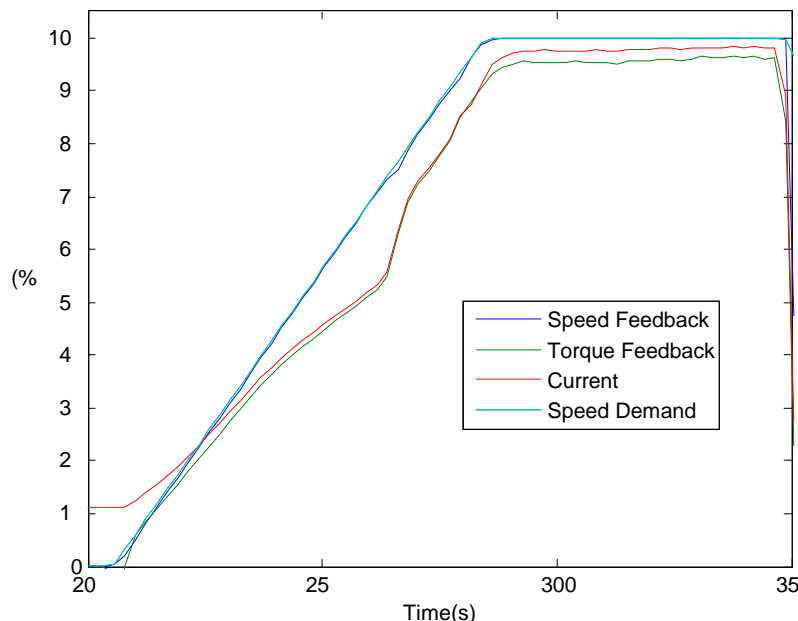


Figure C-12 - Commissioning Test 2; 30% load; Speed incremental steps

Commissioning Test #5a

This test is run to help determine the cause of the motor load non-linearity seen during acceleration and also determine if there may be any issues with the gearbox. The running parameters are as shown below

Table C-15 - Commissioning Test 5a Data

Step	Speed (%)	Load (%)	Ramp time	Step Time (s)
1	0	100	-	60
2	100	100	300	300
3	0	100	300	300

Figure C-13 shows the complete acceleration and deceleration curve, the total time taken to run the test is 10 minutes, not including the settling time at start-up.

Taking the acceleration phase first, the first notable item from the figure is the non-linear increase in motor load with an increasing speed from 20% to 70%. On reaching 70% speed, the load immediately

increases to a higher value over a very short period of time. From this point on, the increase in loading follows a linear pattern up to approximately 85% speed, where there is another marked increase in load. The deceleration phase shows that the corresponding decrease in load at a particular speed does not mirror the acceleration part of the curve. The decrease in load happens at a lower speed than in the acceleration part.

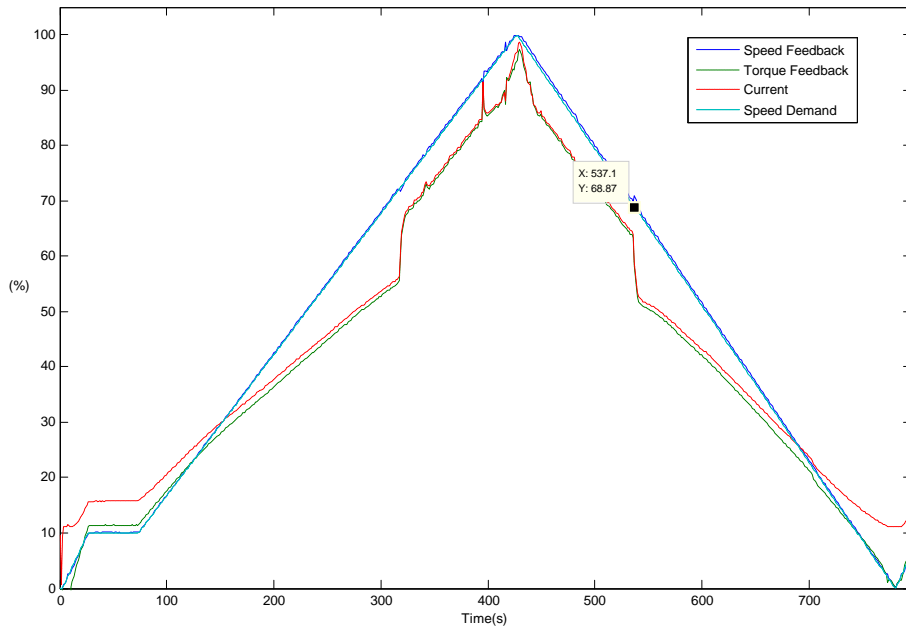


Figure C-13 - Commissioning Test 5a; 100% Load, Speed ramped 0 -100%

The sudden rise in the motor loading can be seen clearly from Figure C-14 when the running speed reaches above 72%. At the same time, the speed feedback drops slightly, indicating that the problem is likely to be with the load to the motor, rather than a characteristic of the AC drive. For a stable load, we would expect the speed feedback to rise at the same rate as the setpoint and lagging slightly behind.

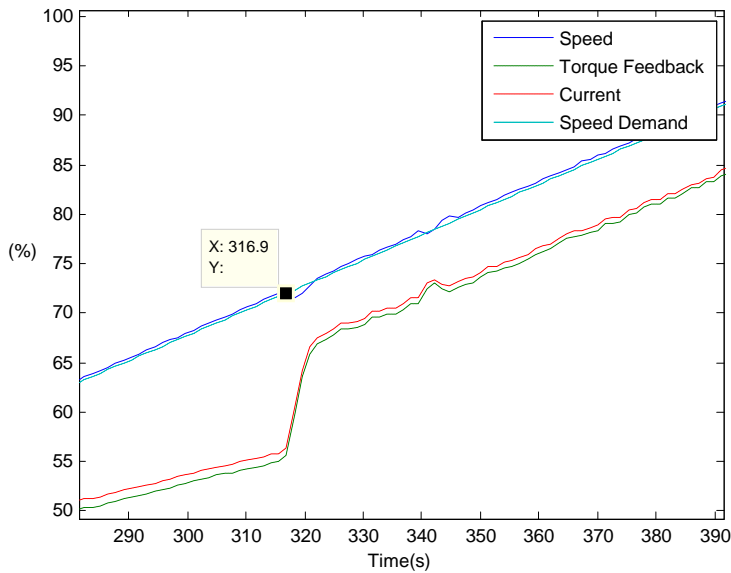


Figure C-14 - Commissioning Test 5a; 100% Load, Speed ramped 0 - 100%

If the speed setpoint of 72% is zoomed into more closely – see Figure C-15 – the drop in speed feedback is easier to see. To be sure that this is the cause of the load it is necessary to monitor the DC motor armature current and also the field current to ascertain if this is stable.

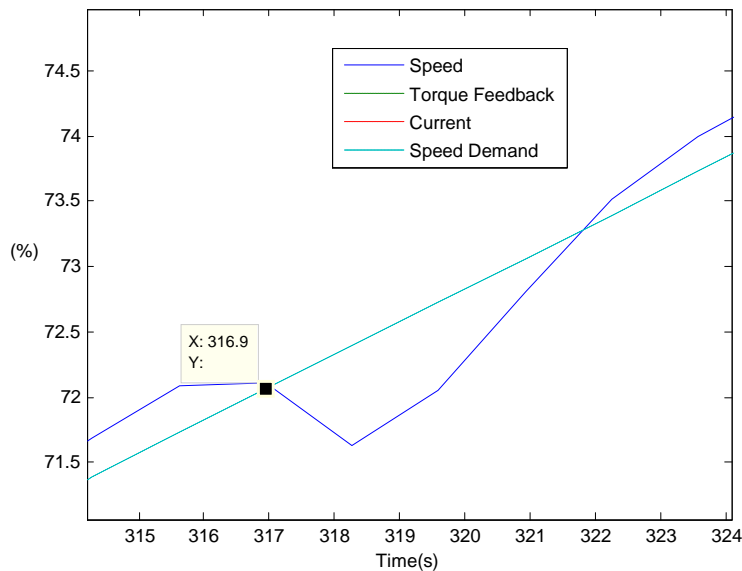


Figure C-15 - Commissioning Test 5a; 100% Load, Speed ramped 0 - 100%

The AC motor speed at 72% will be (1470×0.72) 1058 RPM, the DC motor has a maximum speed of 1470 RPM so is rated correctly for the test rig (the motor does not run above base-speed which may affect the torque/speed curve if this was the case).

Commissioning Test #5b

This test is a repeat of test 5a, and is to clarify that the results of this test can be repeated. The plot in Figure C-16 below indicates the results of this test.

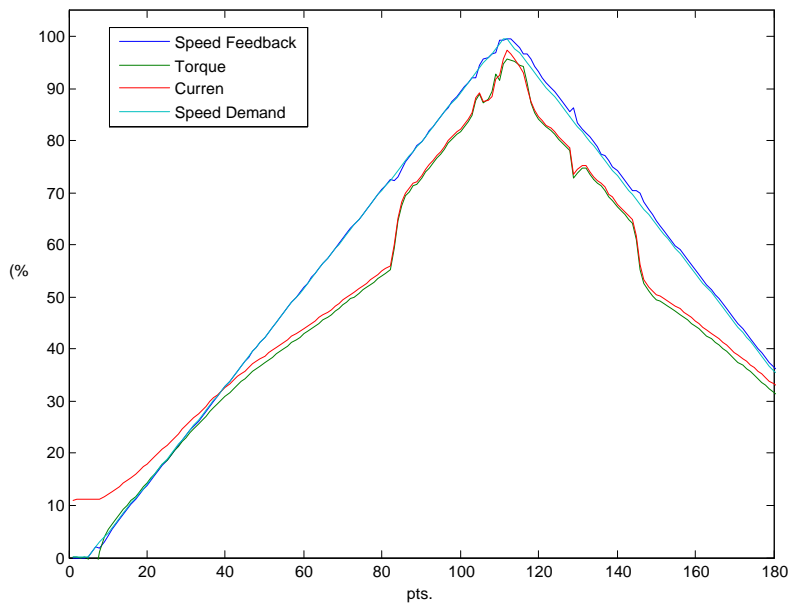


Figure C-16 - Repeat of Commissioning Test 5a; 100% Load, Speed ramped 0 - 100%

This plot has the same characteristics as the initial plot, so there is no need to analyse the results further.

Commissioning Test #5c – Closed-loop vector mode (encoder fitted)

The AC motor is controlled in open-loop vector mode at present. This gives satisfactory operation for most fixed-load, fan and pump applications. Speed holding accuracy is poor by modern motor control methods, achieving 2% over the speed range. This can lead to an accuracy of +/-29RPM for our motor (1470RPM at 50Hz).

Part of the test rig modifications involved closing the motor control loop by fitting an encoder to the motor for speed feedback purposes. This allows the motor torque and speed to be more finely controlled with speed holding of typically +/-0.1%.

The existing motor encoder being used for external data monitoring was a 100PPR unit. This was not sufficient for the Parker SSD drive, which requires a minimum of 350PPR (the drive performs a quadrature function on the encoder A&B signals, so $350 \times 4 = 1400$ PPR) to function in this mode. With encoder feedback, there is a minimum number of encoder pulses required in order to guarantee a reliable speed feedback signal. If this is too low, quantisation errors will occur and the error generated from one encoder value sample to the next can be enough to cause instability in a highly-tuned drive speed loop. A greater number of pulses yields a more accurate speed feedback signal and improved drive performance.

Thus configured, a Parker 690+ drive has an advanced auto-tune feature that allows the drive to accurately model the motor based on such parameters as:

- Motor stator inductance (mH)
- Rotor inertia (kg / m²)
- Magnetisation current (mH)

This is performed on a rotating auto-tune basis and is essential for the drive to control the motor effectively especially when running higher control-loop gains under encoder feedback.

A rotating autotune has already been performed when running without the encoder, but another will be run with encoder feedback. It is imperative that for the rotating autotune to provide a correct motor model, the motor should be disconnected from the load. If this is not done, the drive will obtain an inaccurate measurement for some drive parameters. One instance could be the magnetisation current where a high load on start-up would incorrectly signal to the drive that a larger motor current than is actually necessary is to be applied in order to get the motor to turn. If the motor were free-turning, then the current required to rotate the motor would be far less and the motor obtains an accurate motor model.

The results of this test are shown in the next figure and to illustrate the difference, this can be compared with Figure C-16.

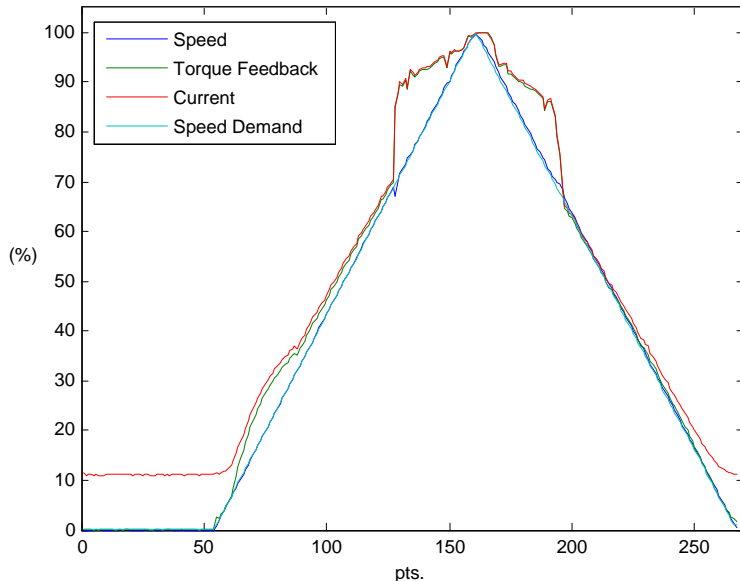


Figure C-17 - Test run 5c; Autotune performed

The motor load behaviour is far more linear up to approximately 70% speed, whereupon there is a more marked increase in motor current from approximately 70% to 90% in a period of 1-2 seconds. What is of note is the improved speed response under acceleration. There is minimal overshoot at the top of the graph when compared with sensorless vector mode.

Commissioning Test 6

Before this test was run, the motor was de-coupled from the gearbox and a rotating drive autotune performed. According to the drives manual, an autotune must be performed when running in either closed loop speed or sensorless vector mode.

Autotune feature identifies motor characteristics for the drive motor modelling algorithm, to allow the drive to control the motor correctly. It loads the values into the parameters below, which are in the QUICK SETUP menu.

Table C-16 - 690+ Drive Autotune Parameters

Parameter	Description
MAG CURRENT	Motor magnetising current (A)
STATOR RES	Per phase stator resistance (Ω)
LEAKAGE INDUC	Per phase stator leakage inductance (mH)
MUTUAL INDUC	Per phase mutual inductance (mH)
ROTOR TIME CONST	Rotor time constant (ms)

This test would chart the no-load speed vs. torque curve from 0% to 100% speed, as given in Table C-17.

Table C-17 - Commissioning Test 6 Data

Step	Speed (%)	Load (%)	Ramp time	Step Time (s)
1	0	0	-	60
2	100	0	300	300
3	0	0	300	300

Figure C-18 shows the results of this test.

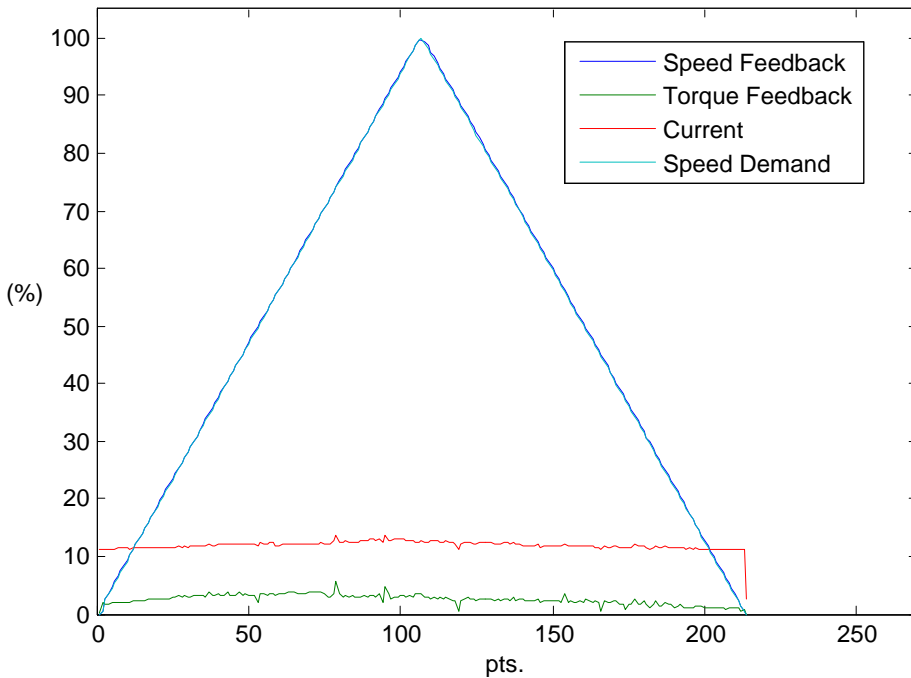


Figure C-18 - AC Motor no-load motor torque/speed plot

There only disturbance to the motor torque comes again at approximately 75% speed – the same point at which the disturbance was discovered under load. Under this test, the DC motor is not loading the AC motor so there is no influence from this. Otherwise, the increase in torque and current is normal and does not show any undue loading of the motor by the mechanical system.

Commissioning Test 7

Test 7 will run the motor to 100% speed, then ramp up the load gradually from 0% to 100% over 3 minutes. This is to verify that the DC motor is providing a linear increase in load as the field current increases.

Table C-18 - Commissioning Test 7 Data

Step	Speed (%)	Load (%)	Ramp time (s)	Step Time (s)
1	100	0	120	120
2	100	100	120	120
3	100	0	120	120
4	0	0	120	120

Figure C-19 verifies this. The initial 10% of AC motor current can be disregarded as this is the sum of motor magnetising current, together with friction and windage losses, resistance of rotor and stator windings and the core losses.

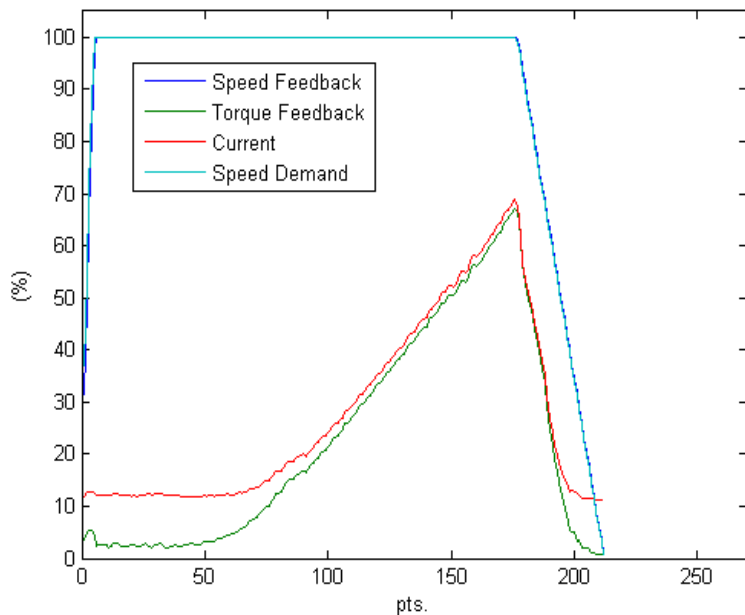


Figure C-19 - Test 7; verification of DC motor loading

The black line drawn through the graph shows there is no deviation from the straight-line increase in motor torque and current and therefore the relationship between motor field current increase and the increase in armature current is linear.

Commissioning Test 8

The test parameters for this are identical to those under test 1a so do not need repeating here. Figure C-20 below illustrates the results of this test and on the initial comparison with Figure C-6 not much difference can be seen, but on zooming into the speed feedback trace, the difference between open-loop and closed-loop mode during stepped load increases is marked.

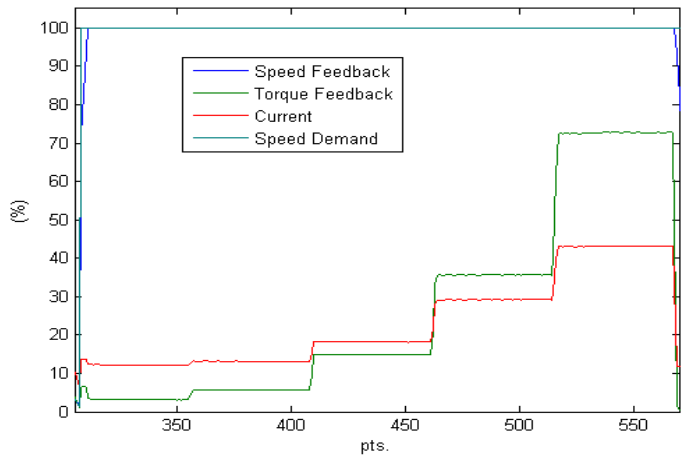


Figure C-20 - Commissioning Test 8

In order to interpret the data correctly, the load settings for each of the figures at the points x-axis are given in Figure C-21 below:

Table C-19 - Graph points vs. load settings

Figure (a)			Figure (b)		
Points	Speed (%)	Load (%)	Points	Speed (%)	Load (%)
955 – 985	100	60	420 – 460	100	60
986 – 1025	100	80	461 – 510	100	80
1026 – 1060	100	100	511 – 560	100	100

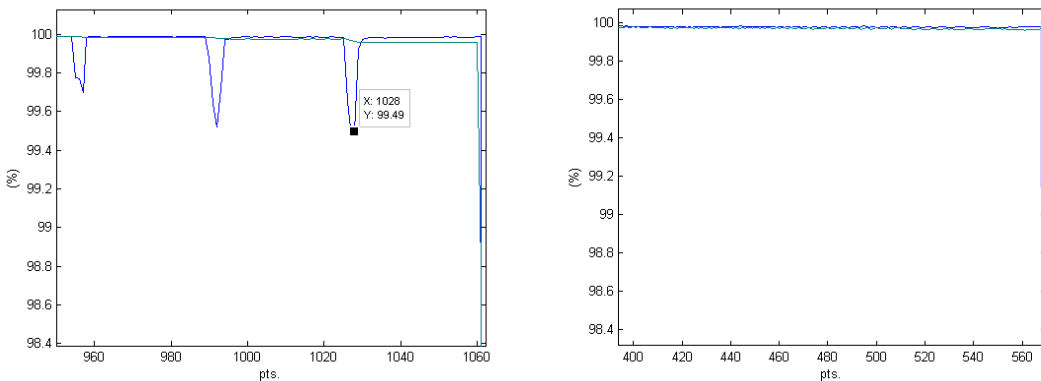


Figure C-21 - Test 8 speed response comparison of

(a) - Sensorless Vector;

(b) - Closed-loop vector modes

The difference between the modes in Figure C-21 is very obvious. Whilst 8-33 (a) shows a speed disturbance of 0.51%, there is no measurable dip in motor speed on 8-33 (b). From this, it can be seen that the full closed-loop control mode offers a significant improvement in motor speed holding. It follows that the rate of change of motor current must be higher under the closed-loop mode in order to bring the motor speed back to the setpoint value as soon as possible and that the drive control loop is of a higher bandwidth as well.

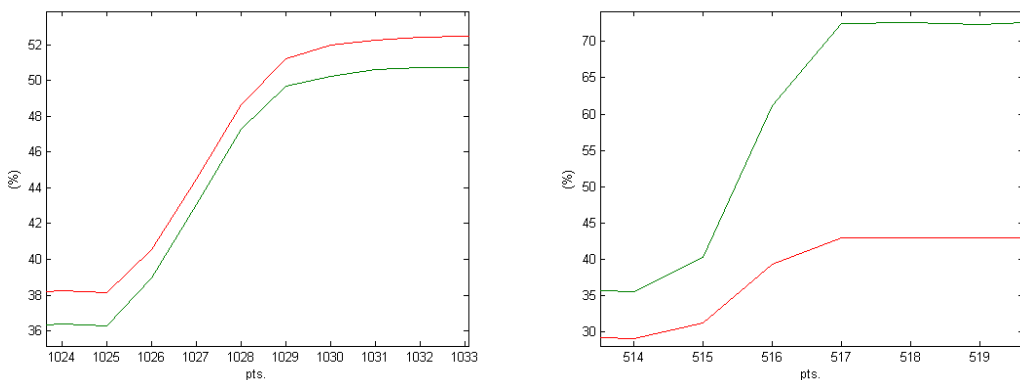


Figure C-22 - Current and torque response comparisons of

(a) - Sensorless Vector;

(b) - Closed-loop vector modes

In Figure C-22, the rate of change of current takes over 7 seconds (1 data point = 1 second) for (a) whereas (b) achieves the required current in less than 3 seconds. With the drive having a benefit of not having to rely on the motor modelling to estimate the speed drop occurring on the motor (there are integration time lags in the motor modelling process that also help to keep the speed control loop stable) and instead has feedback on the speed drop at the next speed loop iteration. This error at the speed loop input allows the current controller to increase the demand current instantly, with the controller proportional term providing the instantaneous error.

What is clear from these results that the drive performance has been improved under full closed-loop vector mode as opposed to operating under sensorless vector mode.

The choice of drive operating mode on the test rig will be determined by the application to which it is simulating. The 690+ vector drive allows a very simple change between these three modes by changing just one menu parameter under the “QUICK SETUP” menu.

Motors in some variable-speed drive applications do not require motor encoder feedback as the absolute shaft speed of the motor does not require such a fine degree of control. Fan and pump applications would be good examples of this. A machine that was controlling a sectional drive of a printing press for example, would require speed control of the motor down to 0.1% or less. This can only be achieved by true closed-loop vector drive operation – despite what some drive manufacturers may otherwise claim.

C.4 Actual Test Rig Operation Screenshots

Included below are images taken during commissioning of the test rig software.

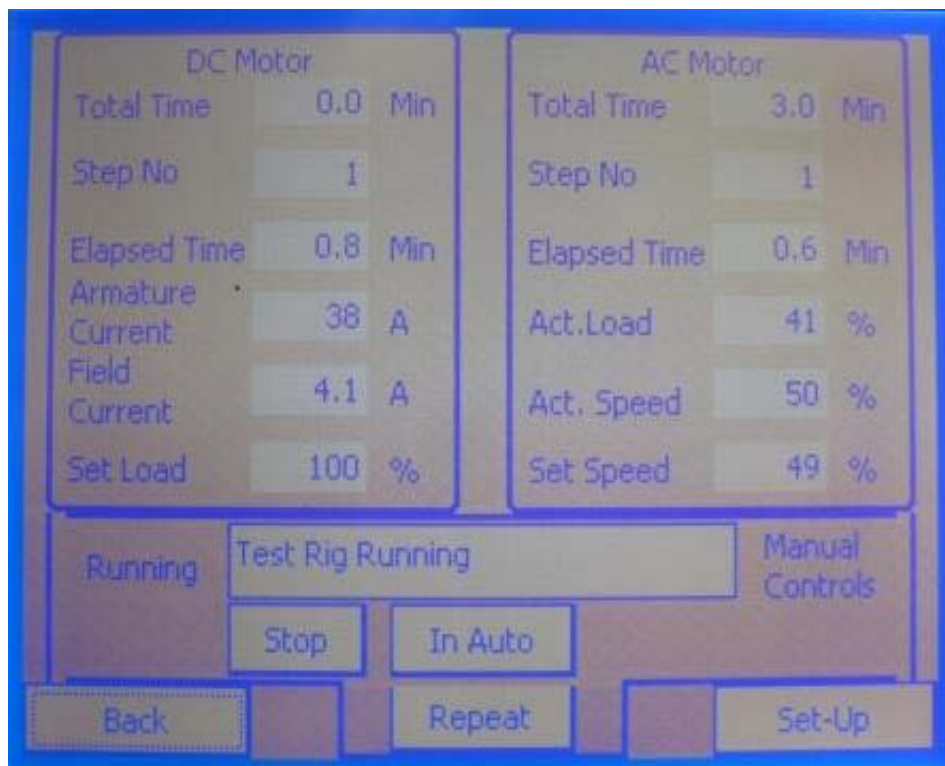


Figure C-23 - Operator Screen; Test Rig running in Auto

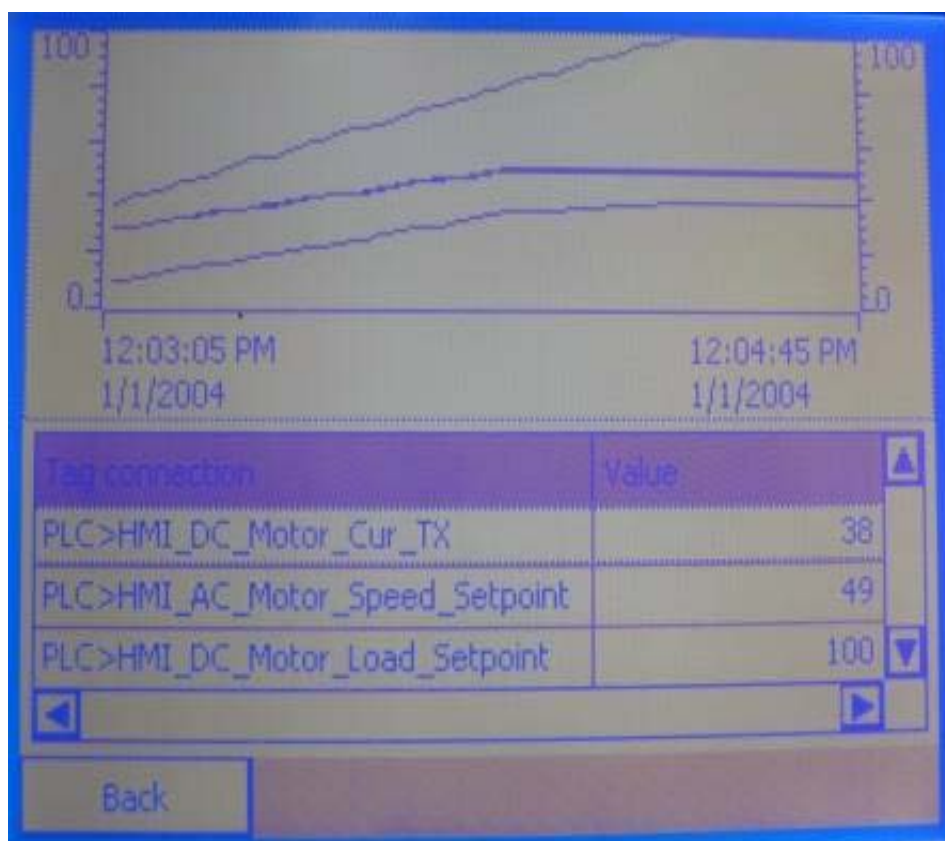
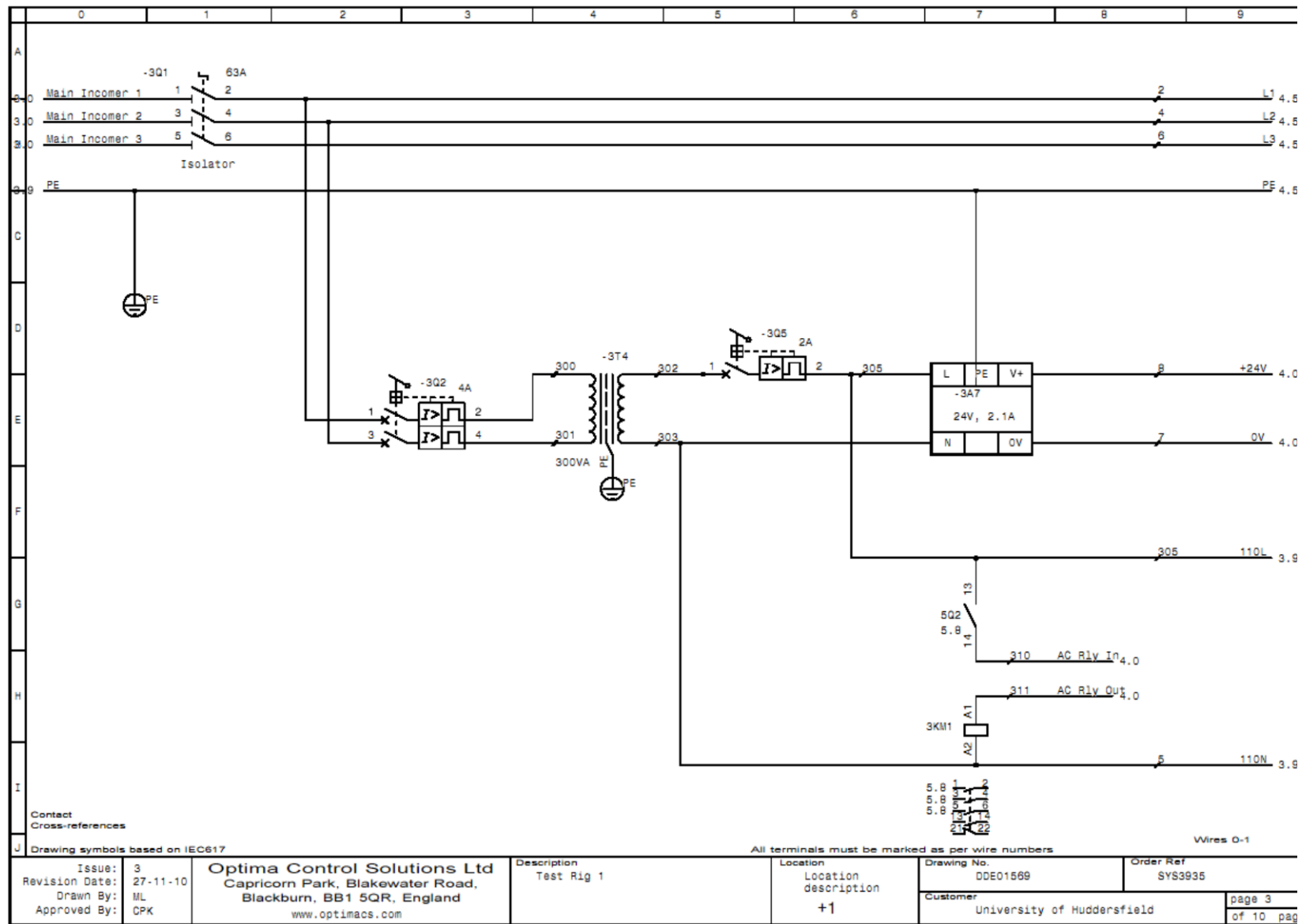


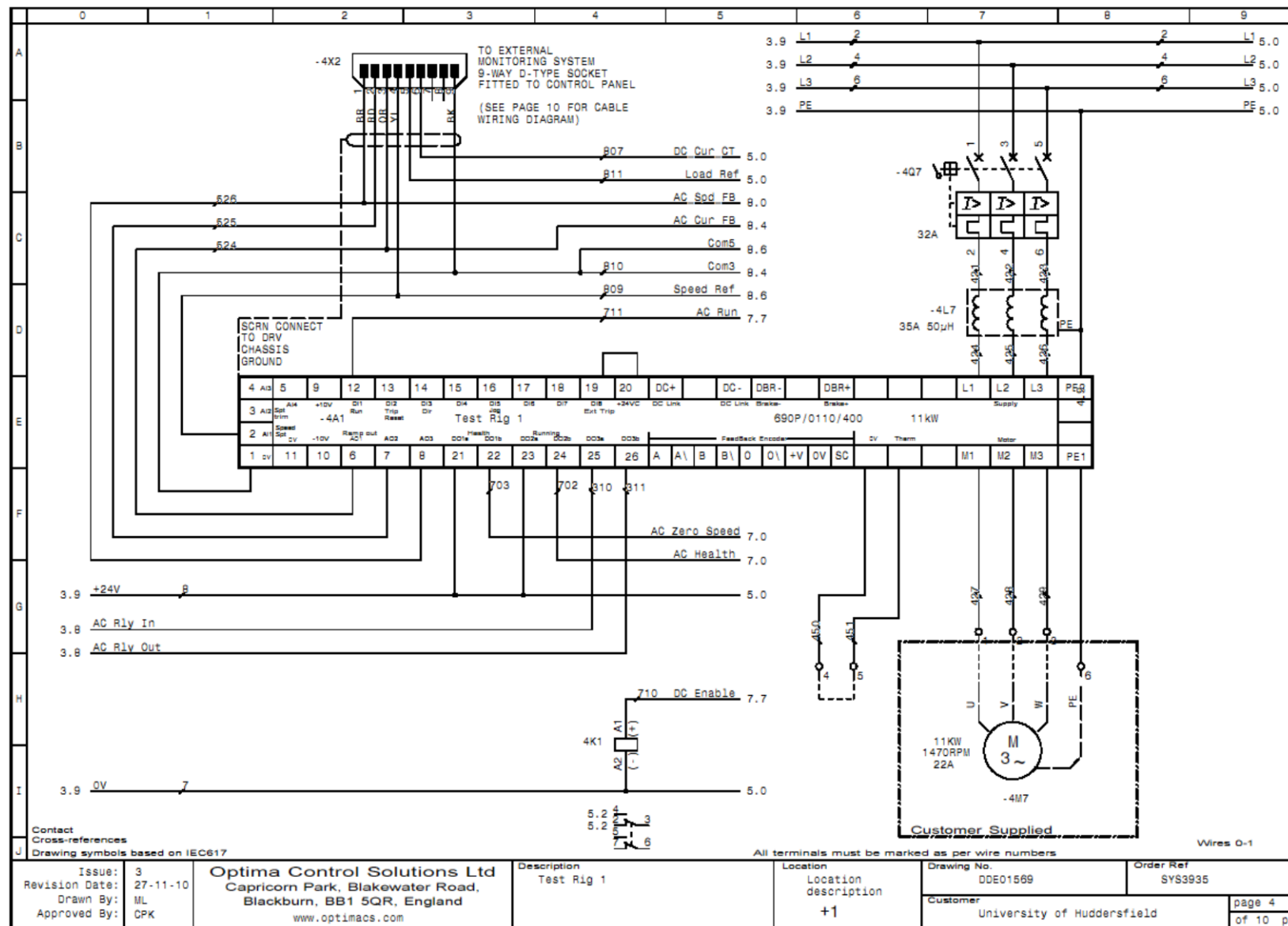
Figure C-24 - Trending Screen

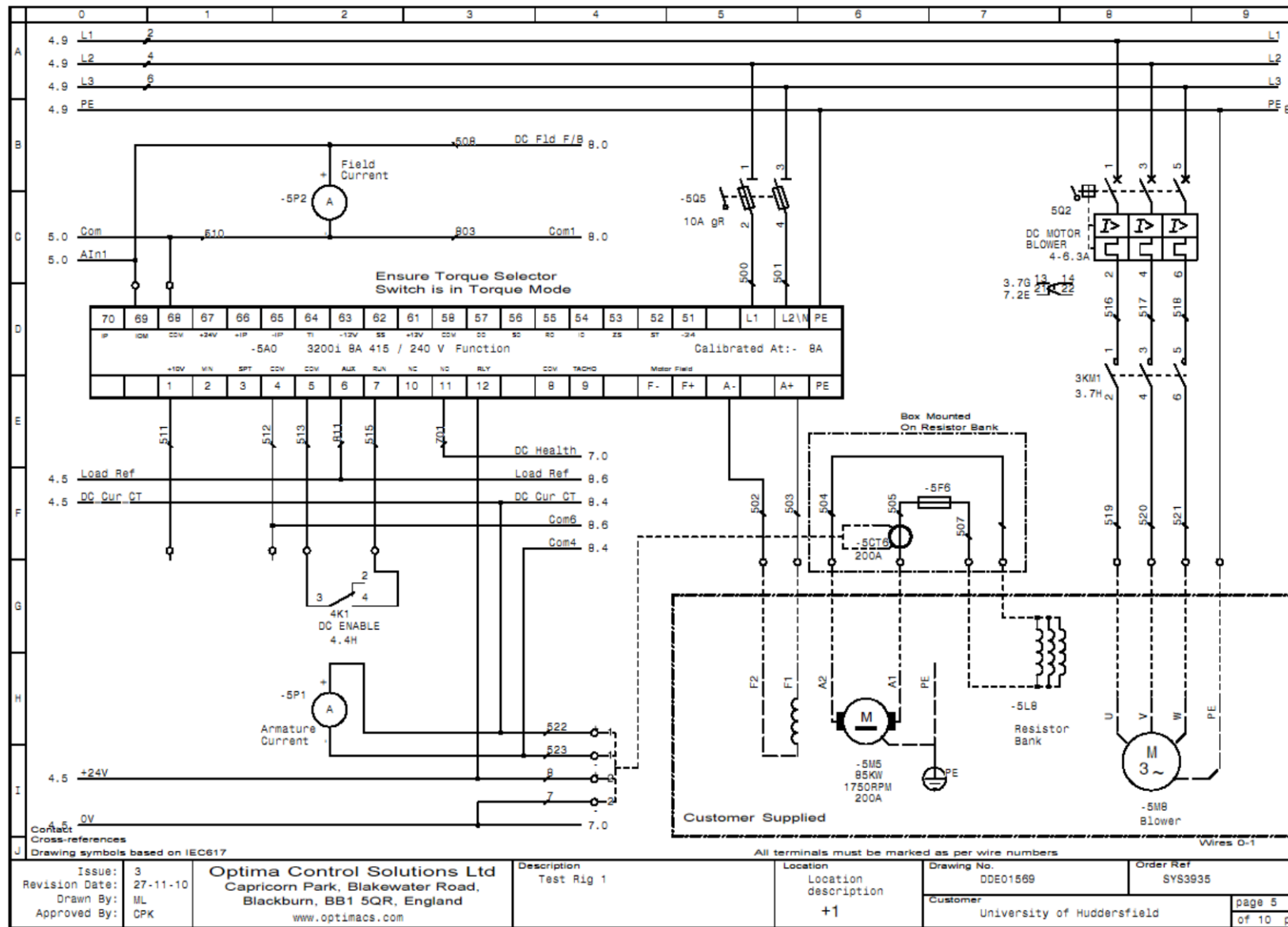
Appendix D Test rig schematics

	0	1	2	3	4	5	6	7	8	9
A										
B										
C										
D										
E										
F										
G										
H										
I										
Contact Cross-references										
J Drawing symbols based on IEC617										
Issue: 3	Revision Date: 27-11-10	Optima Control Solutions Ltd Capricorn Park, Blakewater Road, Blackburn, BB1 5QR, England www.optimacs.com	Description Test Rig 1	Location +1	Drawing No. DDE01569	Order Ref. SYS3935	Wires 0-1			
Drawn By: ML	Approved By: CPK							Customer University of Huddersfield	page 1 of 10 pa	

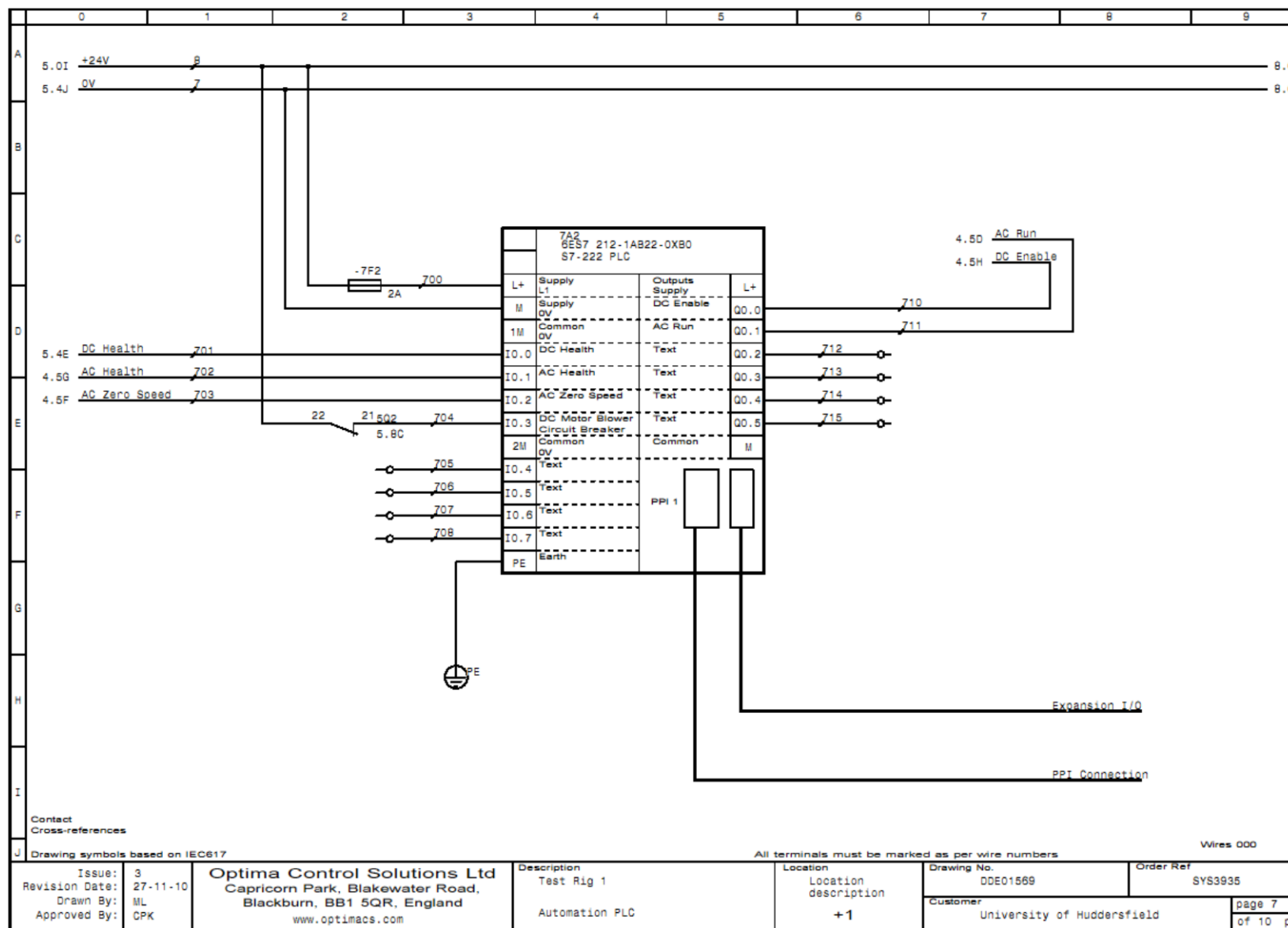
Page 2 intentionally left blank

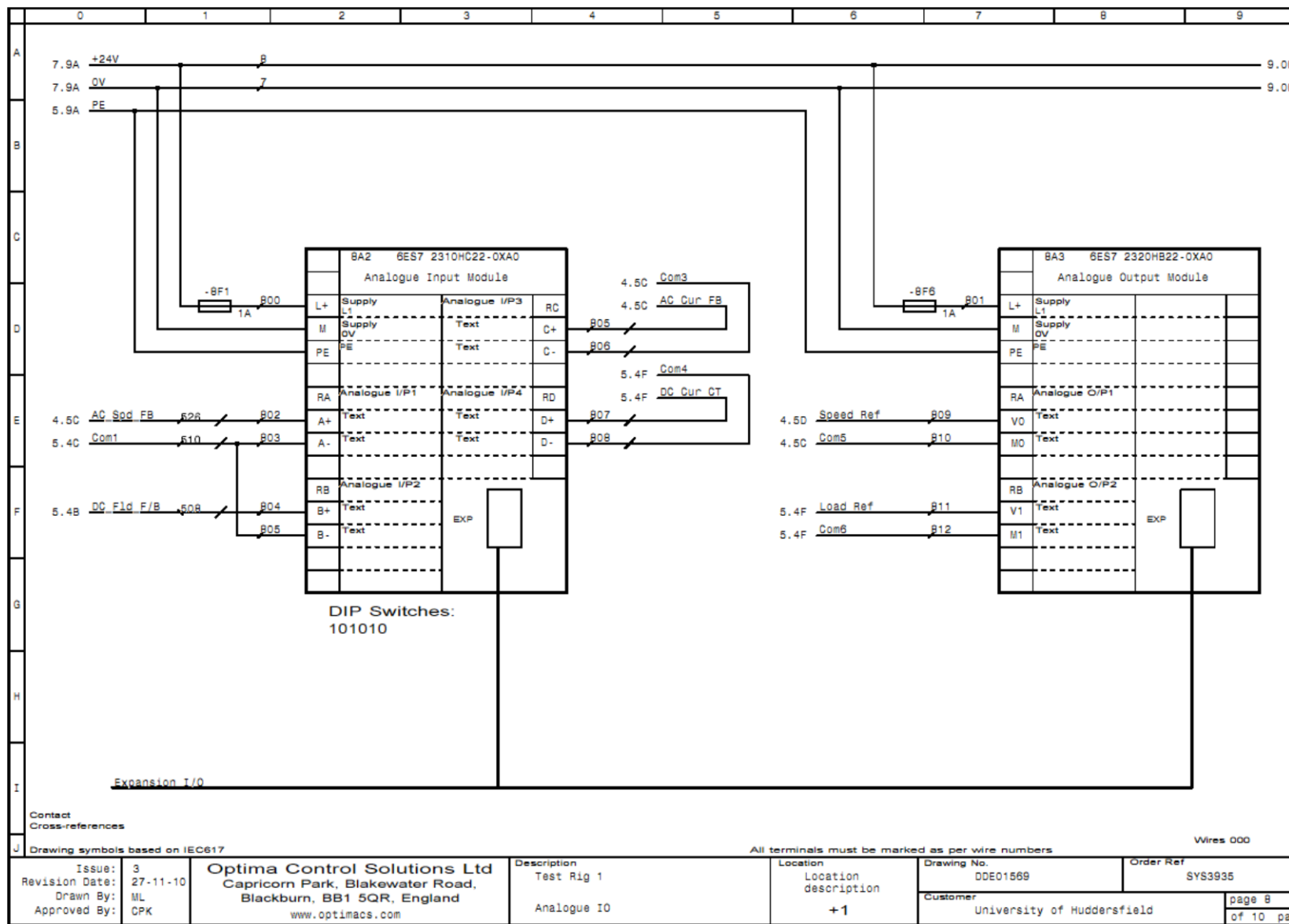


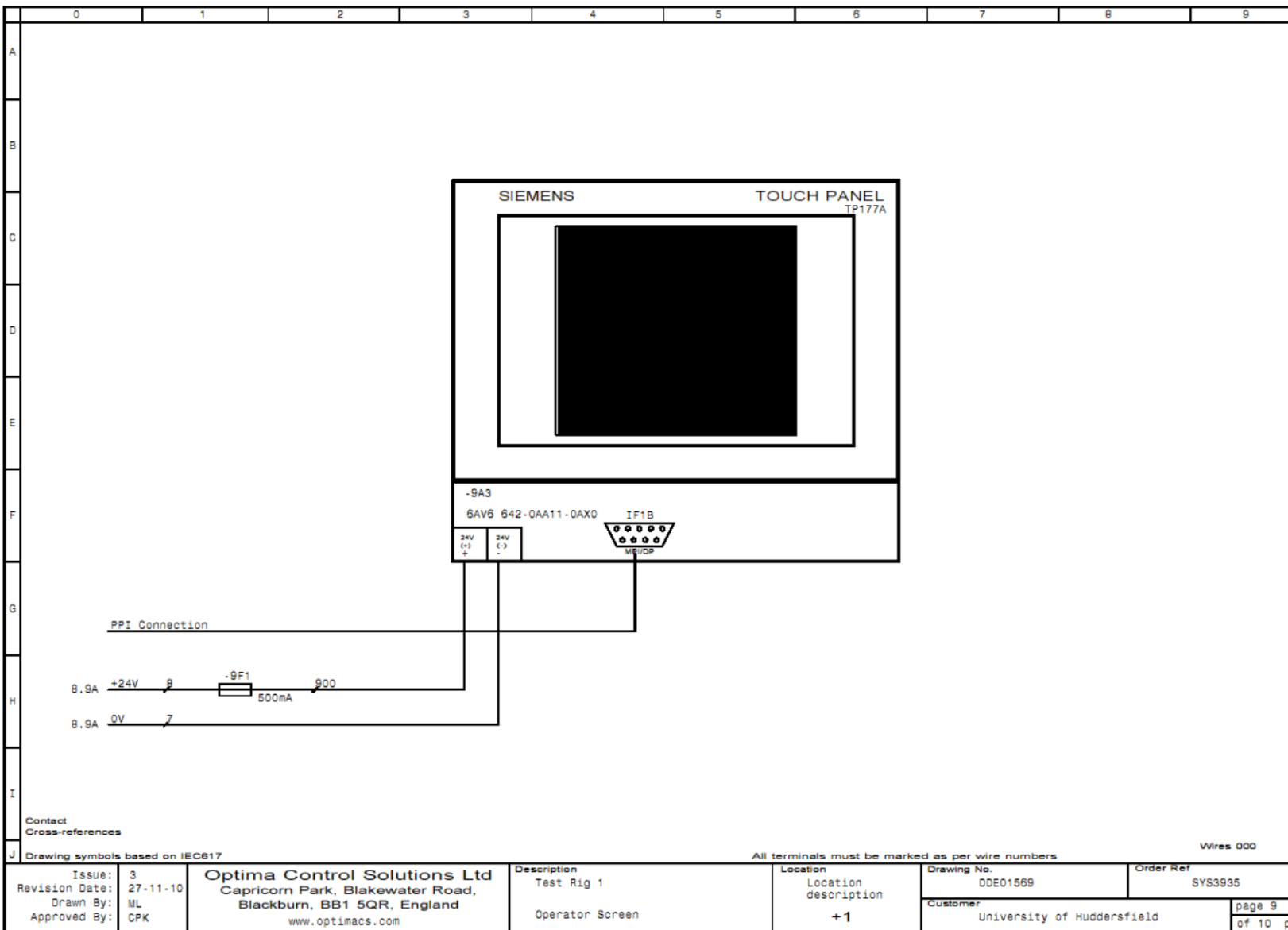




Page 6 intentionally left blank.







	0	1	2	3	4	5	6	7	8	9
A										
B										
C										
D										
E										
F										
G										
H										
I										
J	Contact Cross-references									
	Drawing symbols based on IEC617									
Issue:	3									
Revision Date:	27-11-10									
Drawn By:	ML									
Approved By:	CPK									
Optima Control Solutions Ltd Capricorn Park, Blakewater Road, Blackburn, BB1 5QR, England www.optimacs.com	Description Test Rig 1 External data monitoring connection lead	Location +1	Drawing No. DDE01569	Order Ref SYS3935	Wires 000					
		Customer University of Huddersfield	page 10 of 10 pages							